Valorization of insects as an alternative source of chitin and chitosan for pollutant removal applications and 3D bioprinting

Zhenying Mei

Valorisation des insectes comme source alternative de chitine et de chitosane pour les applications d'élimination des polluants et la bio-impression 3D

Zhenying Mei

Institut de Physique de Nice

Présentée en vue de l'obtention
du grade de docteur en Chimie
d'Université Côte d'Azur

Dirigée par : Pavel Kuzhir/ Guilhem Godeau

Soutenue le : 16 Décembre 2024

Devant le jury, composé de :

Modesto Torcuato López-López,
Professeur, University of Granada

Philippe Barthélémy,
Professeur, Université de Bordeaux

Aman Ullah,
Professeur, University of Alberta

Cédric Delattre,
Professeur, Université Clermont Auvergne

Guilhem Godeau,
Maître de conférences, Université Côte d'Azur

Pavel Kuzhir,
Professeur, Université Côte d'Azur

Valorisation des insectes comme source alternative de chitine et de chitosane pour les applications d'élimination des polluants et la bio-impression 3D

***

Valorization of insects as an alternative source of chitin and chitosan for pollutant removal applications and 3D bioprinting

Jury :

Rapporteurs

Philippe Barthélémy, Professeur, ARNA Laboratory, INSERM, U1212, CNRS 5320, Université de Bordeaux

Cédric Delattre, Professeur, CNRS, SIGMA Clermont, Institut Pascal, Université Clermont Auvergne

Examinateurs

Modesto Torcuato López-López, Professeur, Department of Applied Physics, University of Granada

Aman Ullah, Professeur, Department of Agricultural Food and Nutritional Sciences, University of Alberta

Directeurs de thèse

Pavel Kuzhir, Professeur, Institut de Physique de Nice (INPHYNI), CNRS, Université Côte d'Azur

Guilhem Godeau, Maître de Conférences (HDR), Institut de Physique de Nice (INPHYNI), CNRS, Université Côte d'Azur

Résumé

La chitine et le chitosane présentent un potentiel considérable pour de nombreuses applications dans divers domaines, notamment la biotechnologie, l'ingénierie, l'agriculture, l'industrie alimentaire, les sciences de l'environnement et ainsi de suite, en raison de leurs propriétés distinctives et de leur capacité d'adaptation. La chitine est un polysaccharide linéaire composé d'unités de N-acétylglucosamine (GlcNAc) liées en β-(1-4). Le chitosane est obtenu par désacétylation partielle de la chitine via l'élimination des groupes acétyles des unités GlcNAc. Le degré de désacétylation détermine l'étendue de la conversion de la chitine en chitosane et influe sur ses propriétés physicochimiques. La chitine et le chitosane sont principalement issu des déchets de fruits de mer, car les exosquelettes des crustacées (crevettes, homards, crabes, *etc.*) sont riches en chitine. Toutefois, cette ressource n'est pas en mesure de répondre aux besoins croissants et aux projections de futurs besoin en matière de chitosane. La taille du marché mondial de la chitine devrait être évaluée à environ 1 801,3 millions de dollars américains en 2023 et devrait atteindre 5 746,2 millions de dollars américains d'ici 2033. La demande mondiale de chitosane continue d'augmenter à un taux annuel de 15,4 %. Il existe un besoin pressant de sources alternatives et durables de chitine et de chitosane afin de surmonter les limitations associées aux sources conventionnelles et d'étudier de nouveaux matériaux aux propriétés améliorées. Les insectes peuvent donc être considérés comme une source abondante et durable de chitine et de chitosane. Les insectes ont des taux de reproduction rapides, des cycles de vie courts et nécessitent des ressources minimales pour leur élevage, ce qui garantit un approvisionnement constant en chitine et donc en chitosane.

Cette thèse commence par une revue complète de l'état actuel de la chitine et du chitosane dérivés d'insectes, en se concentrant sur leurs sources, leurs méthodes de production, leur caractérisation, leurs propriétés physiques et chimiques, ainsi que leurs diverses applications. Ensuite, nous avons étudié 11 espèces d'insectes différentes comme matériau de départ pour l'extraction de la chitine et la préparation du chitosane. Il s'agit de neuf espèces appartenant à la famille des *Curculionidae*, d'*Heteronitis castelnaui* appartenant à la famille des Scarabaeidae et d'*Eurycantha calcarata* appartenant à la famille des *Lonchodidae*. La chitine et le chitosane obtenus ont été soigneusement caractérisés à l'aide de diverses techniques analytiques telles que la spectroscopie infrarouge à transformée de Fourier (FTIR), la diffraction des rayons X (XRD), la microscopie électronique à balayage (SEM), la résonance magnétique nucléaire (NMR), l'analyse thermogravimétrique (TGA) et la calorimétrie différentielle à balayage (DSC). Ensuite, le chitosane *Heteronitis castelnaui* et le chitosane *Eurycantha calcarata* obtenus ont fait l'objet d'études plus approfondies en vue d'applications. Le chitosane *Heteronitis castelnaui* a démontré d'excellentes performances dans la formation d'hydrogels et a présenté une capacité d'adsorption remarquable pour le bleu de méthylène et l'orange de méthyle. L'hydrogel à base de chitosane d'*Eurycantha calcarata* a présenté des caractéristiques d'imprimabilité 3D favorables, une biocompatibilité élevée et une nature non toxique. Ces données préliminaires confirment que les espèces étudiées peuvent être considérées comme des sources potentielles de chitine et de chitosane pour des utilisations industrielles.

Mots clés: Chitine, chitosane, matériaux biosourcés, caractérisation physico-chimique, adsorption de colorants, bio-impression 3D

Abstract

Chitin and chitosan have considerable potential for a number of applications in a variety of fields, including biotechnology, engineering, agriculture, the food industry, environmental sciences and so on, due to their distinctive properties and adaptability. Chitin is a linear polysaccharide composed of β-(1-4)-linked N-acetylglucosamine (GlcNAc) units. Chitosan is obtained by the partial deacetylation of chitin via removal of the acetyl groups from the GlcNAc units. The degree of deacetylation determines the extent of conversion from chitin to chitosan and impacts its physicochemical properties. Chitin and chitosan are derived mainly from seafood wastes (shrimp, lobster, crabs, etc.). However, this resource is unable to support the growing needs and future projections for chitin and chitosan. The global chitin market size is set to be valued at around US$ 1,801.3 million in 2023 and is anticipated to reach US$ 5,746.2 million by 2033. And global demand for chitosan continues to rise at an annual rate of 15.4%. There is a pressing need for alternative and sustainable sources of chitin and chitosan to overcome limitations associated with conventional sources, and to investigate novel materials with enhanced properties. Hence, insects may be considered as an abundant and sustainable source of chitin and chitosan. Insects have rapid reproduction rates, short lifecycles, and require minimal resources for breeding, ensuring a consistent available supply of chitin and chitosan.

This thesis provides a comprehensive review on the current state of insect-derived chitin and chitosan, focusing on their sources, production methods, characterization, physical and chemical properties, and various applications. Then, we investigated 11 different insect species as a starting material for chitin extraction and chitosan preparation. These include nine species belonging to *Curculionidae* family, *Heteronitis castelnaui* belonging to Scarabaeidae family, and *Eurycantha calcarata* belonging to Lonchodidae family. All the obtained chitin and chitosan was thoroughly characterized using various analytical techniques such as Fourier-transform infrared spectroscopy (FTIR), X-ray diffraction (XRD), scanning electron microscopy (SEM), nuclear magnetic resonance (NMR), thermogravimetric analysis (TGA), and differential scanning calorimetry (DSC). Then the obtained *Heteronitis castelnaui* chitosan and *Eurycantha calcarata* chitosan were further investigated for the applications. *Heteronitis castelnaui* chitosan demonstrated excellent performance in the formation of hydrogels and exhibited remarkable adsorption capacity for methylene blue and methyl orange. *Eurycantha calcarata* chitosan-based hydrogel exhibited favorable 3D printability characteristics, high biocompatibility and non-toxic nature. These preliminary data confirm that these studied species may be considered as potential source of chitin and chitosan for industrial uses.

Key words: Chitin, chitosan, biosourcesd materials, physicochemical characterization, dyes adsorption, 3D bioprinting

Acknowledgement

The three years I spent at the University of the Côte d'Azur as a PhD student were the most fulfilling, precious, and unforgettable times of my life. I have experienced many days of confusion, anxiety and happiness here. I have also doubted my original intention of studying abroad and lost the meaning and direction of my life. The time I studied here gave me a lot of opportunities to think and made me gradually understand that ordinary is the only answer, and that to create goodness in the ordinary is a kind of heroism of people in this era. Even if it is just to bring a little bit of goodness to the society, or to solve a small problem, such a life is meaningful. It is with this belief, in the continuous psychological construction of self, in the company of friends, in the comfort of parents, I regained confidence again and again, and finally overcame all the difficulties to submit this dissertation.

Thanks to the Chinese Scholar Council for funding my Ph. D. Thanks to my supervisors, Pavel Kuzhir and Guilhem Godeau, for giving me the opportunity to study at the Institut de Physique de Nice three years ago. During these three years, I have been fortunate enough to participate in several research projects, learnt about various experimental instruments, and participated in international conferences and workshops. Université Côte d'azur has provided me with high quality teaching resources and practical opportunities, which have enabled me to exercise my abilities in various aspects and grow up in a solid manner. I would like to thank Pavel for his careful guidance and assistance in my experiments and thesis writing, and his patience in answering my questions no matter how detailed they were; Guilhem for his constant guidance, thanks to his professionalism and for all the discussions to find solutions to the problem encountered.

I respectfully thank Prof. Modesto Torcuato López-López, Prof. Cédric Delattre, Prof. Philippe Barthélémy and Prof. Aman Ullah for being members of my dissertation jury and reviewing my thesis manuscript.

I am grateful to Xiaomin for teaching and encouraging me in my studies and caring for me in my life. Thanks to Arnaud from the Mediterranean Institute of the risk, environment and sustainable development (IMREDD) for his guidance and help with the experimental apparatus. Thanks to Christophe Candet from Phoenix Parc for the constant supply of insect samples.

Thanks to Franck Celestini, Cornelia Meinert, and Luc Vincent for being part of my annual committee and following up on my progress during these 3 years. Thanks to Olivier Montreuil from UMR 7179 MNHN/CNRS, MECADEV, (Muséum National d'Histoire Naturelle, Entomologie) for advice and constructive comments. Thanks to Caroline Szczepanski and René-Paul Godeau for help with articles writing.

Thanks to the members of the Magnetorheology and nanomaterials team (Jordy Queiros Campos, Julie Lagouarde, Jessica Alves Marins, Yassine Bentahar, Sumeyra Seniha Baran, Georges Bossis, Olga Volkova, Charlotte Hurel, Xin Li, Claire Lomenech, Alain Ciffreo, Mariia Savchenko, Maxime Raboisson-Michel, Hongru Tian, and Audrey Sinigaglia) for all these discussions/exchanges/supports! Thanks to everyone in the group for the pleasant and positive atmosphere in my life and experiments. Thanks to everyone at the Institut de Physique de Nice whom I have met and worked alongside during these 3 years.

Finally, thanks to my family for their full support, care and attention over the years, which gave me the greatest courage and freedom.

Content

List of Figures

List of Tables

Nomenclature

Principal acronyms

Cipro/CSNPs	Chitosan nanoparticles loaded with ciprofloxacin
CNPs	Chitosan nanoparticles
CrI	Crystallinity index
DDA	Degree of deacetylation
DES	Deep eutectic solvents
DSC	Differential scanning calorimetry
DTG	Derivative thermogravimetry
ECM	Cell-extracellular matrix
FTIR	Fourier transform infrared
MB	Methylene blue
MO	Methyl orange
NMR	Nuclear magnetic resonance
PEO	Polyethylene oxide
PVA	Polyvinyl alcohol

SEM	Scanning electron microscopy
TGA	Thermogravimetric analysis
3D	Three-dimensional

Principal symbols

C_e **(mg·L^{-1})**	Equilibrium concentrations of adsorbate [Eqs. (3.4), (3.8), (3.9)]
C_r **(mol·L^{-1})**	Standard concentration of the adsorbate [Eq. (3.11)]
C_o **(mg·L^{-1})**	Initial concentrations of adsorbate [Eqs. (3.4), (3.5)]
C_t **(mg·L^{-1})**	Adsorbate concentration at a specific time [Eq. (3.5)]
d_r **(mm)**	The measured sample dimension [Eq. (3.12)]
d_s **(mm)**	The theoretical dimension [Eq. (3.12)]
DTG$_{max}$	Maximum degradation temperature
H-Ac	The integration of the peak of the three protons of acetyl group [Eq. (3.2)]
H1-D	The integration of the proton H1 of deacetylated saccharide [Eq. (3.2)]
I$_{cr}$	Maximum intensity for crystalline lattices [Eq. (3.1)]
I$_{am}$	Maximum intensity for amorphous region [Eq. (3.1)]
K	Dimensionless Langmuir constant [Eq. (3.11)]
K	Hydrogel consistency [Eqs. (6.1), (6.2)]
k_1 **(min^{-1})**	Rate constants of pseudo-first-order model [Eq. (3.6)]
k_2 **(mg^{-1}·g·min^{-1})**	Rate constants of pseudo-second-order model [Eq. (3.7)]
k_L **(L·mg^{-1})**	Langmuir equilibrium constant [Eq. (3.8), (3.11)]

k_F **(mg$^{1-1/n}$·L$^{1/n}$·g^{-1})**	Freundlich constant [Eq. (3.9)]
L **(mm)**	Nozzle length [Eq. (6.2)]
M_w	Molecular weight [Eq. (6.2)]
n	Power-law index [Eqs. (6.1), (6.2)]
q_e **(mg·g^{-1})**	Equilibrium adsorption capacity [Eqs. (3.4), (3.6), (3.7), (3.8), (3.9)]
q_t **(mg·g^{-1})**	Adsorption capacity at a specific time [Eqs. (3.5), (3.6), (3.7)]
R **(J·mol^{-1}·K^{-1})**	The universal gas constant [Eq. (3.10)]
R **(mm)**	Nozzle radius [Eq. (6.2)]
T **(°C)**	The temperature in Kelvin
v **(mm·s)**	Printing speed [Eq. (6.2)]
W_t **(mg)**	The weight of samples at a specific time [Eq. (3.13)]
W_0 **(mg)**	Initial weight of samples [Eq. (3.13)]
ΔG **(kJ·mol^{-1})**	Gibbs energy change [Eq. (3.9)]

Samples

DC	Dung beetle chitosan
DCA hydrogel	Dung beetle chitosan/sodium alginate hydrogel
DCG hydrogel	Dung beetle chitosan/gelatin hydrogel
EC	*Eurycantha* chitosan
ECG hydrogel	*Eurycantha* chitosan/gelatin hydrogel

Chapter 1 Introduction

Chitin is a chain polymer of N-acetylglucosamine and is the second more abundant polysaccharide polymer after cellulose. In Arthropoda's exoskeleton and as consequence in insect's exoskeleton, the most abundant form of chitin is the α form, which has increased stability due to a fully anti-parallel organization. This organization leads to strong hydrogen interactions. Unfortunately, due to its poor solubility in most common solvents, α-chitin is difficult to use in materials applications in its virgin state. This lack of solubility is a consequence of strong intermolecular interactions and a compact macromolecular structure. Typically, to avoid this solubility limitation, chitin is modified prior to industrial use. For example, chitin is the main raw component in chitosan production once it is partially deacetylated.

Chitosan, derived from chitin through deacetylation, exhibits similar structural features with some modifications [1]. The removal of acetyl groups introduces amino groups, altering the properties of the polymer [2]. The degree of deacetylation (DDA) determines the proportion of glucosamine units in the chitosan structure, influencing its solubility, charge density, and other physicochemical properties [3, 4]. The structural characteristics of chitosan play a crucial role in determining their properties and applications. Because of these favorable properties such as biocompatibility, improved solubility and biodegradability, chitosan has a wide range of applications in the food, biomedical, agricultural and textile fields.

Among the various uses of chitosan, 3D bioprinting is of particular relevance, which are currently a growing area of research [5]. Although 3D printing technology has been extensively investigated for tissue engineering, there has been insufficient research on chitosan-based materials. Further modifications and formulations are required to increase the printability of chitosan-based scaffolds. It is also essential to find natural sources of materials to enhance the

biocompatibility. Regarding water pollution, the persistence and potential toxicity of organic dyes commonly used in industries such as textiles, leather, and printing give rise to substantial environmental concerns. Methylene blue (MB) and methyl orange (MO), which are consumed in large quantities in industry, are toxic and carcinogenic, and are non-biodegradable dyes. Additionally, MB is also widely used as a model molecule for studying the removal of biomedical molecules. Consequently, these dyes represent ideal model contaminants for evaluating pollution due to industrial dyes. The adsorption technique is widely regarded as one of the most effective methods for contaminant removal. This effectiveness is attributed to its simplicity, cost-efficiency, lack of secondary pollution, and extensive applicability across various contexts. A considerable number of studies have been conducted on the use of chitosan for dye adsorption. However, there have been few reports on the application of chitosan derived from insects in this context.

Given that the majority of chitin and chitosan production arises from seafood waste, in recent years there has been growing interest in exploring alternative sources to overcome limitations associated with conventional sources. Insects present an abundant and sustainable source of chitin, making them an attractive option for chitin extraction and chitosan production. Unlike crustaceans, which are commonly utilized for chitin extraction and chitosan production, insects offer several distinct advantages. On the one hand, insects have rapid reproduction rates, short lifecycles, and require minimal resources for breeding, ensuring a consistent and readily available supply of chitin [6]. Chitin is distributed throughout an insect's body, primarily in the exoskeleton but also present in other structures like the wings, antennae, and trachea [7]. This distribution allows for the extraction of chitin from various body parts, maximizing the utilization of insect biomass. Insect exoskeleton is composed mainly of chitin, providing structural support and protection for the insect's body [8]. The use of insects as a raw material reduces the environmental impact associated with crustacean-based sources. This sustainability

aspect aligns with the growing demand for environmentally friendly products. Another advantage of insect-derived chitosan lies in its potential to reduce allergenicity compared to chitosan derived from crustaceans. Allergic reactions to chitosan from crustacean sources can occur due to the presence of allergenic proteins. However, insects possess different protein compositions, potentially lowering the risk of allergic reactions in individuals sensitive to crustaceans [9].

This study investigated the production, characterization and applications of chitin and chitosan from the exoskeletons of different insect species, including nine species belonging to Curculionidae family, *Heteronitis castelnaui* belonging to Scarabaeidae family, and *Eurycantha calcarata* belonging to Lonchodidae family. To this purpose, chitin and chitosan were extracted through a series of chemical treatments. And then the resulting chitin and chitosan was thoroughly characterized using analytical techniques such as Fourier-transform infrared spectroscopy (FTIR), X-ray diffraction (XRD), scanning electron microscopy (SEM), nuclear magnetic resonance (NMR), thermogravimetric analysis (TGA), and differential scanning calorimetry (DSC). Furthermore, the obtained chitosan was used to form hydrogels and then its utilizations for 3D bioprinting and dyes removal from aqueous solutions was evaluated. The outcomes of this investigation contribute to the development of the knowledge on novel sources of chitin and chitosan and their potential applications in 3D bioprinting and wastewater treatment, which offers a sustainable and environmentally friendly approach.

Chapter 2 State of the art and thesis objectives[1]

2.1 Summary of chitin and chitosan

Chitin, the second most abundant polysaccharide in nature after cellulose, composed of β-(1,4)-linked N-acetylglucosamine (GlcNAc) units, is a linear polymer that forms long chains with a crystalline structure (Figure 2.1A) [10]. This arrangement provides chitin with rigidity and insolubility in most solvents, underscore chitin's potential as a biomimetic archetype for materials characterized by exceptional mechanical attributes [11]. One notable aspect of chitin is the presence of three distinct allomorphs: α-chitin, β-chitin, and γ-chitin (Figure 2.1B) [12].

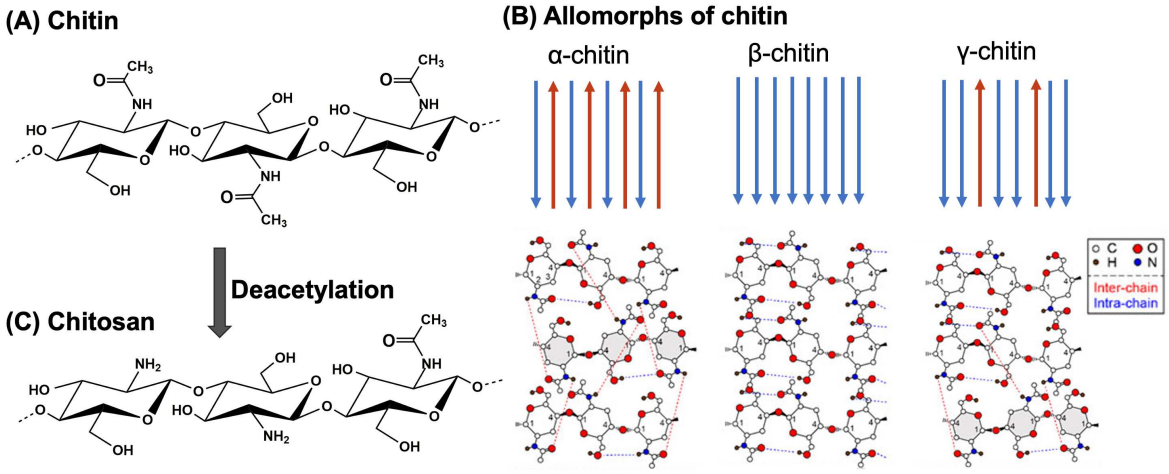

Figure 2.1 (A) Chitin molecular structure. (B) Hydrogen-bonding patterns of different chitin allomorphs. Blue and red dash lines indicate intra-chain and inter-chain hydrogen bonds, respectively. The antiparallel chains in α and γ chitins are in grey. (C) Chitosan molecular structure. The structural schemes are adapted from Liyanage *et al. Front. Mol. Biosci.* 8:727053, Frontiers [13].

[1] Main contents of this chapter are published in the paper Mei, Z.; Kuzhir, P.; Godeau, G. Update on Chitin and Chitosan from Insects: Sources, Production, Characterization, and Biomedical Applications. *Biomimetics* **2024**, *9*, 297. https://doi.org/10.3390/biomimetics9050297

The first allomorph, α-chitin, is the most common and extensively studied. It features tightly antiparallel chains with intra- and intermolecular hydrogen bonding pattern (Figure 2.1B). α-Chitin exhibits a high degree of crystallinity, resulting in exceptional mechanical properties such as stiffness, tensile strength, and hardness [14]. It is commonly found in the exoskeletons of arthropods [15]. The second allomorph, β-chitin, possesses a more open and less ordered crystalline structure compared to α-chitin. It consists of parallel chains with weaker intermolecular hydrogen bonding, leading to reduced crystallinity. β-Chitin exhibits lower mechanical strength but offers improved flexibility and less rigidity compared to α-chitin. It is present in the spines of diatoms, squid pens and pogonophora tubes [16]. The least common and least studied allomorph is γ-chitin. It exhibits a helical arrangement of chains, resulting in a distinct hydrogen bonding pattern different from α-chitin and β-chitin [17]. γ-Chitin is primarily found in fungi, yeasts, and insect cocoons [1, 18, 19]. The crystalline nature of chitin, along with the unique arrangements of the three allomorphs, influences mechanical strength, solubility, and degradation behavior. The hierarchical structure of chitin provides a model for the development of biomimetic materials with tailored mechanical properties. These include lightweight composites, protective coatings, and structural reinforcements. By mimicking the hierarchical organization and composition of chitin-rich structures found in nature, it's possible to engineer materials with superior strength-to-weight ratios, impact resistance, and self-healing capabilities.

Chitosan, a versatile polysaccharide mainly derived from the exoskeletons of crustaceans and insects, has garnered significant attention in recent years for its remarkable properties and potential biomedical applications [20]. Chitosan derived from chitin through deacetylation, exhibits similar structural features with some modifications. The removal of acetyl groups introduces amino groups, altering the properties of the polymer (Figure 2.1C) [21]. The degree

of deacetylation (DDA) determines the proportion of glucosamine units in the chitosan structure, influencing its solubility, charge density, and other physicochemical properties [3, 22].

The structural characteristics of chitin and chitosan play a crucial role in determining their properties and applications. The crystalline nature of chitin, along with the unique arrangements of the three allomorphs, influences mechanical strength, solubility, and degradation behavior. Chitosan, with its improved solubility in acidic solutions and polycationic nature, exhibits enhanced bioactivity and interaction with biomolecules [23].

This transformation unlocks a myriad of opportunities for biomimetic exploration, enabling the development of materials that mimic biological tissues, extracellular matrices, and cellular environments. In biosensing and diagnostic applications, chitosan's inherent biocompatibility and ability to interact with biomolecules make it an attractive candidate for the development of bioactive surfaces, biosensors, and diagnostic assays. The structural characteristics of chitin and chitosan play a crucial role in determining their properties and applications. These distinctive structural and property profiles of chitin and chitosan have made them highly valuable for biomedical applications. Their biodegradability, biocompatibility, and versatile functionalities make them attractive materials for drug delivery systems, tissue engineering, wound healing, and other therapeutic approaches. In particular, chitin and chitosan derived from insect sources has emerged as a promising alternative to traditional sources, offering a multitude of advantages over other origins [24].

2.2 Sources of chitin and chitosan from insects

Abundant insect sources of chitin and chitosan, from the Lepidoptera, Coleoptera, Orthoptera, Hymenoptera, Diptera, Hemiptera, Dictyoptera, Odonata, and Ephemeroptera orders, were comprehensively summarized. Here, data for total number of 82 insect species were collected and analyzed (Table 2.1 and Figure 2.2).

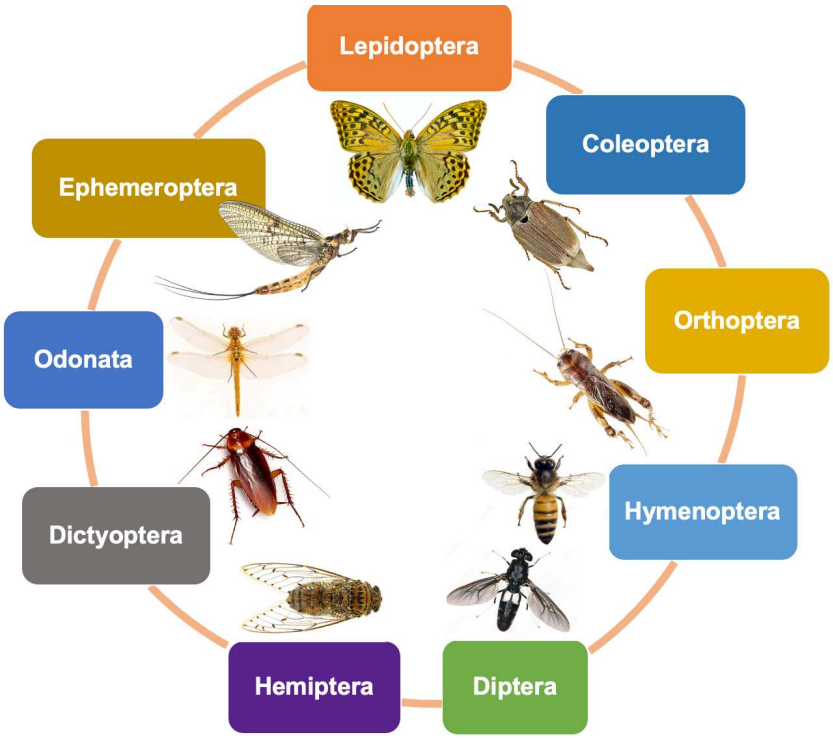

Figure 2.2 Insect sources of chitin and chitosan.

Table 2.1 A summary of chemical methods for chitin purification from insects.

Insect species	Demineralization	Deproteinization	Decoloration	Chitin Yield (%)	Ref.
Lepidoptera					
Silkworm	1 M HCl in 30 °C for 2 h	1 M NaOH in 90 °C for 2 h	2% $KMnO_4$ for 2 h, 2% $H_2C_2O_4$ for 2 h	NA	[25]
Flour moth, *Ephestia kuehniella*	1 M HCl at 100 °C for 20 min	1 M NaOH at 85 °C for 60 min	1% $KMnO_4$ for 60 min	9.5–10.5	[26]
Butterfly, *Argynnis pandora*	2 M HCl at 50°C for 24 h	2 M NaOH solution at 50 °C for 24 h	Distilled water, methanol, and chloroform (4:2:1) for 10 min	Wings-22 Body-8	[27]
Clanis bilineata	7% (v/v) HCl at 25 °C for 24 h	10% (w/v) NaOH at 60 °C for 24 h	NA	NA	[28]
Clanis bilineata	7% (v/v) HCl at 25 °C for 24 h	10% (w/v) NaOH at 60 °C for 24 h	NA	NA	[29]
Clanis bilineata larvae	7% (v/v) HCl at 25 °C for 24 h	10% (w/v) NaOH at 60 °C for 24 h	NA	NA	[30]
Coleoptera					
Mealworm, *Tenebrio molitor*	1 M HCl in 30 °C for 2 h	1 M NaOH in 90 °C for 2 h	2% $KMnO_4$ for 2 h, 2% $H_2C_2O_4$ for 2h	NA	[25]
Comb-clawed beetles, *Omophlus* sp.	2 M HCl for 4 h at 50 °C	2 M NaOH for 20 h at 100 °C	Methanol–chloroform–water (2:1:4)	NA	[31]
Cockchafer, *Melolontha melolontha*	50 mL of 4 M HCl at 75 °C for 2 h	4 M NaOH at 150 °C for 18 h	Water, alcohol and chloroform (4:2:1) for 20 min	13–14	[32]

Cockchafer, *Melolontha* sp.	2 M HCl at 60 °C for 20 h	1 M of NaOH for 20 h at 100 °C	Distilled water, methanol, and chloroform (4:2:1) for 30 min	Male-16.60 Female-15.66	[33]
Colorado potato beetle, *Leptinotarsa decemlineata*	100 mL of 2 M HCl at 65–75 °C for 2 h	50 mL of 2 M NaOH at 80–90 °C for 16 h	Chloroform, methanol and water (in a ratio of 1:2:4) for 1 h	Adult-20 Larvae-7	[34]
Catharsius molossus	1.30 M HCl at 80 °C for 30 min	4.0 M NaOH at 90 °C for 6 h	2% oxalic acid at 70 °C for 30 min	24	[35]
Calosoma rugosa	1 M HCl	1.0 M NaOH at 100 °C for 8 h	NA	5.0	[36]
Calosoma rugosa	*36.5% HCl	*1.0 M NaOH	NA	NA	[37]
Mealworm, *Tenebrio molitor*	3 h in 2 M HCl at 20 °C	500 mL 5% NaOH at 95 °C for 3 h	NA	18.01	[38]
Mealworm, *Tenebrio molitor*	2 M HCl at 50 °C for 24 h	2 M NaOH solution at 50 °C for 24 h	NA	NA	[39]
Mealworm, *Tenebrio molitor*	*1.5 M HCl at 20 °C, 120 rpm for 6 h	*1.25 M NaOH at 80 °C for 24 h	NA	4.72	[40]
Mealworm, *Tenebrio molitor*	2 M HCl at 65-75 °C for 2 h	2M NaOH at 80 to 90 °C	chloroform, methanol, and water (1:2:4) for 1 h	17.7	[41]
Mealworm Beetle, (*Tenebrio molitor, Zophobas morio*) Rhinoceros Beetle (*Allomyrina dichotoma*)	*7% (v/v) HCl at 25 °C for 24 h	*NaOH at 80 °C for 24 h	NA	Larvae-4.60 Adult-8.40 Superworm-3.90 Larvae-10.53 Pupa-12.70 Adult-14.20	[42]

Mealworm, *Zophobas morio*	1.0 M HCl at 35 °C	0.5 M, 1.0 M and 2.0 M NaOH at 80 °C for 20 h	Glacial acetone for 30 min	0.5 M-5.43 1.0 M-5.22 2.0 M-4.77	[43]
Mealworm, *Zophobas morio*	20% HCI for 10 min	1 M NaOH 1:10 ($g \cdot mL^{-1}$) at 80 °C for 3 h	NA	NA	[44]
European stag beetle, *Lucanus cervus* Pine chafer, *Polyphylla fullo*	1 M HCl in 90 °C for 1 h	1 M NaOH in 90 °C for 14 h	chloroform-methanol-water (1:2:4, v/v)	10.9 11.3	[45]
Pentodon algerinum (*Fuessly*)	5% acetic acid at 55°C for 2 h	10% KOH at 40 °C for 48 h	NA	NA	[46]
Wheat weevil, *Sitophilus granarius*	1 M HCl 0.5 h	1 M NaOH at 100 °C, 8 h	ethanol and acetone	NA	[47]
Anoplotrupes stercorosus *Blaps tibialis* Rose chafer, *Cetonia aurata* Dor beetle, *Geotrupes stercorarius*	2 M of HCl at 100 °C for 2 h	2 M NaOH at 140 °C for 20 h	chloroform-methanol–water (1:2:4, v/v) for 2 h at room temperature	20.1 25.2 18.2 20.4	[48]
Blaps lethifera *Pimelia fernandezlopezi*	1 M HCl for 1 h at 40 °C	1 M NaOH at 80 °C for 2 h	10 v/v % H_2O_2 for 30 min at 50 °C	NA	[49]
Banana weevil, *Cosmopolites sordidus*	1.0 M HCl at 50 °C for 24 h	1.0 M NaOH 80 °C for 8 h	NA	11.8	[50]

Orthoptera					
Grasshopper	1 M HCl in 30 °C for 2 h	1 M NaOH in 90 °C for 2 h	2% $KMnO_4$ for 2 h, 2% $H_2C_2O_4$ for 2 h	NA	[25]
Shistocerca gregarea Forsskal	5% acetic acid at 55 °C for 2 h	10% KOH at 40 °C for 48 h	NA	NA	[46]
Mexican katydid, *Pterophylla beltrani*	NA	NA	NA	11.8	[51]
Moroccan locust, *Dociostaurus maroccanus*	2 M HCl in 55 °C for 1 h	2 M NaOH in 50 °C for 18 h	Methanol, chloroform and distilled water (2:1:4)	Nymphs-12 Adults-14	[52]
House cricket, *Brachytrupes portentosus*	*Oxalic acid for 3 h at room temperature	*1 M NaOH at 95 °C for 6 h	1% sodium hypochlorite for 3 h	4.3–7.1	[53]
Celes variabilis, Wart-biter, *Decticus verrucivorus,* Desert Cricket, *Melanogryllus desertus, Paracyptera labiata*	4 M HCl at 75 °C for 2h	4 M NaOH for 20 h at 150 °C	NA	4.71–11.84	[54]
Calliptamus barbarus *Oedaleus decorus*	1 M HCl at 100 °C for 30 min	1 M NaOH at 80–90 °C for 21 h	Chloroform: methanol: distilled water solution (1:2:4) for 1 h	20.5 16.5	[55]
Ailopus simulatrix *Ailopus strepens*	4 M HCl at 75 °C for 1 h	2 M NaOH at 175 °C for 18 h	Chloroform: methanol: distilled water, 1:2:4	5.3 7.4	[56]

Duroniella fracta *Duroniella laticornis* Red-winged grasshopper, *Oedipoda miniata* Blue-winged grasshopper, *Oedipoda caerulescens* *Pyrgomorpha cognata*				5.7 6.5 8.1 8.9 6.6	
Two-spotted cricket, *Gryllus bimaculatus*	2 M HCl	1.25 M NaOH	NA	20.9–23.3	[57]
Calosoma rugosa	1 M HCl	1.0 M NaOH at 100 °C for 8 h	NA	12.2	[36]
Bradyporus sureyai European mole cricket, *Gryllotalpa gryllotalpa*	1 M HCl in 90 °C for 1 h	1 M NaOH in 90 °C for 14 h	Chloroform-methanol-water (1:2:4, v/v)	9.8 10.1	[45]
Two-spotted cricket, *Gryllus bimaculatus*	*Oxalic acid for 3 h at room temperature	*1 M NaOH at 95 °C and 130 rpm for 6 h	APS solution (50% (w/v)) at 50 °C for 30 min	5.1	[58]
Two-spotted cricket, *Gryllus bimaculatus*	2 M HCl at 21 °C for 3 h	1.25 M NaOH at 95 °C for 3 h	50 % NaOH (w/w) at 95 °C and 105 °C for 3 h	79.03-91.14	[59]
Brachystola magna	2 M HCl at 50 °C for 24 h	2 M NaOH solution at 50 °C for 24 h	NA	NA	[39]
House cricket, *Acheta domesticus*	*1 M HCl for 2 h at 98 °C	*1 M NaOH at 80 °C for 24 h	NA	NA	[60]

House cricket, Acheta domesticus *Gryllodes sigillatus*	0.25 M HCl at 85°C for 15 min	1 L NaOH at 70 °C for 22 h	NA	NA	[61]
House cricket, Acheta domesticus	HCl, 1 M for 2 h at 98 °C	NaOH, 1 M at 80 °C for 22 h	NA	7.34	[62]
House cricket, Acheta domesticus *Gryllodes sigillatus*	0.25 M HCl (1:2 w/v) at 85 °C for 15 min	1 M NaOH (1:2 w/v) at 70 °C for 22 h	NA	5.7 ± 0.10 3.4 ± 0.10	[63]
Hymenoptera					
Western Honey Bee, *Apsis mellifera*	2 M HCl at 80 °C for 6 h	2 M of NaOH and refluxed for 20 h at 100 °C	Distilled water (40 mL), methanol (20 mL) and chloroform (20 mL)	Head-8.9 Thorax-6.79 Abdomen-8.61 Legs-13.25 Wings-7.64	[64]
Western Honey Bee, *Apsis mellifera*	1 N HCl	1 M NaOH for 12 h at ambient temperature (20 °C)	NA	8.8	[65]
Western Honey Bee, *Apsis mellifera*	1 M HCl	1.0 M NaOH at 100 °C for 8 h	NA	2.5	[36]
Western Honey Bee, *Apsis mellifera*	36.5% HCl	1.0 M NaOH	NA	NA	[37]

Western Honey Bee, *Apis mellifera*	*6.7% HCl at 25 °C for 3 h	*8% NaOH at 90 °C for 1 h	33% H_2O_2	23	[66]
European hornet, *Vespa crabro* Oriental hornet, *Vespa orientalis* German wasp, *Vespula germanica*	2 M HCl at 75 °C for 2 h	4 M NaOH at 150 °C for 18 h	Distilled water, methanol, and chloroform (4:2:1) for 2 h	8.3 6.4 11.9	[67]
Asian hornet, *Vespa velutina*	100 mL of 1 M HCl at 50 °C for 3 h	1 M NaOH (100 mL) at 60 °C for 8 h	100 mL 1% sodium hypochlorite	11.7	[68]
Oriental hornet, *Vespa orientalis*	1.0 M HCl to a solid ratio of 15 $mL \cdot g^{-1}$ at 100 °C for 20 min	1.0 M sodium hydroxide at 85 °C	H_2O_2/33% HCl 9:1, v/v	NA	[69]
European hornet, *Vespa crabro*	1 M HCl at 50 °C for 6 h	60 °C in 1 M NaOH solution for 16 h	distilled water, methanol and chloroform (4:2:1) solution at room temperature for 40 min at 250 rpm	Larvae-2.2 Pupa-6.2 Adult-10.3	[70]
Oriental hornet, *Vespa orientalis*	5% acetic acid at 55 °C for 2 h	10% KOH at 40 °C for 48 h	NA	NA	[46]
Red-tailed bumblebee, *Bombus lapidaries* *Formica clara*	2 M of HCl at 100 °C for 2 h	2 M NaOH at 140 °C for 20 h	chloroform-methanol–water (1:2:4, v/v) for 2 h at room temperature	9.3 7.8	[48]
Diptera					
Black soldier fly, *Hermetia illucens*	1:10 (m/v) with HCl 1 M at room temperature for 1 h	1 M NaOH treatment (solid: liquid ratio of 1:25 (m/v), 1 h at 80 °C	NA	Larvae-96.3 ± 3.7 Prepupae-94.5 ± 1.5 Pupae-93.9 ± 2.0	[71]

				Shedding-75.7 ± 4.0 Cocoons-96.8 ± 1.8 Flies-95.7	
Black soldier fly, *Hermetia illucens*	1 M HCl for 1 h	1 M NaOH at 80 °C for 24 h	1% $KMnO_4$	NA	[72]
Black soldier fly, *Hermetia illucens*	1 M HCl at 100 °C for 30 min	1 M NaOH at 80 °C for 24 h	NA	pupae exuviae-9 Imago-23	[73]
Black soldier fly, *Hermetia illucens*	NA	1 M NaOH 1 h at 80 °C	NA	8.5 ± 0.1	[74]
Black soldier fly, *Hermetia illucens*	2 M HCl at 55 °C for 1 h	2 M NaOH at 50 °C for 18 h	NaClO at 80 °C for 4 h	Larvae-3.6 Prepupa-3.1 Puparium-14.1 Adults-2.9	[75]
Black soldier fly, *Hermetia illucens*	HCl at 2 h	NaOH at 90 °C for 3 h	NA	21.3	[76]
Black soldier fly, *Hermetia illucens*	2% HCl for 2 h at 20 °C	NaOH 50 °C for 2 h	NA	7	[77]
Black soldier fly, *Hermetia illucens*	*2 N HCl for 24 h at 15 min	*40 mL of 2 N HCl for 24 h at room temperature	NA	9	[78]
Black soldier fly, *Hermetia illucens*	1 M HCl, 1:10 (w/v) for 2 h	1 M NaOH, 1 g·10 mL^{-1} at 80 °C for 6 h	1% $KMnO_4$ in a 1:30 w/v ratio at room temperature for 4 h	late larvae-3.025 Prepupae-5.371	[79]

				Pupal exuviae-18.800 Imagoes-11.846	
Black soldier fly, *Hermetia illucens*	*1 M HCl for 2 h	*1 M NaOH 4 h	NA	10.18 ± 0.42	[80]
Black soldier fly, *Hermetia illucens*	0.5 M CH_2O_2 for 1h at room temperature	2 M NaOH for 2 h at 80 °C	5% H_2O_2 for 1 h at 90 °C	NA	[81]
Black soldier fly, *Hermetia illucens*	1 M HCl for 2 h	1 M NaOH 4 h	NA	NA	[82]
Black soldier fly, *Hermetia illucens*	1 M HCl for 2 h at 100 °C	1 M NaOH for 4 h at 100°C	NA	10.18	[83]
Black soldier fly, *Hermetia illucens*	0.5 M formic acid for 1 h at room temperature	2 M NaOH, 2 h at 80°C	5% (v/v) H_2O_2 for 30–60 min at 90 °C	Larvae-10 ± 0.7 Pupal exuviae-23 ± 1.9 Dead adults- 6 ± 0.1	[84]
Black soldier fly, *Hermetia illucens*	0.5 M HCl at room temperature for 2 h	1.9 M NaOH for 2 h at 50 °C	5% H_2O_2	NA	[85]
Black soldier fly, *Hermetia illucens*	7% HCl for 2 h at room temperature	10% NaOH at 80 °C for 24 h	NA	NA	[86]
Black soldier fly, *Hermetia illucens*	1% HCl at 20 °C for 2 h	30% (w/w) NaOH at room temperature for 30 min, and then at 100 °C for 2 h	NA	NA	[87]

Black soldier fly, *Hermetia illucens*	1 M HCl at 22 °C for 1 h	1 M NaOH at 80 °C for 24 h	1-Without decoloration 2-Water at 100 °C for 24 h 3-9% H_2O_2 at 80 °C for 2.5 h 4-9% H_2O_2 at 80 °C for 5 h 5-1% KMnO4 at 80 °C for 20 min	1-7.95 ± 0.20 2-7.97 ± 0.10 3-7.01 ± 0.12 4-5.98 ± 0.08 5-5.69 ± 0.28	[88]
Common fruit fly *Drosophila melanogaster*	2 M HCl solution for 3 h at 4 °C	NaOH (8% w/w) solution for 20 h at 70 °C	Methanol: chloroform: distilled water (in a ratio of 2:1:4) for 30 min	7.85	[89]
Calliphora vicina	2 M of HCl at 100 °C for 2 h	2 M NaOH at 140 °C for 20 h	chloroform-methanol–water (1:2:4, v/v) for 2 h at room temperature	8.1	[48]
Housefly, *Musca domestica*	1 M HCl for 1 h at 40 °C	2 h of 1 M NaOH at 80 °C	10 v/v % H_2O_2 for 30 at 50 °C	NA	[49]
Housefly, *Musca domestica*	3 h in 500 mL of 2 N HCl at room temperature	500 mL of 1.25 N NaOH at 95 °C for 3 h	NA	8.02	[90]
Tabanus bovinus	1 M HCl for 12 h at room temperature	1M NaOH for 18 h at 70 °C	Water, methanol and chloroform (1:2:4)	NA	[91]
Hemiptera					
Green bugs, *Nezara viridula*	5% acetic acid at 55 °C for 2 h	10% KOH at 40 °C for 48 h	NA	NA	[46]
Dock bug, *Coreus marginatus* Black-and-red-bug, *Lygaeus equestris*	2 M of HCl at 100 °C for 2 h	2 M NaOH at 140 °C for 20 h	chloroform-methanol–water (1:2:4, v/v) for 2 h at room temperature	14.5 11.1 10.6	[48]

Pyrrhocoris apterus					
Cicada slough	1 M HCl in 30 °C for 2 h	1 M NaOH in 90 °C for 2 h	2% $KMnO_4$ for 2 h, 2% $H_2C_2O_4$ for 2 h	NA	[25]
Aquatic bug, *Ranatra linearis*	100 mL of 1 M HCl at 90 °C for 1 h	1 M NaOH at 110 °C for 18 h	Chloroform, methanol, and water (1:2:4)	15–16	[92]
Cicada lodosi *Cicada mordoganensis* *Cicadatra platyptera* *Cicadatra atra* *Cicadatra hyaline* *Cicadivetta tibialis*	2 M HCl for 2 h at 100 °C	2 M NaOH at 100 °C for 20 h	Water, methanol, and chloroform mixed at the ratio of 4:2:1	4.97 6.49 8.84 6.70 5.51 5.88	[93]
Cicada Cryptotympana atrata	1000 mL of 7% (w/w) HCl at room temperature for 24 h	1000 mL of 10% (w/ w) NaOH at 60 °C for 24 h	NA	62.42	[28]
Coridius nepalensis	1 M HCl for 1 h	1 M NaOH at 80 °C for 24 h	1% sodium hypochlorite for 1 h	43.97	[94]
Dictyoptera					
Eupolyphaga sinensis	1.3 M HCl at 80 °C for 1 h, soaked at room temperature for 24 h	4 M NaOH at 90 °C for 6 h	10% H_2O_2 at 80 °C for 30 min	11.63 ± 0.80	[95]
Brazilian cockroach, *Blaberus giganteus*	NA	2 M NaOH at 90 °C for 9 h	Chloroform: methanol: water (1:2:2) at room temperature for 1.5 h	Wing-26.9	[96]

				Dorsal pronotum-21.2	
German cockroach, *Blattela germanic*	5% acetic acid at 55 °C for 2 h	10% KOH at 40 °C for 48 h	NA	NA	[46]
German cockroach, *Blattella germanica*	2 M of HCl at 100 °C for 2 h	2 M NaOH at 140 °C for 20 h	chloroform-methanol–water (1:2:4, v/v) for 2 h at room temperature	4.7	[48]
American cockroach, *Periplaneta americana* German cockroach, *Blattella germanica*	1% sodium hypochlorite solution (1%, w/v)	1 M NaOH at 100°C for 24 h	NA	Nymph-8.4 Adult-15 Nymph-5.4 Adult-6.2	[97]
American cockroach, *Periplaneta americana*	2 N HCl at room temperature for 3 h	1.25 N NaOH at 95 °C for 3 h	NA	3.36	[57]
American cockroach, *Periplaneta americana*	*20 mL of 1% HCl for 24 h	*4% of NaOH for 1 h	50 mL of 2% NaOH for 1 h	NA	[98]
American cockroach, *Periplaneta americana*	4 M HCl for 2 h at 75 °C	4 M NaOH for 20 h at 150 °C	Water, methanol and chloroform (ratio of 4:2:1) for 4 h at 30 °C	Wings-18 Without wings-13	[99]
American cockroach, *Periplaneta americana*	*0.5 M HCl at 60 °C and 500 rpm for 1 h	*0.5 M NaOH at 95 °C and 500 rpm for 20 min, then 4 M NaOH for 160 min	10% H_2O_2 at 80 °C and 500 rpm for 3 h	NA	[100]
American cockroach,	6.7% HCl at 25 °C for 3 h	8% NaOH at 90 °C for 1 h	33% H_2O_2	42	[66]

Pariplaneta americana linnaeus					
American cockroach, *Periplaneta americana*	*1 M HCl for 2h at 75 °C	*2.5% (w/v) NaOH for 6 h at 100 °C	acetone at 50 °C for 2h	NA	[101]
American cockroach, *Periplaneta americana*	5% acetic acid at 55 °C for 2 h	10% KOH at 40 °C for 48 h	NA	NA	[46]
American cockroach, *Periplaneta americana*	NA	4% NaOH for 48 h at 90 °C	NA	NA	[102]
Odonata					
Dragonfly, Sympetrum fonscolombii	1 M HCl at room temperature for 1 h	1 M NaOH solution at 50 °C for 15 h	chloroform: methanol and distilled water (1: 2: 4, v/v)	20.3 ± 0.85	[103]
Downy emerald, *Cordulia aenea* Four-spotted chaser, *Libellula quadrimaculata*	2 M HCl at 100 °C for 2 h	2M NaOH at 140 °C for 20 h	chloroform-methanol–water (1:2:4, v/v) for 2 h at room temperature	9.5 10.1	[48]
Ephemeroptera					
Mayfly	2 M HCl at 50 °C	2 M NaOH at 100 °C	Methanol: chloroform (1:1)	10.21	[104]

* In these literatures, the deproteinization step is performed prior to the demineralization; NA: Not available.

Highlights:

- Abundant insect sources of chitin, from the Lepidoptera, Coleoptera, Orthoptera, Hymenoptera, Diptera, Hemiptera, Dictyoptera, Odonata, and Ephemeroptera orders.
- Hydrochloric acid (HCl) is effective in demineralizing chitin, facilitating the removal of calcium compounds and other minerals.
- Sodium hydroxide (NaOH) and potassium hydroxide (KOH) are commonly used for deproteinization, effectively removing protein residues from the chitin matrix.
- Some methods employ bleaching agents to remove pigments and enhance chitin purity.
- Chitin yields vary depending on the insect species and the purification method employed, ranging from 3.3% to 96.8%.

2.3 Extraction of chitin and chitosan from insects

The production process of insect-derived chitin and chitosan entails a multi-step approach typically involving delipidation, deproteination, demineralization, and deacetylation (Figure 2.3). Various extraction techniques, such as chemical, enzymatic, and microbial methods, have been developed to efficiently extract chitosan from insect sources. These techniques aim to maximize chitosan yield while ensuring the preservation of its structural integrity and desired properties.

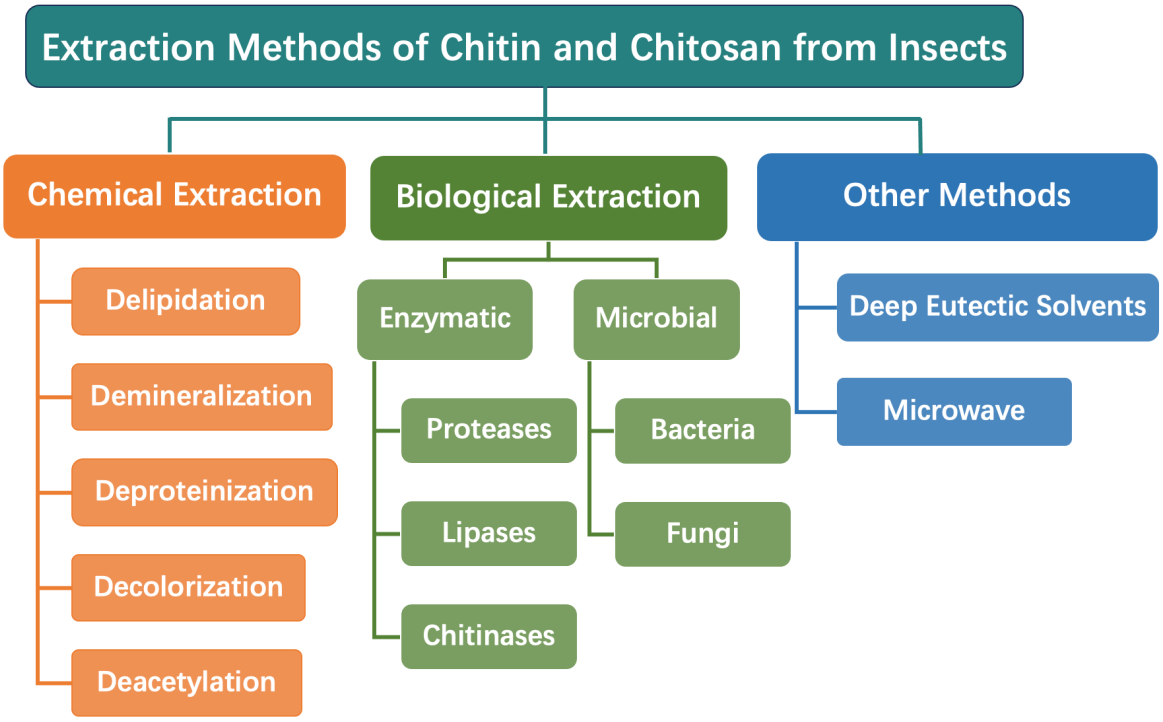

Figure 2.3 Production process for chitin and chitosan from insects.

2.3.1 Chemical extraction

The sequence of the processes involved in the extraction of chitin and chitosan may vary depending on the type of insect source (Table 2.1 and Table 2.2). Regarding delipidation, some literature performs it in the first step and some literature in the last step. In most of the literature, the demineralization step is performed prior to deproteinization. In some of the literature, the

deproteinization step is performed prior to demineralization. The statistics showed that among 80 articles related to insect chitin extraction, only 13 of them report deproteinization first followed by demineralization. Decolorization usually follows demineralization and deproteinization.

2.3.1.1 Delipidation

Delipidation methods for insects can vary significantly across different studies and applications (Table 2.1). Chloroform is a commonly used solvent for delipidation. It is highly effective in extracting lipids, but its high toxicity requires proper safety precautions. Methanol is a safer alternative compared to chloroform, and it is often used alone or as part of a solvent mixture. Chloroform–methanol is a widely used solvent mixture for delipidation. It is a popular choice for its high lipid solubility and relatively low toxicity compared to pure chloroform. Adelya *et al.* used 500 mL of chloroform–methanol (7:3) mixture to treat 100 g of larval shells at 20 °C for 4 h, and the yield of chitin-containing material (defatted material) was 93% [77]. Tsaneva *et al.* extracted the lipid fraction from honeybees (*Apis mellifera*) with n-hexane in a Soxhlet apparatus for 8 h before demineralization and deproteinization. The wax content in the lipid fraction was determined gravimetrically as 24.9 ± 0.28% [65]. Ethanol is also used for delipidation of insect samples, especially in food-related studies [66, 105]. It is relatively safe and can be an appropriate choice for certain applications. Honeybee (*Apis mellifera*) was also defatted with 96% ethanol in Soxhlet's extraction apparatus for 18 h [66]. Kaya *et al.* removed lipids from honeybee (*Apis mellifera*) using a mixture of distilled water (40 mL), methanol (20 mL), and chloroform (20 mL), stirring for 40 min at 250 rpm after demineralization and deproteinization [64]. In another literature, for the defatting of the chitin isolation, Kaya *et al.* used chloroform-methanol-water (1:2:4, v:v) and refluxed for 2 h at room temperature [48]. Son *et al.* removed lipids from mealworms with n-hexane in a shaker at 170 rpm for 6 h [40]. *Eupolyphaga sinensis* Walker insects were defatted with 95% ethanol (m/v, 1/5) and petroleum

ether (m/v, 1/3) at 65 °C for 2 h each time [95]. *Periplaneta americana* was defatted using hexane as the solvent with a Soxhlet extraction method in a water bath at 80 °C for 3 h [100]. In some studies, other solvents like a mixture of acetone and alcohol or petroleum ether have been used for delipidation [78, 106].

2.3.1.2 Demineralization

Demineralization methods for insects involve the removal of mineral components, primarily calcium carbonate, from the exoskeleton to isolate chitin and chitosan. Acetic acid and hydrochloric acid are the most used reagents for demineralization (Table 2.1). Studies have shown that both acids can effectively remove calcium carbonate from insect exoskeletons [25, 46]. Acetic acid is generally considered safer to handle compared to hydrochloric acid. However, using hydrochloric acid might lead to faster and more complete demineralization in some cases. Both acetic acid and hydrochloric acid do not significantly affect the chitin and chitosan structure. They mainly act on the mineral component, leaving the chitin and chitosan intact. However, prolonged exposure to strong acids or elevated temperatures might lead to some degree of depolymerization of chitin and chitosan, reducing their molecular weight and viscosity. In some studies, other acids like sulfuric, nitric, oxalic, and formic acids have been used for demineralization [53, 84, 107, 108]. Except reagents, the choice of duration and temperature in demineralization can significantly affect the efficiency of the process and the properties of the extracted chitin and chitosan. In determining the optimal demineralization conditions, the specific characteristics of the insect species as well as the intended applications of the extracted chitin and chitosan need to be considered.

2.3.1.3 Deproteinization

Deproteinization methods for insects involve removing proteins and organic matter to isolate chitin and chitosan. The solvent concentration in deproteinization is crucial, as it

influences protein removal efficiency and the properties of the extracted chitin and chitosan. The choice of concentration should consider both deproteinization efficiency and the impact on chitin and chitosan properties. Sodium hydroxide (NaOH) is the most used reagent for deproteinization (Table 2.1). Studies have used varying concentrations of NaOH, typically ranging from 1M to 4 M [25, 27, 32], while less commonly used than NaOH, Potassium hydroxide (KOH) has been employed for deproteinization in some studies [46, 109]. High temperature (70-100°C) is commonly used for deproteinization [26, 32, 38]. It helps to improve deproteinization efficiency, especially for more resistant proteins. However, higher temperatures may increase the risk of chitin and chitosan degradation and must be carefully controlled. Optimizing solvent concentration and temperature in deproteinization methods according to the specific insect species and desired properties of extracted chitin and chitosan is essential for efficient protein removal while preserving quality. This is crucial for diverse applications, including industrial, biomedical, or environmental uses.

2.3.1.4 Decolorization

Decolorization methods for insects involve the removal of pigments and other color-causing compounds from the insect material to obtain decolored chitin and chitosan. Sodium hypochlorite, potassium permanganate, hydrogen peroxide and chloroform-methanol are commonly used as bleaching agents for decolorization (Table 2.1) [25, 48, 49, 110]. In some studies, acidic solutions such as oxalic acid or hydrochloric acid have been used for decolorization [35, 111]. Acidic conditions can help in breaking down pigments, but care must be taken to prevent excessive degradation of chitin and chitosan. The choice of solvents, duration, and temperature in decolorization can significantly impact the efficiency of the process and the properties of the resulting chitin and chitosan. Room temperature (20-25°C) is a common temperature range for decolorization [48, 79]. Room temperature decolorization

generally minimizes chitin and chitosan degradation. Mild heating (40-100°C) can enhance decolorization efficiency, especially for more resistant pigments [35, 49].

2.3.1.5 Deacetylation

Deacetylation methods for insects involve the removal of acetyl groups from chitin to produce chitosan. NaOH is the most used reagent for deacetylation (Table 2.2). Concentrations of NaOH ranging from 40% to 70% (w/w) have often been used in different studies [25, 51, 101, 112]. Deacetylation conditions can vary depending on the insect species and DDA. The concentration of these alkalis, durations and temperature should be optimized for efficient deacetylation while preserving the integrity of chitosan. 80-120 °C is a common temperature range for deacetylation [29, 57, 95, 113].

Table 2.2 A summary of methods for chitin deacetylation.

Insect species	Deacetylation	Chitosan Yield (%)	DDA (%)	Molecular Weight (Da)	Moisture content (%)		Ash content (%)		Ref.
					Chitin	Chitosan	Chitin	Chitosan	
Lepidoptera									
Silkworm	60% NaOH in 100°C for 8 h	3.1	85.5	(4.090 ± 0.059) ×10^4	NA	0.07 ± 0.008	NA	0.05 ± 0.003	[25]
Mediterranean flour moth, *Ephestia kuehniella*	NA	NA	NA	NA	9.1 ± 0.4	NA	0.14 ± 0.08	NA	[26]
Clanis bilineata	55% NaOH (w/w), 120°C for 4 h	95.9	NA	NA	NA	3.8	NA	0.3	[29]
Coleoptera									
Mealworm, *Tenebrio molitor*	60% NaOH in 100°C for 8 h	2.5	85.9	(3.975 ± 0.072) ×10^4	NA	0.19 ± 0.012	NA	0.50 ± 0.016	[25]
Mealworm, *Tenebrio molitor*	500 mL of NaOH at 95 or 105°C for 3 h or 5 h	9.2	95.5			NA			[38]
Mealworm, *Tenebrio molitor*	50% NaOH at 100°C for 3h	78.26	75.84			NA			[41]
Mealworm, *Tenebrio molitor*	60% NaOH contained NaBH4 (0.004 g), 120°C for 2 h	NA	88.55	812.30×10^3			NA		[39]
Mealworm, *Tenebrio molitor*	NaOH 40% (w/v) at 90°C, 500 rpm for 8 h	31.9	53.9	NA	6.2 ± 0.5	4.2 ± 0.1	3.6 ± 0.2	3.7 ± 0.1	[114]
Mealworm, *Tenebrio molitor*	50% NaOH at 80°C for 4 h	NA	89.4			NA			[40]

Mealworm Beetle, *Tenebrio molitor, Zophobas morio*	55% (w/v) NaOH at 90°C for 9 h	Larvae-80.00 Adult-78.33 Superworm-83.33	Larvae-75.59 Adult-75.63 Superworm-75.67			NA			[42]
Rhinoceros Beetle, *Allomyrina dichotoma*		Larvae-83.37 Pupa-83.37 Adult-75.00	Larvae-75.66 Pupa-75.67 Adult-74.66						
Mealworm, *Zophobas morio*	50 wt % NaOH in 90°C for 30 h	65.84-75.52	64.82-81.06			NA			[43]
Mealworm, *Zophobas morio*	NaOH 100 g/mL at 80°C for 16 h	15–18%	NA			NA			[44]
Catharsius molossus	8 M NaOH at room temperature for 24 h	17%	94.9 ± 0.85	4.5 ± 0.07 $\times 10^5$	NA	6.55 ± 0.05	NA	0.34 ± 0.04	[35]
Calosoma rugosa	50% NaOH (15 mL·g^{-1}) at 100°C for 8 h	NA	95	NA	NA	8.8	NA	2.0	[36]
Calosoma rugosa	50% NaOH at 100°C for 8 h	NA	95			NA			[37]
Colorado potato beetle, *Leptinotarsa decemlineata*	50% NaOH (w/v, 1:20) at 100°C for 3 h	Adult-72 Larvae-67	Adult-82 Larvae-76	Adults-2.722 $\times 10^3$ Larvae-2.676 $\times 10^3$		NA			[34]

European stag beetle, *Lucanus cervus,*	NA	NA	NA	NA	6.6 5.9	NA	0.6 1.7	NA	[45]
Pine chafer, *Polyphylla fullo*	50 w/v% NaOH	50.0 ± 0.3 41.7 ± 0.5	87.1 ± 0.2 88.2 ± 0.1	NA	NA	14.3 ± 0.3 17.2 ± 0.2	NA	1.5 ± 0.1 2.0 ± 0.1	[49]
Blaps lethifera,	50% NaOH at 90°C for 10 h	70.2	77.8 ± 0.39	343 ± 37.3	NA	2.4	6.4	2.2	[50]
Orthoptera									
Grasshopper	60% NaOH in 100°C for 8 h	5.7	89.7	(3.989 ± 0.021) $\times 10^4$	NA	1.8 ± 0.213	NA	0.89 ± 0.025	[25]
Mexican katydid, *Pterophylla beltrani*	70% NaOH in 1:3 ratio for 1.5 h at 120°C	58.8	NA			NA			[51]
Moroccan locust, *Dociostaurus maroccanus*	60% NaOH at 150°C for 4 h	Nymphs-77.38 Adults-81.69	NA	Adults-7.2×10^3 Nymphs-5.6×10^3		NA			[52]
Brachytrupes portentosus	50% (w/v) NaOH at 121°C for 5 h	2.4–5.8	NA	NA	4.00	3.33	1.00	1.00	[53]
Calliptamus barbarus, *Oedaleus decorus*	50% NaOH (w/v 1:15) at 130°C for 2 h	70–75 74–76	70-75	NA	NA	NA	NA	NA	[55]
Desert locust, *Schistocerca gregaria*	50% NaOH (15 mL· g^{-1}) at 100°C for 8 h	NA	98	NA	NA	NA	14.1	1.6	[36]
Bradyporus sureyai,	NA	NA	NA	NA	5.2,	NA	3.8,	NA	[45]

					6.0		2.1		
European mole cricket, *Gryllotalpa gryllotalpa*	(50–67% NaOH) at 95°C at 130 rpm	41.75	56.47-84.98	NA	NA	NA	NA	NA	[58]
Two-spotted cricket, *Gryllus bimaculatus*	60% NaOH contained NaBH4 (0.004 g), 120°C for 2 h	NA	89.89 ± 1.34	696.95×10^3	NA	NA	NA	NA	[39]
Brachystola magna	50% NaOH for 3 h at 130°C	88.0	62.9	86.8×10^3	NA	NA	NA	NA	[60]
House Crickets, *Acheta domesticus*	40% NaOH at 120°C for 2 h	90.6	88.5	NA	NA	NA	NA	NA	[112]
House Crickets, *Acheta domesticus*	67% w/v NaOH for 2, 4 6, 10 h	2h-76.0 ± 6.7 65.0 ± 1.6 4h-77.3 ± 1.9 63.7 ± 1.2 6h-80.5 ± 2.1 60.3 ± 3.3 10h-69.0 ± 2.2 62.3 ± 0.9	2h-72.5 ± 1.0 73.5 ± 1.4 4h-76.3 ± 1.3 74.9 ± 1.3 6h-79.1 ± 1.9 77.2 ± 1.8 10h-79.4 ± 1.3 81.3 ± 1.1	344×10^3 524×10^3	NA	NA	NA	NA	[63]
Hymenoptera									
Western honey bee, *Apsis mellifera*	NA	NA	NA	NA	7.7 ± 0.09	NA	2.4 ± 0.03	NA	[65]
Western honey bee, *Apsis mellifera*	50% NaOH at 100°C for 8 h	NA	96	NA	NA	17.6	NA	9.2	[36]

Oriental hornet, *Vespa orientalis*	50% NaOH at 100°C for 2 h	NA	96	NA	NA	NA	NA	NA	[111]
Diptera									
Black soldier fly, *Hermetia illucens*	NaOH at 100°C for 2 h	32	90	NA	NA	NA	NA	NA	[115]
Black soldier fly, *Hermetia illucens*	50% (w/v) NaOH (1: 50) for 4 h at 95 °C	late larvae-81.034 Prepupae-73.656 Pupal exuviae-79.701 Imagoes-63.158	NA	NA	NA	NA	NA	NA	[79]
Black soldier fly, *Hermetia illucens*	40% NaOH for 8h	6.58	NA	NA	NA	NA	NA	NA	[80]
Black soldier fly, *Hermetia illucens*	12 M NaOH for 4 h at 100°C	Larvae-3 pupal exuviae-10 dead adults-3	Larvae-92 pupal exuviae-90 dead adults-93	Larvae-21×10^3 pupal exuviae-35×10^3	NA	NA	NA	NA	[84]

				dead adults- 36×10^3					
Black soldier fly, *Hermetia illucens*	100°C for 2 h	81	66	505×10^3	NA	NA	NA	NA	[87]
Common fruit fly, *Drosophila melanogaster*	10 mL of NaOH solution (60%, w/w) for 48 h at 150°C	70.91	NA	NA	NA	NA	NA	NA	[89]
Oriental blue fly, *Chrysomya megacephala*	100 mL NaOH (1 mol/L) at 95°C for 6 h	26.2	89.6	501×10^3	NA	NA	NA	NA	[116]
Housefly, *Musca domestica*	50% NaOH	57.9 ± 0.2	84.1 ± 0.3	NA	NA	7.8 ± 0.1	NA	8.2 ± 0.2	[49]
Hemiptera									
Cicada slough	60% NaOH at 100°C for 8 h	28.2	84.1	(3.779 ± 0.068) $\times10^4$	NA	0.18 ± 0.016	NA	0.03 ± 0.004	[25]
Aquatic bug, *Ranatra linearis*	NA	70	NA	NA	NA	NA	NA	NA	[92]
Dictyoptera									
American cockroach, *Periplaneta americana*	50% NaOH in 100°C for 4 h	5.80, 2.95	36.8, 31.5	NA	NA	NA	NA	NA	[113]
German cockroach, *Blattella germanica*	40% NaOH in 120°C for 2 h	99.7	90.3	NA	NA	NA	NA	NA	[112]

American cockroach, *Periplaneta americana*	10% NaOH at 80°C for 3 h	NA	90.85 ± 3.37	(16 ± 0.746) ×10^3	NA	NA	NA	NA	[100]
American cockroach, *Periplaneta americana*	50% (w/v) NaOH for 8h at 120°C	74.51	NA	NA	NA	NA	NA	NA	[101]
American cockroach, *Periplaneta americana*	50% NaOH at 90°C for 24h	5.48 ± 0.32	96.57 ± 0.48	(127.79 ± 1.35) ×10^3	NA	5.19 ± 0.11	NA	0.55 ± 0.05	[117]
Ephemeroptera									
mayfly	60% NaOH at 150°C for 6 h	78.43	84.3	3.69×10^3	NA	NA	NA	NA	[118]

*NA: Not available.

Highlights:

- Abundant insect sources of chitin, from the Lepidoptera, Coleoptera, Orthoptera, Hymenoptera, Diptera, Hemiptera, Dictyoptera, and Ephemeroptera orders.
- Sodium hydroxide (NaOH) is commonly used for deacetylation.
- Yields, degree of deacetylation (DDA) and molecular weight (Mw) of chitosan vary depending on the insect species and the purification method employed, ranging from 2.5% to 99.7%, 31.5% to 96.57%, and 2.676×103 Da to 8.123×105 Da, respectively.

Moisture content and ash content of chitin and chitosan ranged from 4.0% to 9.1%, and 0.07% to 17.6%, respectively.

Ash content of chitin and chitosan ranged from 0.14% to 14.1%, and 0.03% to 9.2%, respectively.

2.3.2 Biological extraction

Biological extraction methods for chitin and chitosan from insects involve the use of enzymatic, microbial processes to break down the insect material and release the desired biopolymers. These methods offer a more environmentally friendly and sustainable approach compared to chemical extraction methods.

Enzymatic extraction involves the use of specific enzymes that can selectively degrade the non-chitin components of the insect material, leaving behind chitin and chitosan. Enzymes such as proteases, lipases, and chitinases are used to break down proteins, lipids, and chitin-protein complexes in the insect material. Andressa *et al.* used Alcalase enzyme in a proportion of 2% (w/w; enzyme/substrate) for the deproteinization of mealworm's (*Tenebrio molitor*) cuticles [114]. The enzymatic extraction process is typically carried out under controlled conditions, including optimized pH and temperature, to ensure the effectiveness of the enzymes. Enzymatic extraction offers the advantage of specific targeting, minimal damage to chitin and chitosan structures, and reduced chemical waste.

Microbial extraction involves the use of microorganisms, such as bacteria or fungi, that naturally produce enzymes capable of degrading the insect material. Microbes can be cultivated in a suitable growth medium containing the insect material, allowing them to release enzymes that break down proteins, lipids, and other organic matter. Yun *et al.* used purified protease from *Bacillus licheniformis* and *Bacillus subtilis* for deproteinization and defatting of black soldier fly exoskeleton, respectively [119]. Lin *et al.* used *Bacillus licheniformis* A6 strain in the fermentation of spent pupal shell of Black Soldier Fly (*Hermitia illucens*) for the chitin extraction [120]. Marios *et al.* isolated chitin from House Crickets (*Acheta domesticus*) by comparing microwave-assisted demineralization to chemical method, fermentation with *Lactococcus lactis*, citric acid treatment, and leading to a degree of demineralization of 85.8 ± 1.3%, 91.1 ± 0.3%, 97.3 ± 0.8% and 70.5 ± 3.5%, respectively [60]. The microbial fermentation

process is typically carried out under controlled conditions to promote the growth and activity of the microorganisms. The resulting mixture is then processed to separate and isolate the chitin and chitosan from the microbial biomass and other residual components.

Biological extraction methods offer a sustainable and eco-friendly approach by minimizing the use of harsh chemicals and reducing chemical waste. These methods, milder in nature, help to preserve the inherent properties of chitin and chitosan structures. While scalable for industrial production, challenges include the need for optimization due to factors like enzyme or microbial choice, process conditions, and insect species. Despite their environmental benefits, biological extraction methods may entail additional steps, such as enzyme production or microbial cultivation, potentially increasing overall production costs compared to chemical methods. Scaling up these methods to meet industrial demands may pose challenges in terms of process control, scalability, and cost-effectiveness.

2.3.3 Other extraction methods

During recent years, several alternative methods have been suggested to replace the chemical treatments in chitin isolation and chitosan preparation, including deep eutectic solvents (DES) and microwave extraction. Ionic liquids are liquid salts composed of ions, typically consisting of an organic cation and an inorganic or organic anion. Ionic liquids have shown promise in the extraction of chitin and chitosan from insect exoskeletons due to their ability to dissolve and solvate biomolecules effectively [121]. They allow liberating chitin with simultaneous removal of the protein–mineral matrix, without the need of prior isolation and purification of chitin polymer. The process reduces the amount of required chemicals and decreases the volume of process waste while avoiding the necessity of handling boiling acidic solution used in the traditional preparation process [122]. Furthermore, ionic liquids can be tailored by choosing specific cations and anions to optimize their interactions with target molecules, thus enhancing the efficiency of the extraction process [123]. DES is a subclass of

ionic liquids formed by the combination of hydrogen bond acceptors and donors. Unlike traditional ionic liquids, DES are typically composed of inexpensive and biodegradable components, making them environmentally friendly alternatives [124]. Their ability to disrupt hydrogen bonds in the insect exoskeleton facilitates the dissolution of chitin, enabling efficient extraction [125]. Gaël *et al.* compared the impact of both DES/IL-pretreatments on the efficiency of the chemical deacetylation of chitin carried out over two insect sources (*Bombyx eri* and *Hermetia illucens*) and shrimp shells, leading to the results that chitosan obtained from IL-pretreated chitins from *Bombyx eri* larvae, present lower acetylation degrees (13–17%) than DES-pretreated samples (18–27%) [126].

Furthermore, microwave-assisted extraction is a modern and efficient technique for extracting chitin and chitosan from insect exoskeletons. This method utilizes microwave energy to accelerate the extraction process, leading to faster and higher yields compared to traditional extraction methods. Microwave extraction relies on the principle of selective heating. When exposed to microwave radiation, polar molecules like water and certain solvents absorb the energy and convert it into heat. This localized and rapid heating promotes the breakdown of exoskeleton and enhances the diffusion of the solvent into the insect exoskeleton, facilitating the extraction of chitin [127]. Leke *et al.* compared the extraction of chitin from black soldier fly (*Hermetia illucens*) meal using conventional and alternative methods; enzyme-, microwave- and ultrasound-assisted extraction. Results showed that the conventional method resulted in 9.7% chitin yield, while the enzyme-, microwave- and ultrasound-assisted extractions gave 42.3%, 11.4% and 13.7% chitin on dry weight basis, respectively [3].

2.4 Characterization of insect chitin and chitosan

The characterization of insect-derived chitin and chitosan plays a pivotal role in evaluating its quality and suitability for diverse biomedical applications. Employing an array of analytical

techniques including spectroscopy, microscopy, thermal analysis, and rheology, enables the assessment of its physicochemical properties involving molecular weight distribution, degree of deacetylation, and other pertinent characteristics. The resulting characterization data furnish invaluable insights into the structure-function relationships of insect chitosan, thus facilitating tailored modification of its properties to suit specific applications.

2.4.1 Extraction yield

The yield of chitin and chitosan from insects refers to the quantitative measure of these biopolymers obtained after the extraction process. It is a critical parameter that assesses the efficiency of the extraction method and the potential feasibility of using insects as a viable source for chitin and chitosan production. Typically expressed as a percentage or weight relative to the initial mass of the insect exoskeleton, the yield is an essential determinant of the success of chitin and chitosan extraction. The yield of chitin and chitosan from insects are shown in Table 2.1 and Table 2.2. Numerous factors influence the yield of chitin and chitosan from insects. Different insect species exhibit varying chitin and chitosan contents in their exoskeletons. Variations in chitin content among insect species can result in significant differences in yield. The chitin yield extracted from various Coleoptera insects were found to vary in a wide range, such as *Tenebrio molitor* (3.9–4.6%), *Melolontha melolontha* (13-14%), *Leptinotarsa decemlineata* (7-20%), *Heliocopris dilloni* (22.1%), *Catharsius molossus* (24%), *Blaps tibialis* (25%) and *Mecynorhina torquata* (27 %), respectively [32, 34, 35, 42, 48, 49]. The chitin yield extracted from various Orthoptera insects such as *Gryllodes sigillatus, Brachytrupes portentosus, Pterophylla beltrani, Oedaleus decorus* and *Gryllus bimaculatus* were found to be 3.4%, 4.3-7.1%, 11.8%, 16.5% and 79.03- 91.14%, respectively [51, 53, 55, 59, 63]. The chitosan yield extracted from various Lepidoptera insects were found to be vary in a broad range, such as silkworm chrysalis (*Bombyx mori*, 3.1%) and *Clanis bilineata* (95.9%), respectively[25, 29]. The contents of chitin and chitosan can vary with age and molting stage

of insects. Different life cycle stages may lead to fluctuations in overall yield. The yields of chitin from *Leptinotarsa decemlineata* varied between adult (20%) and larvae (7%) [34]. The yields of chitin from *Hermetia illucens* varied between late larvae (3.025%), prepupae (5.371%), pupal exuviae (18.800%) and imagoes (11.846%), respectively [79]. Various experimental parameters, including extraction time, temperature, solvent concentration and solid-liquid ratio, play pivotal roles in determining the yield. Many studies have been reported on chitin extraction and chitosan preparation from *Hermetia illucens*, the chitin and chitosan content varied greatly between 3.1 and 96.3% and 3–81% [71-80, 82-88]. Finding and selecting new sources of chitin and chitosan that can replace crustacean shells and optimizing the yield is particularly important for industrial applications, as it directly affects the cost-effectiveness of the extraction process.

2.4.2 Degree of deacetylation (DDA)

The DDA of chitosan refers to the extent of acetyl group removal from the chitin polymer, resulting in the formation of chitosan. Recall that chitosan is a linear polysaccharide composed of β-(1→4)-linked D-glucosamine (GlcN) and N-acetyl-D-glucosamine (GlcNAc) units. The deacetylation process involves the hydrolysis of GlcNAc units to GlcN units, and the DDA is expressed as a percentage representing the proportion of GlcN units in the chitosan chain. The DDA of chitosan from insects is a crucial parameter as it directly influences its physicochemical and biological properties, making it suitable for a wide range of applications in various industries.

The DDA of chitosan from insects can be determined using various analytical methods, such as nuclear magnetic resonance (NMR), Fourier-transform infrared spectroscopy (FTIR), potentiometric titration method and the acid-base titration method. It is essential to control and optimize the deacetylation process to achieve chitosan with the desired DDA for specific applications. The DDA of chitosan from insects are shown in Table 2.2. It was reported that the DDA of chitosan of Lepidoptera insect like silkworm (*Bombyx mori*) was 85.5% [25]. The

DDA of chitosan of Coloptera insect like *Tenebrio molitor, Zophobas morio, Allomyrina dichotoma, Catharsius molossus, Calosoma rugosa, Leptinotarsa decemlineata, Blaps lethifera, Pimelia fernandezlopezi* and banana weevils (*Cosmopolites sordidus*) was found to be 53.9-95.5%, 64.82-81.06%, 74.66-75.67%, 94.05-95.75%, 95%, 76-82%, 86.9-87.3%, 88.1-88.3%, 77.41-78.19%, respectively [34-44, 49, 50, 114]. The DDA of chitosan of Orthoptera insect like *Calliptamus barbarous, Schistocerca gregaria, Oedaleus decorus, Gryllus bimaculatus, Brachystola magna, Acheta domesticus* and *Gryllodes sigillatus* was 70-75%, 98%, 70-75%, 56.47-84.98%, 88.55-91.23%, 62.9- 88.5% and 73.6-81.3%, respectively [36, 39, 55, 58, 60, 63, 112]. The DDA of chitosan of Hymenoptera insect like *Apsis mellifera* and *Vespa orientalis* was same as 96% [36, 111]. The DDA of chitosan of Diptera insect like *Hermetia illucens*, *Chrysomya megacephala* and *Musca domestica* was reported *as* 66-93%,89.6% and 83.8-84.4%, respectively [49, 77, 79, 80, 84, 87, 116]. The DDA of chitosan of Hemiptera insect like Cicada slough was 84.1% [25]. The DDA of chitosan of *Dictyoptera* insect like *Periplaneta americana, Blattella germanica* and *Eupolyphaga sinensis* was 36.8-90.85%, 31.5% and 96.09-97.05%, respectively [95, 100, 112, 113]. The DDA of chitosan of *Ephemeroptera* insect like mayfly was 84.3% [118]. A higher DDA indicates a higher proportion of GlcN units, leading to increased positively charged amino groups, which enhances chitosan's cationic and polycationic properties. Chitosan with a high DDA exhibits enhanced cationic characteristics, making it effective for applications such as antimicrobial agents, drug delivery systems, and flocculants in wastewater treatment. Chitosan with a low DDA is more hydrophobic and can be used for applications in biodegradable films, coatings, and controlled-release systems.

2.4.3 Molecular weight

The molecular weight of chitosan from insects refers to the average size of chitosan molecules obtained from the deacetylation of chitin found in insect exoskeletons. The molecular

weight of chitosan is typically expressed in terms of its number-average molecular weight (M_n) or weight-average molecular weight (M_w).

The M_w of chitosan from insects are shown in Table 2.2. Different insect species may have variations in the molecular weight of their chitin, which can affect the resulting molecular weight of chitosan. It was reported that the M_w of chitosan of Lepidoptera insect like silkworm (*Bombyx mori*) was 40.90 kDa [25]. The M_w of chitosan of Coleoptera insect like *Tenebrio molitor, Catharsius molossus, Leptinotarsa decemlineata* and banana weevils (*Cosmopolites sordidus*) was found to be 39.75 kDa, 812.3 kDa, 450 kDa, 2676-2722 Da and 343 kDa, respectively [25, 34, 35, 39, 50]. The M_w of chitosan of Orthoptera insect like grasshopper, *Dociostaurus maroccanus, Brachystola magna, Acheta domesticus* and *Gryllodes sigillatus* reported to be 39.89 kDa, 5.6-7.2 kDa, 696.95 kDa, 86.8-344 kDa, 524 kDa, respectively [25, 39, 53, 60, 63]. The M_w of chitosan of Diptera insect like *Hermetia illucens* and *Chrysomya megacephala* was 21-505 kDa and 501 kDa, respectively [84, 87, 116]. The M_w of chitosan of Hemiptera insect like Cicada slough was 37.79 kDa [25]. The M_w of chitosan of Dictyoptera insect like *Periplaneta americana* and *Eupolyphaga sinensis* was 16 kDa and 127.79 kDa, respectively [95, 100]. The M_w of chitosan of *Ephemeroptera* insect like mayfly was found to be 3.69 kDa [118]. The deacetylation process conditions, such as temperature, time, and the concentration of the deacetylating agent, can influence the molecular weight of chitosan. Higher temperatures and longer deacetylation times may lead to lower molecular weights. For example, the M_w of *Acheta domesticus* measured by different studies vary widely from 86.8 to 344 kDa [60, 63]. Various methods have been developed to measure the M_w of chitosan, including gel permeation chromatography (GPC), size exclusion chromatography (SEC), and viscometry [128, 129]. Leke *et al.* revealed that chitosan samples from black soldier fly (*Hermetia illucens*) meal, extracted by three different sources: enzyme-, microwave- and ultrasound-assisted methods, displayed both antioxidant and antimicrobial activity. Chitosan M_w had effects on

biological activities; high M_w chitosan showed better antimicrobial activity [3]. Controlling and tailoring the M_w of chitosan from insect sources is important for customizing its properties to suit specific applications.

2.4.4 Moisture content and ash content

The measurements of moisture content and ash content provide valuable information about the quality and purity of the chitosan obtained from insects, which are crucial considerations for its various applications. Analytical methods such as gravimetric analysis are commonly employed to determine moisture content and ash content in chitosan samples from insects. The moisture content and ash content of chitin and chitosan from insects are shown in Table 2.2. The moisture content of chitin from *Ephestia kuehniella* (9.1%), *Tenebrio molitor* (6.2%), *Lucanus cervus* (6.6%), *Polyphylla fullo* (5.9%), *Brachytrupes portentosus (*4.00%), *Bradyporus sureyai* (5.2%), *Gryllotalpa gryllotalpa* (6.0%) and *Apsis mellifera* (7.7%) was measured [26, 45, 53, 65, 114]. The moisture content of chitosan from silkworm (*Bombyx mori,* 0.07%), *Clanis bilineata* (3.8%), *Tenebrio molitor* (0.19%-4.2%), *Catharsius molossus* (6.55%), *Calosoma rugosa* (8.8%), *Blaps lethifera* (14.3%), *Pimelia fernandezlopezi* (17.2%), banana weevils (*Cosmopolites sordidus*, 2.4%), grasshopper (1.8%), *Brachytrupes portentosus* (3.33%), *Apsis mellifera* (17.6%), *Musca domestica* (7.8%), Cicada slough (0.18%), *Eupolyphaga sinensis* (5.19%) was reported [25, 29, 35, 36, 49, 50, 53, 114]. Ash content refers to the inorganic residue left behind after chitosan is incinerated at high temperature. It represents the amount of non-organic or mineral matter present in the chitosan sample. Lower ash content indicates higher purity of the chitosan sample. High ash content may negatively affect the performance of chitosan in specific applications, such as biomedical or food-related uses. The ash content of chitin from *Ephestia kuehniella* (0.14%), *Tenebrio molitor* (3.6%), *Lucanus cervus* (0.6%), *Polyphylla fullo* (1.7%), banana weevils (*Cosmopolites sordidus*, 6.4%), *Brachytrupes portentosus* (1.00%), *Schistocerca gregaria* (14.1%), *Bradyporus sureyai*

(3.8%), *Gryllotalpa gryllotalpa* (2.1%) and *Apsis mellifera* (2.4%) was reported. The ash content of chitosan from silkworm (*Bombyx mori,* 0.05%), *Clanis bilineata* (0.3%), Mealworm (0.50%), *Tenebrio molitor* (3.7%), *Catharsius molossus L.* (0.34%), *Calosoma rugosa* (2.0%), *Blaps lethifera* (1.5%), *Pimelia fernandezlopezi* (2.0%), banana weevils (*Cosmopolites sordidus*, 2.2%), grasshopper (0.89%), *Brachytrupes portentosus* (1.00%), *Schistocerca gregaria* (1.6%), *Apsis mellifera* (9.2%), *Musca domestica* (8.2%), Cicada slough (0.03%) and *Eupolyphaga sinensis* (0.55%) was measured [25, 29, 35, 36, 49, 50, 53, 95, 114]. By carefully controlling and optimizing moisture and ash content, researchers and industries can produce high-quality chitosan with desired properties, making it suitable for a wide range of applications in areas such as biomedicine, agriculture, and environmental science.

2.4.5 Elemental analysis

Elemental analysis of chitin and chitosan from insects provides valuable information about the presence and relative abundance of different elements. The percentage of C and N (C%, N%) in chitin and chitosan can vary depending on factors such as the insect species, the extraction process, and the degree of deacetylation. Elemental analysis of chitin from different types of insects, including the carbon, nitrogen, hydrogen and carbon-nitrogen ratio are shown in Table 2.3. The percentage of C atoms from chitin and chitosan originating from various insects ranged from 32.09% to 48.90% and 38.98% to 42.76%, respectively. The N% value of chitin and chitosan from various insects ranged from 4.63% to 6.9% and 5.93% to 7.3%, respectively. The carbon/nitrogen (C/N) ratio of chitin and chitosan for various insects ranged from 6.13 to 9.49 and 5.35 to 6.57, respectively. For chitosan, the C/N ratio is used to calculate the DDA, which is a measure of the extent of acetyl group removal during the conversion of chitin to chitosan [116, 130]. A higher C/N ratio corresponds to a lower DDA, indicating a higher degree of acetylation in the chitosan [131]. Accurately determining the C and N percentages in chitin and chitosan is crucial for quality control, ensuring compliance with

industry standards. This information also aids in optimizing extraction and purification processes, producing chitin and chitosan with desired properties for diverse applications.

Table 2.3. Elemental analysis (EA) results of chitin and chitosan from insects.

Insect species	Chitin (%)				Chitosan (%)				Ref.
	Carbon (C)	Hydrogen (H)	Nitrogen (N)	Carbon/ Nitrogen	Carbon (C)	Hydrogen (H)	Nitrogen (N)	Carbon/ Nitrogen	
Flour moth, *Ephestia kuehniella*	43.12	6.11	5.89	7.057	NA	NA	NA	NA	[26]
Butterfly, wings *Argynnis pandora*	44.89	6.53	6.62	6.781	NA	NA	NA	NA	[27]
Butterfly, OBP *Argynnis pandora*	44.91	6.45	6.48	6.931	NA	NA	NA	NA	
Common cockchafer, *Melolontha melolontha*	45.09	6.29	6.72	6.71	NA	NA	NA	NA	[32]
Superworm, *Zophobas morio*	0.5 M-43.27	0.5 M-6.77	0.5 M-6.60	0.5 M-6.56	42.76	7.47	6.55	6.53	[43]
	1.0 M-43.07	1.0 M-6.73	1.0 M-6.38	1.0 M-6.75	42.27	7.09	6.76	6.25	
	2.0 M-43.32	2.0 M-6.77	2.0 M-6.29	2.0 M-6.89	42.08	7.40	6.56	6.41	
European stag beetle, *Lucanus cervus*	45.9	7.6	5.3	8.5	NA	NA	NA	NA	[45]
Pine chafer, *Polyphylla fullo*	45.4	7.5	5.1	8.9					
Moroccan locust,	Adult-42.35	Adult-5.64	Adult- 4.63	Adult-9.15	Adult-41.63	Adult-6.38	Adult-7.20	Adult-5.78	[52]

Dociostaurus maroccanus	Nymph-47.32	Nymph-6.64	Nymph- 5.66	Nymph-8.36	Nymph-42.01	Nymph-6.28	Nymph-6.45	Nymph-6.51	
House cricket, *Brachytrupes portentosus*	41.30	NA	6.022	6.858	38.98	NA	5.932	6.571	[53]
Celes variabilis	45.05-49.0	6.31-6.92	5.68-6.43	7.01-8.24	NA	NA	NA	NA	[54]
Wart-biter, *Decticus verrucivorus*									
Melanogryllus desertus									
Paracyptera labiata									
Bradyporus sureyai	46.6 ± 0.1	7.7 ± 0.1	5.3 ± 0.1	8.8 8.8	NA	NA	NA	NA	[45]
European mole cricket, *Gryllotalpa gryllotalpa*	44.2 ± 0.1	7.6 ± 0.1	5.0 ± 0.1						
European hornet, *Vespa crabro*	46.62	6.42	6.85	6.81	NA	NA	NA	NA	[67]
Oriental hornet, *Vespa orientalis*	46.01	6.34	6.71	6.86					
German wasp, *Vespula germanica*	44.94	5.95	6.90	6.51					
Asian hornet, *Vespa velutina*	43.47	6.94	6.85	6.35	NA	NA	NA	NA	[110]
European hornet, *Vespa crabro*	Larval-45.6 Pupa- 46.2 Adult-45.5	Larval-6.5 Pupa- 6.4 Adult- 6.3	Larval-6.5 Pupa- 6.3 Adult- 6.49	Larval-7.02 Pupa-7.33 Adult-7.01	NA	NA	NA	NA	[70]

Black soldier fly, *Hermetia illucens*	Pupal exuviae-35.23 Imago-32.09	Pupal exuviae-5.11 Imago-4.80	Pupal exuviae-3.73 Imago-3.9	Pupal exuviae-9.45 Imago-8.23	NA	NA	NA	NA	[72]
Black soldier fly, *Hermetia illucens*	Pupae exuviae-43.74 Imago-39.74	Pupae exuviae-5.82 Imago-5.46	Pupae exuviae-6.14 Imago-6.00	Pupae exuviae-6.62 Imago-7.12	NA	NA	NA	NA	[132]
Black soldier fly, *Hermetia illucens*	41.84	6.74	5.96	7.02	NA	NA	NA	NA	[115]
Oriental blue fly, *Chrysomya megacephala*	NA	NA	NA	NA	39.06 ± 0.20	7.16 ± 0.08	7.30 ± 0.08	5.35	[116]
American cockroach, *Periplaneta Americana*	45.74	6.59	6.69	6.84	NA	NA	NA	NA	[99]
Dragonfly, Sympetrum fonscolombii	47.09	6.65	6.83	6.89	NA	NA	NA	NA	[103]
American cockroach, *Pariplaneta Americana linnaeus*	47.23	7.32	7.20	6.56	NA	NA	NA	NA	[66]
Western honey bee, *Apis mellifera linneaus*	52.65	8.42	5.55	9.49	NA	NA	NA	NA	[66]
Coridius nepalensis	42.175	6.551	6.878	6.13	NA	NA	NA	NA	[94]
American cockroach, *Periplaneta americana*	43.84	6.93	6.33	6.92	NA	NA	NA	NA	[102]
German cockroach, *Blattella germanica*	46.28	6.84	6.84	6.77	NA	NA	NA	NA	[48]

Dor beetle, *Anoplotrupes stercorosus*	40.6	7.66	6.35	6.39					
Blaps tibialis	45.17	6.85	6.43	7.02					
Rose chafer, *Cetonia aurata*	43.6	7.13	6.87	6.35					
Geotrupes stercorariu	43.1	6.49	6.77	6.37					
Calliphora vicina	48.9	6.54	6.79	7.2					
Dock bug, *Coreus marginatus*	39.2	6.95	6.03	6.5					
Black-and-red-bug, *Lygaeus equestris*	46.59	6.34	6.74	6.91					
Pyrrhocoris apterus	46.38	6.02	6.77	6.85					
Red-tailed bumblebee, *Bombus lapidaries*	40.1	7.48	6.11	6.56					
Formica clara	46.48	6.45	6.59	7.05					
Downy emerald, *Cordulia aenea*	44.6	6.86	6.66	6.70					
Four-spotted chaser, *Libellula quadrimaculata*	43.0	6.95	6.42	6.70					
Pale giant horse-fly, *Tabanus bovinus*	47.60	6.55	6.57	7.24	41.99	6.42	7.18	5.85	[91]

*NA: Not available.

Hightlights：

- The percentage of C atoms from chitin and chitosan originating from various insects ranged from 32.09% to 48.90% and 38.98% to 42.76%, respectively.
- The N value of chitin and chitosan from various insects ranged from 4.63% to 6.9% and 5.93% to 7.3%, respectively.
- The carbon/nitrogen (C/N) ratio of chitin and chitosan for various insects ranged from 6.13 to 9.49 and 5.35 to 6.57, respectively.

2.4.6 Fourier transform infrared spectroscopy

Fourier Transform Infrared Spectroscopy (FTIR) is a powerful analytical technique used to characterize the molecular structure and functional groups present in chitin and chitosan extracted from insects. Figure 2.4 presents the classical FT-IR spectra of chitin and chitosan extracted from insects. Peak at around 1615-1665 cm^{-1} corresponds to the carbonyl (C=O) stretching vibration of the acetyl (Ac) groups in chitin. It confirms the presence of N-acetylglucosamine units in the chitin structure. Peak at around 1635-1670 cm^{-1} is still present in the chitosan spectrum, but it is usually broader and slightly shifted to lower wavenumbers compared to chitin. This change is due to the partial deacetylation, indicating the presence of both acetyl and amino groups in chitosan [41, 55, 133-135]. Peak at around 1570-1605 cm^{-1} corresponds to the amide I band, indicating the presence of amide groups (N-H bending) in chitosan [55, 133-135]. It becomes more prominent with increasing deacetylation, reflecting the higher proportion of glucosamine units. Peak at around 3330-3490 cm^{-1} indicates the presence of hydroxyl (OH) groups in chitin and chitosan, which are involved in hydrogen bonding and contribute to its crystalline structure [41, 55, 133-135]. To differentiate between α-form and β-form chitin content, an additional peak related to the amide I band in the FTIR spectrum can be observed. For example, Soon *et al.* reported that the chitin isolated from *Zophobas morio* was in α-form because the amide I band was split into two bands, namely, 1620 cm^{-1} and 1650 cm^{-1}, respectively [43]. Kaya *et al.* reported characteristic band of α form chitin from *Calliptamus barbarus* (observed at 1652 cm^{-1} and 1621 cm^{-1}) and *Oedaleus decorus* (1655 cm^{-1} and 1620 cm^{-1}) [55]. Furthermore, the degree of deacetylation in chitosan can be quantified based on the intensity ratio of specific peaks in the FTIR spectrum. One common method is to calculate the DDA as the ratio of the areas under the peaks of acetyl groups and amide groups. A higher DDA value indicates a greater proportion of glucosamine units and a more deacetylated chitosan structure [136].

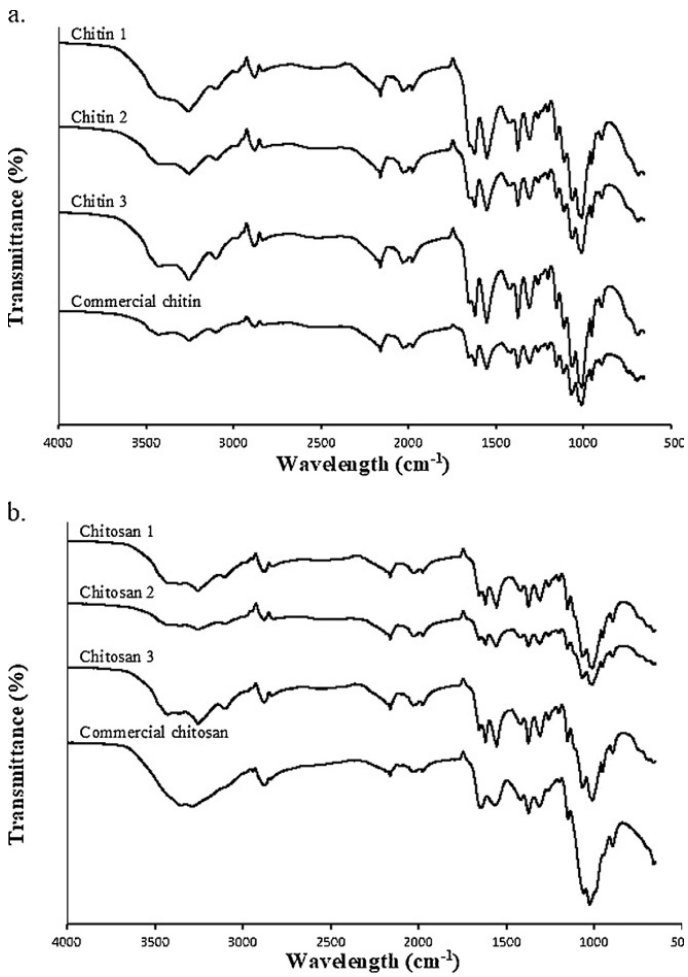

Figure 2.4 FTIR spectrograms of (a) chitin and (b) chitosan extracted from *Zophobas morio* larvae in varying sodium hydroxide concentration. Reprinted with permission (5846050212462) from Soon *et al., Int. J. Biol. Macromol.*, 108, 2018, 135-142, Elsevier [43]

2.4.7 Thermogravimetric analysis

Thermogravimetric Analysis (TGA) is a widely used technique to study the weight loss of chitin and chitosan from insects as a function of temperature, it offers valuable information about their thermal behavior, stability, and decomposition characteristics (Table 2.4). The maximum degradation temperature (DTG_{max}), representing the temperature at which the sample loses maximum weight due to thermal decomposition. For chitin, the DTG_{max} is usually higher due to its more crystalline and stable structure, while chitosan may have a lower DTG_{max} due to the presence of more amorphous regions [34, 52, 55, 91, 92]. As reported in many papers,

the DTG_{max} of chitin and chitosan extracted from different insect orders ranged between 307 and 412.7°C or between 289 and 317.7°C, respectively. The TGA analysis of chitin and chitosan from various insects shows that mass loss typically occurs in two stages; the first mass loss both occurred around 100°C, followed by a second mass loss (100-750°C and 200-650°C), respectively. For all the chitin and chitosan from various insects, the first mass loss (corresponds to water loss) was noted to be 1.1%-9% and 3%-13.37%, respectively, while the second mass loss (corresponds to degradation) was 48%-94.5% and 45.76%-96%, respectively. The TGA curve also shows any residue formation, indicating the presence of inorganic or non-volatile components in the chitin and chitosan samples after thermal decomposition.

Table 2.4. Thermogravimetric analysis (TGA) of insect chitin and chitosan.

Insect species	Chitin (%)					Chitosan (%)					Ref.
	First		Second		DTG_{max}	First peak		Second peak		DTG_{max}	
	mass loss (%)	T (°C)	mass loss (%)	T (°C)	(°C)	mass loss (%)	T (°C)	mass loss (%)	T (°C)	(°C)	
Lepidoptera											
Silk worm, *Bombyx mori*	NA	NA	NA	NA	NA	NA	80–90	NA	290–300	NA	[25]
Butterfly, *Argynnis pandora*	Wings-4.85 OBP-4.82	30-100	Wings-82.23 OBP-80	100-650	Wings-386.9 OBP-399.6	NA	NA	NA	NA	NA	[27]
Coleoptera											
Mealworm, *Tenebrio molitor*			NA			NA	80–90	NA	290–300	NA	[25]
Omophlus sp.	3.6% (α) 7.7% (β)	NA	78.8% (α) 63.5% (β)	NA	385.3 (α) 334.2 (β)	NA	NA	NA	NA	NA	[31]
Melolontha melolontha	4	0-150	78	150-600	380	NA	NA	NA	NA	NA	[32]
Melolontha sp.	1.1- 5.4	NA	51.2-94.5	NA	female-392.2 male-378.3	NA	NA	NA	NA	NA	[33]
Colorado potato beetle, *Leptinotarsa decemlineata*	3–5	NA	Adult-74 Larval-48	NA	Adult-379 Larval-307	3–5	NA	94-96	NA	Adult-289 Larval-292	[34]
Catharsius molossus			NA			13.37	25-290	45.76	290-400	317.70	[35]

European stag beetle, *Lucanus cervus*	6.6	100	70	300-420	379.9	NA	NA	NA	NA	NA	[45]
Pine chafer, *Polyphylla fullo*	5.9	100	73		374.7						
Dor beetle, *Anoplotrupes stercorosus*	4	NA	74	NA	387	NA	NA	NA	NA	NA	[48]
Blaps tibialis	7		76		385						
Rose chafer, *Cetonia aurata*	7		82		361						
Geotrupes stercorarius	5		77		390						
Orthoptera											
grasshopper			NA			NA	80–90	NA	290–300	NA	[25]
Moroccan locust, *Dociostaurus maroccanus*	4	NA	Adult-77 Nymph-82	NA	Adult-386 Nymph-383	Adult-5 Nymph-7	NA	Adult-62 Nymph-59	NA	Adult-302 Nymph-308	[52]
Celes variabilis	3–6	0–150	73–96	150–400	350-387	NA	NA	NA	NA	NA	[54]
Wart-biter, *Decticus verrucivorus*											
Melanogryllus desertus											
Paracyptera labiata											
Calliptamus barbarus	8	0–150	72	150-	381	8	0–150	61	300	296	[55]
Oedaleus decorus	6		77	650	390	6		57		305	
Ailopus simulatrix	NA	0–150	82	150-	383	NA	NA	NA	NA	NA	[56]
Ailopus strepens			78	600	382						
Duroniella fracta			74		381						

Duroniella laticornis			72		382						
Red-winged grasshopper, *Oedipoda miniata*			76		385						
Oedipoda caerulescens			77		384						
Pyrgomorpha cognata			74		384						
Bradyporus sureyai	5.2	0-100	72	300-420	382.4	NA	NA	NA	NA	NA	[45]
European mole cricket, *Gryllotalpa gryllotalpa*	6.0		70	300-412	374.6						
House Crickets (*Acheta domesticus*)	7.4	0-150	53	200-400	359.2	NA	NA	NA	NA	NA	[60]
Hymenoptera											
Western honey bee, *Apsis mellifera*	Head-6 Thorax-4 Abdomen-3 Legs-5 Wings-3	NA	Head-67 Thorax-56 Abdomen-68 Legs-68 Wings- 60	NA	Head-308 Thorax-360 Abdomen-367 Legs- 359 Wings-359	NA	NA	NA	NA	NA	[64]
European hornet, *Vespa crabro*	Larvae-3.51 Pupaand-2.7 Adult-6.5	30-180	Larvae-88.7 Pupa-69.9 Adult-78.3	NA	Larvae-384.8 Pupa-381.7 Adult-382.4	NA	NA	NA	NA	NA	[70]
Red-tailed bumblebee, *Bombus lapidarius*	5	NA	72	NA	384	NA	NA	NA	NA	NA	[48]

Formica clara	4		78		374						
Diptera											
Black soldier fly, *Hermetia illucens*	2–3	0–122	62-63	122–450	Imago-387 Larval-389	NA	NA	NA	NA	NA	[72]
Black soldier fly, *Hermetia illucens*	5-6	74-110	70-80	250	Imago-363 Pupae exuvia-371	NA	NA	NA	NA	NA	[132]
Black soldier fly, *Hermetia illucens*	Larvae-4.42 Prepupa-6.74 Puparium-8.52 Adults-7.5	0–150	Larvae-69.48 Prepupa-71.16 Puparium-71.25 Adults-3.31	150–400	Larvae-372 Prepupa-373 Puparium-371 Adults-372	NA	NA	NA	NA	NA	[75]
Common fruit fly, *Drosophila melanogaster*	4.4	NA	75.6	NA	378.7	4.47	NA	61.12	NA	304.7	[89]
Calliphora vicina	4	NA	65	NA	379	NA	NA	NA	NA	NA	[48]
Pale giant horse-fly, *Tabanus bovinus*	4.6	30- 150	80.2	200-650	370.50	7.3	30-150	59.3	200-650	295.4	[91]
Hemiptera											
Cicada slough			NA			NA	80–90	NA	290–300	NA	[25]
Aquatic bug Ranatra linearis	6	0–150	78	150–650	393	9	0–150	50	150–650	289	[92]
Cicada lodosi	4.41	0–200	83.94	200–750	411.70	NA	NA	NA	NA	NA	[93]
Cicada mordoganensis	4.88		80.44		412.40						

Cicadatra platyptera	3.80		81.78		412.20						
Cicadatra atra	4.54		83.75		411.50						
Cicadatra hyaline	5.4		66.78		412.70						
Cicadivetta tibialis	4.04		73.49		339.90-402.30						
Dock bug, *Coreus marginatus*	9	NA	73	NA	389	NA	NA	NA	NA	NA	[48]
Black-and-red-bug, *Lygaeus equestris*	3		66		375						
Pyrrhocoris apterus	5		78		387						
Dictyoptera											
Periplaneta americana	5	100	76	350–390	389	NA	NA	NA	NA	NA	[99]
Blattella germanica	4	NA	77	NA	389	NA	NA	NA	NA	NA	[48]
Odonata											
Dragonfly, *Sympetrum fonscolombii*	2.9	25-100	73.2	100-750	369.2	NA	NA	NA	NA	NA	[103]
Cordulia aenea	4	NA	75	NA	378	NA	NA	NA	NA	NA	[48]
Libellula quadrimaculata	6		76		384						

*NA: Not available. The typical DTG_{max} of chitin and chitosan extracted from different insect orders ranged between 307-412.7 °C and 289-317.7 °C, respectively.

2.4.8 Crystalline properties

The crystalline analysis of insect-extracted chitin and chitosan is vital for understanding their molecular structure and degree of crystallinity, influencing mechanical properties, solubility, and interactions. Common techniques, such as X-ray diffraction (XRD) and solid-state nuclear magnetic resonance (NMR), reveal distinct peaks in classical XRD patterns, indicating crystalline regions. Chitin displays well-defined peaks, showcasing a highly ordered structure. Chitosan, with partial deacetylation, may exhibit broader or less intense peaks, signifying a less ordered structure than chitin. The degree of crystallinity, a critical parameter obtained from XRD analysis, quantitatively measures the proportion of crystalline regions compared to amorphous regions. Higher crystallinity suggests a more ordered molecular arrangement, while lower crystallinity indicates a more disordered and amorphous structure. As showed in Table 2.5, the crystallinity of chitin and chitosan from different insect species ranged from 24.9 to 96.4% and 32.9% to 86.64%, respectively. Wang *et al*. found that the crystallinity of chitin from *Hermetia illucens*, varies greatly at different growth stages such as larvae (33.09%), prepupa (35.14%), puparium (68.44%), adult (87.92%) [75]. Kaya *et al.* also attempted to compare the crystallinity of chitin from different body parts of Lepidoptera insect *Argynnis pandora*, results showed that the crystallinity of wings (64%) close to other parts (66%) [27]. For the same insect sample, *Hermetia illucens*, the crystallinity of chitin obtained by different methods varied greatly from 24.9% to 94% [71-73, 75, 84]. Crystalline analysis of chitin and chitosan from insect sources are important for under-standing the fundamental properties of these biopolymers and for tailoring their characteristics to fit with future applications.

Table 2.5. XRD peaks and crystalline index value (%) of chitin and chitosan from insects.

Insect species	Chitin (%)		Chitosan (%)		Ref.
	XRD peaks at 2θ	CrI (%)	XRD peaks at 2θ	CrI (%)	
Lepidoptera					
Silk worm	9.6, 19.7, 12.7, 23.2, 26.3, 39	59.21	10, 20	32.9	[25]
Butterfly, *Argynnis pandora*	Wings-9.3, 9.3, 12.84, 21.04, 22.9, 26.36	Wings-64	NA	NA	[27]
	OBP-8.5, 19.3, 12.84, 21.14, 23.06, 6.66	OBP-66	NA	NA	
Coleoptera					
Mealworm	9.6, 19.7, 12.7, 23.2, 26.3, 28.1, 39	81.11	10, 20	51.9	[25]
Omophlus sp.	9.42, 12.72, 19.34, 20.84, 23.32, 26.44	82.9	NA	NA	[31]
Cockchafer, *Melolontha melolontha*	NA	75.2	NA	NA	[32]
Cockchafer, *Melolontha* sp.	9.32−9.70, 12.12−13.22, 12.78−13.22, 19.18−19.76,	74. 1- 88.9	NA	NA	[33]
	20.06−21.48, 23.06−23.78，26.02−26.80				
Colorado potato beetle, *Leptinotarsa*	Larvae-9.6,13.22, 19.68, 21.42, 23.26, 26.7	Larvae-72	NA	NA	[34]
decemlineata	Adults-9.66, 13.18, 19.48, 21.06, 23.16, 26.76	AMdults-76			
Calosoma rugosa	NA	NA	9.7°, 20.3°, 22.6°	49	[36]
Calosoma rugosa	NA	NA	9.7°, 20.3°	49	[37]
Mealworm Beetle, *Tenebrio molitor*	9.6, 19.6, 21.1, 23.7, 36	57.85	NA	NA	[40]
Mealworm Beetle, *Tenebrio molitor*	9.011, 9.034, 19.119, 19.167, 21.38, 21.44, 22.68,	NA	NA	NA	[137]
	22.74				

Mealworm Beetle, *(Tenebrio molitor, Zophobas morio)*	NA	NA	10.62°, 20.02°	58.11	[42]
Rhinoceros beetle, *Allomyrina dichotoma*	NA	NA	10.74°, 19.92°	62.77	
European stag beetle*, Lucanus cervus*	9.67, 12.40, 19.60, 23.41, 26.26, 39.1	85.2	NA	NA	[45]
	9.2, 12.40, 19.46, 23.50, 26.21, 28.1, 39.5	86.1			
Sitophilus granarius L.	8.9, 9.2, 18.7, 25.6, 12.3, 22.8	78.77	NA	NA	[47]
Dor beetle, *Anoplotrupes stercorosus*	9.58, 13.36, 19.66, 21.14, 23.18, 26.52	83.5	NA	NA	[48]
Blaps tibialis	9.48, 12.76, 19.38, 21.08, 23.04, 26.64	80.1			
Rose chafer, *Cetonia aurata*	9.44, 13.04, 19.52, 21.28, 23.46, 26	86.3			
Geotrupes stercorarius	9.64, 13.14, 19.56, 21.38, 23.22, 26.76	80.1			
Blaps lethifera	NA	NA	10.7, 19.9	84	[49]
Pimelia, fernandezlopezi			11.5, 20.4	73	
Banana weevil, *Cosmopolites sordidus*	NA	NA	19.5	41	[50]
Orthoptera					
Grasshopper	9.6, 19.7, 12.7, 23.2, 26.3, 28.1, 39.0	83.4	10, 20	50.1	[25]
Moroccan locust, *Dociostaurus maroccanus*	Adult-9.56, 12.76, 19.72, 21.12, 23.96, 26.64 Nymph-9.42, 12.86, 19.72, 21.56, 23.38, 26.66	Adult-71 Nymph-74	Adult-10.96, 20.14 Nymph-10.76, 20.3	NA	[52]
House cricket, *Brachytrupes portentosus*	9.4, 12.8, 17.1, 19.4, 21.1, 23.2, 26.3, 28.5, 35.0, 39.0	88.02	9.6, 19.6, 21.2	86.64	[53]

Celes variabilis	9, 19, 12, 21, 23, 26	75-80	NA	NA	[54]
Wart-biter, *Decticus verrucivorus*					
Melanogryllus desertus					
Paracyptera labiata					
Calliptamus barbarus	9.26, 19.28, 21.24, 23.28, 26.36, 31.78	70.9	10.92, 20.08	NA	[55]
Oedaleus decorus	9.6, 19.6, 21.1,23.7, 26.64	76.8	10.08, 20.14		
Ailopus simulatrix	9.3, 12.7, 19.6, 21.1, 23.8, 26.6	76	NA	NA	[56]
Ailopus strepens	9.5, 12.8, 19.6, 20.8, 23.8, 26.4	75			
Duroniella fracta	9.5, 12.6, 19.4, 20.9, 23.5, 26.8	72			
Duroniella laticornis	9.5, 12.8, 19.3, 20.7, 23.2, 26.5	71			
Red-winged grasshopper, *Oedipoda miniata*	9.7, 12.9, 19.6, 21, 23.7, 26,8	74			
Oedipoda caerulescens	9.3, 12.7, 19.3, 20.7, 23.1, 26.9	74			
Desert locust, *Schistocerca gregaria*	NA	NA	9.3, 20.2, 24.4	69	[36]
Bradyporus sureyai	9.62, 12.5, 19.72, 23.74, 26.22, 27.8, 39.2	83.1	NA	NA	[45]
European mole cricket, *Gryllotalpa gryllotalpa*	9.44, 12.3, 19.41, 23.31, 26.2, 27.9, 39.0	80.6			
Gryllus bimaculatus	NA	NA	10.50, 20.07	57.52	[58]
Shistocerca gregarea Forsskal	9.2, 19.1,12.6, 22.9, 26.2	71.4	NA	NA	[46]
Hymenoptera					

Apsis mellifera	NA	NA	9.7, 20.3	59	[36]
Apsis mellifera	NA	NA	9.7, 20.3	59	[37]
European hornet, *Vespa crabro*	9.64, 12.74, 19.38, 20.94, 23.92, 26.88	69.88	NA	NA	[67]
Oriental hornet, *Vespa orientalis*	9.68, 12.72, 19.32, 21.6, 23.74, 26.8	53.92			
European wasp, *Vespula germanica*	9.32, 12.92, 20.l04, 21.24, 23.16, 25.9	50			
Vespa orientalis L.	9.2, 19.1,12.6, 22.9, 26.2	39.4	NA	NA	[46]
Red-tailed bumblebee, *Bombus lapidarius*	9.64, 13.02, 19.58, 21.22, 23.44, 26.78	75.5	NA	NA	[48]
Formica clara	9.5, 13.38, 19.78, 20.84, 23.1, 26.76	69.8			
Diptera					
Musca domestica	NA	NA	10.5, 20.2	81	[49]
Black soldier fly, *Hermetia illucens*	9.4, 13.0, 19.3, 20.8, 23.2, 29.5	Prepupae-94 Cocoons-94 Sheddings-89 Larvae-89	NA	NA	[71]
Black soldier fly, *Hermetia illucens*	9, 19, 22, 24, 30	Larval-35 Imago-24.9	NA	NA	[72]
Black soldier fly, *Hermetia illucens*	9.3, 19.8, 23, 26.0	Pupae exuvia-25.2 Imago-49.4	NA	NA	[132]
Black soldier fly, *Hermetia illucens*	Larvae-9.30, 12.78, 19.26, 21.82, 23.31, 26.41 Prepupa-9.38, 12.93, 19.33, 21.19, 23.42, 26.37	Larvae-33.09 Prepupa-35.14	NA	NA	[75]

	Puparium-9.30, 12.67, 19.29, 20.77, 23.38, 26.45 Adult-9.50, 12.82, 19.33, 20.81, 23.31, 26.34	Puparium-68.44 Adult-87.92			
Black soldier fly, *Hermetia illucens*	9, 19, 13, 21, 23, 26	Larvae-84 Pupal exuviae-62 Dead adults-93	10, 20	Larvae-77 pupal exuviae-80 dead adults-86	[84]
Calliphora vicina	9.38, 12.88, 19.3, 20.8, 22.84, 26.8	67.1	NA	NA	[48]
Hemiptera					
Cicada slough	9.6, 19.7, 12.7, 23.2, 26.3, 39	85.21	10, 20, 23.2	49.1	[25]
Aquatic bug Ranatra linearis	9.34, 12.38, 19.66, 20.88, 23.22, 26.56, 38.96	84.8	NA	NA	[92]
Coridius nepalensis	9, 20, 20.5, 22.8, 26.4	86.33	NA	NA	[94]
Dock bug, *Coreus marginatus*	9.7, 13.2, 19.86, 21.24, 23.42, 26.54	76.9	NA	NA	[48]
Black-and-red-bug, *Lygaeus equestris*	9.64, 13, 19.76, 21.16, 22.8, 26.7	59.7			
Pyrrhocoris apterus	9.44, 12.52, 19.14, 20.84, 22.66, 26.7	62.1			
Dictyoptera					
American cockroach, *Periplaneta americana*	9.14, 19.58, 12.88, 20.98, 23.12, 26.8	86.7	NA	NA	[99]
American cockroach, *Periplaneta americana*	12, 19, 20.5, 21.5, 23, 26	83.72	NA	NA	[102]
German cockroach, *Blattela germanica*	9.2, 19.1, 12.6, 22.9, 26.2	44.2	NA	NA	[46]
German cockroach, *Blattella germanica*	9.4, 12.7, 19.5, 20.68, 23.33, 26.66	70.1	NA	NA	[48]

Odonata					
Dragonfly, *Sympetrum, fonscolombii*	9, 13, 19, 21, 26	96.4	NA	NA	[103]
Downy emerald, Cordulia aenea	9.54, 13.18, 19.62, 21.4, 23.76, 26.92	73.2	NA	NA	[48]
Four-spotted chaser, Libellula quadrimaculata	9.54, 13.24, 19.68, 21.06, 23.1, 26.88	63.9			

NA: Not available.

- The crystallinity of chitin and chitosan from different insect species ranged from 24.9 to 96.4% and 32.9% to 86.64%, respectively.
- The typical peaks at 2θ for chitin are around 9-10°, 13°,20-22°,23° and 26°. The typical peaks at 2θ for chitosan are around 10° and 20-25°.

2.4.9 Nuclear magnetic resonance spectroscopy

Analyzing chitin and chitosan from insects using Nuclear Magnetic Resonance (NMR) spectroscopy is a powerful technique that provides detailed structural information about these biopolymers. Solid-state NMR allows for the investigation of materials that do not readily dissolve in traditional liquid-state NMR solvents [138]. As showed in Table 2.6 and Figure 2.5, there are some specific peaks and their approximate chemical shifts in the ^{13}C NMR spectra of chitin and chitosan [63, 68, 73, 139-141]. The acetyl carbon (C=O, CH_3-CO) in chitin typically appears in the region of 170-175 ppm. Due to the deacetylation process, chitosan may have a peak at a slightly lower chemical shift, around 165-170 ppm, corresponding to the acetyl carbon. The carbon at the anomeric position (C-1) in the glycosidic linkage of both chitin and chitosan typically appears in the range of 100-105 ppm. This carbon is part of the sugar ring structure. C-2, C-3, C-4, and C-5 (Carbon Atoms in Sugar Ring) in the sugar ring structure exhibit chemical shifts in the range of 55-85 ppm, depending on their specific positions within the ring. For example, the peaks of C-2 and C-3 normally appear at 55 ppm and 75 ppm, respectively. Carbon C-6 (Carbon in Sugar Ring) in the sugar ring typically appears in the range of 55-65 ppm. Chitosan contains hydroxyl groups (OH) introduced during the deacetylation process. The carbons associated with these hydroxyl groups can give rise to peaks in the region of 70-80 ppm, reflecting their different chemical environment. The carbons in the CH_2 groups within Glucosamine and N-Acetylglucosamine units usually appear in the range of 20-40 ppm. In both chitin and chitosan, carbons associated with the amide linkages can be found in the range of 150-175 ppm. The DDA of chitin and chitosan could be estimated using ^{1}H NMR by comparing signals from acetylated and deacetylated glucosamine units [133, 134]. It's important to note that the exact NMR chemical shifts can vary depending on factors such as the source of chitin or chitosan, their DDA, and the molecular conformation.

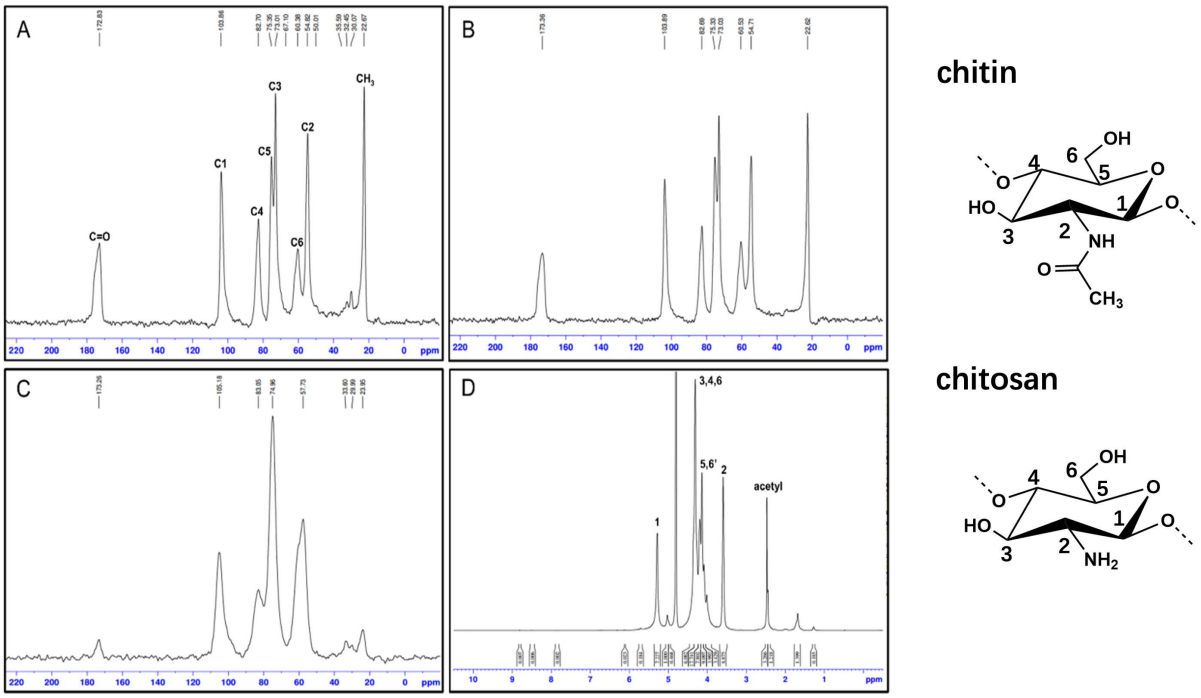

Figure 2.5 ^{13}C NMR data of mealworm chitin (A), shrimp chitin (B), and mealworm chitosan (C). ^{1}H NMR data of mealworm chitosan (D). Reprinted from Son et al. *Foods* 2021, 10, 640, MDPI [40].

Table 2.6. ^{13}C NMR spectral data of chitin and chitosan in different insect sources.

Insect species	**Chemical shift (ppm)**								**Ref.**
	C1	**C2**	**C3**	**C4**	**C5**	**C6**	**C=O**	**CH_3**	
Blowfly larvae, chitosan	104.47	56.78	75.14	85.31	75.14	60.41	NA	22.64	[63]
Black soldier fly, chitin	104.6	55.7	74.2	84.0	76.4	61.5	173.9	23.4	[73]
European rhinoceros beetle, *Oryctes nasicornis*, chitin film	104	55	73	83	75	61	NA	NA	[139]
Asian hornet, *Vespa velutina,* chitin	104.12	55.94	NA	82.74	75.34	60.34	173.17	22.79	[68]
Black soldier fly, *Hermetia illucens* Pupal, chitin	104.3	55.2	73.5	83.2	75.8	60.9	173.1	22.9	[140]
Mealworm, *Tenebrio molitor* Linnaeus 1758, chitin	104.63	55.71	76.14	83.63	76.14	61.46	173	23	[141]
Monarchs, Swallowtails, chitin	104	NA	73	83	76	NA	173	23	[138]

*NA: Not available.

2.4.10 Scanning electron microscopy

The surface morphology of chitin and chitosan, derived from insects and analyzed via Scanning Electron Microscopy (SEM), offers profound insights into their microstructural characteristics. Surface morphologies of insect chitin and chitosan normally showed following properties: (I) nanofiber, (II) nanopore, (III) smooth surface, and (IV) rough surface, as showed in exemplary Figure 2.6. Chitin from *Ephestia kuehniella*, *Vespa crabro*, *Vespa orientalis*, Vespula germanica, *Blaberus giganteus*, *Sympetrum fonscolombii (*dragonfly*), Melolontha melolontha, Omophlus* sp., *Celes variabilis*, *Decticus verrucivorus*, *Melanogryllus desertus*, *Paracyptera labiate*, *Hermetia illucens*, *Mecynorhina torquata*, exhibit highly ordered structure composed of microfibers [26, 31, 32, 54, 67, 72, 96, 103, 133]. These microfibers are the fundamental building blocks of the material and contribute to its strength and rigidity. Chitin from *Ephestia kuehniella*, *Vespa crabro*, *Vespa orientalis*, *Vespula germanica*, *Bradyporus* (*Callimenus*) *sureyai*, *Gryllotalpa gryllotalpa*, *Polyphylla fullo*, *Blaberus giganteus*, *Melolontha melolontha, Omophlus* sp., *Mecynorhina torquata* exhibit nanopores, which are nano-sized, high-aspect-ratio rods with a distinct surface morphology [26, 31, 32, 45, 67, 96, 133]. These nanostructures are of interest for various applications, including nanocomposites. Kaya *et al.* compared chitins extracted from male and female of *Celes variabilis*, *Decticus verrucivorus*, *Melanogryllus desertus*, *Paracyptera labiate*, SEM revealed that male chitin normally showed obvious nanopores structure [54]. Chitin from different body parts of *Argynnis pandora* butterfly showed several different types under SEM, such as microfibers, smooth porous zones, plane areas having no pores, tough and rough surface [27]. Chitin from *Lucanus cervus* showed rough surface [45]. Chitosan, which is derived from chitin through deacetylation, generally has a less crystalline and more amorphous structure. As a result, the surface of chitosan usually appears more irregular and porous under SEM. Luo *et al.* compared morphologic properties of chitosan from four insects [25]. Surface structure of cicada slough

chitosan was compact and intertwined with each other and showed needle and highly tighter shape. Silkworm chrysalis (*Bombyx mori*) chitosan was similar to the reticular structure. Mealworm chitosan has a surface with soft and irregular fibers. Grasshopper chitosan revealed irregular block and rough structure without any of porosity. Marei *et al.* revealed that the surface of locust chitosan with short thick regularly arranged nanofibers and some pores, beetle chitosan with randomly distributed nanofibers, honeybee chitosan with a hard and regular rough surface without pores or nanofibers [36]. Kaya *et al.* revealed that chitin and chitosan from larvae and adult Colorado potato beetle (*Leptinotarsa decemlineata*) have similar nanofiber structures [34]. Ibitoye *et al.* revealed that chitin and chitosan from house cricket showed similar rough and smooth layers of flakes with big pores and fibers [53]. Chitin and chitosan from *Drosophila melanogaster* also showed similar nanofiber structures [89]. Chitin and chitosan from *Goliathus orientalis* showed similar morphologic properties with a well-defined network and layer-by-layer structure [135]. The above studies indicated that source, sex, body part and life stage all affected the surface morphology of insect chitin and chitosan. The structures of insect chitin and chitosan have provided sources of inspiration for the fabrication of many novel materials for various biomimetics applications, such as nano-composites.

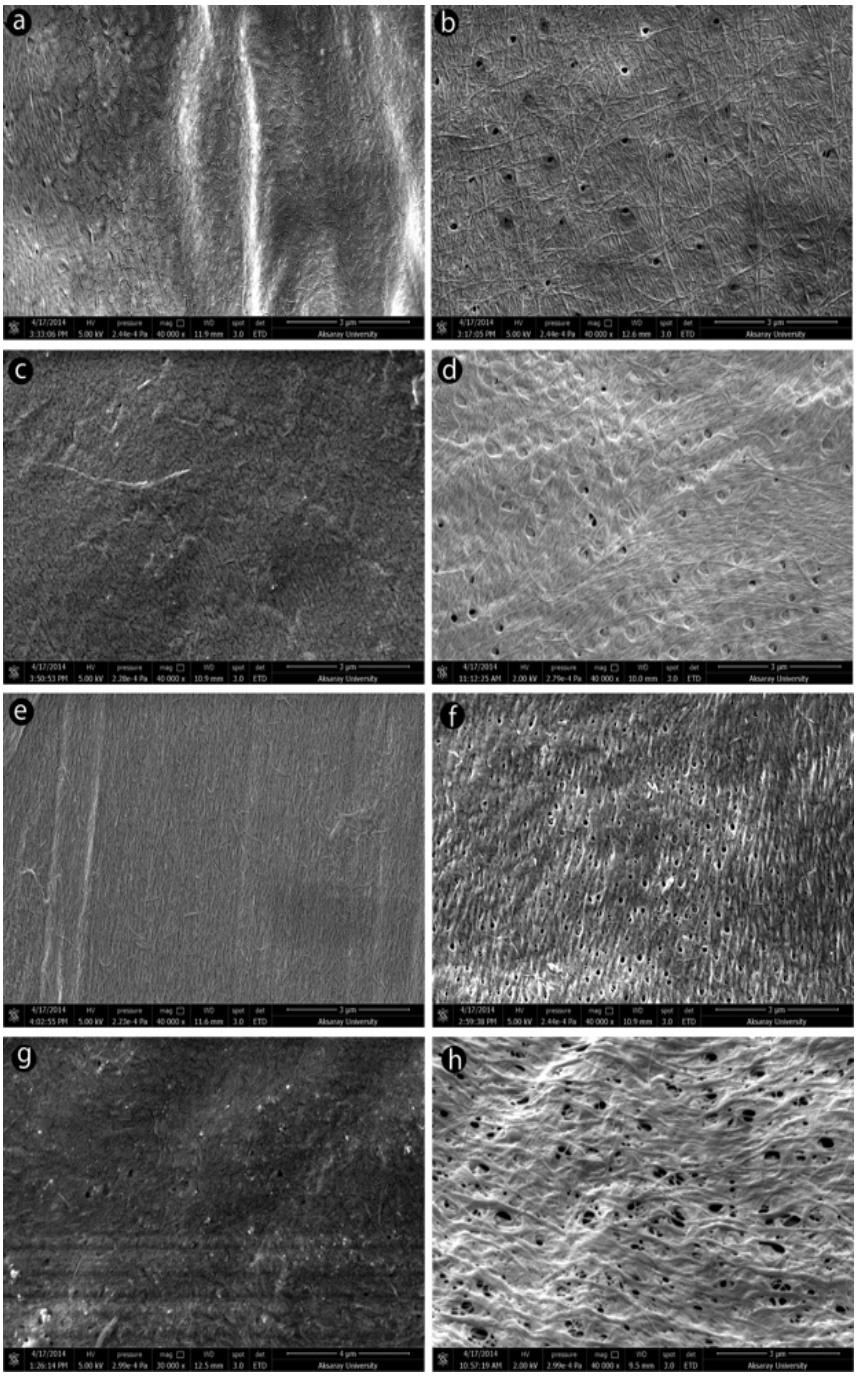

Figure 2.6 SEM images of four insect species: a) *Celes variabilis* female, b) C. *variabilis* male, c) *Decticus verrucivorus* female, d) D. *verrucivorus* male, e) *Melanogryllus desertus* female, f) *M. desertus* male, g) *Paracyptera labiate* female, h) *P. labiate* male. Reprinted from Kaya *et al.*, 2015, 10, Plos One [54].

2.4.11 Solubility

Chitin from insects, as chitin in general, is typically insoluble in water and most common organic solvents, such as ethanol, methanol, acetone, and chloroform, due to many hydrogen

bonds and crystalline structure [142]. On the contrary, chitosan, with its partial deacetylation, exhibits improved solubility in water [143]. To investigate the solubility of chitosan, Luo *et al.* added 0.1 g of chitosan into pre-weighed centrifuge tube, then dissolved in 10 mL of 1% aqueous acetic acid at 30°C under constant stirring for 1 h and centrifuged. The supernatant was removed, and the pellet was dried at 60°C overnight. The solubility was calculated by (initial weight of sample– final weight of sample) / initial weight of sample. The solubility of chitosan from four different insects were tested as: cicada slough, silkworm chrysalis (*Bombyx mori*), mealworm, and grasshopper were 99.3%, 98.7%, 97.4%, 94.3%, respectively [25]. Lucas *et al.* measured solubility by the same method as Luo *et al*. and revealed that the solubility of chitosan from mealworm's cuticles was 40.3 ± 0.6% [114]. The solubility of chitosan depends on several factors, including its molecular weight, DDA, and the chemical properties of the solvent, such as pH, polarity, and acidity [144]. High molecular weight and high DDA chitosan tend to form aggregates due to intermolecular hydrogen bonding and hydrophobic interactions, leading to decreased solubility [145]. At acidic pH smaller than 6.2, the amino groups (pKa from 6.2 to 7.0) are protonated, and solubility of chitosan increases. At alkaline pH, chitosan deprotonates, and its solubility decreases due to the formation of insoluble salts [146, 147]. The solvent's polarity and acidity also play critical roles in solubilizing chitosan, with polar, acidic solvents like hydrochloric acid and acetic acid facilitating solubility through protonation of amino groups. Chitosan's solubility can be enhanced by modifying its structure, such as by introducing more charged groups, such as carboxyl, hydroxyl, amino, or sulfate groups, into the polymer chain [148]. Additionally, chitosan can be chemically modified to form water-soluble derivatives, such as N-carboxymethyl chitosan or N-succinyl chitosan, which have improved solubility and other properties [149]. For chitin, grafting hydrophilic groups, such as polyethylene glycol or acrylic acid, onto the structure can enhance its solubility in water and polar solvents [150, 151]. Understanding the solubility behavior of chitin and chitosan is crucial

for designing its applications in various fields, such as drug delivery, wound healing, and tissue engineering [152, 153]. Solubility properties influence the processing and fabrication of chitin and chitosan-based materials, such as films, hydrogels, and nanocomposites [17, 154, 155].

2.5 Applications of chitin and chitosan from insects

2.5.1 Wastewater treatment

Adsorption was found to be a very effective and cheap method of wastewater treatment, attracting considerable attention due to its simplicity, low cost and high efficiency in removing pollutants from water [156]. Among various adsorbents, chitosan and its derivatives stand out as particularly promising materials, with a high concentration of hydroxyl (-OH) and amino (-NH_2) groups in its polymer backbone. These functional groups play a crucial role in the adsorption process by providing active sites for the binding of contaminants. The presence of these groups not only enhances the adsorption capacity of chitosan, but also makes it an environmentally friendly option. Chitosan and its derivatives have been extensively studied and shown to be effective in adsorbing a wide range of pollutants, including dyes and heavy metals [157]. Its biodegradability, non-toxicity and renewability further contribute to its suitability as a sustainable adsorbent in wastewater treatment applications. Few studies on the use of insect chitosan for wastewater treatment have also been reported. Ilham *et al.* extracted chitosan from three different sources: *Blaps lethifera* chitosan, *Pimelia fernandezlopezi* chitosan, and *Musca domestica* chitosan and investigated the effect of the DDA of chitosan on and the azo dyes (like methylene blue - MB) removal from wastewater. The MB dye removal of *Blaps lethifera* chitosan, *Pimelia fernandezlopezi* chitosan, and *Musca domestica* chitosan reached 37%, 87%, and 26%, respectively, at a contact time of 2 h, a low initial dye concentration of 13 ppm, a solution temperature of 25 °C, and a pH = 7 [49]. The possibility of using chitin from the molts of *Tenebrio molitor* to remove anionic (RB5, RY84) and cationic (BV10, BR46) dyes from

aqueous solutions was investigated by Tomasz *et al.* The sorption efficiency of anionic dyes on mealworm (*Tenebrio molitor*) chitin was highest at pH 2-3 and for cationic dyes at pH 6. The equilibrium sorption time of anionic dyes was 240-300 min and that of cationic dyes was 180-240 min. The experimental data on dye sorption kinetics were best described by the pseudo-second-order model. The maximum sorption capacity of mealworm (*Tenebrio molitor*) chitin for the anionic dyes RB5 and RY84 was 121.15 $mg \cdot g^{-1}$ and 138.55 $mg \cdot g^{-1}$ and was higher than that of some carbon-based materials. Regarding cationic dyes, the sorption capacity of the chitin tested was lower, reaching 3.22 $mg \cdot g^{-1}$ and 59.56 $mg \cdot g^{-1}$ for BV10 and BR46, respectively [158]. Katarzyna et al revealed that chitin isolated from Black Soldier Fly (*Hermetia illucens*) exuviae had relatively high efficiency and good biosorption properties for nickel ions [88].

2.5.2 3D printing and bioprinting

Chitosan is becoming increasingly popular in 3D printing due to its unique properties. This natural biopolymer is biocompatible, biodegradable and non-toxic, making it ideal for medical applications such as tissue engineering, wound healing and drug delivery. Its antimicrobial properties are beneficial in the creation of medical implants and devices. Chitosan's chemical structure allows it to be easily modified to improve its mechanical properties and solubility, making it versatile for various applications. It is also environmentally friendly as it is derived from renewable sources and is biodegradable. Chitosan can be processed into hydrogels, films and fibers suitable for various 3D printing techniques. Its excellent printability allows the creation of stable, high-resolution structures, essential for complex and precise objects. Few studies have reported the use of insect chitosan for 3D printing. A study carried out by our group reports the preparation of chitosan from giant dung beetles (Genus *Heliocopris*) and possibility to use it for formation of hydrogels and then for 3D printing. Measurements on the printed shapes showed well defined structures with printing accuracy (comparison between the printed shape and the model) between 85% and 95 % [134]. In another study from our group,

the extracted chitosan from *Mecynorhina torquata* has also been employed to form a hydrogel. Utilizing extrusion enables preparation of various 3D morphologies including a rigid block, fibers, beads and even enables printing out specific letters [133].

Bioprinting is a specialized branch of 3D printing that involves the layer-by-layer deposition of bioinks, typically composed of living cells and biomaterials. *In vitro* cell culture is an essential part of regenerative biology and preclinical evaluation. In traditional 2D cell culture, cells are grown on a flat surface such as a Petri dish or flask. They adhere and spread to form a monolayer. Cell-cell and cell-extracellular matrix (ECM) interactions are restricted to a single plane. This may not fully recapitulate the complexity of cellular interactions *in vivo*. Cells often have a flattened morphology and may behave differently from their *in vivo* counterparts. Biomechanical cues, such as matrix stiffness and elasticity, are missing. In 3D cell culture, however, cells are embedded in a three-dimensional matrix, such as a hydrogel, which more closely mimics the natural cellular microenvironment. Cells interact with neighboring cells and the surrounding ECM in three dimensions, allowing for more realistic cell signaling, migration and differentiation processes. Cells can adopt more physiologically relevant morphologies and functions, such as forming tissue-like structures or exhibiting specialized behaviors such as cell migration or differentiation. 3D cell culture is more suitable for modelling complex diseases and studying drug responses in a microenvironment that better mimics *in vivo* conditions [159]. Hydrogels can be designed to mimic the biomechanical properties of specific tissues, providing additional cues that influence cell behavior. In summary, while 2D cell culture remains a valuable tool for certain applications, 3D cell culture offers a more physiologically relevant model system that better recapitulates the complexity of tissues and organs *in vivo*. Although there have been many reports on the use of chitosan in 3D bioprinting, there have been no reports on insect-derived chitosan in this regard.

2.5.3 Biomedical applications

2.5.3.1 Antioxidant and anti-aging activity

Free radicals can damage cells, proteins, and DNA, contributing to various health issues and accelerating the aging process. Antioxidants work by neutralizing free radicals, thus reducing the risk of cellular damage and chronic diseases [160]. Anti-aging approaches focus on promoting skin health, maintaining cognitive function, preventing chronic diseases, and enhancing overall quality of life [161]. The relationship between antioxidants and anti-aging is rooted in the idea that antioxidants can help protect the body from the damage caused by oxidative stress, potentially slowing down the aging process and promoting longevity [162]. Many studies have reported the antioxidant and anti-aging activities of insect chitosan-based biomimetic materials. Chitosan film from the American cockroach *(Periplaneta americana*) could resist UV light effectively and keep scavenging DPPH radicals in 8 h [100]. Wu *et al.* found that chitosan of *Clanis bilineata* larva skin exhibited high antioxidant activity *in vitro* and anti-aging activities in D-gal-induced mice [30]. The antioxidant capacities of the chitosan from two gregarious Orthoptera species (*Calliptamus barbarus* and *Oedaleus decorus*) was evaluated using the free radical scavenging activity (2,2-diphenyl-1-picrylhydrazyl, DPPH) and ferric reducing power assays, and the scavenging effect increased with increasing concentrations of the extracts [55]. Chu *et al.* found that both DPPH radical scavenging and ferric-chelating assay showed positive correlation with DDA of chitosan isolated from superworm (*Zophobas morio*) larvae [43]. Tafi *et al.* reported that chitosan from *Hermetia illucens* as a coating for the preservation of a fresh food product, generally able to increase the phenolics and flavonoids content and the antioxidant activity of tomatoes at both room temperature and cold storage [163].

2.5.3.2 Antibacterial activity

Chitosan have gained significant attention for their antibacterial properties, which are attributed to their unique chemical structure and versatile applications. The present literature of antibacterial properties of insect chitin and chitosan are summarized in Table 2.7. Kaya *et al.* reported that the antimicrobial activities of the chitosan (250 μg/disc) from two gregarious Orthoptera species (*Calliptamus barbarus* and *Oedaleus decorus*) were more effective than traditional antibiotics (Amikacin, Ampicillin, Gentamicin, Erythromycin and Kanamycin) against some of the pathogenic bacteria strains studied. The chitosan from these two species generally showed stronger antibacterial effectiveness against the Gram-negative bacteria than the Gram-positive bacteria [55]. The negative charge on the cell surface of the Gram-negative bacteria is higher than that on the Gram-positive bacteria, which causes a greater amount of chitosan to be adsorbed and a higher inhibitory effect against the Gram-negative bacteria [164]. Mahboub *et al.* reported that chitosan nanoparticles prepared from the American cockroach, *Periplaneta americana*, inhibit the growth of *Escherichia coli, Klebsiella pneumoniae, Staphylococcus aureus,* and *Bacillus subtilis.* Chitosan nanoparticles were found to cause the deformation and rupture of the selected bacteria by TEM investigation [101]. The chitosan from Mealworm Beetle (*Tenebrio molitor, Zophobas morio*) showed an antibacterial effect against *Pseudomonas aeruginosa* [41]. Shin *et al.* also confirmed that *Tenebrio Molitor* chitosan had about 1–2 mm inhibition zones against four strains of bacteria: *Bacillus cereus, Listeria monocytogenes, Escherischia coli,* and *Staphylococcus aureus,* indicating antimicrobial activity [42]. Chitosan extracted from *Blaps lethifera, Pimelia fernandezlopezi,* and *Musca domestica*, showed good antibacterial activity against *Listeria innocua, Bacillus subtiliis, Staphylococcus aureus, Salmonella typhimurium,* and *Pseudomonas aeruginosa* [49].

Many researchers have been focusing on chitosan from black soldier fly (BSF), *Hermetia illucens*. Teo *et al.* found that BSF chitosan could restrict bacterial growth at concentrations of

0.25% or 0.5%, with the two most susceptible species being identified as *Pseudomonas aeruginosa* and *Serratia marcescens* [79]. Lagat also revealed that BSF chitosan concentrations of 2.5 and 5 $g \cdot mL^{-1}$ significantly inhibited the growth of *Escherichia coli, Bacillus subtilis, Pseudomonas aeruginosa, Staphylococcus aureus* and *Candida albicans* [80]. Anna *et al.* revealed that chitosan from different biomasses (larvae, pupal exuviae and dead adults) of BSF had a good antimicrobial ability both against Gram-negative and Gram-positive bacteria species [81]. Because of antibacterial activity, insect chitosan has been considered to use in the textile field and food packaging. Parag *et al.* used BSF chitosan as a finishing agent for polyester fabrics using citric acid as a cross-linking agent [165].

Malm *et al.* have confirmed that chitosan from *Acheta domesticus* and *Gryllodes sigillatus* effectively inhibited *Escherichia coli* and *Listeria innocua*. And their antimicrobial activity against *Escherichia coli* was more effective at higher DDA values, compared to shrimp chitosan [63]. Chitosan from three species of American cockroach, *Periplaneta american*, the German cockroach, *Blattella germanica* and the Mealworm beetle, *Tenebrio molitor* were investigated for their anti-bacterial properties. Results showed that the anti-bacterial influence of the chitosan is based upon the insect species and chitosan concentration, the American cockroach chitosan at a concentration of 1% had the greatest effect on *Proteus mirabilis*, while German cockroach chitosan at a concentration of 0.01% had the greatest effect on *Klebsiella pneumoniae* [113]. Hamidreza *et al.* also confirmed that chitosans from adults and nymphs of American cockroach, *Periplaneta american*, the German cockroach, *Blattella germanica* had antibacterial and antifungal activities [97]. Chen *et al.* reported that the chitosan film from *Periplaneta americana* resisted the growth of *Serratia marcescens* and *Escherichia coli* more effectively than shrimp chitosan film did [100]. Khayrova *et al.* found that low molecular weight chitosan from *Hermetia illucens* larvae depolymerized by enzymes (*Myceliophthora thermophila* and *Trichoderma harzianum*) had significant influence on antibacterial and anti-

fungal activities [87]. Chitosan from *Hylobius abietis* was reported to have antimicrobial activity against 18 bacterial strains [166]. Nanoparticles Based on Egyptian Wasp (*Vespa orientalis*) chitosan (WCSNPs) showed the antibacterial activities against extended-spectrum beta-lactamase (ESBL)- and carbapenemase-producing *Klebsiella pneumoniae*, *Escherichia coli*, and *Pseudomonas aeruginosa*. The zeta potential indicated stable WCSNPs capable of binding to cellular membrane and increasing the cellular uptake [111]. Chitosan from banana weevils (*Cosmopolites sordidus*) revealed concentration dependent antibacterial activity against *Escherichia coli* and *Klebsiella pneumoniae* and followed with mean growth inhibition zones of 5 mm (3 $mg \cdot mL^{-1}$) and 7 mm (4 $mg \cdot mL^{-1}$) [50].

Various materials based on insect chitosan such as films, nanoparticles etc. have also been developed and in turn used for antimicrobial purposes. Chitosan-based film from two reared cricket species (*Acheta domesticus* and *Gryllodes sigillatus*) showed the potential to be used as bio-based packaging material for food and pharmaceutical applications because of good mechanical and barrier properties, and improved water resistance and light barrier characteristics [61]. Sedef *et al.* revealed that quercetin (80 $\mu g \cdot mL^{-1}$) loaded chitosan membranes from *Tabanus bovinus* corneal lenses presented antibacterial effectivity, as much as commercial gentamicin antibiotic. Quercetin loaded chitosan membranes had higher antimicrobial effect against Gram-negative bacteria (*Escherichia coli*) than against Gram-positive bacteria (*Staphylococcus aureus*). It has been shown to work with nanoparticles and adoptable to the releasing or nano-based fluidic systems for various biomedical applications [91]. Marei *et al.* prepared nanoparticles loaded with ciprofloxacin (Cipro/CSNPs) with chitosan isolated from desert locusts, beetles, honeybee exoskeletons and shrimp shells, which could inhibit the growth of *Escherichia coli*, *Bacillus thuringiensis*, Methicillin resistant *Staphylococcus aureus* (MRSA) and, *Pseudomonas aeruginosa* and showed higher antibacterial activity than nanoparticles or chitosan itself. CSNPs had highest antibacterial

activity against E. coli and MRSA with MIC varying from 0.0043 to 0.01 μg·mL^{-1} and from 0.07 to 0.14 μg·mL^{-1}, respectively. The locust chitosan-based nanoparticles had the smallest particle size 36.7 ± 3.59 nm which increased the drug penetration into the Escherichia coli bacterial cell and improve its antibacterial activity after drug loading. MIC value was 85.6% lower than the MIC of the free drug itself [37].

Table 2.7 Antibacterial activity of insect chitin and chitosan.

Insect Order	**Insect Species**	**Bacteria Strains**	**Ref.**
Coleoptera	banana weevils, *Cosmopolites sordidus*	*Escherichia coli, Klebsiella pneumoniae*	[50]
	Tenebrio molitor	*Proteus mirabilis, Klebsiella pneumoniae, Enterococcus faecalis Staphylococcus epidermidis*	[113]
	Tenebrio Molitor	*Bacillus cereus, Listeria monocytogenes, Escherischia coli, Staphylococcus aureus*	[42]
	Hylobius abietis L.	*Enterococcus faecalis, Enterobacter aerogenes, Bacillus subtilis, Streptococcus pneumonia, Vibrio parahoe molyticus, Acinetobacter baumannii, Bacillus megaterium, Bacillus cereus, Micrococcus luteus Klebsiella oxytoca, Pseudomonas aeruginosa, Shigella sonnei, Staphylococcus epidermitis wt, Staphylococcus aureus,*	[166]

		Klebsiella pneumoniae subsp. Pneumoniae, *Pseudomonas aeruginosa,* *Pseudomonas aeruginosa,* *Escherichia coli*	
	Tenebrio molitor	*Pseudomonas aeruginosa*	[41]
	Blaps lethifera, *Pimelia fernandezlopezi*	*Listeria innocua,* *Bacillus subtiliis,* *Staphylococcus aureus,* *Salmonella typhimurium,* *Pseudomonas aeruginosa*	[49]
	Tenebrio molitor	*Proteus mirabilis,* *Klebsiella pneumoniae,* *Enterococcus faecalis* *Staphylococcus epidermidis*	[113]
Dictyoptera	American Cockroach German Cockroach	*Micrococcus luteus,* *Staphylococcus aureus,* *Pseudomonas aeruginosa,* *Escherichia coli*	[97]
	American cockroach, *Periplaneta americana*	*Escherichia coli,* *Klebsiella pneumoniae,* *Staphylococcus aureus,* *Bacillus subtilis*	[101]
	Periplaneta americana	*Serratia marcescens* *Escherichia coli*	[100]
	Periplaneta americana *Blattella germanica*	*Proteus mirabilis,* *Klebsiella pneumoniae,* *Enterococcus faecalis* *Staphylococcus epidermidis*	[113]
Diptera	black soldier fly, *Hermetia illucens*	*Pseudomonas aeruginosa,* *Serratia marcescens*	[79]
		Escherichia coli, *Bacillus subtilis,*	[80]

		Pseudomonas aeruginosa, *Staphylococcus aureus,* *Candida albicans*	
		Escherichia coli, *Micrococcus favus*	[81]
		Escherichia coli, *Staphylococcus epidermidis*	[87]
	Musca domestica	*Listeria innocua,* *Bacillus subtiliis,* *Staphylococcus aureus,* *Salmonella typhimurium,* *Pseudomonas aeruginosa*	[49]
Orthoptera	*Calliptamus barbarous,* *Oedaleus decorus*	*Listeria monocytogenes,* *Bacillus subtilis,* *Salmonella enteritidis,* *Yersinia enterocolitica,* *Candida albicans*	[55]
	Acheta domesticus, *Gryllodes sigillatus*	*Escherichia coli,* *Listeria innocua*	[63]
Hymenoptera	*Vespa orientalis*	*Klebsiella pneumoniae,* *Escherichia coli,* *Pseudomonas aeruginosa*	[111]

2.5.3.3 Anticancer activity

The anti-cancer activity of insect chitosan has been demonstrated by many studies. Hasaballah *et al.* investigated the anticancer activity of chitosan nanoparticles (CNPs) from maggots of *Musca domestica, Lucilia sericata* and *Chrysomya albiceps* against human liver carcinoma (HepG-2) and human colon carcinoma (HCT-116) cell lines. Their anticancer activities in both tested cell lines were found highly effective and concentration dependent, the highest anticancer activity was recorded at the concentrations of 80, 90 and 100 $\mu g \cdot mL^{-1}$, and

median inhibitory concentrations (IC50) values were in the range of 37.3 to 74.3 $\mu g \cdot mL^{-1}$ [167]. Tan *et al.* revealed that the effects of chitosan have varied depending on cell types, concentration, and chitosan derivatives. At concentrations below 250 $\mu g \cdot mL^{-1}$, mayfly and commercial chitosan with low and medium M_w exhibited strong inhibitory activity on cancer cells (A549 and WiDr cells). Mayfly chitosan induced early and late apoptosis in A549 cells, but late apoptosis and necrosis in WiDr cells [118]. Mahboub *et al.* investigated the anticancer activity of chitosan prepared from the American cockroach against Hepatoblastoma (HepG2) and Breast cancer (MCF7) cell lines by the MTT assay. The cytotoxicity was found a positive relationship with the chitosan concentration and the IC50 were 329 and 195 $\mu g \cdot mL^{-1}$ with HepG2 and MCF7, respectively [168].

2.5.3.4 Wound management

Chitosan from different sources has been widely utilized in various forms, including wound dressings, gels, films, and sponges, to support the wound healing process due to its unique properties of hemostatic, anti-inflammatory, antimicrobial, biocompatibility, biodegradability, and promotion of granulation tissue formation [169, 170]. The wound healing activity of insect chitosan-based biomimetic nanofibers have been reported in some studies. Jiang *et al.* mixed chitosan from *Eupolyphaga sinensis* with polyvinyl alcohol (PVA) and polyethylene oxide (PEO) to create a novel electro spun nanofiber membrane, which activities of accelerating wound healing and collagen regeneration were verified with a rat full-thickness skin defect model. The structure of membrane like the extracellular matrix provides a suitable environment for soft tissue regeneration, which could promote cell growth. It could be used as a carrier for delivering various drugs and active substances or to develop new wound dressings [95]. Marei *et al.* confirmed the biocompatibility and function on accelerating wound healing of chitosan from desert locust (*Schistocerca gregaria*) with *in vitro* and *in vivo* models. Compared to shrimp chitosan, insect chitosan showed earlier granulation as well as dermis

active angiogenesis with a significantly higher count with early marked epithelization and formation of thicker epidermis with minimal inflammation [171].

2.5.3.5 Drug delivery

Chitosan from different sources has been engineered into different types of drug carriers such as nanoparticles, microspheres, membranes, sponges and rods, and used in the design of many for various administration routes such as oral, buccal, nasal, transdermal, parenteral, vaginal, cervical, intrauterine and rectal [172-174]. For the drug delivery activity of insect chitosan, some studies have been reported. Magdalena *et al.* reported that chitosan from crickets was used with alginate for preparation of polymer capsules, which can be applied for the delivery of nisin. Compared to alginate-based capsules, chitosan/alginate-base capsules had two times longer period of release time, indicating a possibility of achieving an extended-release profile of an active substance is a big advantage of the developed systems. Due to the electrostatic interactions between OH^- and COO^- ions, the release was significantly more effective in alkaline solutions [175]. It was predicted that biomaterials based on insect chitosan could be used in medicine as a carrier for various agents for their biocompatibilities.

2.5.3.6 Other biomedical applications

In addition to those listed above, insect chitosan has other biological activities such as antiviral, anti-inflammatory, hypolipidemic and so on. Mahboub *et al.* reported that CNPs from American cockroaches (*Periplaneta americana*) protected the Vero cells from the cytopathic effect of adeno-40 and coxsackie B4 viruses. At the concentration of (80 $\mu g \cdot mL^{-1}$), CNPs substantially reduced adenovirus infectivity titer to 4.2 log (10)/0.1 mL ($p < 0.05$) and coxsackie B4 virus infectivity titer to 4.4 log (10)/0.1 mL ($p < 0.01$). The reduction percentages were about 5 and 26 for adeno-40 and coxsackie B4 viruses, respectively [101]. Son *et al.* revealed that chitosan from Mealworm (*Tenebrio molitor*) had notable NO reduction effect in the LPS-

induced RAW 264.7 cell line assay, and its efficacy was relatively higher than chitosan obtained from other animal sources [40]. Malm *et al.* revealed that chitosan from the house cricket (*Acheta domesticus*) and tropical banded cricket (*Gryllodes sigillatus*) both showed similar ($p > 0.05$) lipid-binding capacity to that of shrimp chitosan. And varying the DDA had no effect on chitosan's lipid-binding capacity [63]. Insect chitosan's biocompatibility, biodegradability, and various biological activity, combined with its ability to support tissue regeneration and controlled drug release, make it a valuable material in a range of biomedical applications. Its versatility continues to drive innovation in the field of healthcare and biotechnology.

2.6 Research objectives and content

According to the literature survey presented above, the increasing demand for chitin and chitosan, driven by their wide-ranging applications in various industries, necessitates the exploration of new and sustainable sources. Traditional sources such as seafood waste, while abundant, may not be sufficient to meet future demands or address environmental sustainability concerns. This thesis aims to investigate alternative sources of chitin and chitosan from insects, particularly invasive species and underutilized arthropods, and to explore their potential applications in environmental remediation and biomedical fields. By addressing the challenges of extraction, characterization, and application, this research seeks to contribute to the development of sustainable practices and innovative materials, offering new insights into the utilization of these biopolymers. In Chapter 4, we explore the potential of 11 different species as the source of chitin and chitosan. These include nine species belonging to Curculionidae family, *Heteronitis castelnaui* belonging to Scarabaeidae family, and *Eurycantha calcarata* belonging to Lonchodidae family. And all the extracted chitin and prepared chitosan were characterized to determine its suitability for further applications.

The increasing concern over the environmental impact of organic dyes, particularly from industries such as textiles and printing, underscores the need for efficient removal strategies [176-180]. While chitin and chitosan have been widely studied for their applications in wastewater treatment, the use of insect-derived chitosan remains relatively underexplored. In Chapter 5, this thesis investigates the production of chitosan from the exoskeletons of *Heteronitis castelnaui*, and its application in the adsorption of methylene blue (MB) and methyl orange (MO) dyes. Through a series of chemical treatments, high-quality chitosan was obtained and fully characterized. The study also examines the formation of hydrogels from the extracted chitosan and evaluates their dye adsorption capacity through batch experiments. This work contributes to the exploration of novel, sustainable sources of chitosan and their potential application in addressing environmental challenges associated with organic dye pollutants.

3D bioprinting represents a frontier in tissue engineering and regenerative medicine, however, research on chitosan-based materials for this purpose, especially insect chitosan, is insufficient. Chapter 6 explores novel insect source by investigating the preparation of chitosan from *Eurycantha calcarata*, and its subsequent use in 3D bioprinting. The study involves a comprehensive characterization of the extracted chitosan and the development of a hydrogel suitable for 3D bioprinting. Rheological properties and cytocompatibility are focused on, with the aim of demonstrating the printability and biocompatibility of the prepared scaffolds. This research provides a foundation for future studies on chitosan-based materials in advanced biomedical applications and emphasizes the potential of natural sources in enhancing biocompatibility.

Chapter 3 Materials and methods

3.1 Materials

Sodium hydroxide (NaOH), hydrochloric acid (HCl, 37 wt.%) and sodium tripolyphosphate (TPP) were purchased from Thermo Fisher Scientific. Hydrogen peroxide (H_2O_2, 30 wt.%), sodium alginate (SA), calcium chloride ($CaCl_2$) and methyl orange (MO, $C_{14}H_{14}N_3NaO_3S$) were purchased from Sigma-Aldrich. Sodium hypochlorite (3.6 wt.%) was purchased from Colgate. Methylene blue (MB, $C_{16}H_{18}N_3CIS{\cdot}3H_2O$) was obtained from REACTIFS RAL-Bordeaux Technopolis. RPMI medium 1640 - GlutaMAXTM, fetal bovine serum (FBS), MEM Non-Essential Amino Acid solution (100X) (NEAA), sodium pyruvate (100 mM), penicillin-streptomycin, live/dead cell staining kit are purchased from Thermo Fisher Scientific. All water mentioned was MilliQ water (resistivity ≥ 18.2 MΩ·cm).

Table 3.1 Studied insect species.

Studied species	**Descriptor**
Eupholus cuvieri	Guérin-Méneville, 1830
Eupholus magnificus	Kirsch, 1877
Lixus albicornis	Fairmaire, 1904
Lixus gigas	Fairmaire, 1904
Lixus sturmii	Boheman, 1835
Holonychus saxosus	Coquillet, 1859
Pachyrhynchus reticulatus	Waterhouse, 1841
Pachyrhynchus gemmatus	Kraatz, 1888
Sipalinus gigas	Fabricius, 1775
Heteronitis castelnaui	Harold, 1865
Eurycantha calcarata	Lucas, 1869

All the studied insect species are listed in Table 3.1. All *Curculionidae* specimens come from the private collection of G. Godeau. Samples of dung beetle *Heteronitis castelnaui* come from O. Montreuil collections. Samples of *Eurycantha calcarata* were collected from Parc Phoenix (405, Promenade des Anglais, 06200 Nice, France). All observations were performed on dried specimens. No specimens were sacrificed for the present work.

3.2 Preparation of chitin and chitosan

3.2.1 Chitin extraction (For Chapter 4)

Demineralization: This step eliminates mineral constituents present in the material. Dry samples of all the species were hydrated by immersing them in a 1M HCl aqueous solution. The resulting mixture was heated at 95°C for 2 hours. The liquid phase was then removed, and the remaining exoskeleton material was rinsed with water until it reached a neutral pH. After rinsing, the demineralized exoskeleton material was used for the deproteination step without any additional purification or drying procedures.

Deproteination: The purpose of this step is to remove proteins and other organic components inherent in the material. The exoskeleton was deproteinated by immersing it in a 2M NaOH aqueous solution, which was heated to 95°C and maintained at this temperature for 36 hours. The solution turned black during the treatment, so the NaOH solution was refreshed every hour during the first 6 hours to address this issue. Following the 36-hour deproteination period, the liquid phase was removed, and the exoskeleton material was rinsed with fresh water until a neutral pH was achieved. The deproteinated exoskeleton was then used directly in the subsequent step without undergoing any further purification or drying procedures.

Bleaching: The exoskeleton was bleached using a bleaching solution at room temperature for 1 hour with the aim to further purify the material. For the different samples of *Curculionidae* specimens, *Heteronitis* and *Eurycantha* specimens, different bleaching solutions including

sodium hypochlorite (3.6 wt.%), hydrogen peroxide (30 wt.%) were used in this step. Then the bleached exoskeleton was thoroughly washed with water and acetone to remove any residual bleaching agents or byproducts. Finally, the washed exoskeleton was dried in an oven at a temperature of 60 °C until it reached a constant weight.

The solid material obtained following these three steps is referred to as chitin and is employed directly in the subsequent deacetylation process without undergoing any additional purification.

3.2.2 Chitin deacetylation (For Chapter 4)

This process facilitates the conversion of chitin into chitosan by the removal of acetyl groups. The dry chitin was rehydrated in an aqueous NaOH solution (50 %, w/w). The solution was then heated at 95 °C overnight. The liquid phase was removed, and the solid was washed with fresh water until reaching a neutral pH. The deacetylated chitin (chitosan) was then washed with acetone and dried in an oven at 60 °C. For the treatment of *Heteronitis* specimens and *Eurycantha* specimens, the step of bleaching followed the step of deacetylation.

3.2.3 Preparation of hydrogels (For Chapter 5 and Chapter 6)

Dung beetle (*Heteronitis castelnaui*) chitosan/alginate (DCA) hydrogel was prepared as follows. 300 mg of dung beetle chitosan (DC) was dissolved in 10 mL of 2 % acetic acid (final concentration: 3 % w/v) at 40 °C using an ultrasonic bath. 300 mg of SA was dissolved in 10 mL of water at 40 °C using an ultrasonic bath. Then, chitosan and SA solutions were mixed with volume ratios of 1:1. The samples were cross-linked with 0.5 M $CaCl_2$ solution for 20 min and then washed with deionized water 3 times to remove unbound $CaCl_2$. The prepared DCA hydrogel were kept at room temperature without cover for one night to obtain the final hydrogel.

Chitosan/gelatin hydrogel was prepared as follows. 600 mg of chitosan was dissolved in 20 mL of 2% acetic acid aqueous solution (chitosan final concentration: 3 % w/v) at 40°C using

an ultrasonic bath. After complete dissolution, the warm solution was filtered. The solution's pH was then systematically increased to 4.7 using a 0.5M aqueous solution of NaOH. 3,6 g of gelatin was dissolved in 20 mL of water at 40°C using an ultrasonic bath. After total dissolution, the warm solution was filtered. DC solution was mixed with gelatin solution at a ratio of 1: 3 (DCG hydrogel). *Eurycantha* chitosan (EC) solution was mixed with gelatin solution at different ratios of 1:3, 1:4 and 1:5 (ECG hydrogel). The mixture pH was increased to 6 by addition of 0.5M aqueous solution of NaOH added drop by drop.

3.3 Characterization

3.3.1 Scanning electron microscopy (SEM)

SEM observations were carried out using Phenom Pro X Desktop SEM from Thermo Fisher Scientific. Samples were observed with gold coating at an accelerating voltage of 5 and 10 kV. The samples were coated using Quorum Q150R S Sputter Coater.

3.3.2 Fourier transform infrared (FTIR) spectroscopy

Infrared spectroscopy was carried out using a Spectrum Two FTIR spectrometer from Perkin Elmer with universal ATR accessory. The measurements were performed between 4000 cm^{-1} and 500 cm^{-1}.

3.3.3 Elemental analysis

Elemental analyses were carried out on an elemental analyzer Flash EA 1112 series (Thermo Finnigan), equipped with Eager Xperience software.

3.3.4 X-ray diffraction (XRD)

XRD was examined by a Panalytical X'Pert Pro with an Xcelerator fast detector operating at 45 kV and 30 mA. The radiation was generated from a Cu Kα (k = 0,15418 nm) source. The diffraction data were collected at 2h values from 2θ =5° to 75°. In an XRD experiment, X-rays are incident on a sample at an angle θ. Bragg's Law: $n\lambda = 2d\sin\theta$,w*h*ere: n is the order of diffraction (usually 1), λ is the wavelength of the X-rays, d is the spacing of the crystal planes, θ is the angle between the incident ray and the crystal plane. Experimental equipment (e.g., XRD instruments) typically fixes the X-ray source and rotates the sample and detector to record the diffraction intensity. Therefore, the angle recorded by the detector is the angle between the incident and diffracted light, i.e., 2θ, and so the angle of diffraction on the XRD pattern is also labeled with 2θ.

The crystallinity index of isolated chitosan samples (CrI) was calculated from XRD data using the following equation [36]:

$$CrI = [(I_{cr}-I_{am})/I_{cr}]*100 \quad (3.1)$$

where I_{cr} is the maximum intensity for crystalline lattices at 2θ = 19.6° for both chitosan and chitin and I_{am} is the maximum intensity at 2θ = 12.6° for chitosan or 2θ = 16° for chitin, corresponding to the amorphous region of both species.

3.3.5 Thermogravimetric analysis (TGA) and differential scanning calorimetry (DSC)

TGA and DSC measurements were performed simultaneously on a STA449 F5 Jupiter ECO from Netzsch. The testing parameters for different samples are summarized in Table 3.2.

Table 3.2 TGA and DSC testing conditions.

Samples	Parameters			
	Temperature range (°C)	**Heating rate ($°C \cdot min^{-1}$)**	**Nitrogen flow rate ($mL \cdot min^{-1}$)**	**waiting time with air atmosphere (h)**
Curculionidae Chitin	25 - 850	10	50	4
Dung beetle (*Heteronitis castelnaui*) chitosan, DCG hydrogels, ECA hydrogels, ECG hydrogels	35 - 650	20	50	4
Eurycantha chitosan	35 - 850	20	50	4

3.3.6 H^1 NMR Characterization (For Chapter 4)

H^1 NMR analysis of *Heteronitis* chitosan and *Eurycantha* chitosan was performed on a Brucker 400 MHz, using CF_3COOD as solvent. The NMR chemical shifts are reported in ppm. The deacetylation degree was determined following a previously reported method by comparing signals from acetylated and deacetylated glycosamine units and estimates deacetylation degree (DDA) as follows [181]:

$$DDA = [H1\text{-}D/(H1\text{-}D + H\text{-}Ac/3)]*100 \quad (3.2)$$

where H1-D is the integration of the proton H^1 of deacetylated saccharide and H-Ac is the integration of the peak of the three protons of acetyl group.

3.3.7 Deacetylation degree titration (For Chapter 4)

Dried chitosan samples were dissolved in 0.1 M HCl solution. Once the chitosan was completely dissolved, the solution was titrated with a 0.1 M NaOH solution. The pH value was

monitored using a pH-meter (Seven Compact™, Mettler Toledo). Deacetylation degree of chitosan was calculated using the following formula [182]:

$$\text{DDA (\%)} = 2.03* \frac{V_2-V_1}{m+0.0042*(V_2-V_1)} \quad (3.3)$$

where m is the sample mass (g), V_1 and V_2 are volumes of NaOH solution corresponding to the deflection points respectively for HCl and chitosan hydrochloride, 2.03 is a coefficient resulting from the molecular weight of chitin monomer unit and 0.0042 is a coefficient resulting from the difference between molecular weights of chitin and chitosan monomer units.

3.3.8 Rheological measurements (For Chapter 6)

Rheological measurements of ECG hydrogels were conducted using MCR502 (Anton Paar) rheometer in parallel plate geometry (PP40/TI, plate radius of 2 cm). A solvent trap was used to prevent solvent evaporation during measurement. Storage (G′) and loss (G″) moduli were measured in a linear viscoelastic regime (strain amplitude $\gamma = 0.5\%$, oscillation frequency f = 1 Hz) as function of temperature imposed on the lower rheometer plate using an integrated Peltier element. The duration of measurements was adjusted so that the moduli achieved their steady state value (with an error of ± 5%) at each tested temperature. The viscosity was measured in a shear rate control mode imposing a continuous shear rate ramp from 10 s^{-1} to 100 s^{-1}.

3.4 Protocol of adsorption (For Chapter 5)

All batch adsorption experiments were executed by adding 30 mg dried hydrogels and 30 mL adsorbate solution in a 50 mL polypropylene centrifuge tube, on an orbital shaker (Fisher Bioblock Scientific) operating at a desired time and a fixed speed (150 rpm) at room temperature. All adsorption experiments were repeated at least three times, and standard errors were calculated.

3.4.1 Determination of adsorbate concentration

The typical cationic MB dye and anionic MO dye were selected to evaluate the adsorption capacity of prepared hydrogels. A series of MB and MO standard solutions were prepared with known concentrations ranging from 0.1 mg·L^{-1} to 10 mg·L^{-1}. The absorbance values (Abs.) of the absorbed light (in UV-visible spectrum) passing through the MB solutions and MO solutions were determined with a UV-Vis spectrophotometry (Shimadzu-UV-1800) at the wavelengths of 658 and 466 nm, respectively. Then the concentration and Abs. data were fitted using the instrument's operating software to generate a standard curve. The concentration of an unknown MB solution and MO solutions can be determined using this standard curve. In cases where the concentration of the adsorbate exceeds the range covered by the standard curve, dilution is required before conducting the measurement.

3.4.2 Calculation of adsorption capacity

The dye adsorption capacity (q_e) of the hydrogels were calculated according to the following equation (3.4) while the adsorption capacity at a specific timepoint was computed by the Equation (3.5) :

$$q_e = \frac{(C_0 - C_e)\, V}{m} \tag{3.4}$$

$$q_t = \frac{(C_0 - C_t)\, V}{m} \tag{3.5}$$

where, q_e (mg·g $^{-1}$) is the equilibrium adsorption capacity; C_o and C_e represent the initial and equilibrium concentrations of adsorbate (mg·L^{-1}), respectively; V (L) and m (g) stand for the volume of adsorbate solution and the weight of adsorbent; q_t (mg·g^{-1}) and C_t (mg·L^{-1}) represent the adsorption capacity and adsorbate concentration at a specific time t (min).

3.4.3 Adsorption kinetics

Adsorption kinetic data were obtained by measuring the adsorption capacities as a function of time. Dried DCA hydrogel samples (30 mg) were immersed in tubes containing aqueous dye solutions (30 mL) with MB concentration of 1000 $mg \cdot L^{-1}$ at pH 12. On the other hand, dried DCG hydrogel samples (30 mg) were immersed in tubes containing aqueous dye solutions (30 mL) with MO concentration of 800 $mg \cdot L^{-1}$ at pH 5. Next, these tubes were placed on an orbital shaker (Fisher Bioblock Scientific) operating at room temperature.

Based on adsorption kinetics, the rate of adsorbate uptake can be quantified, enabling the prediction of the necessary retention time for the adsorption process. The adsorption process can be conceptually divided into three distinct steps, each corresponding to a phase of the adsorbate's movement and interaction with the adsorbent: (i) external diffusion, where the adsorbate diffuses through the boundary layer or liquid film surrounding the adsorbent; (ii) intra-particle diffusion, where the adsorbate migrates within the internal structure of the adsorbent; and (iii) adsorption at active sites, where the adsorbate molecules reach and interact with the active sites on the adsorbent surface, either undergoing adsorption or desorption [183]. To model these adsorption processes, the pseudo-first-order and pseudo-second-order kinetic models are frequently employed. These models effectively describe scenarios where the rate-determining step is the interaction between the adsorbate molecules and the active sites on the adsorbent.

The pseudo-first-order kinetic model was first proposed by Lagergren and can be expressed using the following equations [184]:

$$q_t = q_e \, (1\text{-}e^{-k_1 t}) \tag{3.6}$$

The pseudo-second-order model, developed by Ho et al., is an extension of the pseudo-first-order model. This model was specifically designed to describe adsorption processes under

conditions of (i) low adsorbate concentration, (ii) the final stages of adsorption, and (iii) an abundance of active sites on the adsorbent. It has been widely adopted to more accurately depict the kinetics of adsorption at active sites, particularly in scenarios where the interaction between the adsorbate and the adsorbent's active sites is the rate-determining step. The pseudo-second-order kinetic model can be described as following equations [185]:

$$q_t = \frac{k_2 q_e^2 t}{1 + k_2 q_e t} \tag{3.7}$$

where q_t (mg·g^{-1}) and q_e (mg·g^{-1}) are the adsorption capacity at time t (min) and at equilibrium, respectively; k_1 (min^{-1}) and k_2 (mg^{-1}·g·min^{-1}) are the first-order and the second-order adsorption rate constants, respectively.

3.4.4 Adsorption equilibrium

Dried DCA hydrogel samples (30mg) were immersed in tubes containing aqueous dye solutions (30 mL) with MB concentration range of 100 mg·L^{-1} to 1800 mg·L^{-1} at pH 12 during 24 h. Dried DCG hydrogel samples (30 mg) were immersed in tubes containing aqueous dye solutions (30 mL) with MO concentration range of 100 mg·L^{-1} to 1000 mg·L^{-1} at pH 5. Next, these tubes were placed on an orbital shaker (Fisher Bioblock Scientific) operating at room temperature.

The adsorption equilibrium is quantified in terms of adsorption isotherms: dependencies of the equilibrium adsorption capacity q_e on the free (non-adsorbed) adsorbate concentration C_e. The adsorption isotherm models describe the relationship between solute concentrations in the two phases at equilibrium at a given temperature. Different combinations of adsorbents and adsorbates result in unique adsorption isotherms, reflecting the characteristics of the adsorbent and the nature of interactions with the adsorbate. The Langmuir and Freundlich models are commonly used to describe these isotherms.

Langmuir adsorption isotherm, formulated by Langmuir in 1916, is grounded in a theoretical framework assuming monolayer adsorption on a uniform surface, with no interactions between adsorbed molecules, and that the adsorption process is in dynamic equilibrium. The Langmuir isotherms are presented by the following equation [186]:

$$q_e = \frac{K_L q_m C_e}{1+K_L C_e} \tag{3.8}$$

On the other hand, the Freundlich isotherm is an empirical model proposed by Freundlich in 1907, which describes adsorption on heterogeneous surfaces. Unlike the Langmuir model, the Freundlich model allows for multilayer adsorption and assumes that the heat of adsorption and the affinity between the adsorbent and adsorbate are not uniform, resulting in a non-uniform arrangement of adsorbate molecules on the adsorbent surface. The Freundlich isotherms are presented by the following equations [187]:

$$q_e = K_F C_e^{1/n} \tag{3.9}$$

in which q_m is the maximum Langmuir adsorption capacity ($mg \cdot g^{-1}$), K_L is the Langmuir constant related to adsorption free enthalpy ($L \cdot mg^{-1}$), and C_e is the equilibrium adsorbate concentration ($mg \cdot L^{-1}$); K_F ($mg^{1-1/n} \cdot L^{1/n} \cdot g^{-1}$) is the Freundlich constant related to adsorption capacity, and $1/n$ is the Freundlich exponent related to adsorbent surface heterogeneity.

3.4.5 Adsorption thermodynamics

In the evaluation of adsorption systems, it is essential to consider both measurable and derived thermodynamic properties to fully understand the adsorption process. Directly measurable properties, such as temperature and equilibrium constants, provide a foundation for characterizing the system. However, to gain deeper insights into the adsorption mechanisms and performance, it is also important to consider properties that cannot be directly measured, such as Gibbs free energy change. These thermodynamic parameters play a critical role in predicting the behavior of adsorption systems under various conditions. By analyzing

adsorption isotherms, we can calculate these parameters using established definitions and relationships, thereby enabling a more comprehensive understanding of the system's thermodynamics. Gibbs free energy isotherm can be calculated from the adsorption isotherm, using the following definitions and relationships:

Gibbs free energy isotherm [188]:

$$\Delta G = -RT \ln K \tag{3.10}$$

Dimensionless Langmuir constant [189]:

$$K = K_L * 10^3 * M_w * C_r \tag{3.11}$$

In these equations, ΔG (kJ·mol^{-1}) is the standard Gibbs energy change; R and T are the universal gas constant (8.314 J·mol^{-1}·K^{-1}) and the temperature in Kelvin; K_L (L·mg^{-1}) is Langmuir equilibrium constant [cf. Eq. (3.8)], Cr is the standard concentration of the adsorbate, Cr = 1 mol·L^{-1} ; the factor 10^3 is for unit conversion; M_w (g·mol^{-1}) is the molar mass of adsorbate.

3.5 3D bioprinting (For Chapter 6)

3.5.1 3D printing assays

3D printing of ECG scaffolds was performed using a Bio-X bioprinter from Cellink (Boston, MA, USA). The printing was performed following an extrusion process. The cartridge was kept at room temperature, while the temperature of heated substrate and bed were kept constant at 22 °C and 10 °C, respectively. Bioprinting nozzles (22G) was used to print hydrogels (Figure 3.1).

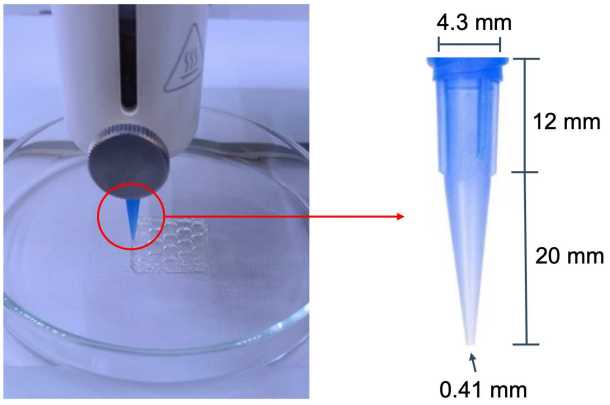

Figure 3.1 Bioprinting nozzles (22G).

Printing parameters: translational speed of the printing head (the jet flow speed) of 5 $mm \cdot s^{-1}$ and the extrusion pressure within 10 kPa were chosen to ensure proper and continuous filament formation and were kept constant throughout the study.

3.5.2 Printing accuracy characterization

The shape fidelity of the 3D printed samples was investigated for each formulation. Measurements were acquired immediately before and after the crosslinking with TPP solution, with consideration given to the dimensions of the printed samples (i.e., length and width). For each formulation considered in this study, the measurements of five samples were obtained. Regarding the fiber dimensions, the diameter of each fiber for each condition was measured at six different points and averaged. The dimensions were acquired with an optical comparator (KEYENCE IM-Series). The quantitative measurements for the different conditions were compared to the theoretical values using the following equation [190]:

$$\text{Accuracy } (\%) = \frac{100}{n} * \sum_{1}^{n} \left(1 - \frac{|d_r - d_s|}{d_s}\right) \tag{3.12}$$

where d_r is the measured sample dimension, d_s the theoretical dimension (i.e., d_s = 10 mm for length, width, n is the number of the considered samples (n = 5 × 6 different points).

3.5.3 Stability Test

Stability test was performed on the samples of different formulations to evaluate the degradation of samples after immersion in medium at 37°C. At established time points (t = 0h, 2h, 3h, 4h, 1 day, 2 days, 3 days, 7 days, 14 days, 21 days), samples were removed from the solution, gently swabbed with tissue paper and weighted. Degradation ratio was calculated with the following equation [191]:

$$\text{Degradation ratio (\%)} = (W_0\text{-}W_t)/W_0 \times 100\% \quad (3.13)$$

where, W_t is the weight of samples at a given time and W_0 is the initial weight of samples before immersed into medium.

3.5.4 *In vitro* cytocompatibility

A preliminary *in vitro* cytocompatibility test was conducted using the HeLa cell line to assess the cytocompatibility of the printed scaffolds. To prevent contamination, the gelatin and chitosan powders were sterilized by UV light for one hour. The 3D structures (10 mm × 10 mm × 5 mm) were placed in contact with HeLa cells. For each tested condition, six replicates were considered. The positive control was constituted by HeLa cells cultured in complete medium (i.e., live cells), while the negative control was constituted by HeLa cells cultured in complete medium and 0.1% Triton X-100 (i.e., dead cells), representing the optimal and the worst cells viability condition, respectively. To prepare complete medium, 500 mL RPMI medium 1640 - GlutaMAXTM was supplemented with 10% (v/v) of fetal bovine serum (FBS), 5 mL MEM Non-Essential Amino Acid solution (100X) (NEAA), 5 mL sodium pyruvate (100 mM), 5mL penicillin-streptomycin solution. 3D printed ECG scaffolds were seeded with 5×10^3 cells/well in 24-well plate and cultured in 500 µL complete medium at 37°C, 5% CO_2. Subsequently, 3 days after seeding, the viability of HeLa cells on the 3D printed ECG scaffolds was evaluated by Tecan Infinite M1000 PRO microplate reader.

After culturing for 3 days, the cell-seeded scaffolds were rinsed with phosphate buffer saline (PBS). Then, a live/dead cell staining kit (Thermo Fisher Scientific) was employed to stain the cells on the scaffolds after cultivation for 3 days. All operations were carried out according to the manufacturer's protocol. Briefly, the staining solution was prepared by mixing 2 μM of Live-Dye (Calcein-AM) and 4 μM Dead-Dye (EthD-1 solution). Then, the staining solution was evenly dripped onto the scaffold surface, which then was incubated at 37 °C for 30 min. Finally, the redundant staining solution was washed away using PBS, and the scaffold will be mounted on microscope slides for observation using an inverse fluorescence microscope (Zeiss Axiovert 200M).

Results are expressed as mean ± standard deviation. One-way ANOVA tests were performed to investigate statistical difference between experimental and control groups. A *p*-value (p) < 0.05 was considered as statistically significant. The *p*-value measures the probability of observing the results, or more extreme results, assuming the null hypothesis is true. In our study using one-way ANOVA, the null hypothesis posits that there are no differences between the experimental and control groups. A *p*-value less than 0.05 indicates that there is less than a 5% chance of obtaining the observed differences by random chance, suggesting that the differences are statistically significant and not due to random variation. If the *p*-value is greater than 0.05, the null hypothesis cannot be rejected, and no significant difference is considered.

Chapter 4 Chitin extraction and chitosan preparation from different insects[2]

In this chapter, the potential of 11 different species as the source of chitin and chitosan was investigated, which include nine species belonging to *Curculionidae* family, *Heteronitis castelnaui* belonging to Scarabaeidae family, and *Eurycantha calcarata* belonging to Lonchodidae family. Some of *Curculionidae* species are invasive insects, which pose a significant threat to agriculture due to their ability to destroy crops, represent a potential, underexplored source of chitin. The challenge lies in finding methods to extract valuable products from these species, which would not only provide new resources but also offer a strategy to mitigate the impact of invasive pests. This study aims to provide insights into the utilization of these invasive species as a sustainable source of chitin, with the potential to inform future materials development. Not all *Curculionidae* are classified as pest insects. Some are beneficial as pollinators. However, for this study we chose various *Curculionidae* species from different genus to determine best candidates for chitin extraction which can inform future strategies for materials development. *H. castelnaui*, was selected for its thick exoskeleton and unstudied chitin content. Similarly, *E. calcarata,* a large, robust insect, was chosen due to its highly developed exoskeleton, which suggests a significant chitin content, but it has also not been researched for extraction. Both species are valuable, underexplored sources of chitin-rich exoskeletons. This work includes the chitin extraction and chitosan preparation. Subsequently, a series of comprehensive characterizations were conducted on the obtained chitin and chitosan, including IR, SEM, NMR, XRD, TGA, ash content, and water content analyses.

[2] The contents of *Curculionidae* species in this chapter are published in the paper Mei, Z.; Vincent L.; Szczepanski, C. R.; Godeau, R.; Kuzhir, P.; Godeau, G. Investigation on 9 true weevil (*Curculionidae* Latreille, 1802) species for chitin extraction. *Biomimetics.* (Accepted)

4.1 Studied species

Curculionoidae also known as true weevils are one of the most diverse groups of phytophagous *Coleoptera*. More than 51,000 species belonging to approximately 4600 genera of *Curculionidae* have been described [192]. Among this wide diversity, many weevils can be described as pest insects that harm various crops or ornamental plants. For example, *Lixus* and *Sipalinus* genera are considered pests. To capture the diversity of the *Curculionidae* family, 9 species belonging to 5 genera (including *Lixus* and *Sipalinus*) were investigated in this work. With this design, both beneficial and pest insects are considered. *H. castelnaui* belonging to Scarabaeidae family*, and E. calcarata* belonging to Lonchodidae family were also studied here. The selection of *H. castelnaui* and *E. calcarata* is driven by their robust exoskeletons, which indicate substantial chitin content. Both species have not been previously investigated for chitin extraction, presenting valuable opportunities for exploring these underutilized resources. The complete list of the studied species is reported in Figure 4.1 and Table 4.1.

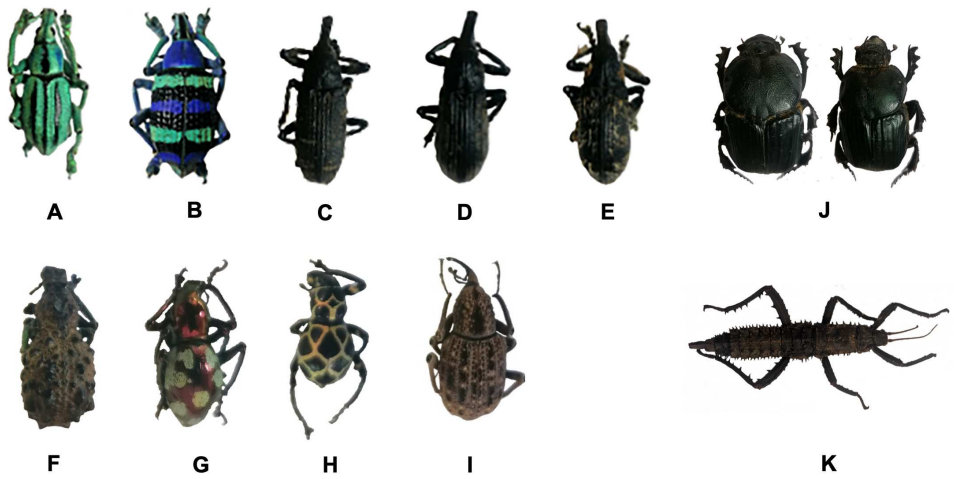

Figure 4.1 Examples of studied species. *Curculionidae* specimens: A) *Eupholus cuvieri*, B) *Eupholus magnificus*, C) *Lixus sturmii*, D) *Lixus gigas*, E) *Lixus albicornis*, F) *Holonychus saxosus*, G) *Pachyrhynchus gemmatus*, H) *Pachyrhynchus reticulatus* and I) *Sipalinus gigas*; J) *Heteronitis castelnaui*; K) *Eurycantha calcarata*.

Table 4.1 Studied species data.

Studied species	Descriptor	Specimens collection area
Eupholus cuvieri	Guérin-Méneville, 1830	Indonesia
Eupholus magnificus	Kirsch, 1877	Indonesia
Lixus albicornis	Fairmaire, 1904	Madagascar
Lixus gigas	Fairmaire, 1904	Madagascar
Lixus sturmii	Boheman, 1835	Madagascar
Holonychus saxosus	Coquillet, 1859	Madagascar
Pachyrhynchus reticulatus	Waterhouse, 1841	Philippines
Pachyrhynchus gemmatus	Kraatz, 1888	Philippines
Sipalinus gigas	Fabricius, 1775	Australia
Heteronitis castelnaui	Harold, 1865	Australia
Eurycantha calcarata	Lucas, 1869	Australasia

4.2 Chitin extraction and chitosan preparation

All the *Curculionidae* specimens were treated for chitin extraction. The selected chitin extraction strategy is the classical chemical approach described decades ago for shrimp's chitin extraction [193, 194]. It is a three-step treatment including demineralization, deproteination and bleaching as descripted in section 3.2. Between each step, the material is washed with water. The final isolated material can be reported as *Curculionidae*'s chitin.

Of course, the selected *Curculionidae* species went through the chitin extraction process separately, in order to obtain species-specific data. All the data collected at each stage of the extraction are reported in Table 4.2, including yields for demineralization, deproteination and overall.

Table 4.2 Chitin extraction data from *Curculionidae* species.

Species	Demineralization yield (%)	Deproteination yield (%)	Overall yield (%)
Eupholus cuvieri	84.7	19.9	16.7
Eupholus magnificus	85.8	22.6	19.3
Lixus albicornis	78.1	21.2	16.4
Lixus gigas	84.6	19.2	15.9
Lixus sturmii	84.9	21.2	18.0
Holonychus saxosus	84.9	18.4	15.5
Pachyrhynchus reticulatus	86.5	15.5	13.5
Pachyrhynchus gemmatus	80.6	15.2	12.1
Sipalinus gigas	94.9	16.7	15.7

The *Curculionidae* chitin extraction data mostly shows homogeneous results. The demineralization step has an associated yield between 80 and 90 %. For deproteination, the yield is roughly 15 -25 % and the overall yield is between 12 and 19 %. These values remain similar and are consistent with chitin extraction yields reported for other *Coleoptera* in the literature [45].

In addition to the chitin extraction from *Curculionidae*, we conducted independent studies on *H. castelnaui* and *E. calcarata* to evaluate their potential for chitosan preparation. After a series of processes, including demineralization, deproteinization, and bleaching, these samples underwent deacetylation. The overall yield of the final product, chitosan derived from *H. castelnaui* and *E. calcarata*, was determined to be 11.7% and 22.2%, respectively. Chitosan, represents a polymer consisting of β-(1-4)-D-glucosamine units with the presence of N-acetyl-D-glucosamine units occurring randomly (Figure 4.2). Confirmation of the successful deacetylation and removal of acetyl groups was achieved through the observation that the isolated chitosan exhibited full solubility in slightly acidic water. This solubility characteristic

serves as an indication of the absence of acetyl groups, which are responsible for the insolubility exhibited by chitin.

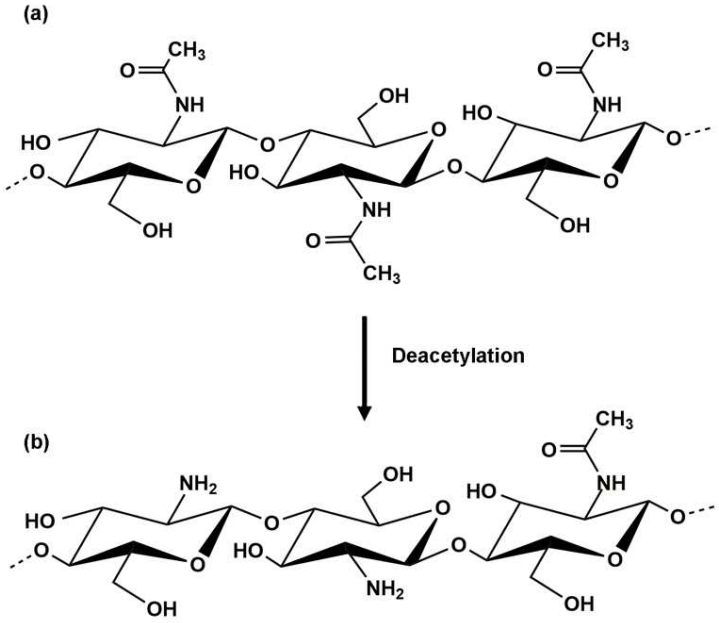

Figure 4.2 Theoretical chemical structures of (a) chitin and (b) chitosan.

4.3 SEM observation

The samples of obtained chitin and chitosan were then considered for characterisations. All treated surfaces were first investigated for their morphologies, using SEM as descripted in section 3.3.1 and compared with the corresponding virgin surfaces. Not surprisingly, depending on the species, the surface morphologies were very different. For example, some *Curculionidae* genera are known to exhibit structural coloration like *Eupholus* (Figure 4.3) and *Pachyrhynchus* (Figure 4.4).

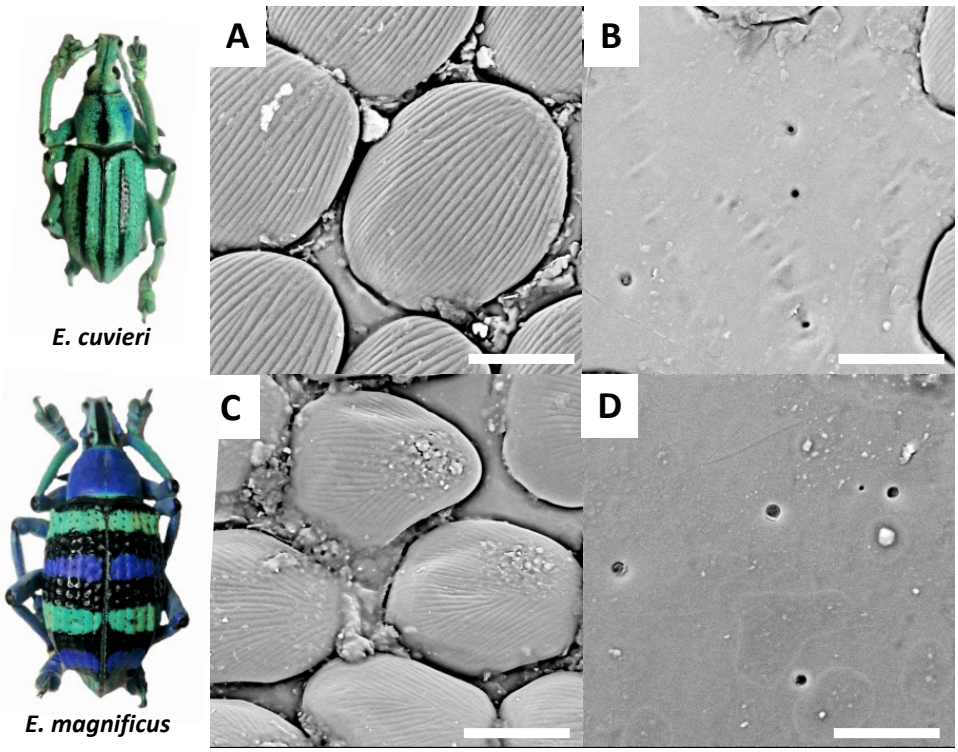

Figure 4.3 Examples of SEM images (scale bar = 30 μm) observed for raw surfaces of *E. cuvieri* (A and B), *E. magnificus* (C and D).

For both genera, the surface morphology varies across the specimen. For example, the colored parts (blue or green) of *E. cuvieri* (Figure 4.3A) and *E. magnificus* (Figure 4.3C) show nanostructured (wrinkled) microscales which contribute to the structural color, as has been previously described in the literature [195].

Not surprisingly, the black part of both species, which lacks any structural color is smooth when observed via microscopy (Figure 4.3B for *E. cuvieri* and 4.3D for *E. magnificus*). Similar microscales are observed for *P. reticulatus* and *P. gemmatus purpureus*. Here, these microscale structures correspond to the golden network present on *P. reticulatus* (Figure 4.4A) and the large green spots on *P. gemmatus purpureus* (Figure 4.4C).

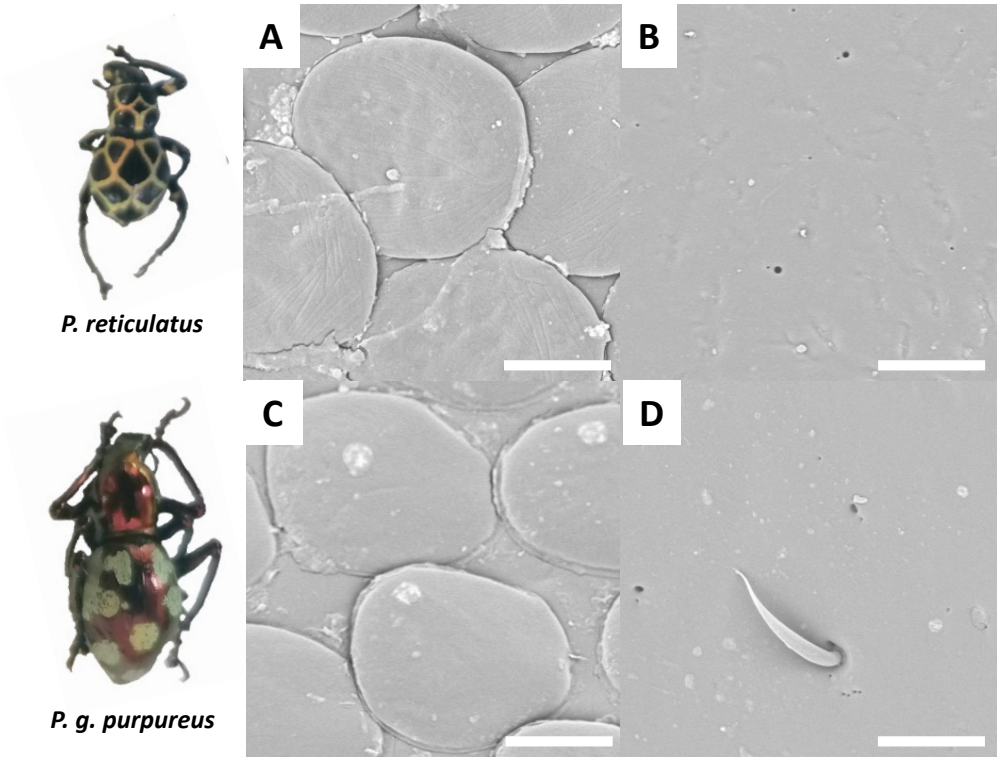

Figure 4.4 Examples of SEM images (scale bar = 30 μm) observed for raw surfaces of *P. reticulatus* (A and B) and *P. gemmatus purpureus* (C and D).

On these species a second kind of surfaces are observed, the black part of *P. reticulatus* (Figure 4.4B) and the metallic red surface of *P. gemmatus purpureus* (Figure 4.4D) may be reported as smooth compared with the previous one. Of course, the red metallic surface of *P. gemmatus purpureus* is structurally colored but the structuration remains under the surface.

For the *Lixus genus*, all species present similar surface morphologies. These surfaces are highlighted in Figure 4.5. For *Lixus species*, most of the observed surfaces are smooth, with or without hairs depending on the position imaged (Figure 4.5).

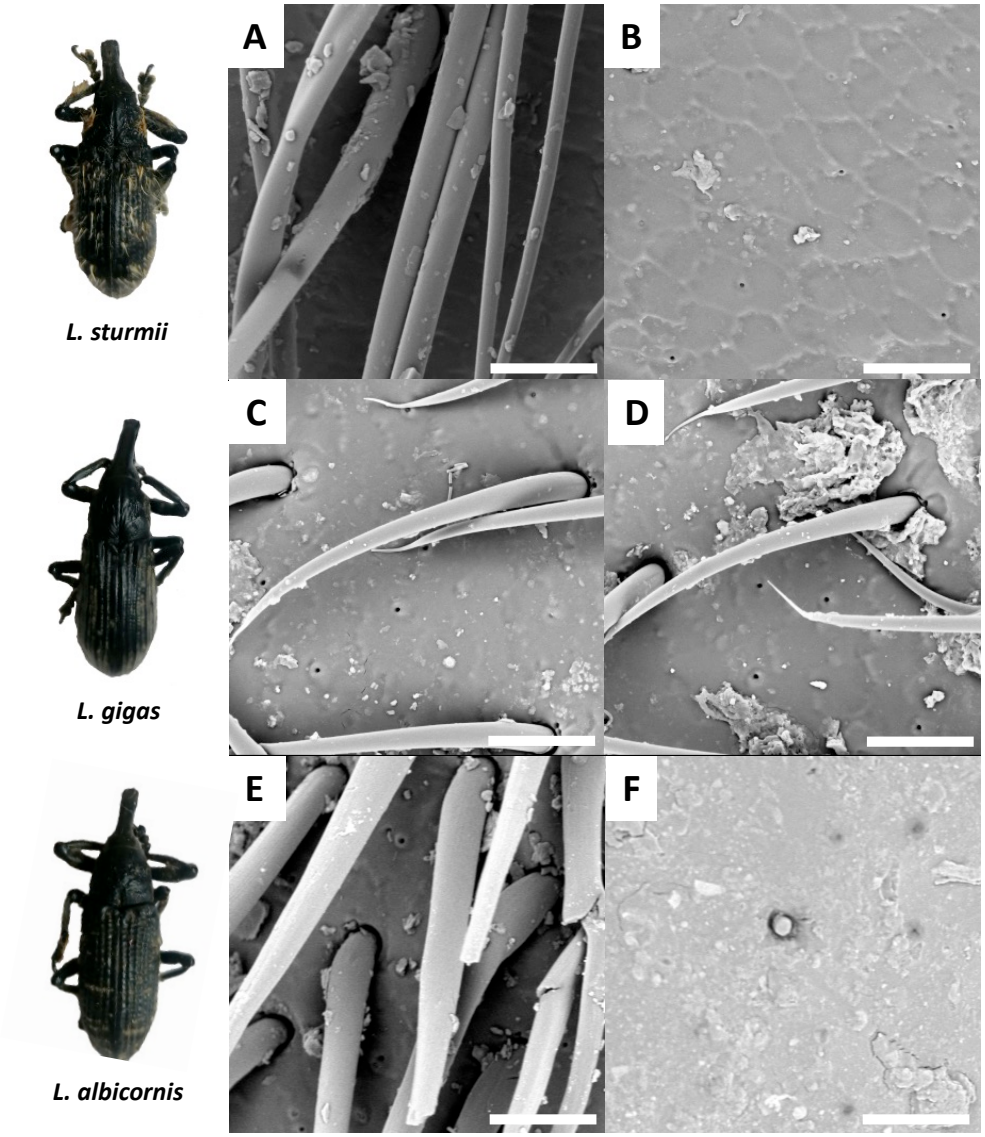

Figure 4.5. Examples of SEM images (scale bar = 30 μm) observed for raw surfaces of *L. sturmii* (A and B), *L. gigas* (C and D) and *L. albicornis* (E and F).

Observations of *H. saxosus*, which lacks any structural coloration, reveals dense microscale organizations (Figure 4.6 A and B). *S. gigas* presents surface with straightly aligned pins (Figure 4.6 C and D). This structuration appears to be quite homogeneous along the darkest surface.

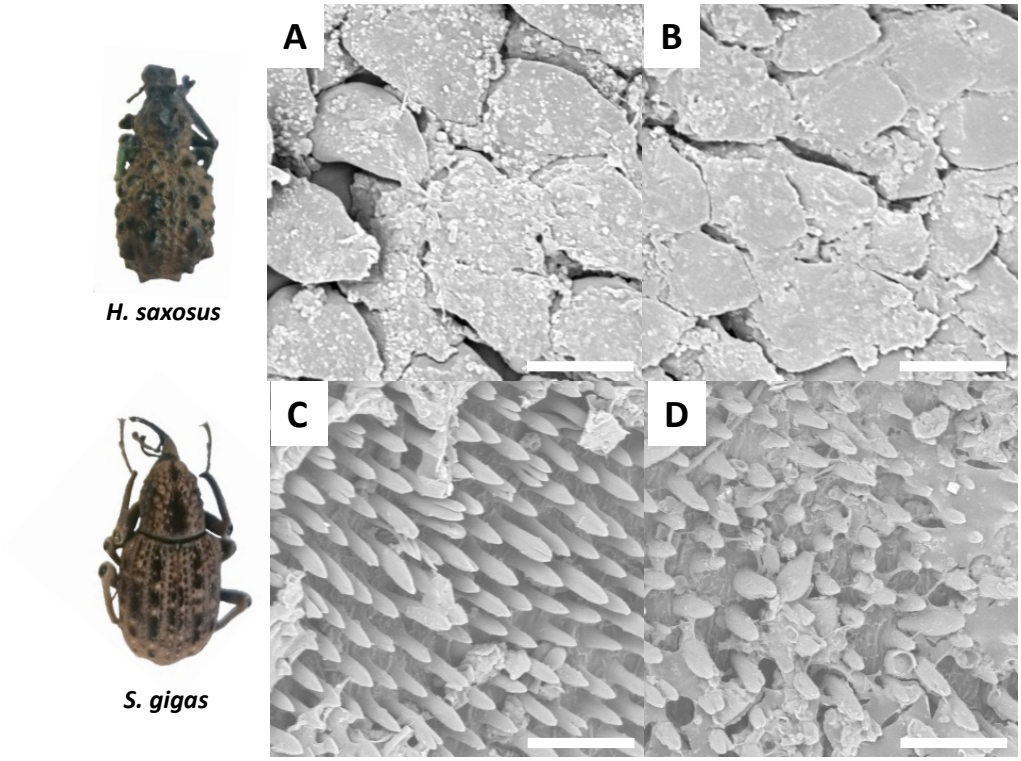

Figure 4.6 Examples of SEM images (scale bar = 30 μm) observed for raw surfaces of *H. saxosus* (A and B) and *S. gigas* (C and D).

After the treatment used to extract chitin, surfaces reveal an inner-connected chitin network (Figure 4.7-4.9). Most of the treated surfaces revealed holes instead of the microscales previously observed.

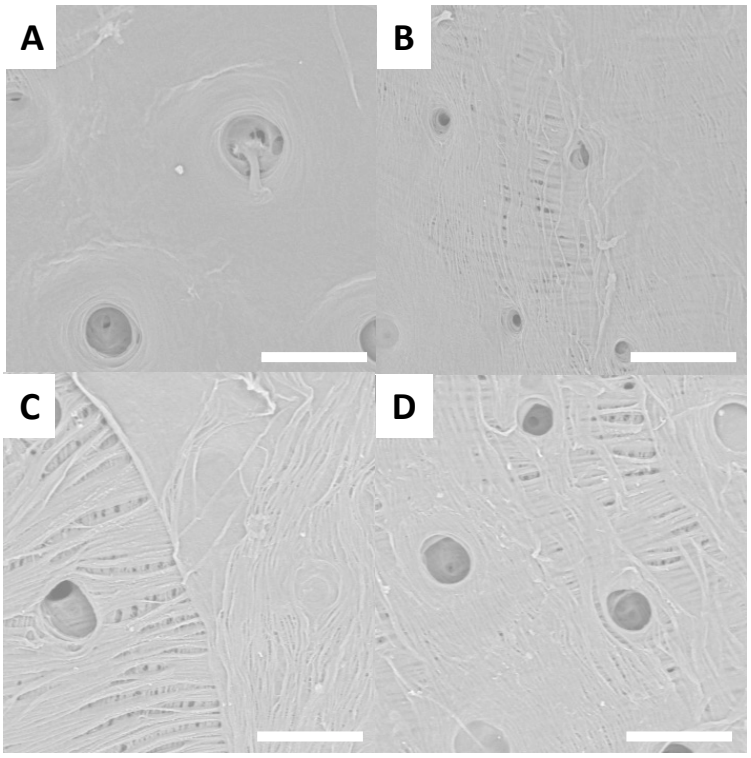

Figure 4.7 Examples of SEM images (scale bar = 30 μm) observed for treated surfaces of *E. cuvieri* (A and B), *E. magnificus* (C and D).

SEM images of *Pachyrhynchus* species treated surfaces are presented Figure 4.8A to D.

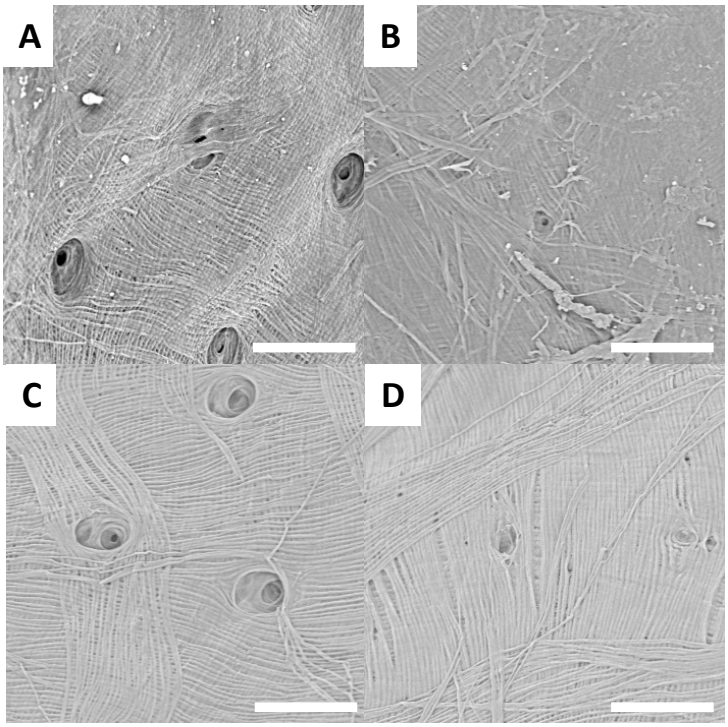

Figure 4.8 Examples of SEM images (scale bar = 30 μm) observed for treated surfaces of *P. gemmatus purpureus* (A and B) and *P. reticulatus* (C and D).

Different *Lixus* species surfaces after treatment are presented in Figure 4.9 A to F.

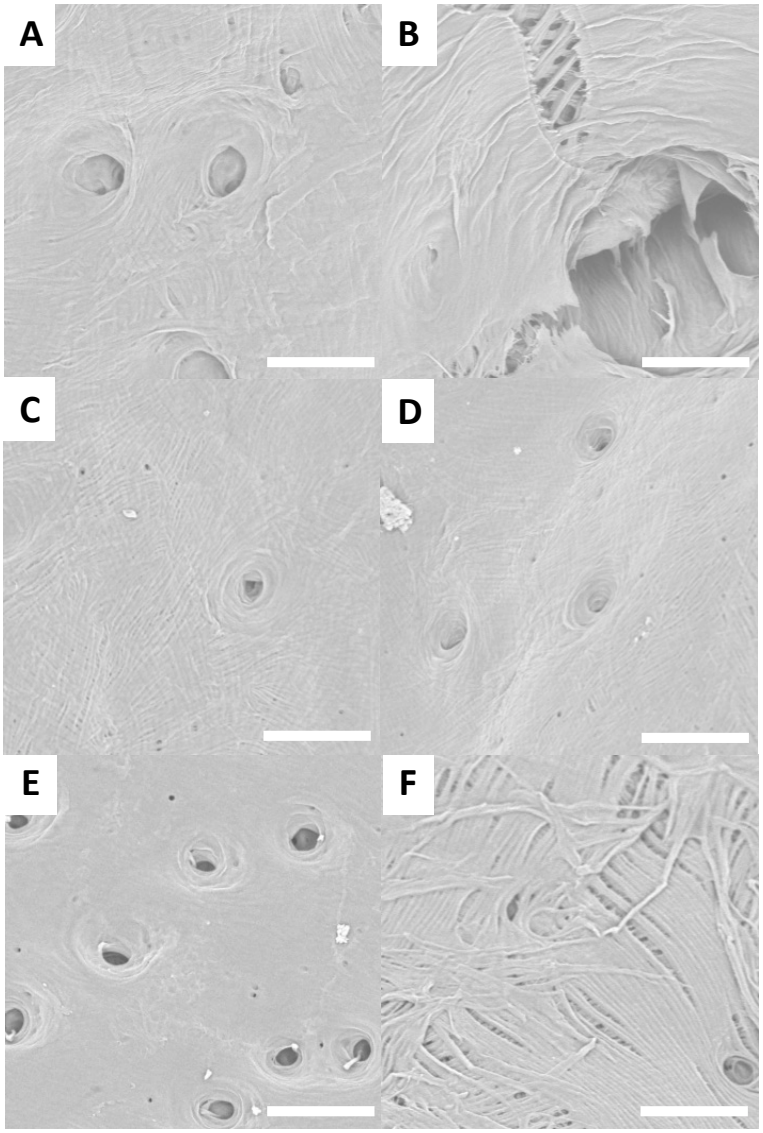

Figure 4.9. Examples of SEM images (scale bar = 30 μm) observed for treated surfaces of *L. sturmii* (A and B), *L. gigas* (C and D) and *L. albicornis* (E and F).

Treated surfaces from *H. saxosus* are presented in Figure 4.10 A and B and treated surfaces from *S. gigas* are presented in Figure 4.10 C and D.

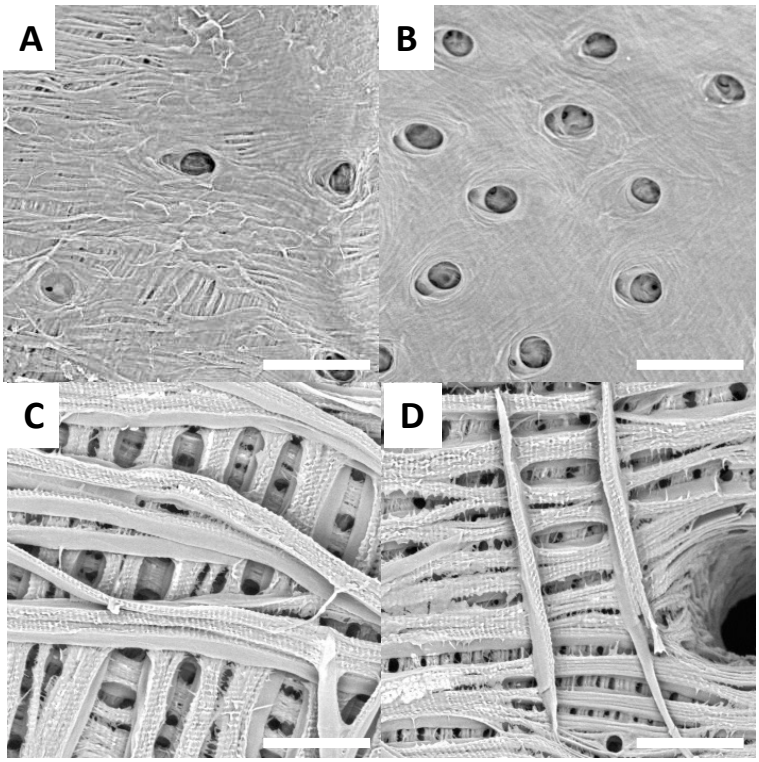

Figure 4.10 Examples of SEM images (scale bar = 30 μm) observed for raw surfaces of *H. saxosus* (A and B) and *S. gigas* (C and D).

For *H. saxosus* surface, holes are observed. For most of the treated surfaces, it is possible to consider that a fiber network is observed even if the network change from one specie to the other. All examples of SEM images observed for treated surfaces of other *Curculionidae* species are provided in the Appendix (Figure SI 1-9) at the end of the thesis.

Chitin and chitosan from *H. castelnaui* were compared here as example to show the change of surface after deacetylation (Figure 4.11). Slight roughness of the surfaces is revealed for *H. castelnaui* chitin, which likely results from the natural structural composition of the chitin matrix, which contribute to the mechanical strength and rigidity of the exoskeleton. The surface morphology did not display significant changes before and after deacetylation, indicating that the chemical treatment preserved the overall structural integrity of the chitin matrix. This consistency in morphology suggests that the deacetylation process, while effective in converting chitin to chitosan, does not significantly alter the surface features at the microscopic level. In addition, the consistency in morphology across both samples before and after

deacetylation can be further understood in the context of the biological characteristics of the *H. castelnaui*. Unlike some insects that exhibit structural coloration—a phenomenon where micro- and nano-scale surface features create iridescent colors due to light interference—*H. castelnaui* does not possess such complex surface microstructures.

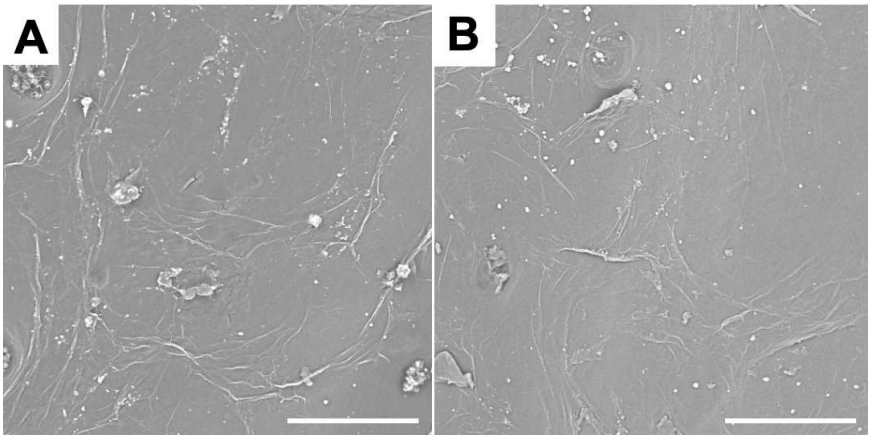

Figure 4.11 Examples of SEM images (scale bar = 80 μm) of chitin (A) and chitosan (B) from *H. castelnaui*.

For *E. calcarata*, the surfaces of raw sample and chitosan were compared here as example to show the change of surface after a series of treatments, both of them did not show significative structuration, only revealing slight roughness with some pores (Figure 4.12).

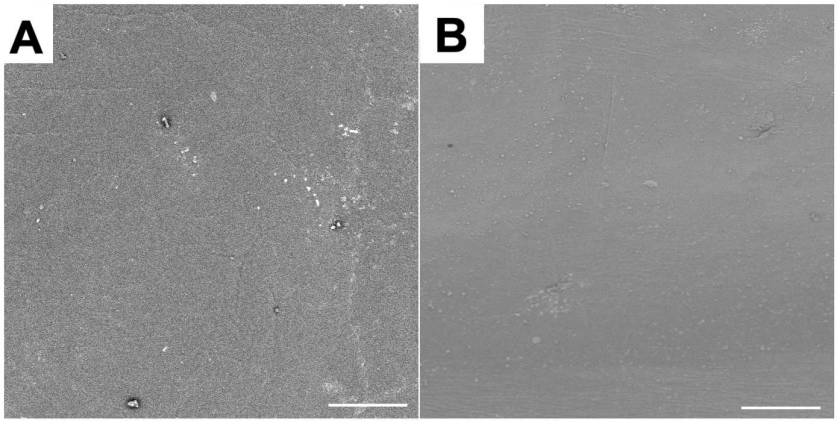

Figure 4.12 Examples of SEM images (scale bar = 100 μm) of raw sample (A) and chitosan (B) from *E. calcarata*.

These observations of *H. castelnaui* and *E. calcarata* made after treatments are not surprising, as this genus is not known for structural color.

If SEM observation reveals interesting information on observed surfaces, it remains only morphological observations. To improve surface characterization, additional experiments are needed.

4.4 FTIR spectroscopy analysis

FTIR analyses were performed on all obtained chitin and chitosan samples as descripted in section 3.3.2. Examples of FTIR spectra for extracted chitin from *Curculionidae* species are shown Figure 4.13, and all other FTIR spectra collected are provided in the Appendix supplementary data (Figure SI 10-18) at the end of the thesis.

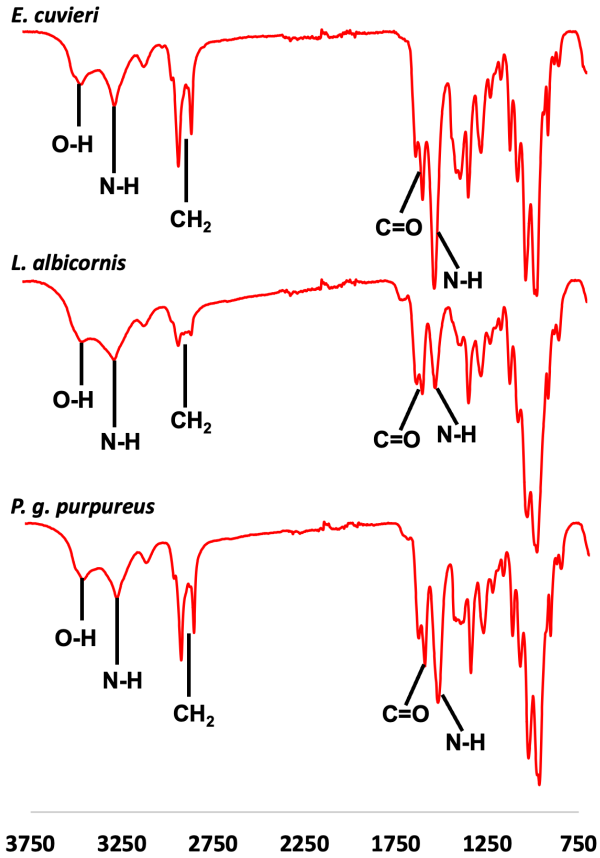

Figure 4.13 Examples of IR spectra observed for extracted chitin from *Curculionidae* specimens.

The FT-IR spectra for each extract have results consistent with chitin material and expected bands. For example, strong bands at 3380-3450 cm^{-1} and 3250-3300 cm^{-1} are observed, consistent with the stretching of O-H and N-H bonds, respectively. Additionally, a band

corresponding to sp^3 CH_2 vibration is observed at 2850-2950 cm^{-1}, and the C=O band from amide group is observed at 1635 -1660 cm^{-1}. Finally, the bending and vibration bands from N-H are observed at 1560-1580 cm^{-1}. As expected, the observed IR bands for chitin from all studied species are consistent with data reported in the literature for shrimp chitin [196].

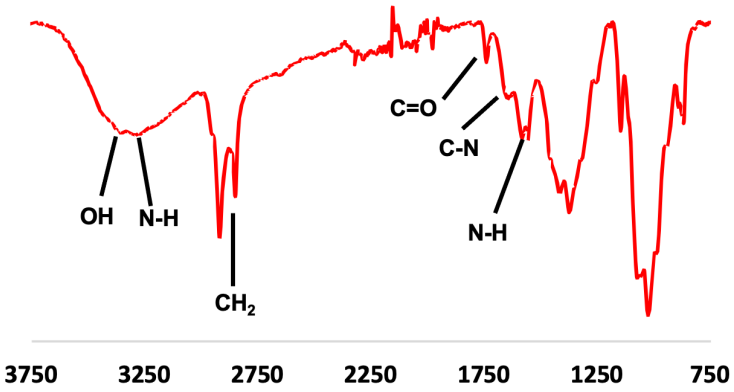

Figure 4.14 FTIR spectra of *E. calcarata* chitosan.

FTIR spectra of prepared chitosan from *E. calcarata* presents strong bands at 3430-3330 cm^{-1} and 3250-3320 cm^{-1} (Figure 4.14), which are consistent with the stretching of O-H and N-H bonds, respectively. The band corresponding to sp3 CH_2 vibration is observed at 2820-2960 cm^{-1} and the C=O band from the amide group can be observed at 1630-1660 cm^{-1}. Lastly, the bending and vibration bands from N-H can be observed at 1540-1575 cm^{-1}. As expected, the observed IR bands for chitosan from *E. calcarata* are consistent with data reported in the literature for shrimp chitosan [133].

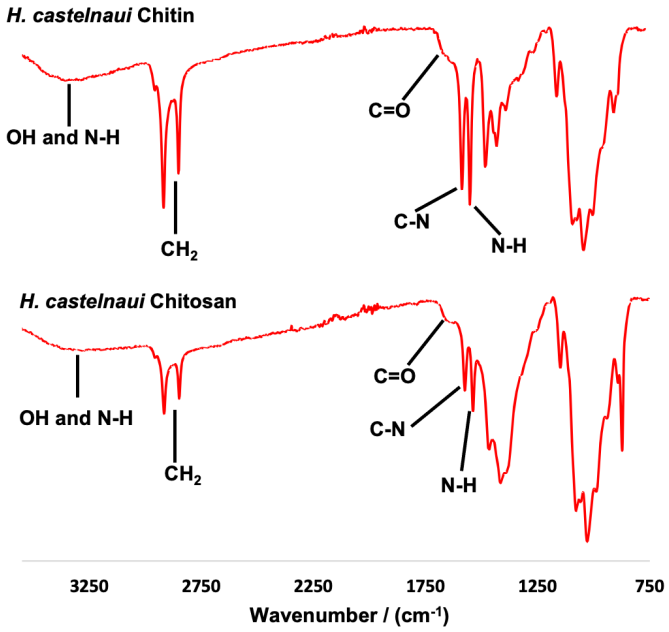

Figure 4.15 FTIR spectra of *H. castelnaui* chitin and chitosan.

FTIR spectra of *H. castelnaui* chitin and chitosan were compared here as example to show the change of structure after deacetylation (Figure 4.15). The observed IR bands for chitin and chitosan from *H. castelnaui* are consistent with data reported in the literature. IR bands from C=O (1610-1660 cm^{-1}) bonds are significantly weakened in chitosan, demonstrating the efficiency of the deacetylation reaction [133].

4.5 Thermal analysis

The extracted materials were also characterized using TGA as descripted in section 3.3.5. Examples of TGA curves of extracted chitin from *Curculionidae* specimens are presented in Figure 4.16, the data for other species are provided in Appendix (Figure SI 19-27) at the end of the thesis.

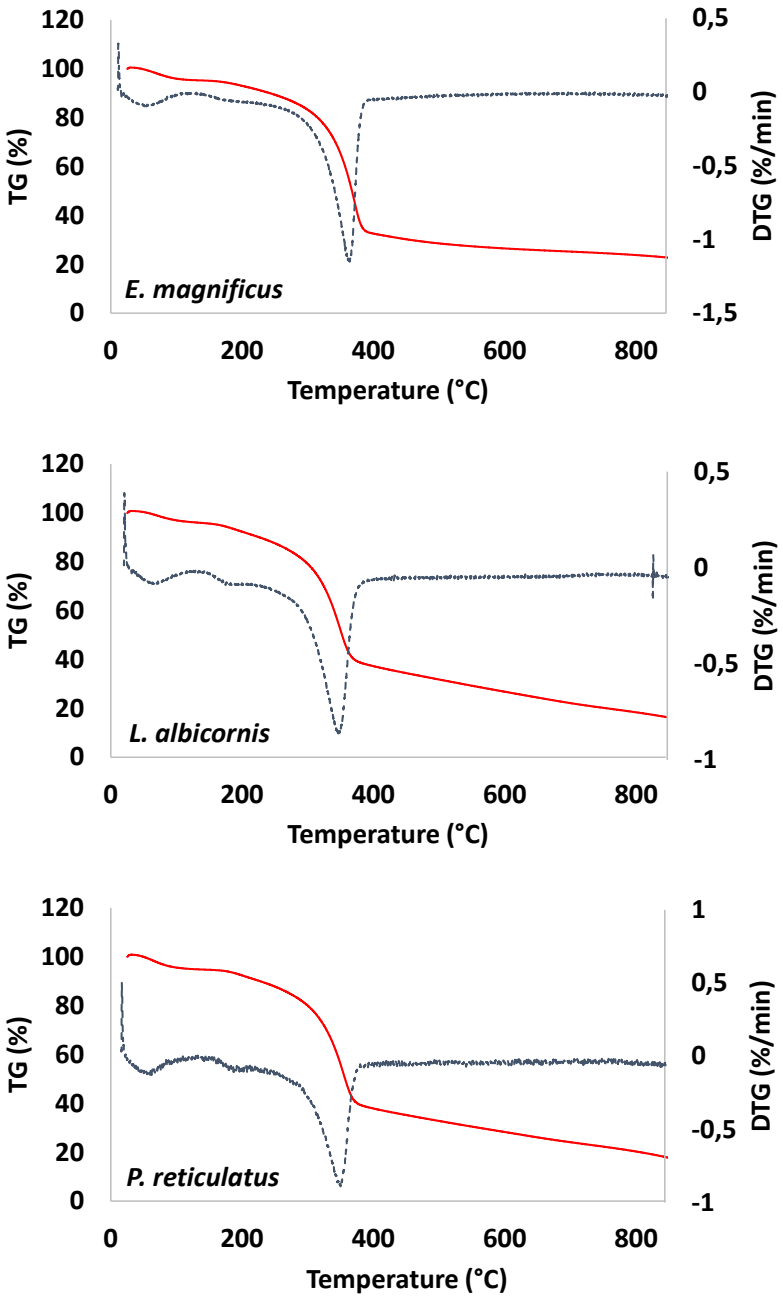

Figure 4.16 Examples of thermal analysis observed for *Curculionidae* specimens (TG: red and DTG: Blue).

TGA is used here to determine thermal degradation temperature, then ash and water content. The ash content is related with the remaining mineral fraction of the extracted chitin and the water content corresponds to the amount of water spontaneously trapped in the material (Table 4.3).

Table 4.3 Thermal analysis data of chitin from *Curculionidae* species.

Species	Thermal degradation temperature (℃)	Ash content (%)	Water content (%)
Eupholus cuvieri	370.5	4.0	3.8
Eupholus magnificus	373.7	3.7	4.0
Lixus albicornis	350.5	3.5	3.1
Lixus gigas	366.5	5.3	3.5
Lixus sturmii	371.5	5.0	3.5
Holonychus saxosus	371.8	3.9	4.2
Pachyrhynchus reticulatus	356.3	5.6	4.4
Pachyrhynchus gemmatus	368.2	9.7	1.8
Sipalinus gigas	369.8	4.7	4.7

The TGA data reveals a degradation temperature greater than 350 °C for all extracted chitin. This is consistent with temperatures reported in the literature for α-chitin [197]. For most species, the ash content is reported near or below 5 % except for *P. gemmatus purpureus* which is higher (9.7%). All these values remain consistent with values previously reported for beetles in the literature [45]. Regarding the measured water content, the reported data are from 2 to 5 % and remain in the range described in the literature for natural chitin.

The thermal behavior of *H. castelnaui* chitosan and *E. calcarata* chitosan was also analyzed as detailed in section 3.3.5. The thermal degradation profile of them both exhibited two distinct steps (Figure 4.17). The first step, observed up to 100 °C, corresponded to the loss of moisture from the chitosan, resulting in a 5 % weight loss for *H. castelnaui* chitosan and 10% weight loss for *E. calcarata* chitosan. The second step represented the decomposition of the chitosan itself. The thermal degradation of *H. castelnaui* chitosan and *E. calcarata* chitosan was around 287℃ and 271℃. The ash percentage is an important parameter for characterizing

chitosan, as it can impact the solubility and viscoelastic properties of the derived material [198-201]. In many applications of chitosan, particularly the formation of hydrogels, a low ash level is preferred. The residual ash content of *H. castelnaui* chitosan and *E. calcarata* chitosan was determined to be 5.7 % and 10 % of the initial sample mass, which is consistent with the previous literature [134].

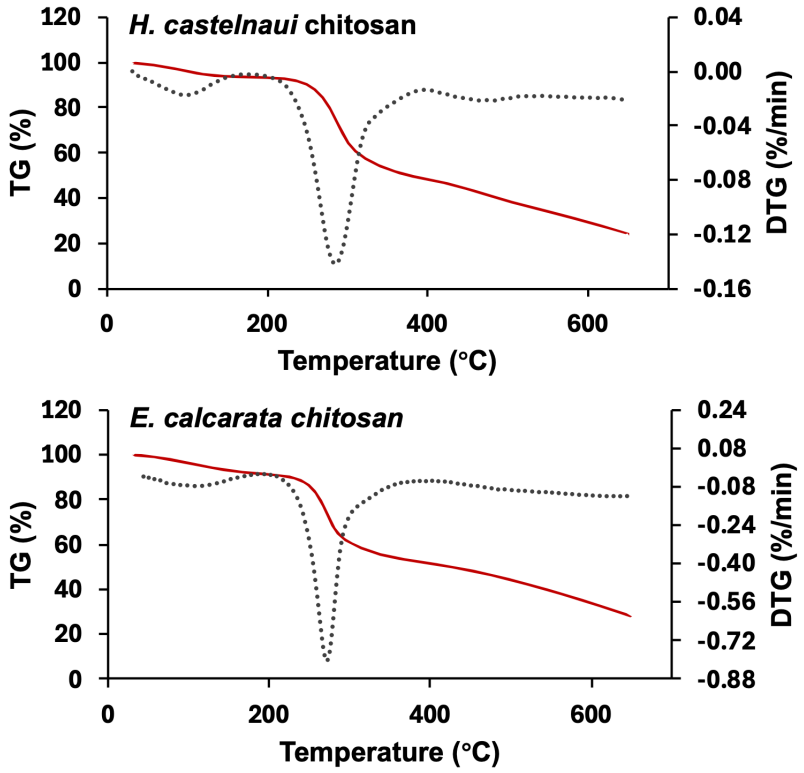

Figure 4.17 TGA curve for *H. castelnaui* chitosan and *E. calcarata* chitosan (TG: red and DTG: Blue).

The insights into the thermal behavior of prepared chitosan were further provided through the DSC curve. A degradation peak associated with chitosan was observed at 315 °C for both *H. castelnaui* chitosan and *E. calcarata* chitosan (Figure 4.18), similar observations made with commercial shrimp chitosan under the same test conditions. This degradation temperature aligns with values reported in the literature for chitosan [202]. The analysis of thermal behavior and determination of ash content contribute valuable information regarding the stability and purity of the chitosan sample, essential considerations for its potential applications [203]. The *H. castelnaui* chitosan and *E. calcarata* chitosan, with its comparable thermal stability and

purity to commercial chitosan, presents a valuable alternative source. This offers significant potential for sustainable and high-quality chitosan production, reducing reliance on traditional marine sources and expanding the scope of its industrial applications.

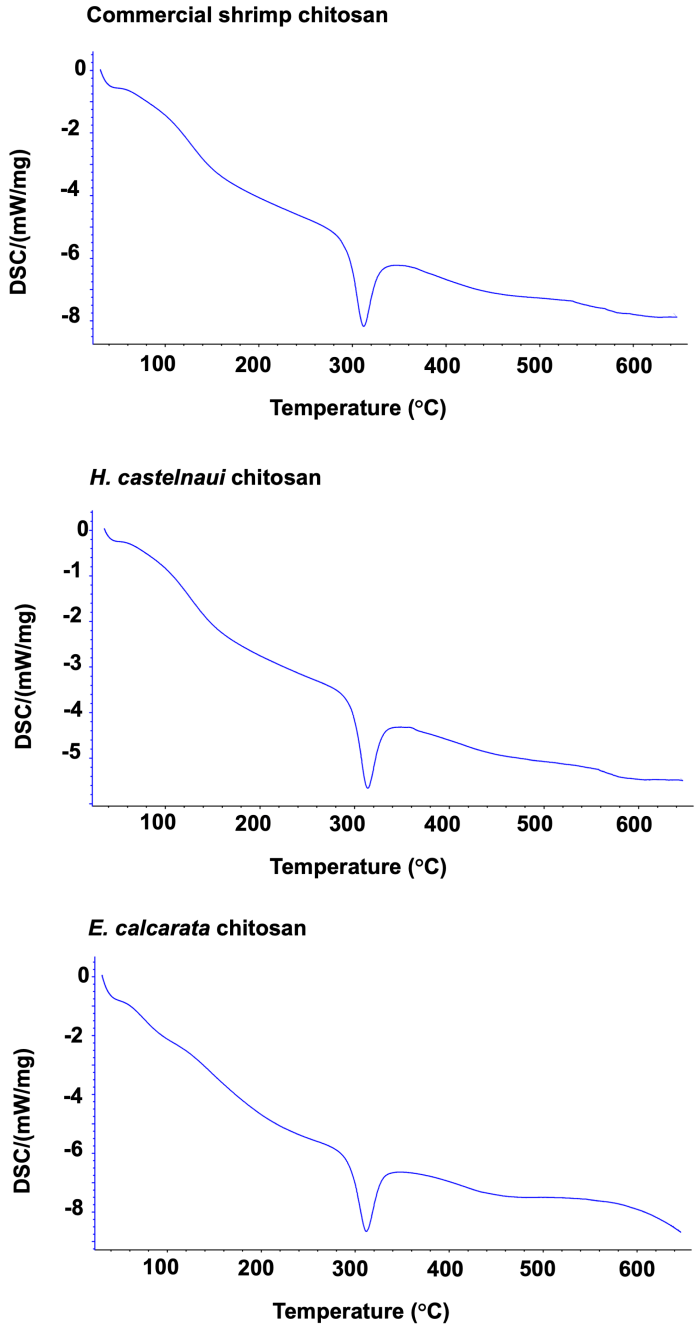

Figure 4.18 DSC observation for chitosan from shrimp, *H. castelnaui* and *E. calcarata.*

The inconsistency between the degradation temperatures measured by DSC and TGA for the same chitosan sample is common due to the differing principles of these techniques. DSC

focuses on thermal events such as phase transitions and heat flow changes, which may indicate melting or other transformations in the chitosan. In contrast, TGA measures mass loss with temperature, providing insights into thermal stability and decomposition. As a result, the degradation temperature from DSC may reflect a specific thermal event, while TGA captures the actual decomposition temperature associated with weight loss. Thus, it is important to interpret DSC and TGA results together with other characterization methods for a comprehensive understanding of chitosan's thermal behavior.

4.6 Elemental analysis

The extracted chitin and prepared chitosan were characterized using elemental analysis as descripted in section 3.3.3, specifically assessing the ratios of carbon, hydrogen, and nitrogen. These elemental percentages are crucial for confirming the purity of the chitin and ensuring that its composition aligns with theoretical values expected for high-quality chitin and chitosan. Accurate elemental composition is essential for verifying the material's suitability for its intended applications and its potential performance in further studies or industrial use. All elemental analysis data of chitin from *Curculionidae* species are reported in Table 4.4 and are consistent with theoretical values considered for chitin. Therefore, the extracted chitin can be used for further research and industrial applications.

Table 4.4 Elemental analysis data of chitin from *Curculionidae* species.

Species	**C (%)**	**H (%)**	**N (%)**
Theoretical value	46.8	6.5	6.8
Eupholus cuvieri	42.8	6.4	6.1
Eupholus magnificus	42.7	6.2	6.2
Lixus albicornis	42.6	6.3	6.2
Lixus gigas	41.9	6.2	6.1
Lixus sturmii	42.6	6.4	6.3
Holonychus saxosus	41.2	6.2	6.0

Pachyrhynchus reticulatus	42.3	6.2	6.3
Pachyrhynchus gemmatus	43.8	6.5	5.4
Sipalinus gigas	40.6	6.1	5.8

Elemental analysis was also performed on the obtained chitosan from *H. castelnaui* and *E. calcarata*. The results from this analysis are shown in Table 4.5. The experimental elemental proportions are all consistent with the expected theoretical elemental proportions for chitosan [134].

Table 4.5 Elemental analysis for *H. castelnaui* chitosan and *E. calcarata* chitosan.

Species	**C (%)**	**H (%)**	**N (%)**
Theoretical value	44.32	6.87	7.95
H. castelnaui	39.81	7.19	6.77
E. calcarata	39.43	6.90	7.61

High nitrogen content in *H. castelnaui* chitosan and *E. calcarata* chitosan reflects the number of amino groups (NH_2) present. Amino groups are key active sites for adsorption due to their ability to form hydrogen bonds and electrostatic interactions with dye molecules. Chitosan with high nitrogen content may provide a sustainable natural alternative for dye removal applications, thus increasing its practical utility in environmental management. Besides, high amino group quantity in chitosan significantly affects its solubility, viscosity, and compatibility. These factors contribute to its effectiveness in 3D printing applications by enhancing flowability, improving material interactions, and ensuring structural stability. Amino groups can increase the viscosity of chitosan solutions by forming more hydrogen bonds, ensuring it has the right flow characteristics for 3D printing. Amino content affects the gelation and hardening rates, which in turn impacts the accuracy and stability of printed structures. In addition, high amino content may enhance compatibility with other materials, such as

biopolymers or synthetic materials, by reacting with acidic groups in those materials, potentially improving the overall performance of the 3D-printed structures [204].

4.7 XRD analysis

Finally, the extracted chitin and prepared chitosan were evaluated using x-ray diffraction as descripted in section 3.3.4. Examples of the X-ray observations for *Curculionidae* specimens are shown in Figure 4.19.

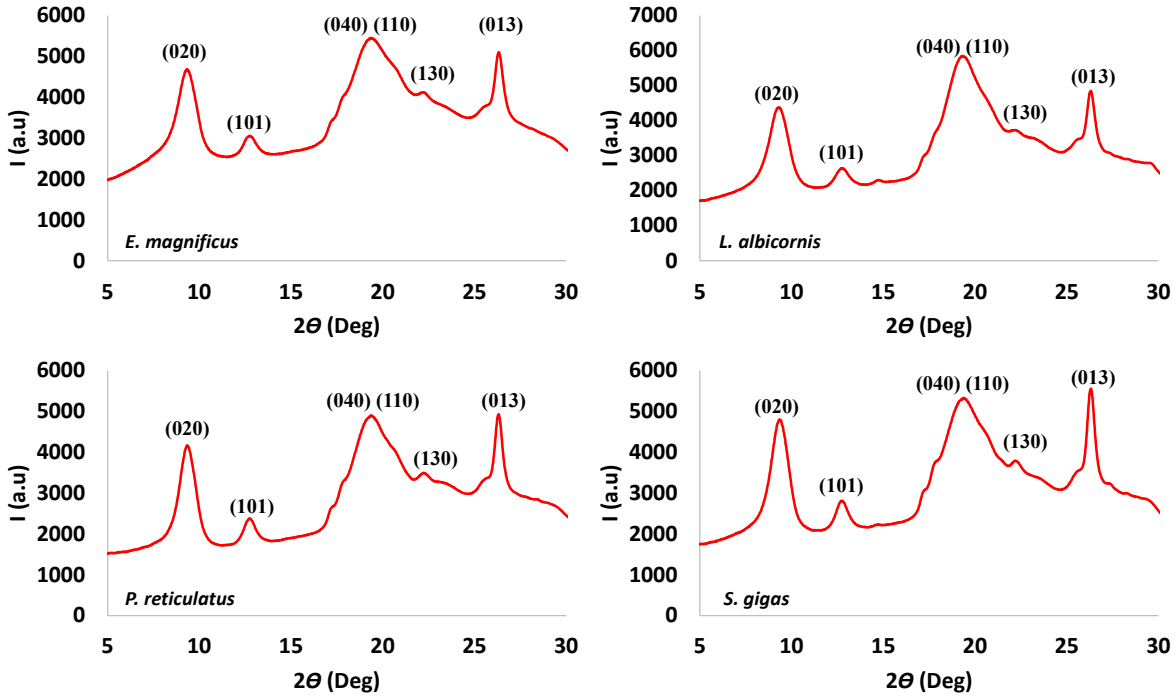

Figure 4.19 Examples of X-ray spectra observed for *Curculionidae* specimens.

In x-ray diffraction, a plane is formed by the arrangement of atoms in a crystal, which can be expressed by Miller indices such as (020), (101), etc. The Miller index is a direction vector in a three-dimensional crystal lattice that expresses the relationship between the crystal plane and the crystal axis. Miller indices are direction vectors in a three-dimensional crystal lattice that are used to represent the relationship between crystal planes and crystal axes [205]. With a known crystal structure, the *d* values corresponding to different Miller indices can be calculated to obtain the expected diffraction angle 2θ. The peak position 2θ from the experimental data is

then matched with the calculated angle to determine which peak corresponds to which crystal plane.

All chitin samples from *Curculionidae* specimens have similar XRD patterns, which are at 2θ values of 9.4°, 12.9°, 19.6° shouldering with 20.6°, 22.3° and 26.4°. These values can be attributed to the plane (020), (101), (040) shouldering with (110), (130) and (013). The small shoulder peak may represent a secondary diffraction phenomenon or be due to minor structural differences in the crystal. All these values are consistent with that reported in the literature for α-chitin characterized by XRD [206]. The crystallinity results are presented in Table 4.5.

Table 4.5 Calculated crystallinity index of chitin from *Curculionidae* species.

Species	Crystallinity index (%)
Eupholus cuvieri	46.4
Eupholus magnificus	48.9
Lixus albicornis	59.7
Lixus gigas	48.3
Lixus sturmii	34.8
Holonychus saxosus	48.3
Pachyrhynchus reticulatus	58.7
Pachyrhynchus gemmatus	56.9
Sipalinus gigas	56.4

For all *Curculionidae* species, the crystallinity index remains between 45 and 60 %. This index can be described as low compared with crystallinity index reported in the literature for other coleopters [43, 45]. With all the performed characterizations, it is concluded that the extracted material has similar characteristics to classical shrimp chitin. The average overall yield less than 20 % for *Curculionidae* is lower compared to other beetle chitin yields [45]. However, compared with shrimp the yield remains greater. As a consequence, it is reasonable to consider *Curculionidae* as potential source of chitin for future industrial exploitation.

For the comprehensive characterization of obtained chitosan, XRD investigations were also undertaken on *H. castelnaui* chitosan and *E. calcarata* chitosan as shown in Figure 4.20. Major, sharp peaks for *H. castelnaui* chitosan observed at 10.2° and 20.1°, as well as a shoulder at 22.0°. Major, sharp peaks for *E. calcarata* chitosan observed at 10.8° and 20.0°, as well as a shoulder at 22.0°. These values are consistent with chitosan and allow determination of the crystallinity index (Crl) [25]. The CrI of them were found to be 12.1 % and 12.2 %, revealing that the prepared chitosan is mostly amorphous. The amorphous regions in chitosan are typically associated with higher surface activity and more active sites, which are essential for dye adsorption. Lower crystallinity suggests more amorphous regions, enhancing the interaction with dye molecules and improving adsorption capacity [207]. By understanding the crystallinity from XRD, the adsorption capacity can be predicted and optimized, allowing for better performance in dye removal. Additionally, more amorphous regions chitosan tend to be more mobile and flexible and typically increase the flexibility and hydration capacity of the material, making it more suitable for gel formation and use in 3D bioprinting [208].

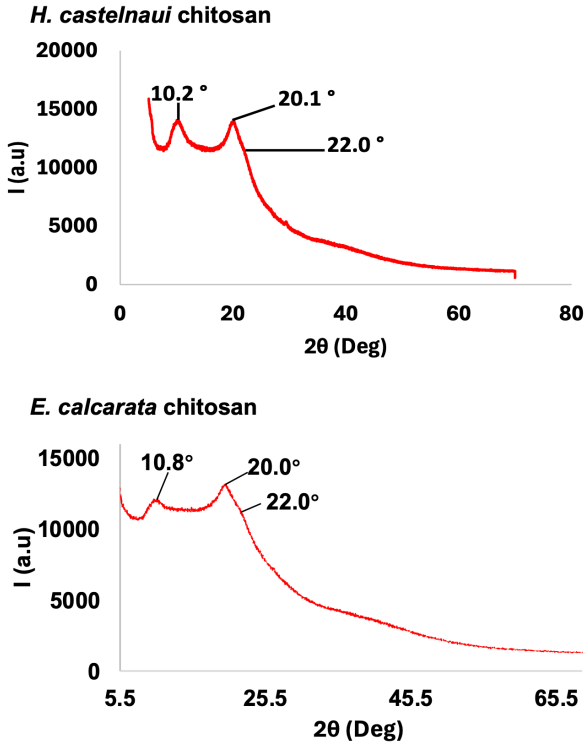

Figure 4.20 XRD observation on *H. castelnaui* chitosan and *E. calcarata* chitosan.

4.8 DDA characterization of *H. castelnaui* chitosan and *E. calcarata* chitosan

The DDA was estimated using both ^{1}H-NMR (Figure 4.21 and Figure 4.22) and titration (Figure 4.18) as descripted in section 3.3.6 and 3.3.7, respectively. Due to the polymer structure, all reported signals of chitosan are relatively broad. Chitosan from *H. castelnaui* presented the following chemical shifts: (400 MHz, CF_3COOD, ppm): 2.68 (H-Ac); 3.91 (H_2-Deacetylated); 4.06 - 4.90 (H_2 to H_6); 5.23 - 5.48 (H_1-Acetylated); 5.50 - 5.90 (H_1-Deacetylated). The areas under pics corresponding to H1-D and H-Ac were found to be equal to 1.55 and 1, respectively. Thus, the DDA calculated using NMR (Eq. (3.2)) for chitosan from *H. castelnaui* in this study is 82.4%.

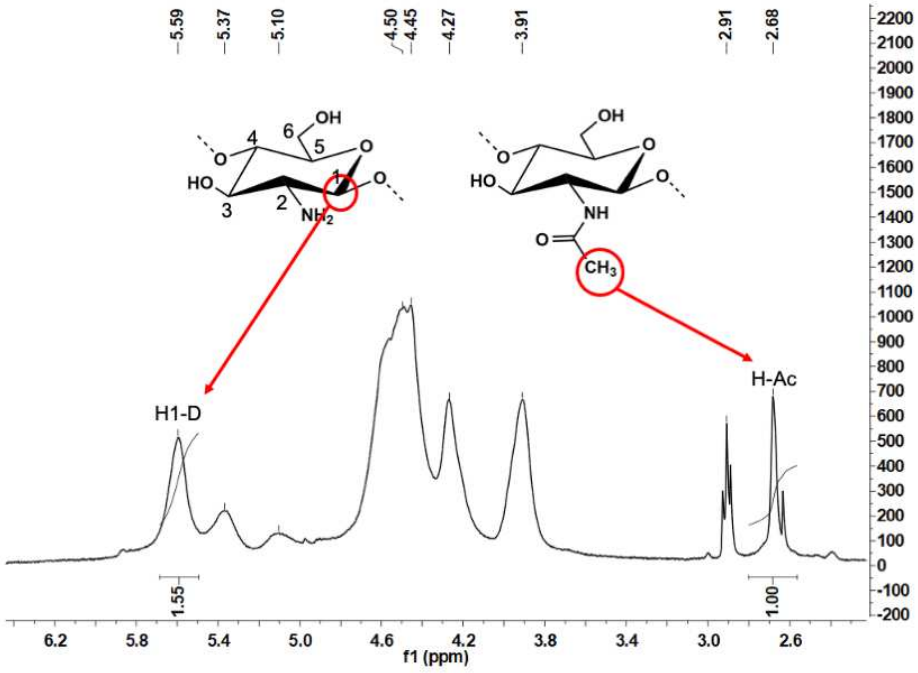

Figure 4.21 Example of ^{1}H NMR for *H. castelnaui* chitosan.

The chemical shift values for chitosan from *E. calcarata* are as follows: δH (400 MHz, CF3COOD, ppm): 2.65 (H-Ac); 3.97 (H2-Deacetylated); 4.10 - 4.90 (H2 to H6); 5.25 - 5.50

(H1-Acetylated); 5.55 - 5.85 (H1-Deacetylated). Following the Eq. (3.2) in Chapter 3, H1-D and H-Ac integrated to 1.2 and 1.0, respectively, and the DDA is calculated to be equal to 78.2%.

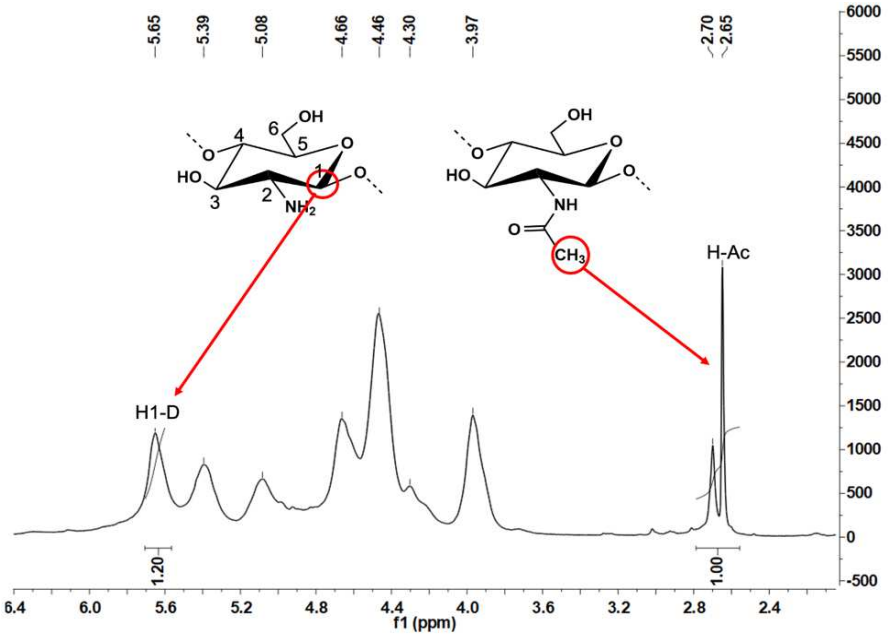

Figure 4.22 Example of ^{1}H NMR for *E. calcarata* chitosan.

For the titration method, the curve obtained exhibited two distinct deflections, each corresponding to different stages of the reaction (Figure 4.23). The initial deflection indicated the presence of excess hydrochloric acid (HCl) in the reaction mixture, while the subsequent deflection indicated the formation of chitosan hydrochloride. Based on the titration results, the DDA of *H. castelnaui* chitosan and *E. calcarata* chitosan were determined to be 78.1 ± 1.8 % and 77.3 ± 2.0 %, which is consistent with the DDA determined by NMR method. The obtained deacetylation degree is consistent with the findings reported in existing literature for chitosan derived from various beetle sources [42].

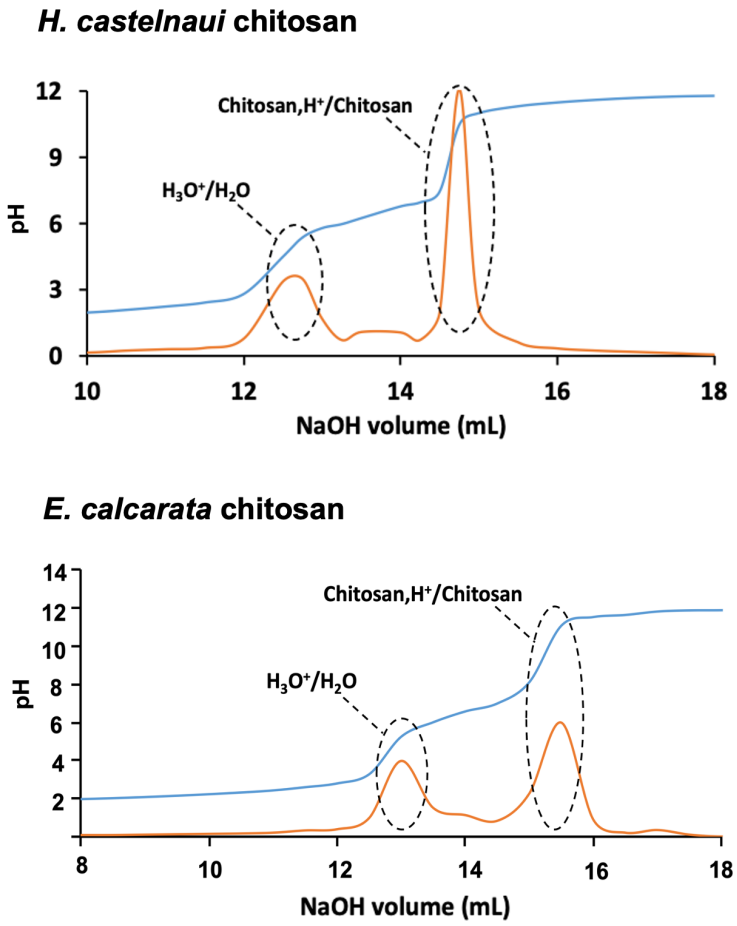

Figure 4.23 Example of titration curve for determination of DDA of *H. castelnaui* chitosan and *E. calcarata* chitosan (Blue: titration curve and orange: first derivative of the titration curve).

4.9 Summary of this chapter

In this chapter, we present for the first time the extraction of chitin from nine species within the *Curculionidae* family, spanning five distinct genera. The chitin was successfully isolated using straightforward chemical procedures, including demineralization, deproteination, and bleaching. Following these three steps, the treated insect cuticles yielded chitin in the range of 12% to 20%. Although these yields are modest compared to those reported for other beetle species, they are relatively high when compared to the extraction yields typically obtained from shrimp shells. The extracted chitin was thoroughly characterized using a suite of analytical

techniques, including FTIR, TGA, XRD, SEM, and elemental analysis. The chitin obtained from the nine *Curculionidae* species exhibited typical characteristics, with ash content ranging from 3% to 10% and water content between 2% and 5%. The consistency of these properties with standard chitin profiles confirms that the extracted material is indeed chitin. Given these findings, *Curculionidae* species can be considered as a potential alternative source of chitin for industrial applications. Moreover, the utilization of pest insect invasions as a biosourced material origin offers an innovative approach to managing these invasions while contributing to sustainable material production.

In addition, chitosan was successfully derived from *H. castelnaui* and *E. calcarata*, with yields of 11.7% and 22.2%, respectively. The obtained chitosan was subjected to comprehensive characterization using FTIR, TGA, XRD, SEM, and elemental analysis, as well as NMR, titration, and DSC. Preliminary data revealed that chitosan from *H. castelanui* and *E. calcarata* exhibited low ash contents (5.7% and 10%), low water content (5% and 10%), and high DDA of 78.1% and 78.2%, respectively. These promising results suggest that *H. castelanui* and *E. calcarata* are viable candidates as sustainable sources for chitosan production, potentially offering new avenues for industrial application.

The outcomes of this work not only expand the knowledge base on chitin and chitosan extraction from lesser-studied insect species but also highlight the potential of these materials as valuable resources in various industrial sectors. By exploring the use of insect-derived chitin and chitosan, particularly from species considered pests, this research contributes to the development of sustainable bioprocesses and materials, offering innovative solutions to both material science and environmental challenges.

Chapter 5 Novel chitosan from dung beetle *Heteronitis castelnaui* for organic dyes removal from aqueous solution[3]

The study in this chapter focuses on exploring a novel chitosan source derived from the dung beetle and evaluates its potential for organic dye removal from aqueous solutions (Figure 5.1). The research involves the preparation of hydrogels by *H. castelnaui* chitosan and characterization using various analytical techniques, including SEM, FTIR, TGA. Then the obtained hydrogels were evaluated for its adsorption capacity through batch adsorption experiments using methylene blue (MB) and methyl orange (MO) as model pollutants. The adsorption capacity for MB was around 1300 $mg \cdot g^{-1}$ at pH = 12 and MB concentration of 1800 $mg \cdot L^{-1}$. The adsorption capacity for MO was around 190 $mg \cdot g^{-1}$ at pH = 5 and MO concentration of 1000 $mg \cdot L^{-1}$. Furthermore, the kinetics of the adsorption process was fitted to pseudo-first-order and pseudo-second-order models to understand the rate of adsorption. The adsorption isotherms were fitted to Langmuir and Freundlich models to highlight the adsorption mechanisms.

[3] Main contents of this chapter are published in the paper Mei, Z.; Szczepanski, C. R.; Montreuil, O; Kuzhir, P.; Godeau, G. Investigation on novel chitosan from dung beetle *Heteronitis castelnaui* (Harold, 1865) and its potential application for organic dyes removal from aqueous solution, *International Journal of Biological Macromolecules*, 2024, 280 (1), 135605.

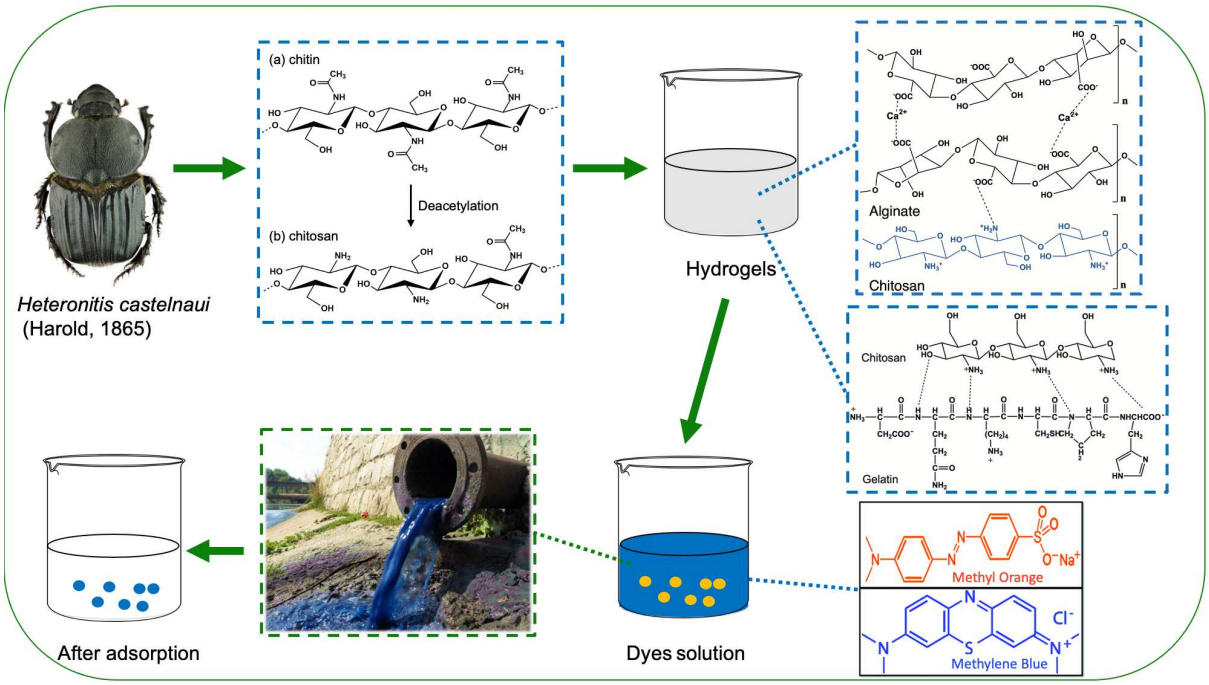

Figure 5.1 Schematic illustration of chitosan from dung beetle *H. castelnaui* for organic dyes removal from aqueous solution.

5.1 Hydrogel preparation and characterization

5.1.1 SEM observation of hydrogels

SEM observation was performed to study the microstructure of the prepared hydrogels (Figure 5.2) as descripted in section 3.3.1. It was observed that the surface was irregular after the hydrogels were dried in air, with numerous cracks and large wrinkles. These irregularities in shape and the presence of cracks and wrinkles are structural changes that occur during the drying process. Specifically, when the hydrogel beads were subjected to dehydration, the polymer network partially collapsed, resulting in the formation of cracks and wrinkles on the surface. These features contribute to the generation of a large surface area and a loose structure within the beads. These characteristics are advantageous for various applications, particularly for molecular diffusion and the adsorption of dyes [209]. The large surface area provides ample opportunities for molecules to interact with the hydrogel, while the loose structure offers sufficient space for the adsorption of dyes or other substances [210].

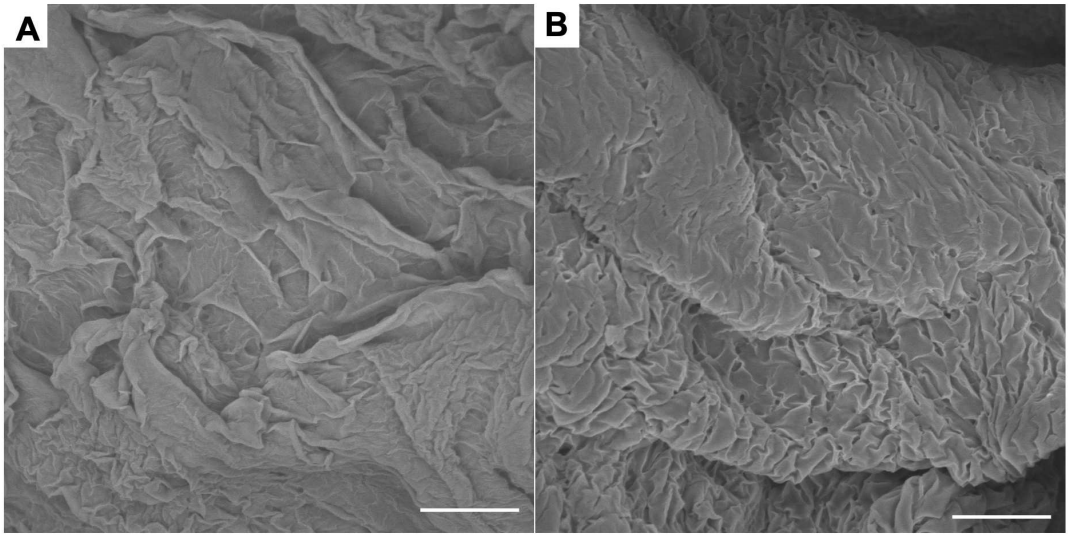

Figure 5.2 SEM images (scale bar = 10 μm) of (A) *H. castelnaui* chitosan/sodium alginate (DCA hydrogel) (B) *H. castelnaui* chitosan/gelatin (DCG hydrogel).

5.1.2 FTIR analysis of hydrogels

Figure 5.3 shows the FTIR spectra of *H. castelnaui* chitosan, SA and DCA hydrogel, respectively, tested as descripted in section 3.3.2. For chitosan, strong bands are observed at 3410–3323 cm^{-1} and 3250–3310 cm^{-1}, corresponding to the stretching of O-H and N-H bonds, respectively. The band corresponding to CH_2 vibration is observed at 2835–2945 cm^{-1} and the C=O band from the amide group is weak but can be observed at 1610–1660 cm^{-1}. Lastly, the bending and vibration bands from N-H can be observed at 1550–1605 cm^{-1}. The band at 1530-1550 cm^{-1} corresponded to the C-N stretch. As expected, the observed IR bands for chitosan from *H. castelnaui* are consistent with data reported in the literature for shrimp chitosan [211].

The characteristic peaks of SA were the peaks at 1596 cm^{-1} (C=O bond) and 1407 cm^{-1}. As seen from Figure of DCA gel, these two characteristic absorption bands shifted to a higher wavelength, 1602 cm^{-1} and 1425 cm^{-1}, by the presence of chitosan into the gel. The spectra of chitosan, SA and DCA gel indicated the broad band at 3336 cm^{-1} corresponding O–H stretching which shows intermolecular hydrogen bonding and also overlaps with the N–H streching in chitosan in the same region. Another characteristic peak of SA appeared at 814 cm^{-1} (Na–O band). This peak was also observed in the spectrum of DCA gel at 822 cm^{-1}, respectively. The prominent peaks at 2920 cm^{-1} and 2854 cm^{-1} showed the presence of asymmetric CH stretching and symmetric CH stretching, respectively. The spectra confirm that the carboxylate group of SA was dissociated to COO^- group which complexes with protonated amino group from chitosan via electrostatic interactions [212]. Moreover, as blend formation proceeded the hydrogen bonding would also be expected due to an increase in intermolecular attraction between SA and chitosan.

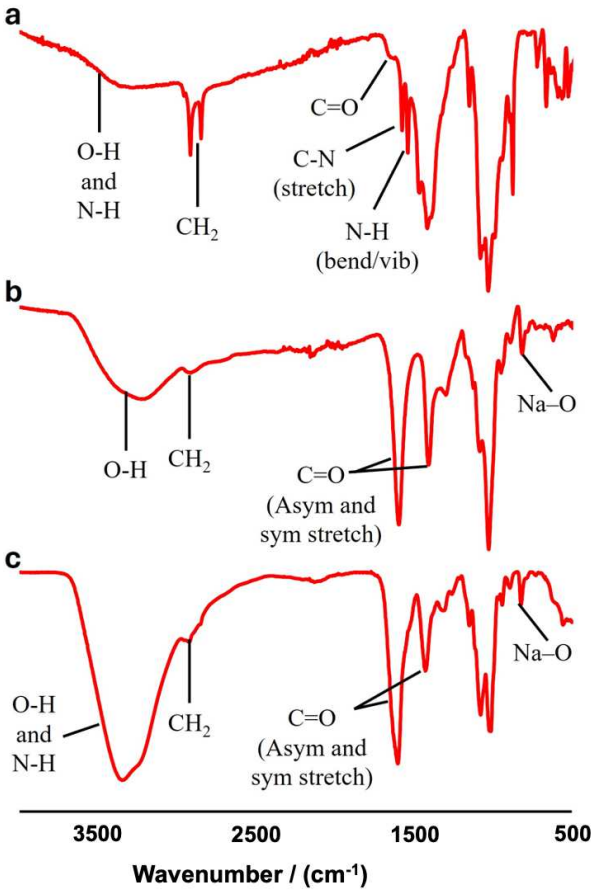

Figure 5.3 FTIR spectra of (a) *H. castelnaui* chitosan (DC), (b) sodium alginate (SA), (c) *H. castelnaui* chitosan/alginate dry hydrogel (DCA hydrogel).

Figure 5.4 showed the FTIR spectra of *H. castelnaui* chitosan (DC), gelatin, and gelatin/chitosan hydrogel (DCG gel). Gelatin showed characteristic bands at 3265 cm^{-1} (O–H stretching vibration), 1625 cm^{-1} (C=O stretching vibration), 1521 cm^{-1} (N–H bending vibration) and 1437 cm^{-1} (symmetric stretching of –COOH groups). For DCG hydrogel, the peaks at 3240 cm^{-1} attributed to O–H and N–H stretching vibration. The DCG gel showed that the band of gelatin at 1625 cm^{-1} shifted to 1635 cm^{-1} and the strengthened band at 1404 cm^{-1} from gelatin (symmetric stretching of –COO− groups) was observed, indicating that gelatin was mixed well with DC. The interaction might be due to the ammonium ($-NH_3^+$) ions of the DC and the carboxyl (–COO−) ions of the gelatin through partial conversion of electrostatic bonds into chemical bonds by the hydrogen bonding [213].

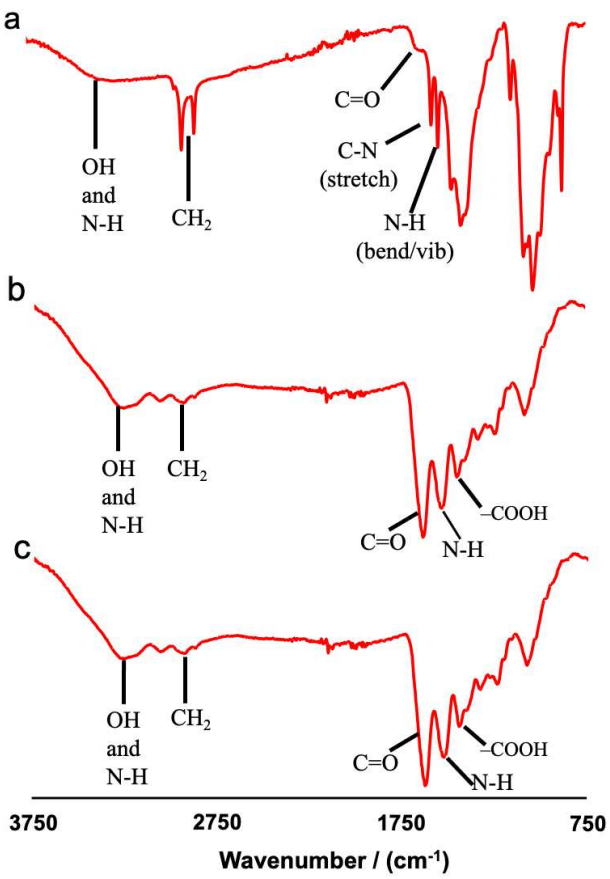

Figure 5.4 FTIR spectra of (a) *H. castelnaui* chitosan (DC), (b) gelatin, (c) *H. castelnaui* chitosan/gelatin dry hydrogel (DCG hydrogel).

5.1.3 Thermal analysis of hydrogels

The TGA and DTG results (Figure 5.5) exhibited that thermal degradation of DC, SA and DCA hydrogel occurred in multiple steps, tested as descripted in section 3.3.5. Typical DTG curves show two intensive peaks distinguishable for SA around 260 °C and 575 °C. For DCA hydrogel, two peaks for DTG_{max} are found around 208 °C and 298 °C, respectively. These peaks are related to the interactions between polymers inside the hydrogel, as it was explained before when more free end chains are added to the polymeric material, less temperature is needed to the decomposition because polysaccharide-based hydrogels presented an abundance of hydroxyl and carboxyl groups which made them highly absorbent and thermally susceptible.

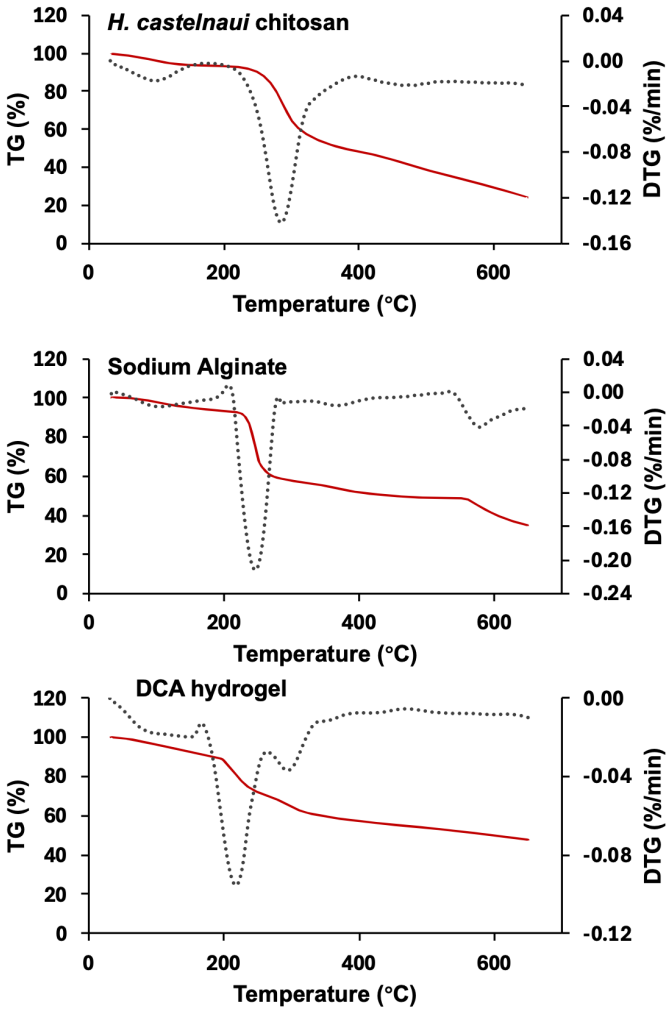

Figure 5.5 Thermogravimetric analysis of *H. castelnaui* chitosan (DC), sodium alginate (SA), chitosan/alginate dry hydrogel (DCA hydrogel) (TG: red and DTG: grey).

As shown in Figure 5.6, all the samples (including gelatin formulations) degraded in three steps and had similar thermal degradation behaviors. The less weight loss around 100 °C was observed for the first step, which was mainly due to the evaporation of moisture in the samples. The second step was owned to thermal degradation of samples. The weight loss in the last step was attributed to carbonization process of organic compounds. The degradation of DC and gelatin starts at 220 and 229 °C and becomes most intense at 283 °C and 315 °C respectively. For DCG hydrogel, the degradation starts at 200 °C with a temperature of maximum volatilization rate, DTG_{max}, at 295 °C showing a behavior in between DC and gelatin. The degraded process of DCG hydrogel did not exhibit two separated process corresponding DC

and gelatin. This may be attributed to the fact that the protonation of primary amino groups ($-NH_3^+$) on chitosan together with carboxylate ($-COO-$) ions of the gelatin form polyelectrolyte network structure by strong ionic bond electrostatic action. On the other hand, other intermolecular forces such as hydrogen bonds between carboxyl ($-COOH$), hydroxyl ($-OH$) and amino ($-NH_2$) groups in chitosan and gelatin molecules also existed [214].

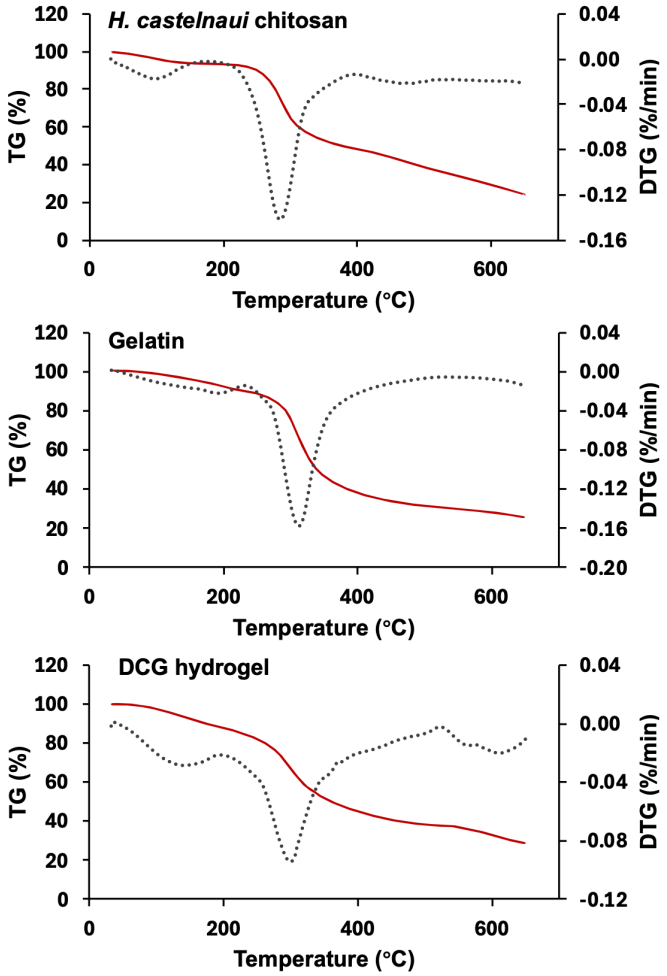

Figure 5.6 Thermogravimetric analysis of *H. castelnaui* chitosan (DC), gelatin, chitosan/gelatin dry hydrogel (DCG hydrogel) (TG: red and DTG: grey).

5.2 Adsorption assays

5.2.1 Adsorption kinetics

The DCA hydrogel and DCG hydrogel were used to further study the adsorption kinetics of MB and MO, respectively, performed as descripted in section 3.4. Figure 5.7 shows

adsorption kinetics of MB and MO dyes on hydrogels. The adsorption rates of both dyes were rapid in the initial stage and then gradually slowed down until the equilibrium was reached. This might be due to the abundant vacant adsorption sites are initially available, which enable the dye molecules to interact easily on the sample surface. The adsorption of MB on the hydrogels took 6 h to reach equilibrium, while the plateau was not really reached at the maximal contact time of 9 h for MO dye. The characteristic adsorption time scale for MO will therefore be determined through fitting of the experimental points to kinetic models. With the increase of adsorption time, the dye molecules occupied the vacant sites of the adsorbent surface and diffused into the internal pores, resulting in the decrease of adsorption rate.

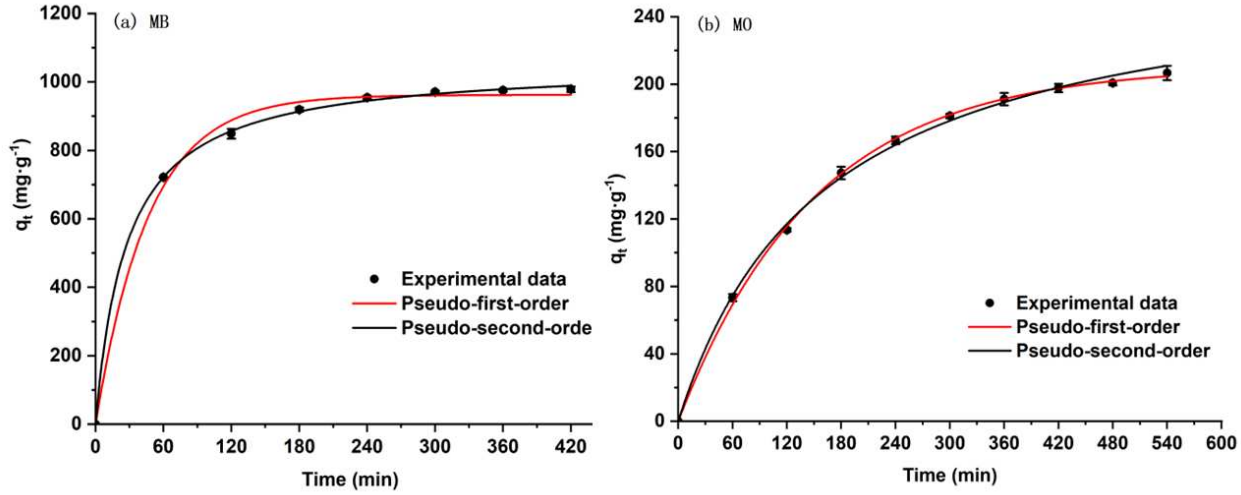

Figure 5.7 Adsorption kinetics, the pseudo-first-order and pseudo-second-order non-linear fitting curves of MB on the DCA hydrogel and MO on the DCG hydrogel. (m = 30 mg, V = 30 mL, T = 298 K, for MB, C_0 = 1000 mg·L^{-1}, pH = 12, t = 7 h; for MO, C_0 = 800 mg·L^{-1}, pH = 5, t = 9 h)

As showed in Table 5.1, both the pseudo-first-order (PFO) and pseudo-second-order (PSO) models demonstrate strong correlation coefficients, with R^2 values exceeding 0.98. This indicates a favorable agreement between the experimental data and these two models, suggesting their capability to describe the adsorption process to a considerable extent. Moreover, the entire adsorption process may involve concurrent physical and chemical adsorption phenomena. For MB adsorption, the comparison of obtained data showed that the regression

coefficient R^2 of the PSO model was superior to that of the PFO model, suggesting that MB adsorption process onto the hydrogels could be better explained by the PSO kinetic model. MO adsorption was better described by PFO kinetic model. Note that k_1 coefficient of the PFO model stands physically for inverse characteristic timescale of the adsorption process. We can therefore determine the characteristic time of the MO adsorption to be 1/0.006≈170 min≈3 h. Note that according to Eq. (3.6), this timescale reflects the time needed for the amount of adsorbed molecules to reach ~63% of its maximal value for a given initial concentration of adsorbate.

Table 5.1 Kinetic parameters of the pseudo-first-order and pseudo-second-order models for MB on the DCA hydrogel and MO on the DCG hydrogel.

Dye	$q_{e,exp}$ ($mg \cdot g^{-1}$)	Pseudo-first-order			Pseudo-second-order		
		k_1 (min^{-1})	q_e ($mg \cdot g^{-1}$)	R^2	k_2 ($mg^{-1} \cdot g \cdot min^{-1}$)	q_e ($mg \cdot g^{-1}$)	R^2
MB[(a)]	980	0.02	962.1	0.996	3.43×10^{-5}	1053.8	0.999
MO[(b)]	210	0.006	210.4	0.999	2.28×10^{-5}	273.6	0.996

(a) C_o = 1000 $mg \cdot L^{-1}$, pH = 12, t = 7 h, m = 30 mg, V = 30 mL, T = 298 K
(b) C_o = 800 $mg \cdot L^{-1}$, pH = 5, t = 9 h, m = 30 mg, V = 30 mL, T = 298 K

5.2.3 Adsorption isotherm

The adsorption capacities of hydrogels were enhanced significantly with the growing initial dye concentration, and the maximal adsorption capacity of MB and MO reached to 1300 $mg \cdot g^{-1}$ at pH=12 and 190 $mg \cdot g^{-1}$ at pH=5, respectively (Figure 5.8). In the cases of MB and MO adsorption, the experimental data fitted well with Langmuir isotherm model (Table 5.2), even though the adsorption plateau was not reached at the considered concentration range of adsorbate. The theoretical maximum adsorption capacity of MB and MO dyes onto the hydrogels using Langmuir equation were 1900 $mg \cdot g^{-1}$ and 220 $mg \cdot g^{-1}$, respectively. Moreover, the value of the isotherm constant K_L of MB and MO dyes are 0.005 $L \cdot mg^{-1}$ and 0.009 $L \cdot mg^{-1}$. According to Eq.（3.10 and 3.11）, the value of Gibbs free energy ΔG of MB and MO dyes are

calculated as -19 kJ·mol^{-1} and -20 kJ·mol^{-1}, indicating that the adsorption of both dyes on the hydrogel is a spontaneous and advantageous process. The initial studies on adsorption primarily focused on the behavior of gases adsorbing onto solid surfaces. These early investigations revealed that the adsorption process is thermodynamically driven by intermolecular forces, resulting in a decrease in Gibbs free energy ($\Delta G<0$). This negative change in Gibbs free energy indicates that the adsorption process is spontaneous, as the system naturally progresses towards a more stable, lower-energy state. Over time, this understanding of gas-solid adsorption laid the groundwork for further exploration of adsorption phenomena, extending to liquid-solid interfaces and complex multi-component systems [215].

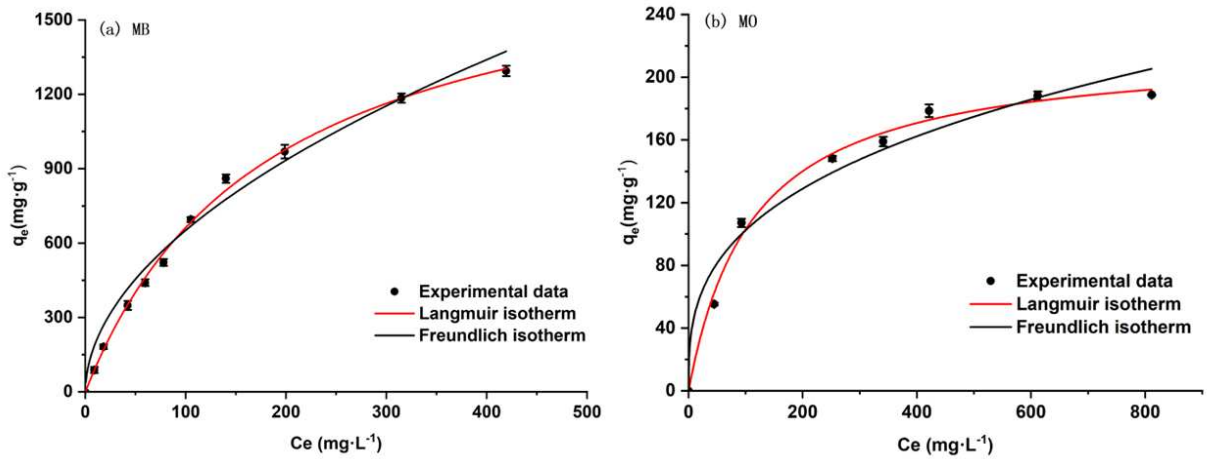

Figure 5.8 Adsorption isotherms, the Langmuir and Freundlich non-linear fitting curves of MB on the DCA hydrogel and MO on the DCG hydrogel. (m = 30 mg, V = 30 mL, T = 298 K, t = 24 h, for MB, C_0 = 100-1800 mg·L^{-1}, pH = 12; for MO, C_0 = 100-1000 mg·L^{-1}, pH = 5)

Table 5.2 Isotherm parameters of Langmuir and Freundlich models for MB on the DCA hydrogel and MO on the DCG hydrogel.

Dye	T(k)	Langmuir isotherm			Freundlich isotherm		
		q_{max} (mg·g^{-1})	K_L (L·mg^{-1})	R^2	K_F (mg$^{1-1/n}$·L$^{1/n}$·g^{-1})	n	R^2
MB[(a)]	298	1900	0.005	0.997	59.27	1.92	0.984
MO[(b)]	298	220	0.009	0.983	22.18	3.01	0.960

(a) C_o = 1800 mg·L^{-1}, pH = 12, t = 24 h, m = 30 mg, V = 30 mL
(b) C_o = 1000 mg·L^{-1}, pH = 5, t = 24 h, m = 30 mg, V = 30 mL

5.2.4 Adsorption mechanism

Figure 5.9 showed the formation of DCA hydrogel with crosslinker agent $CaCl_2$ for MB absorption. MB is a synthetic dye with a complex structure that includes a thiazine ring, which is a heterocyclic ring containing both nitrogen (N) and sulfur (S) atoms. This ring is fused to a planar aromatic system known as the phenothiazine moiety, characterized by alternating single and double bonds that allow for the delocalization of π-electrons across the conjugated system. This conjugation is critical for the chromophore groups in MB, which are responsible for its intense blue coloration by absorbing light in the red–orange region of the electromagnetic spectrum. MB features dimethylamino group ($-N(CH_3)_2$), which enhances its reactivity and electron-donating properties. This group significantly strengthens MB's capacity to engage in hydrogen bonding with other molecules, due to the electron-donating effect of the methyl groups attached to the amino nitrogen atom [216]. Although the schematic representation (Figure 5.9) might imply that the positive charge of MB is localized on one end of the molecule, the electron charge distribution of the monomer stands between those of the resonance forms. This delocalization means that the negative charge of the adsorbent molecule interacts with the overall positive charge of MB rather than a single fixed point, leading to a more dynamic and distributed electrostatic interaction [217].

Chitosan is composed mainly of glucosamine units. It is characterized by three primary functional groups that play key roles in its adsorption capability. Amino groups ($-NH_2$), rich in lone pairs of electrons, can form coordination bonds with positively charged ions [218]. They also contribute to hydrogen bonding and electrostatic interactions, enhancing the polymer's ability to bind various pollutants. Attached to the sugar units of chitosan, hydroxyl groups (-OH) participate in hydrogen bonding, contributing to the hydrophilic nature of chitosan. This property is crucial for dissolving chitosan in water and allowing it to form strong hydrogen bonds with functional molecules. Although less abundant than the amino and hydroxyl groups,

acetyl groups (-$COCH_3$) enhance the structural integrity of chitosan and improve its adsorption properties for MB.

SA is a naturally occurring polysaccharide extracted from brown seaweed, consists of mannuronic and guluronic acid units. Carboxyl Groups (-COO-) impart a strong anionic character to alginate, enabling it to interact electrostatically with cationic species, including the amino groups in chitosan and the positive groups in MB [219]. Alginate's ability to form gels in the presence of divalent cations like Ca^{2+} is a critical property. SA chains are cross-linked by electrostatic interactions between the Ca^{2+} ions and the anionic alginate carbonyl ends (-COO-), forming an "egg box" polymer network by replacing the Na that enhances the mechanical strength and stability of the resulting hydrogel [220].

The combination of chitosan and alginate creates a hydrogel through crosslinking, primarily mediated by Ca^{2+} ions. The anionic carboxyl groups of alginate interact with the cationic amino groups of chitosan, leading to the formation of a 3D porous network [219]. The functional groups in chitosan and alginate enable multiple modes of interaction with MB, mainly including electrostatic attractions and hydrogen bonding [221-223]. Additionally, chitosan has amino groups (-NH_2) that contain lone pairs of electrons, which can interact with the π orbital of MB, which has aromatic rings, forming an n-π interaction [224]. When MB molecules are adsorbed onto the hydrogel, there may be some degree of π-π stacking between MB molecules that are closely packed on the surface [225].

Overall, the synergistic combination of chitosan's functional groups and alginate's gelling properties, along with the structural characteristics of MB, results in a highly effective system for the adsorption of methylene blue from aqueous solutions. This makes the chitosan-alginate hydrogel a potent material for water purification and environmental remediation.

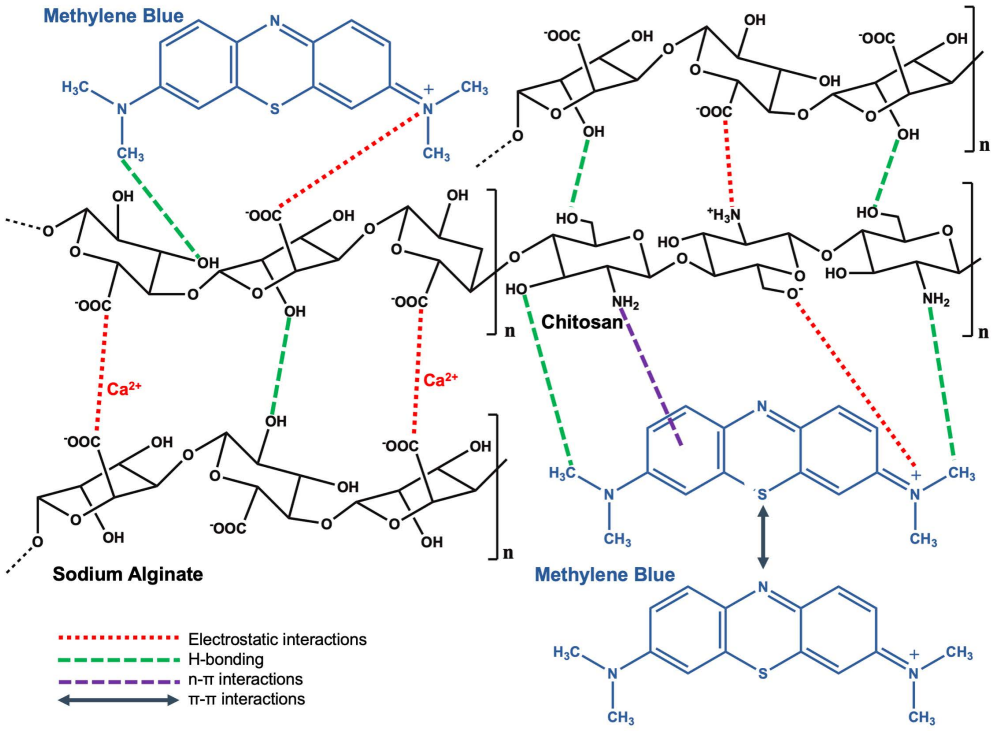

Figure 5.9 Formation of DCA hydrogel with crosslinker agent $CaCl_2$ for MB absorption.

Figure 5.10 shows the formation of DCG hydrogel for MO absorption. Chitosan-gelatin composite can exhibit a variety of interactions. During cross-linking, free radical sites on the covalent cross-linker react with those on the polymer chains of chitosan and gelatin, forming a three-dimensional network through covalent bond formation [226]. Ionic crosslinkers interact with chitosan and gelatin via ionic interactions that require the protonation or deprotonation of functional groups (-COOH, $-NH_2$ and -OH). These charged functional groups then interact by electrostatic interactions [227]. The DCG hydrogel formed by chitosan and gelatin for MO adsorption involves several interaction mechanisms. The electrostatic attractions occur between the negatively charged sulfonate groups (SO_3^-) of the MO dye and the positively charged amino groups (NH_3^+) on the DCG hydrogel surface [228]. Hydrogen bonding also plays a role, with free hydrogen atoms on the DCG hydrogel surface forming bonds with oxygen and nitrogen atoms in the MO dye [229, 230]. In addition, the lone pair electrons of the oxygen and nitrogen atoms in the hydrogel can induce n-π interactions with the π orbitals of the aromatic rings of

the MO dye [231]. These combined interactions facilitate the effective adsorption of the MO dye onto the DCG hydrogel.

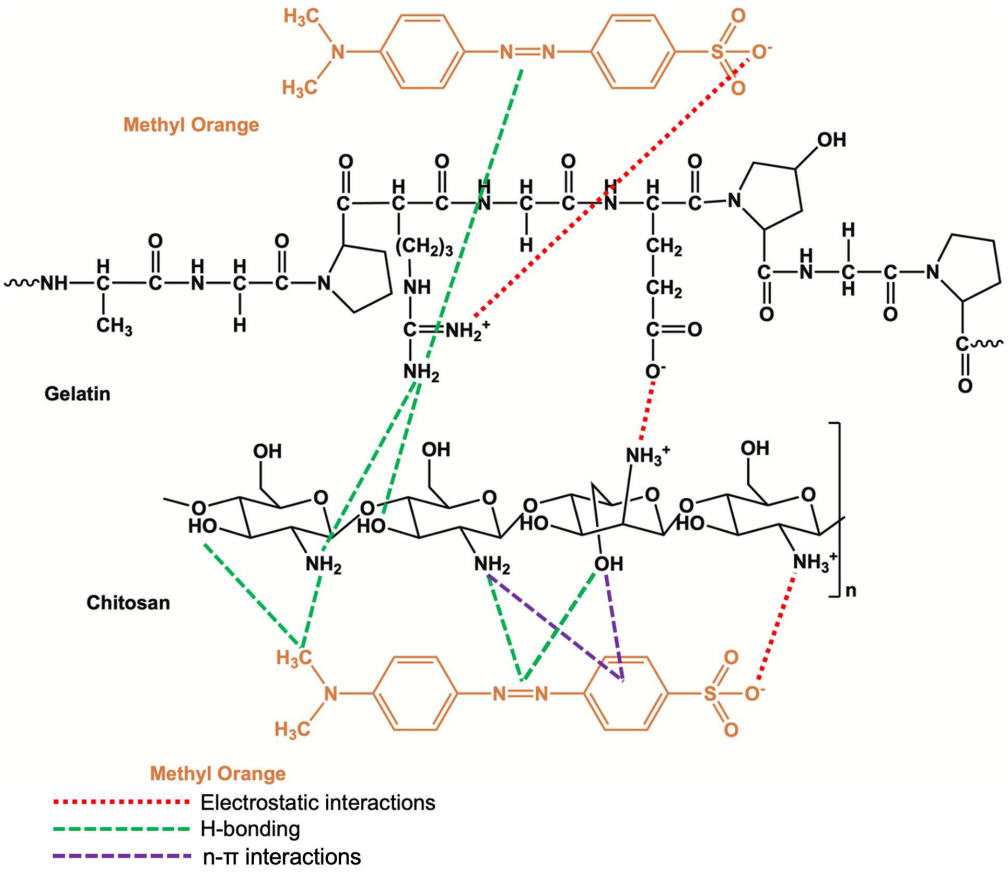

Figure 5.10 Formation of DCG hydrogel for MO absorption.

5.2.5 Comparison with published studies

Chitosan-based hydrogels have gained significant attention for their potential in environmental applications, particularly in the adsorption and removal of dyes such as MB and MO from wastewater (Table 5.3). A three-dimensional porous β-cyclodextrin/chitosan functionalized graphene oxide hydrogel was used for the removal of MB from aqueous solution, and showed an adsorption capacity of 1134 $mg \cdot g^{-1}$ at pH = 12 [232]. Zhao *et al.* prepared fibrous chitosan/sodium alginate composite foams by lyophilization with ternary acetic acid/water/tetrahydrofuran solvents, which showed adsorption capacity for MB of 1488.1 $mg \cdot g^{-1}$, the adsorption capacity shows an overall upward trend with the pH increasing [233].

Ecaterina *et al.* prepared a kind of macroporous composite interpenetrating polymer networks hydrogels based on poly(acrylamide) and chitosan with adsorption capacity of MB, around 750 $mg \cdot g^{-1}$, at 25 °C [234]. Qi *et al.* investigated the self-assembly of graphene oxide sheets in the presence of chitosan, a natural polyaminosaccharide, into sponges, and the sponge with chitosan content of 9% had adsorption capacity of 275 $mg \cdot g^{-1}$ for MB [235]. Thi *et al.* reported a similar adsorption capacity of graphene oxide/chitosan hydrogel for MB (275.5 $mg \cdot g^{-1}$). Plus, adsorption capacity for MO was tested as 150 $mg \cdot g^{-1}$ [236]. Yan *et al.* also tested adsorption capacity of magnetic chitosan–graphene oxide composite for MO, the maximum was 398.08 $mg \cdot g^{-1}$ [237]. Mahdi *et al.* synthesized hydrogel polymer by incorporation of acrylic acid, vinylphosphonic acid and N-maleyl chitosan, which showed maximum adsorption capacity for MB of 66.89 $mg \cdot g^{-1}$ [238]. Li *et al.* reported a versatile bio-based material prepared by simple thermal cross-linking chitosan and polyacrylic acid, which exhibits adsorption capacity of 990.1 $mg \cdot g^{-1}$ for MB [239]. Qi *et al.* prepared composite hydrogel beads by the dropping and pH-precipitation method, which contains chitosan and halloysite nanotubes at the ratio of 1:1 and exhibits adsorption capacity of 303 $mg \cdot g^{-1}$ for MB [240]. Atefeh *et al.* used formaldehyde as crosslinking agent to form the graphene-chitosan composite hydrogel, the maximum adsorption capacity for MO was reported as 102.84 $mg \cdot g^{-1}$ [241]. Zhao *et al.* prepared Semi-IPN hydrogel composites via photopolymerization of poly(ethylene glycol) macromer and acrylamide monomer in the presence of chitosan, which exhibits adsorption capacity of 185.2 $mg \cdot g^{-1}$ for MO at pH = 2 [242]. Wang *et al.* prepared magnetic chitosan/poly (vinyl alcohol) hydrogel beads through a freezing-thawing method, which exhibits adsorption capacity of 6.936 $mg \cdot g^{-1}$ (with the dye concentration of 30 $mg \cdot L^{-1}$) at pH = 4 [243]. Compared to these approaches for the hydrogel preparation, the processes in this thesis are simpler and faster. Furthermore, the sodium alginate and gelatin components chosen in this study are more

economical and eco-friendly. In terms of adsorption capacity, the hydrogels prepared in this work showed higher performance than many reported chitosan-based hydrogels.

Table 5.3 Summary of MB and MO adsorption of various chitosan-based hydrogels reported in literature.

Composition of Hydrogels	**Adsorption performance**		**Ref.**
	Dye	**Adsorption capacity($mg \cdot g^{-1}$)**	
β-cyclodextrin/chitosan functionalized graphene oxide	MB	1134	[232]
Chitosan/sodium alginate	MB	1488.1	[233]
IPN poly (acrylamide) and chitosan	MB	750	[234]
Graphene oxide/chitosan	MB	275	[235]
Graphene oxide-chitosan	MB	275.5	[236]
Poly (AA-co-VPA) cross-linked with *N*-maleyl chitosan	MB	66.89	[238]
Cross-linked chitosan and polyacrylic acid	MB	990.1	[239]
Chitosan–halloysite nanotubes	MB	303	[240]
H. castelnau chitosan/alginate (DCA)	MB	1900	This study
Graphene-chitosan composite hydrogel	MO	102.84	[241]
Graphene oxide-chitosan	MO	150	[236]
Magnetic chitosan–graphene oxide composite	MO	398	[237]
Semi-IPN poly (ethylene glycol), acrylamide and chitosan	MO	185.2	[242]
Magnetic chitosan/poly (vinyl alcohol)	MO	6.936	[243]
H. castelnaui chitosan/gelatin (DCG)	MO	220	This study

5.3 Summary of this chapter

In conclusion, this study presents a significant advancement in the investigation of novel chitosan derived from *H. castelnaui* and its potential application in the removal of MB and MO organic dyes from aqueous solutions. *H. castelnaui* chitosan demonstrated excellent performance in the formation of hydrogels and exhibited remarkable adsorption capacity, highlighting the efficient and favorable nature of the chitosan as a sorbent for organic dyes. For

MB, adsorption capacity reached ~1300 $mg \cdot g^{-1}$ at solution pH = 12 and MB concentration of 1800 $mg \cdot L^{-1}$, while the theoretical maximal adsorption capacity obtained through fit of adsorption isotherm to the Langmuir model was ~1900 $mg \cdot g^{-1}$ for the same pH. For MO, adsorption capacity was ~190 $mg \cdot g^{-1}$ at MO concentration of 1000 $mg \cdot L^{-1}$ and the theoretical maximal adsorption capacity was ~220 $mg \cdot g^{-1}$, both at solution pH = 5 and. The equilibrium and kinetics of the adsorption process followed the Langmuir isotherm (at least in the experimental dye concentration range without reaching adsorption plateau) and pseudo-second-order kinetic model, respectively.

By utilizing insect waste for chitosan production, this study contributes to the valorization of industrial by-products and offers a sustainable and environmentally friendly approach to address the challenges associated with organic dye removal. Moreover, considering the growing global demand for chitosan production for various purposes, this research not only demonstrates the efficient utilization of insect resources but also promotes the development of sustainable strategies for water treatment and environmental protection.

Chapter 6 Chitosan from *Eurycantha calcarata* for 3D bioprinting[4]

In this chapter, we investigated the potential of *Eurycantha calcarata* chitosan for hydrogel formation and 3D bioprinting (Figure 6.1). Prepared hydrogels were characterized by FTIR and TGA. The rheological properties were characterized to demonstrate the printability of the prepared hydrogel. Cell viability assay and fluorescence staining were performed to demonstrate the cytocompatibility of the printed scaffolds. The printed scaffolds showed great printability and interacted well with cells, making them a potential candidate for future biomedical applications.

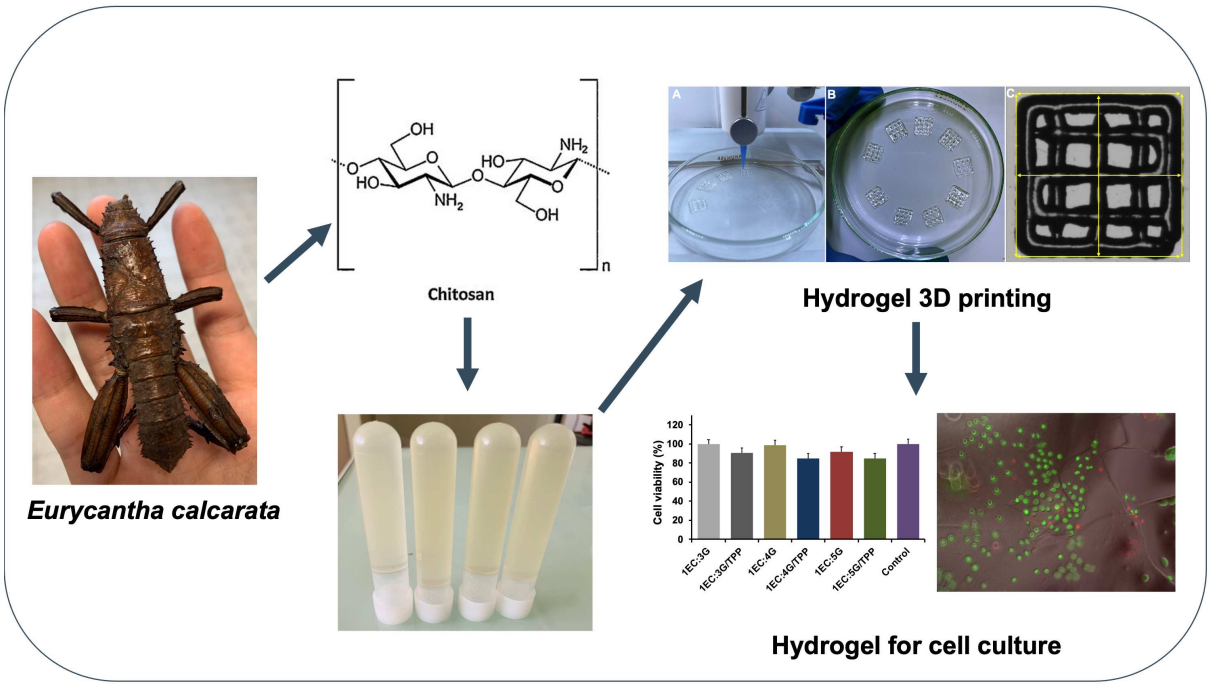

Figure 6.1 Schematic illustration of chitosan from *E. calcarata* for 3D bioprinting.

[4] Main contents of this chapter are submitted in the paper Mei, Z.; Lagouarde, J.; Volkova, O; Candet, C; Kuzhir, P.; Godeau, G. Investigation on chitosan hydrogel from *Eurycantha calcarata* and its potential application for 3D bioprinting.

6.1 *Eurycantha calcarata* chitosan-gelatin (ECG) hydrogels characterization

6.1.1 TGA analysis of ECG hydrogels

The thermal stability and thermal decomposition of the dried ECG hydrogels were investigated using TGA and the results are shown in Figure 6.2, tested as descripted in section 3.3.5. The curve of non-crosslinked ECG hydrogels showed a main zones of weight loss about 45.0%, at 295-310 °C, denoted the intermolecular disintegration and the decomposition of polymeric chains between *E. calcarata* chitosan and gelatin. These results are consistent with the chitosan-gelatin gels in the literature [244]. The curve of ECG hydrogels crosslinked with TPP showed the weight loss about 12.2% to 13.3%, at 195-202 °C, was thought to be the disintegration between TPP and chitosan-gelatin gels; the weight loss about 29.8% to 36.2%, at 329-338 °C, represented the decomposition of polymeric chains between *E. calcarata* chitosan and gelatin. All these results indicate that the thermal stability of the ECG hydrogels was improved by crosslinking with TPP.

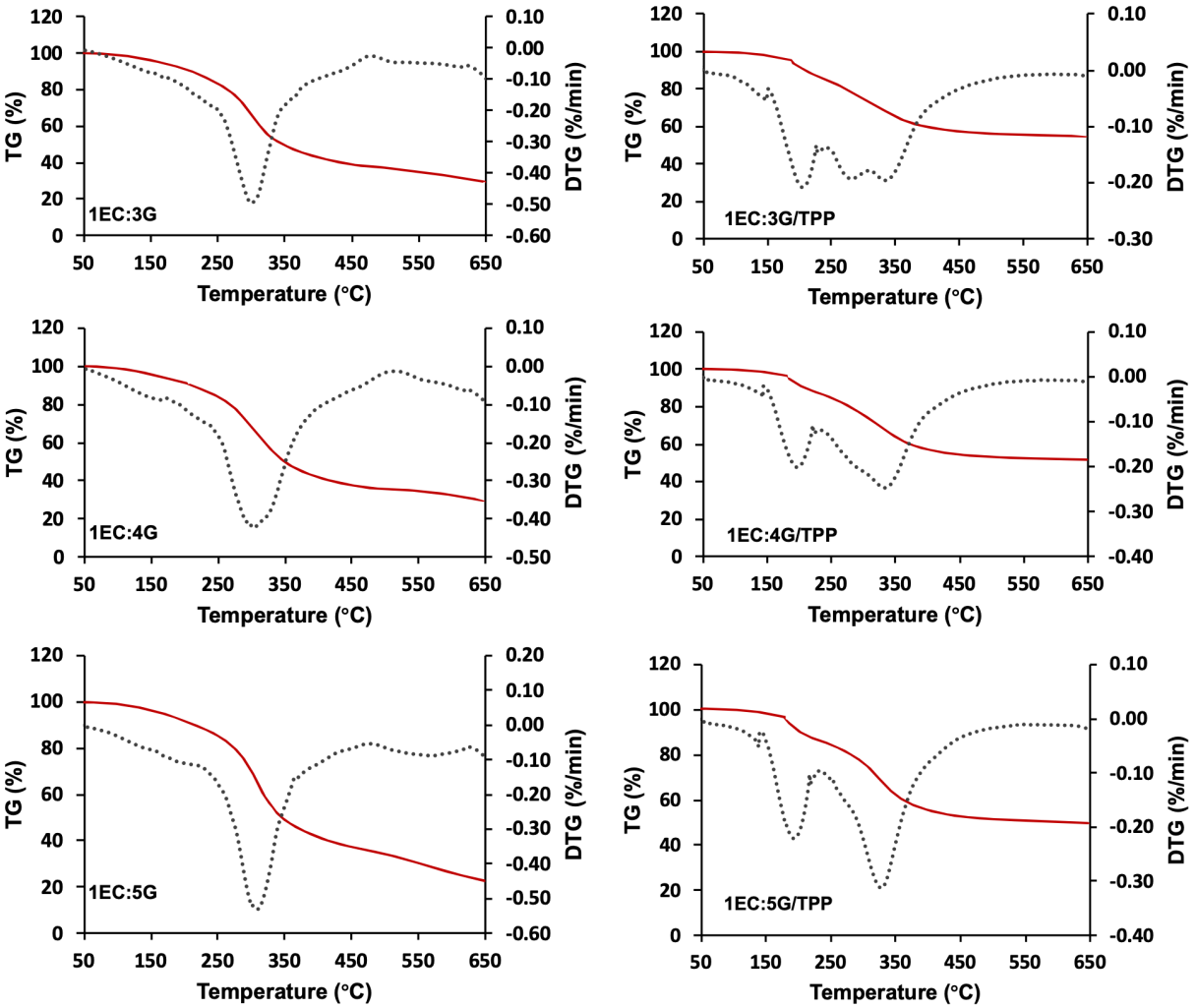

Figure 6.2 Thermogravimetric analysis of ECG hydrogels (TG: red and DTG: grey).

6.1.2 FTIR analysis of ECG hydrogels

The interactions between *E. calcarata* chitosan and gelatin within the blend and the effect of the TPP crosslinking for each crosslinking condition (Table 6.1) were evaluated by FTIR analysis as descripted in section 3.3.2. The C-N and N-H bond vibrations in amide III, the N-H and C-N vibrations in amide II, the C = O and N-H vibrations in amide I (peak of the carbonyl group), and the N-H vibrations in amide A were observed. A comparison of the spectra of the pristine materials and those obtained from the blend for each crosslinking condition revealed the presence of shifts and the disappearance of certain peaks (Figure 6.3). In all the FTIR spectra

acquired for ECG hydrogels, for each ratio and crosslinked condition, it was observed that the carbonyl groups shifted from 1624 cm^{-1} to 1632-1637 cm^{-1}, and the amino groups shifted from 1560 cm^{-1} to 1535-1543 cm^{-1}. Furthermore, it was observed that the gelatin peak at 3063 cm^{-1}, which is attributed to amide A, and the peak at 2933 cm^{-1}, which is attributed to amide B, disappeared in the blend due to the chitosan-gelatin electrostatic interactions (Table 6.1). The observed IR bands for chitosan, gelatin and ECG hydrogels blend are consistent with data reported in the literature [190].

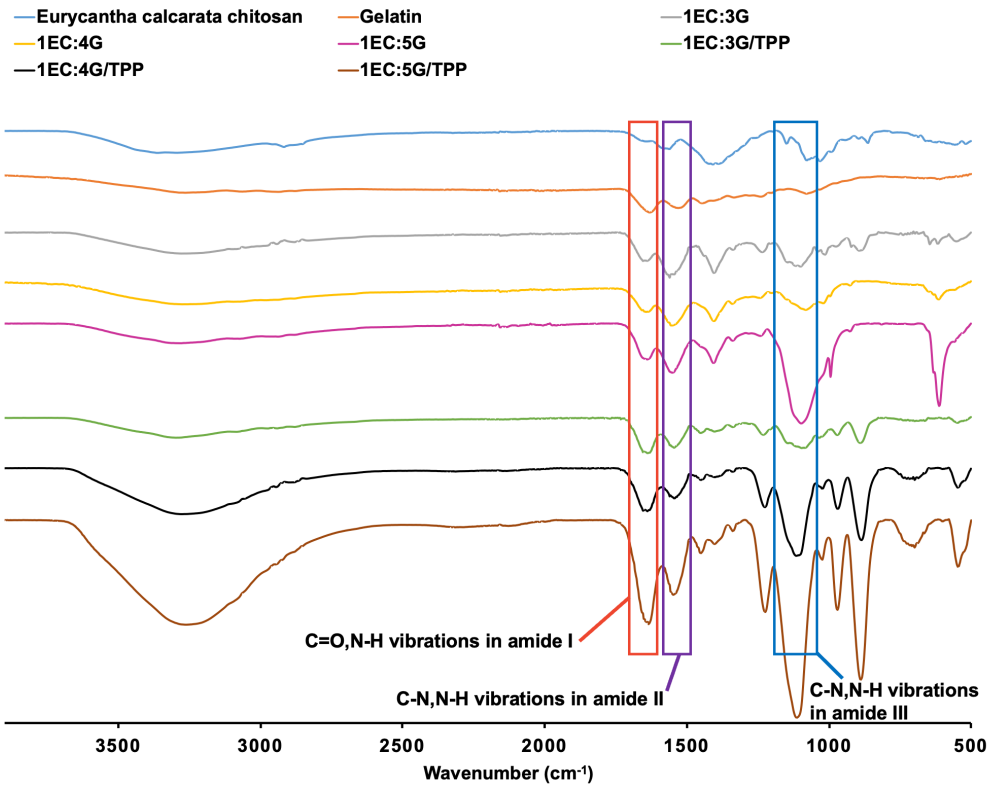

Figure 6.3 FTIR spectra of ECG hydrogels.

Table 6.1 FT-IR functional groups of *E. calcarata* chitosan (EC), gelatin and ECG hydrogels.

Functional group	EC peaks	Gelatin peaks	ECG hydrogels blend
C-N, N-H vibrations in amide III	1251 cm^{-1}	1234 cm^{-1}	1234-1225 cm^{-1}
C-N, N-H vibrations in amide II	1560 cm^{-1}	1518 cm^{-1}	1535-1543 cm^{-1}
C=O, N-H vibrations in amide I	1641 cm^{-1}	1624 cm^{-1}	1632-1637 cm^{-1}
N-H vibrations in amide A	-	3063 cm^{-1}	/
C-H vibrations in amide B	-	2933 cm^{-1}	/

6.1.3 Rheological measurements of ECG hydrogels

The measurements were tested as descripted in section 3.3.8. The results presented in Figure 6.4 show that the storage modulus is greater than the loss modulus at low temperature for three different formulations. For 1EC:3G gel, the storage modulus slowly decreases between 10 and 24 °C, revealing the beginning of gel melting. At temperatures above 24 °C, the modulus dramatically decreases indicating that the gel is molten. At the highest temperature tested, 29°C, the storage modulus becomes nearly equivalent to the loss modulus, indicating a solid-liquid transition of the gel at this temperature. This observation indicates that the 1EC:3G gel should be totally molten at 29 °C but will remain solid at 24 °C. For 1EC:4G gel, the storage modulus slowly decreases between 10 and 25 °C, dramatically decreases at temperatures above 25 °C, and becomes nearly equivalent to the loss modulus 30°C. This observation indicates that the 1EC:4G gel should be totally molten at 30 °C but will remain solid at 25 °C. For 1EC:5G gel, the storage modulus slowly decreases between 10 and 26 °C, dramatically decreases at temperatures above 26 °C, and becomes nearly equivalent to the loss modulus 32°C. This observation indicates that the 1EC:5G gel should be totally molten at 32 °C but will remain solid at 26 °C. These properties are suitable for 3D printing applications.

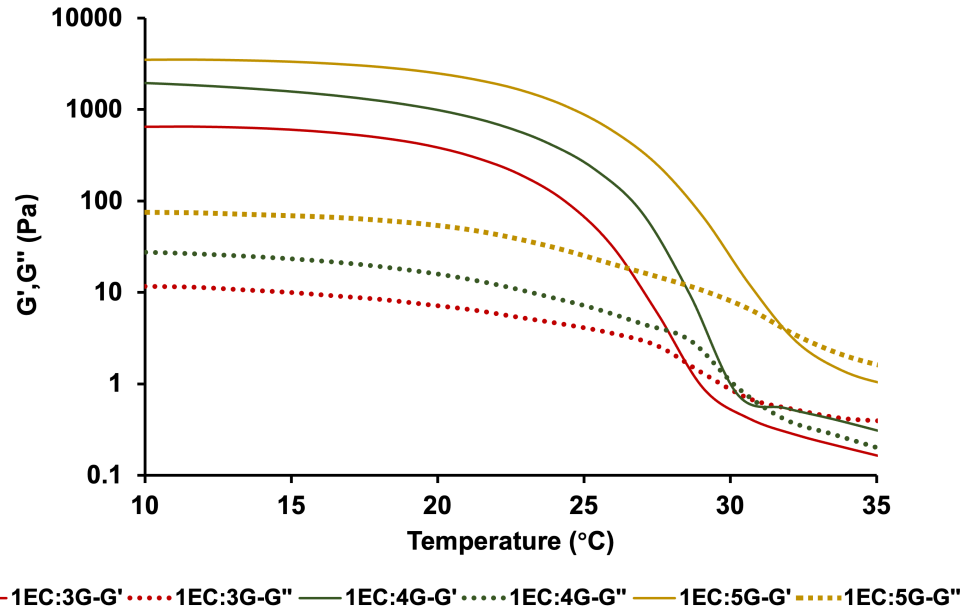

Figure 6.4 Measurement of storage moduli (G') and loss moduli (G'') as function of the temperature (γ = 0.5%, f = 1 Hz) for ECG hydrogels with different formulations.

The second set of rheological measurements of viscosity as a function of shear rate for ECG hydrogels was conducted at 22 °C, which is consistent with the temperature of 3D print process. The shear rate range was chosen to fit the one of the flow though the injector of the 3D printer used in our study, which can be evaluated as the shear rate at the internal wall of the printer nozzle (needle): $\dot{\gamma} = \frac{4Q}{\pi R^3} = \frac{4v}{R} = \frac{8v}{D} = 97.56\ s^{-1}$, where Q is volume flow rate, the nozzle internal diameter $D = 0.41\ mm$, $v = 5\ mm \cdot s^{-1}$ is the flow rate and the speed of the hydrogel through the nozzle. As we can see from Figure 6.5, viscosity decreased with the increasing shear rate, indicating shear-thinning behavior of ECG hydrogels, which is consistent with the previous literature published by my hosting team [134].

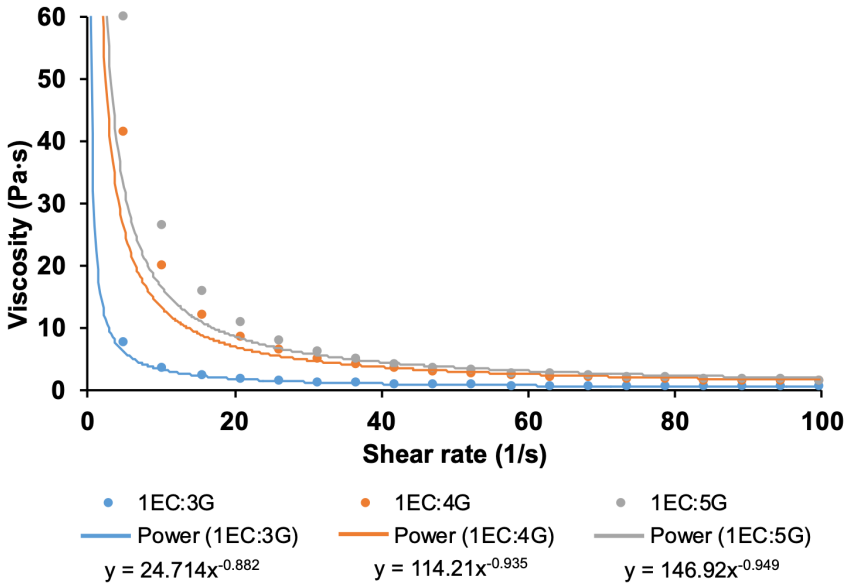

Figure 6.5 Measurement of viscosity as a function of shear rate for ECG hydrogels.

For a deeper insight into the 3D printing process, we will now evaluate the pressure difference applied to the hydrogel by the 3D printer to extrude the hydrogel at a desired speed v through the nozzle. To this purpose, we fit the viscosity curves of Figure 6.5 by a power law model:

$$\eta = K\dot{\gamma}^{n-1} \tag{6.1}$$

where K is the hydrogel consistency and n is a power-law index. Using Origin software, we get the following values of the rheological parameters K and n for the three considered hydrogels (Table 6.2).

Table 6.2 The consistency coefficient K and power-law index n of hydrogels.

Hydrogels	K	n
1EC:3G	24.71 Pa·s$^{0.12}$	0.12
1EC:4G	114.21 Pa·s$^{0.06}$	0.06
1EC:5G	146.92 Pa·s$^{0.05}$	0.05

The flow consistency coefficient K is a key parameter in power-law fluid modelling, which reflects the basic magnitude of the fluid's viscosity properties or resistance to flow. Specifically, the larger K is, the higher the viscosity of the fluid. Hence, as the proportion of gelatin in the hydrogels increases, the viscosity of the hydrogels increases. The value of power-law index n determines the type of fluid: when $n = 1$, the fluid is Newtonian with constant viscosity; when $n < 1$, the fluid exhibits shear-thinning behavior (viscosity decreases with increasing shear rate); and when $n > 1$, the fluid exhibits shear-thickening behavior (viscosity increases with increasing shear rate) [245]. As showed in Table 6.2, all the hydrogels exhibit shear-thinning behavior, which is ideal for 3D printing.

The pressure loss through the nozzle is evaluated using the following expression obtained from [246]:

$$\Delta P = \frac{2KL_1}{R_1}\left(\left(3+\frac{1}{n}\right)\frac{vR_2^2}{R_1^3}\right)^n + \frac{2KL_2}{3n(R_1-R_2)}\left(1-\left(\frac{R_2}{R_1}\right)^{3n}\right)\left(\left(3+\frac{1}{n}\right)\frac{v}{R_2}\right)^n \quad (6.2)$$

where L_1 = 12 mm, L_2 = 20 mm, is the nozzle (needle) length; $D_1 = 2R_1 = 4.3$ mm, $D_2 = 2R_2 = 0.41$ mm as showed in Figure 3.1, nozzle includes cylindrical and conical sections. Using Eq. (6.2), the values of the total pressure loss for hydrogels 1EC:3G, 1EC:4G and 1EC:5G were calculated as 1800 Pa, 7800 Pa and 9800 Pa. The print pressure applied by the 3D printer must be at least equal to or greater than the pressure loss in the nozzle to ensure that the fluid can pass through the entire extrusion system and be extruded correctly. During 3D print, the extrusion pressure around 10 kPa was set to ensure proper and continuous filament formation. These calculated values are of the same order of magnitude that experimental values of the applied pressure.

In summary, all these observations again confirm that the prepared ECG hydrogels are good candidate to prepare bio-ink for bio-printing.

6.2 3D printing assays of ECG hydrogels

6.2.1 Print accuracy

In the context of 3D printing, the preservation of the printed shape is of great importance. Indeed, following printing, the risk exists that the hydrogel will flow and lose the printed shape due to the combined effects of gravity and gel fluidity. The investigation of shape fidelity for each formulation of 3D printed scaffolds was performed by measuring the dimensions, such as length and width (Figure 6.6) as descripted in section 3.5.2.

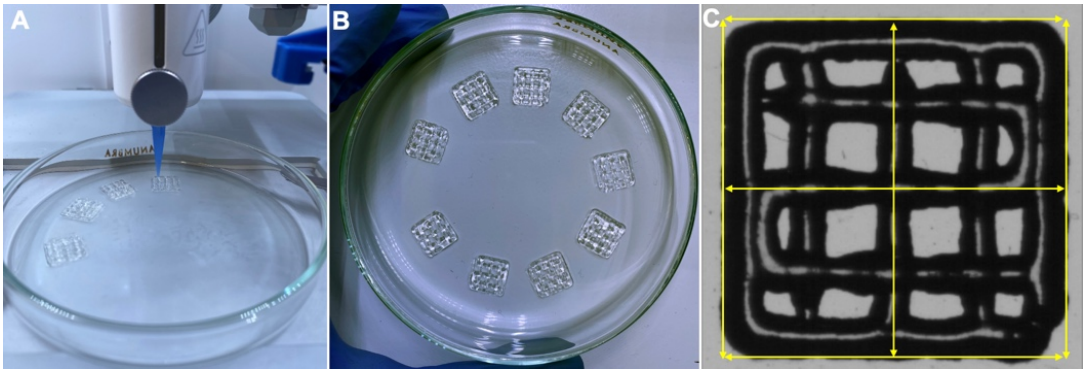

Figure 6.6 Example of 3D printed scaffolds.

The printing accuracy was calculated according to Eq. (3.12). In comparison with the designed structures, all the presented printed structures exhibit a high degree of similarity, with a 10% variation in size. The formed hydrogels did not flow after printing, since the printing shapes were preserved for a few hours at room temperature (observations in Figure 6.7 were made 2 h after printing). This observation indicates that the prepared hydrogel is compatible with bioprinting.

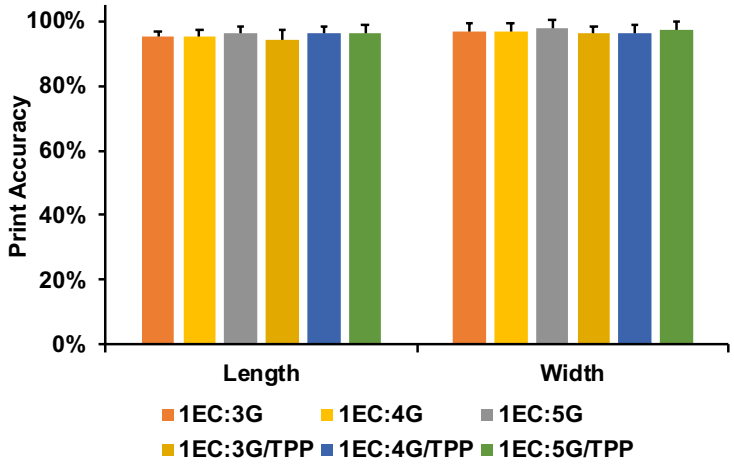

Figure 6.7 Print accuracy compared with the theoretical model.

6.2.2 Stability Test

A stability test was conducted *in vitro* on the printed samples for each gel ratio as descripted in section 3.5.3, maintaining the samples in the medium at 37°C for up to 21 days (Figure 6.8). A comparison of the 1EC:3G, 1EC:4G, and 1EC:5G conditions revealed that the weight variation was not statistically significant ($p > 0.05$) between the 1EC:3G and 1EC:4G conditions at any time point during the stability test. In particular, the 1EC:3G and 1EC:4G conditions exhibited greater weight stability than the 1EC:5G conditions, with the greatest stability observed after two days. Over time, at later time points, the effect of chains cleaving due to bulk erosion on gels with a higher ratio of gelatin becomes more dominant than in gels with a lower ratio of gelatin, which is consistent with previous literature [190]. This could be attributed to the higher presence of gelatin. The higher the concentration of gelatin, the greater its hydrophilicity. Consequently, the effect of water penetrating the bulk and cleaving chemical bonds is greater, resulting in the rupture of long chains into water-soluble fragments. It has been demonstrated that gelatin dissolution in the presence of water is accelerated when the gelatin concentration is elevated [247]. The comparison of stability results for the scaffolds with or without crosslinking indicated that the stability of the scaffolds without crosslinking was higher than that of the TPP-crosslinked ones under the same conditions. The crosslinking process with

TPP can alter the structure and physical properties like porosity and solubility of the hydrogel, which in turn can influence its stability and compatibility with cell culture conditions. In addition, TPP may potentially react with certain components present in the cell culture media, leading to ion release or structural modifications within the gel matrix, thus influencing cell behavior and stability.

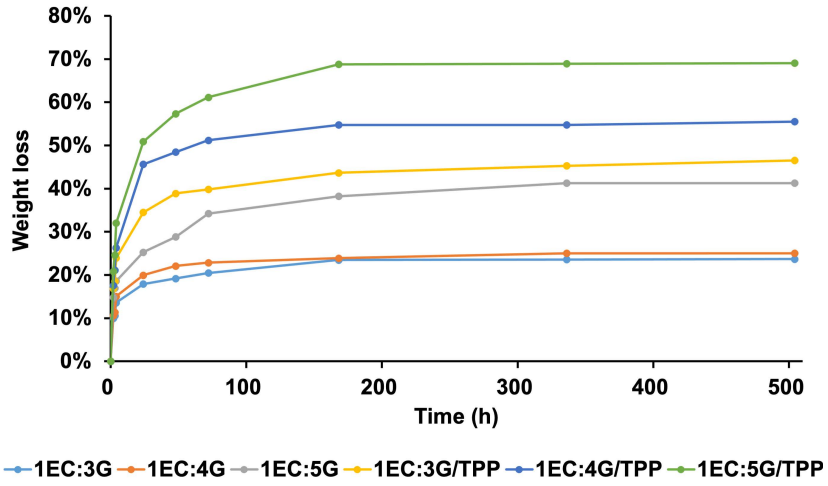

Figure 6.8 Stability of ECG hydrogels at different test times.

6.2.3 *In vitro* cytocompatibility test of ECG scaffolds

The cytocompatibility of tissue-engineering scaffolds is an essential factor to evaluate the feasibility of their clinical application as descripted in section 3.5.4. To evaluate this parameter for the ECG scaffolds, HeLa cells were seeded on the surface of different scaffolds, cultured for 3 days, and stained for live/dead cell assay. The quantitative statistics of cell viability and the fluorescence images of live/dead-stained cells and are shown in Figure 6.9 and Figure 6.10. The viability of cells seeded onto the 1EC:3G scaffolds was the highest among all scaffolds with a value of 99.6 % on day 3. A similar result was found for 1EC:4G scaffolds, the cell viability was 98.7 % on day 3. Meanwhile, 1EC:5G, 1EC:3G/TPP, 1EC:4G/TPP, 1EC:5G/TPP scaffolds also presented high viability, as the value was 91.9%, 90.7%, 84.7%, 84.6% for HeLa cells on day 3, respectively. The scaffolds before and after TPP crosslinking showed no

significant difference compared to each other. The comparison of cell viability results for the scaffolds with or without crosslinked by TPP demonstrated that the cell viability of the scaffolds without crosslinking was higher than that of the TPP-crosslinked ones under the same conditions. This observation is consistent with the results revealed by stability test (Figure 6.16). In comparison to similar studies in the literature, the observed cell viabilities are consistent with findings reported for chitosan-based scaffolds used in tissue engineering applications. For example, previous studies have shown that chitosan-gelatin scaffolds are typically highly cytocompatibility, showing increased cell viability within 72 hours with no significant difference compared to negative controls [190].

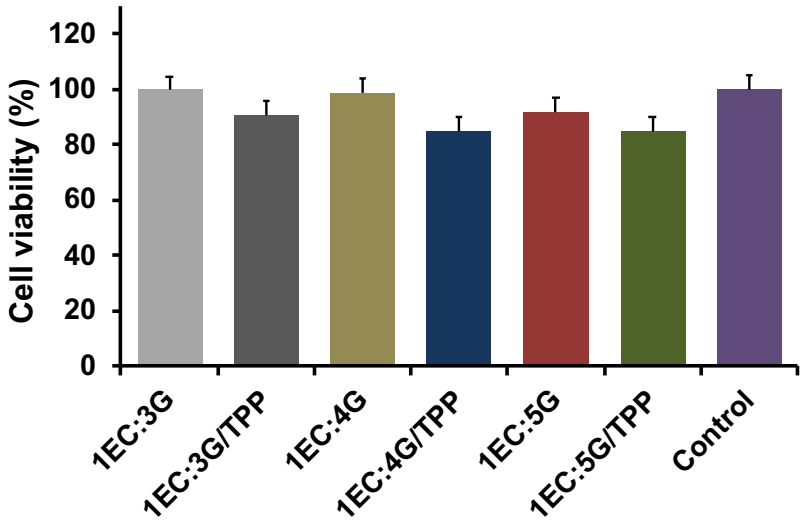

Figure 6.9 *In vitro* cytotoxicity test performed on the printed ECG scaffolds.

The fluorescence images of the live/dead cell staining on the printed ECG scaffolds exhibited high viability, whereas only a few dead cells were found. As can be seen from the arrow marks in the fluorescence images, the cells are embedded within a three-dimensional matrix in the gels, mimicking the natural cellular microenvironment more closely. As we know, traditional 2D cell culture involves cells growing on a flat surface, resulting in a monolayer with limited cell-cell and cell-ECM interactions. This fails to fully mimic *in vivo* cellular complexities, leading to flattened cell morphology and lacking biomechanical cues. 3D cell

culture is more suitable for modeling complex diseases and studying drug responses in a microenvironment that better mimics *in vivo* conditions [159, 248]. These results confirmed that the printed ECG scaffolds featured favorable cytocompatibility and non-toxicity, providing an optimal candidate for future 3D bioprinting explore. Our results align with findings from other studies, where chitosan-based scaffolds have been shown to support high cell viability and promote more natural cell morphologies in 3D cultures. For example, Mohammad *et.* have reported that dental pulp stem cells cultured on chitosan-gelatin scaffolds exhibit enhanced cell proliferation and viability compared to traditional 2D cultures due to the more physiologically relevant environment provided by the 3D matrix [249].

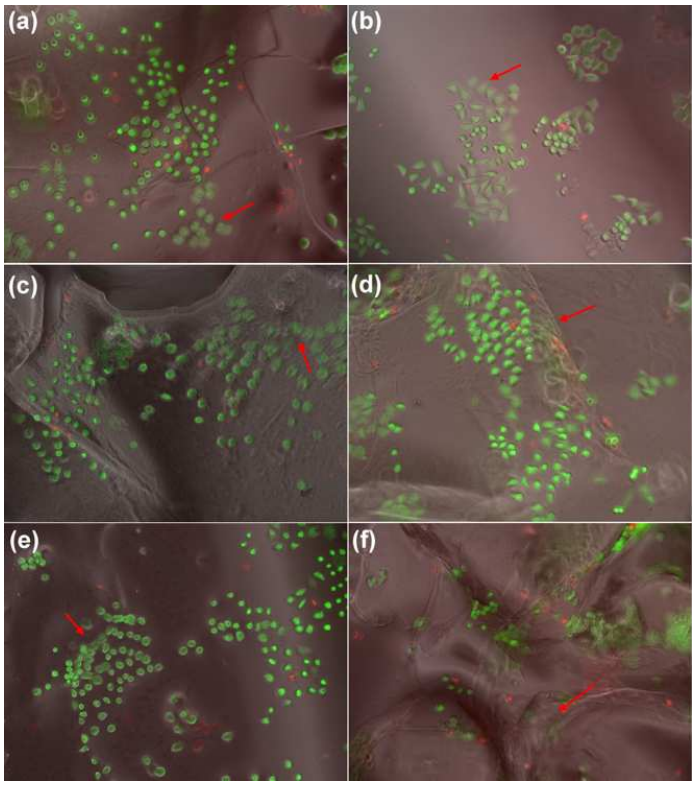

Figure 6.10 Fluorescence images (10×) of HeLa cells seeded on printed ECG scaffolds with different formulations: (a)1EC:3G (b)1EC:4G (c)1EC:5G (d)1EC:3G/TPP (e)1EC:4G/TPP (f)1EC:5G/TPP. (Live cells (green fluorescent) and dead cells (red fluorescent), red arrows indicate cells growing embedded in the ECG scaffolds)

6.3 Summary of this chapter

In this chapter, we report here for the first time the preparation of hydrogels based on *E. calcarata* chitosan and its application in 3D bioprinting. Comprehensive characterization of the prepared hydrogels was conducted utilizing a suite of analytical techniques, including SEM, FTIR, TGA, DSC. The rheological properties of ECG hydrogels were also visualized. Firstly, the rheological test conditions were determined based on the 3D printing parameters, and then the rheological data were substituted into the power law rheological constitutive equation and the pressure drop equation, and the calculated theoretical pressure drop was consistent with the actual value of the applied pressure through the 3D printer nozzle. Notably, the hydrogel exhibited favorable printability characteristics, enabling the fabrication of intricate three-dimensional constructs with a shape accuracy exceeding 90%. Furthermore, *in vitro* cytocompatibility evaluations demonstrated the high viability of cells seeded onto the printed constructs, underscoring the biocompatibility and non-toxic nature of ECG hydrogels. The findings presented in this study hold significant promise for the utilization of *E. calcarata* as a sustainable source for chitosan production, thereby opening avenues for its integration into advanced biomedical applications such as tissue engineering and regenerative medicine. Moreover, this research represents a pioneering endeavor in the valorization of insect-derived waste materials, offering a sustainable and economically viable solution for the exploitation of industrial by-products originating from insect farming activities.

Chapter 7 General conclusion and perspectives

7.1 General conclusion

This thesis aims to valorize insects as an alternative source of chitin and chitosan, focusing on its sources, production methods, characterization techniques, various applications, and highlighting the distinctive advantages it holds over from other sources.

Initially, after a short introduction (Chapter 1) a comprehensive review was summarized in Chapter 2, providing a meticulous exploration of the current state of insect-derived chitin and chitosan, focusing on their sources, production methods, characterization, physical and chemical properties, and emerging biomedical applications. Abundant insect sources of chitin and chitosan, from the Lepidoptera, Coleoptera, Orthoptera, Hymenoptera, Diptera, Hemiptera, Dictyoptera, Odonata, and Ephemeroptera orders, were comprehensively summarized. A variety of characterization techniques were concluded, including spectroscopy, chromatography, and microscopy, used to reveal its physical and chemical properties like molecular weight, degree of deacetylation, and crystallinity, laying a solid foundation for its wide application. The examination of insect-derived chitin and chitosan extends into wide realm of biomedical applications, highlighting their unique advantages in wound healing, tissue engineering, drug delivery, and antimicrobial therapies. Their intrinsic biocompatibility and antimicrobial properties position them as promising candidates for innovative solutions in diverse medical interventions.

After detailed description of characterization techniques (Chapter 3), Chapters 4 investigated the extraction and characterization of chitin and chitosan from various insect

species. The characterization of these materials was performed using techniques such as FTIR, TGA, XRD, SEM, elemental analysis, titration and NMR. Chitin was extracted from nine *Curculionidae* species using demineralization, deproteination, and bleaching, resulting in yields of 12-20%. The extracted chitins from nine *Curculionidae* species showed typical properties with ash content between 3-10% and water content of 2-5%. All the extracted materials present characterization consistent with chitin and can be reported as chitin. Chitosan was derived from *H. castelnaui* with a yield of 11.7% and from *E. calcarata* with a yield of 22.2%. The chitosan from *H. castelnaui* and *E. calcarata* exhibited low ash contents (5.7% and 10%), water content (5% and 10%) and high DDA (78.1% and 78.2%), respectively. These obtained data hold significant promise for the utilization of *H. castelnaui* and *E. calcarata* as sustainable source for chitosan production.

In terms of adsorption performance, in Chapter 5, chitosan derived from *H. castelnaui* was tested for its ability to remove methylene blue and methyl orange dyes from aqueous solutions. For methylene blue, maximum adsorption capacity was 1900 $mg \cdot g^{-1}$ at solution pH = 12; for methyl orange, it was 220 $mg \cdot g^{-1}$ at solution pH = 5 as inferred from fitting the adsorption isotherms to the Langmuir adsorption model. The kinetics of the adsorption process followed the pseudo-second-order kinetic model. The obtained chitosan demonstrated excellent performance in the formation of hydrogels and exhibited remarkable adsorption capacity with respect to published results on other chitosan-based materials or other insect sources, highlighting the efficient and favorable nature of the obtained chitosan as a sorbent for organic dyes. This study provides valuable insights for the development of sustainable dye adsorption technologies, specifically investigating a novel chitosan source derived from the *H. castelnaui*.

Lastly, in Chapter 6, the application of chitosan based on *E. calcarata* for hydrogels formulation and 3D bioprinting was investigated. The rheological properties and microstructure of ECG hydrogels were studied before its application in 3D printing. Notably, the hydrogel

exhibited favorable printability characteristics, enabling the fabrication of intricate three-dimensional constructs with a shape accuracy exceeding 90%. Furthermore, *in vitro* cytocompatibility evaluations demonstrated the high viability of cells seeded onto the printed constructs, underscoring the biocompatibility and non-toxic nature of ECG hydrogels. The findings presented in this study hold significant promise for the utilization of *E. calcarata* as a sustainable source for chitosan production, thereby opening avenues for its integration into advanced biomedical applications such as tissue engineering and regenerative medicine.

In summary, with the increasing global demand for chitin and chitosan in various applications, this study demonstrates the use of insect waste to produce chitin and chitosan, thereby contributing to the valorization of insect resources. This approach provides a sustainable and environmentally friendly solution to the challenges associated with organic dye removal and 3D bioprinting. The use of insect-derived chitin and chitosan not only promotes the conservation of natural resources by converting insect waste into a valuable and renewable resource, but also reduces dependence on non-renewable materials.

7.2 Perspectives

While chitin and chitosan has been extensively studied and applied in various fields, the utilization of insects as a source of chitin and chitosan for industrial application is relatively new and explored incompletely. The applications and product development in the marketplace are still in the research stage, and there are no mature products for medical use. Very limited information on the commercial use of insect-derived chitin and chitosan can be searched. The company, Sfly®, utilizes *Hermetia illucens* larvae for high-quality chitin/chitosan production. In the meanwhile, production techniques of chitin and chitosan from insects have advanced toward sustainability and became greener. The methods such as fermentation, deep eutectic solvents, and microwave extraction, which reduce energy consumption and environmental

impact, are being explored. Stable models for large-scale production, including insect species selection and purification methods, should be further explored. Various advanced characterization techniques have empowered the fine-tuning of biopolymer properties to meet specific application demands. For example, chitosan with lower molecular weight tends to have better solubility in water and other solvents, making it more suitable for certain applications like film-forming and solution-based formulations. Higher molecular weight chitosan is often associated with improved mechanical strength, making it more suitable for applications requiring structural integrity, such as biomedical scaffolds. The ability to customize chitin and chitosan properties for specific applications holds tremendous promise for biomimetic innovation. Building on nature's design principles, such as the adaptability and biocompatibility of insect-derived chitin and chitosan, offers potential for diverse applications.

To further this potential, future studies could expand the pollutant classes addressed by these biopolymers to include heavy metals and pharmaceuticals and explore bioprinting applications with other insect species and in *in-vivo* contexts. Additionally, as research and applications in the medical field evolve, regulatory standards will need to adapt to ensure the safety and efficacy of these biopolymers.

Appendix

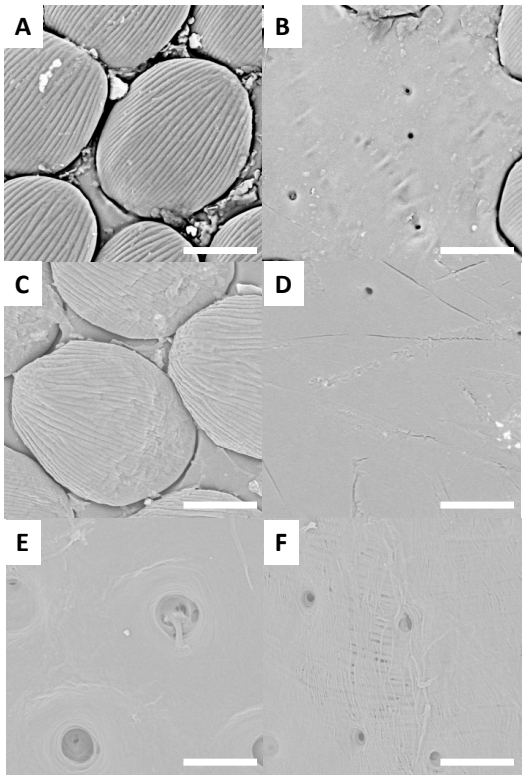

Figure SI 1. SEM image for *E. cuvieri* (Scale bar = 30 µm), Cuticle (A, B, C and D) and extracted chitin (E and F).

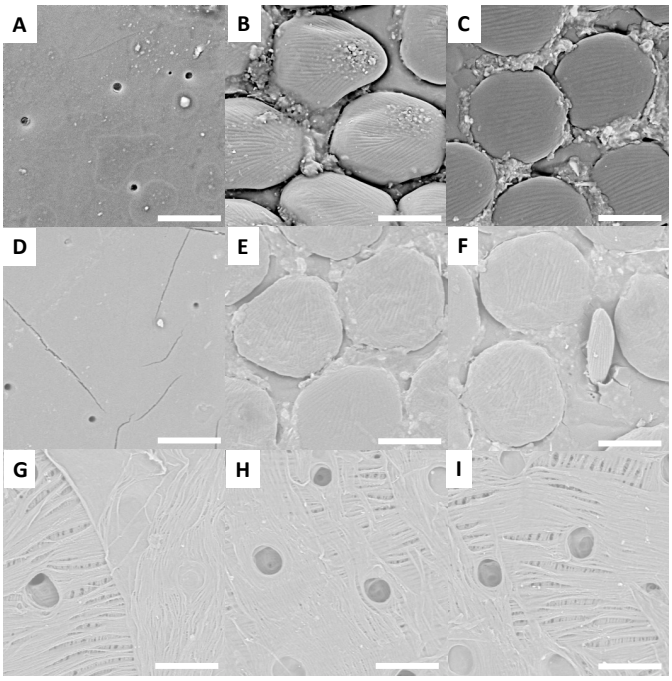

Figure SI 2. SEM image for *E. magnificus* (Scale bar = 30 µm), Cuticle (A to F) and extracted chitin (G, H and I).

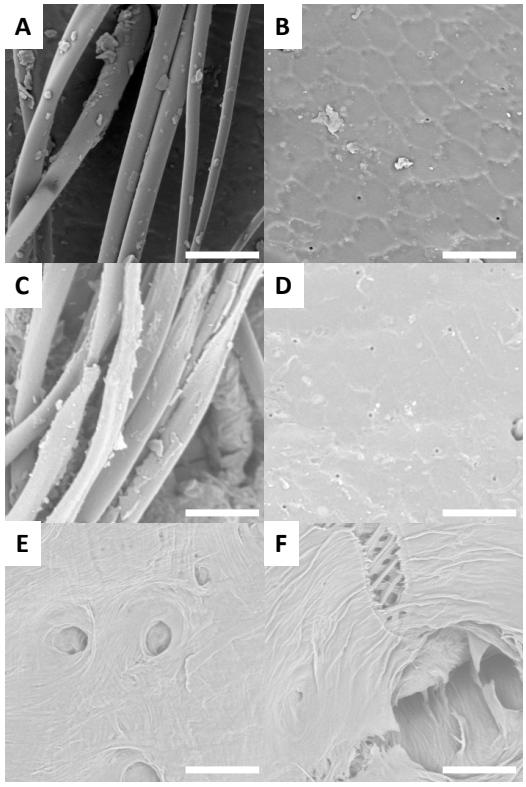

Figure SI 3. SEM image for *L. albicornis* (Scale bar = 30 µm), Cuticle (A, B, C and D) and extracted chitin (E and F).

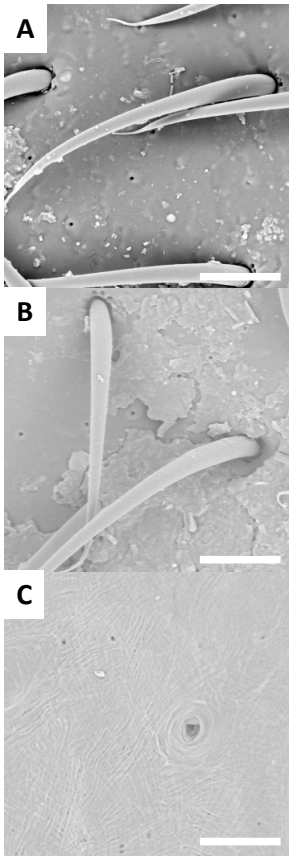

Figure SI 4. SEM image for *L.gigas* (Scale bar = 30 µm), Cuticle (A and B) and extracted chitin (C).

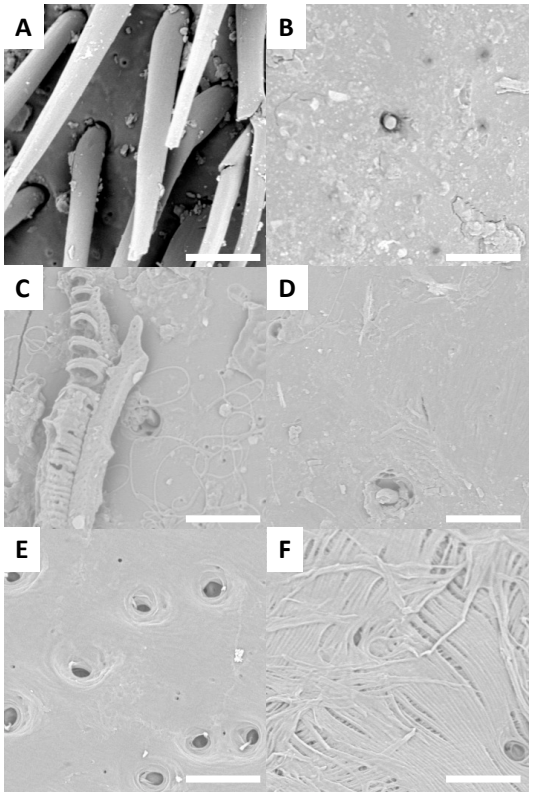

Figure SI 5. SEM image for *L. sturmii* (Scale bar = 30 µm), Cuticle (A, B, C and D) and extracted chitin (E and F).

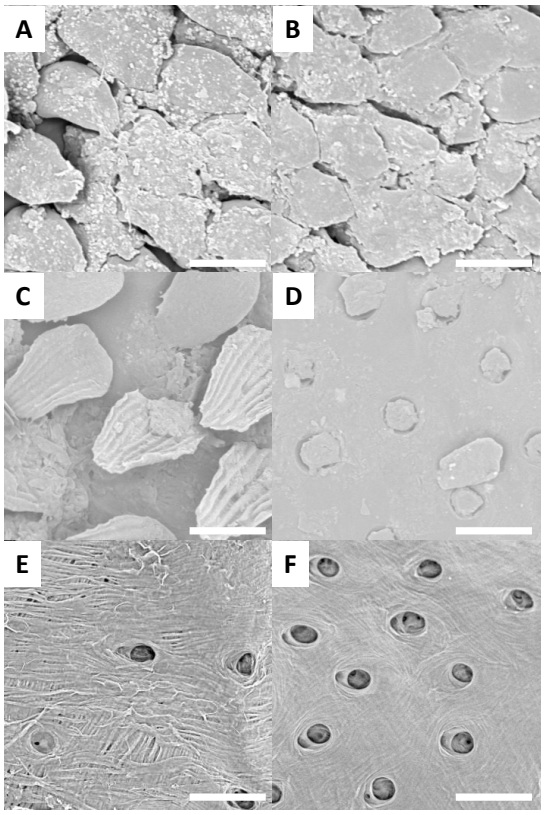

Figure SI 6. SEM image for *H. saxosus* (Scale bar = 30 µm), Cuticle (A, B, C and D) and extracted chitin (E and F).

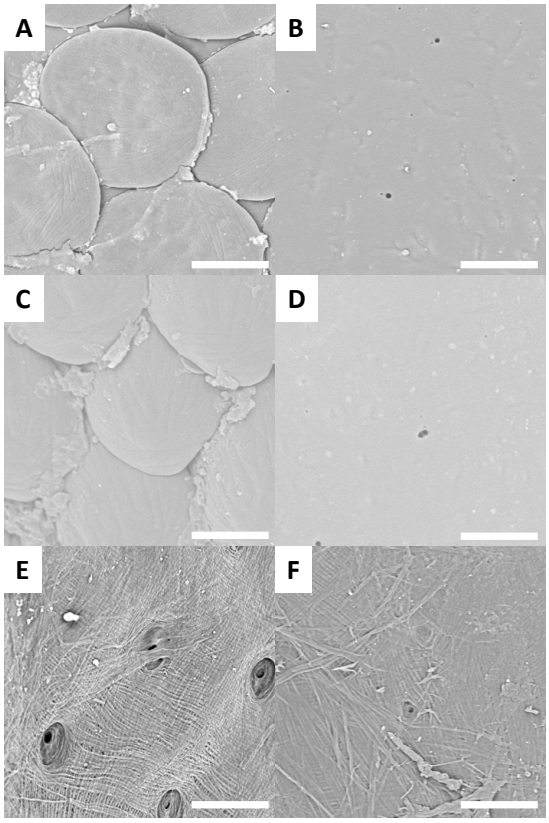

Figure SI 7. SEM image for *P. reticulatus* (Scale bar = 30 µm), Cuticle (A, B, C and D) and extracted chitin (E and F).

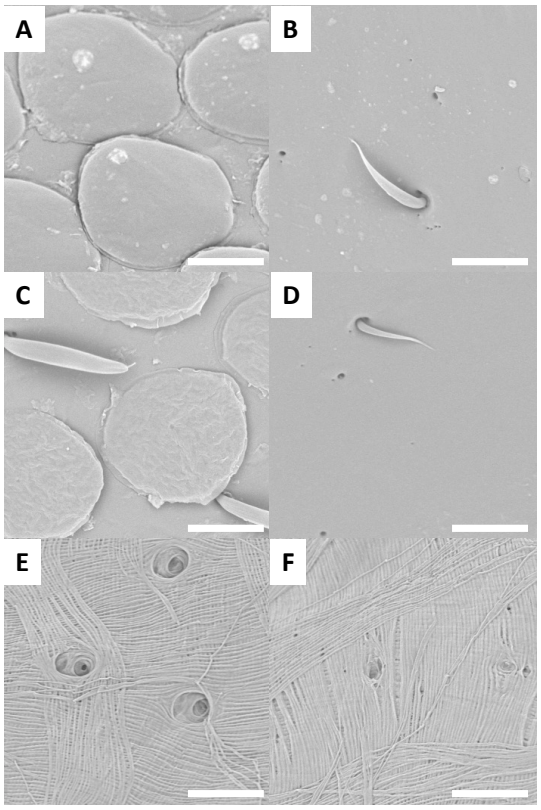

Figure SI 8. SEM image for *P. purpureus* (Scale bar = 30 µm), Cuticle (A, B, C and D) and extracted chitin (E and F).

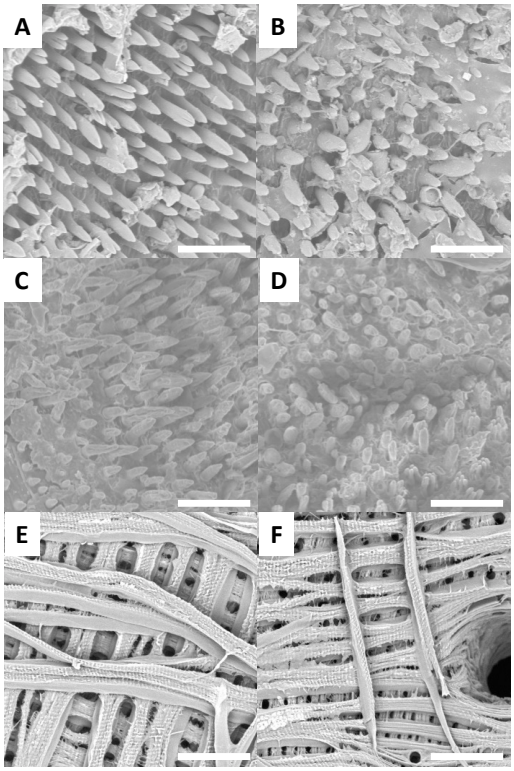

Figure SI 9. SEM image for *S. gigas* (Scale bar = 30 µm), Cuticle (A, B, C and D) and extracted chitin (E and F).

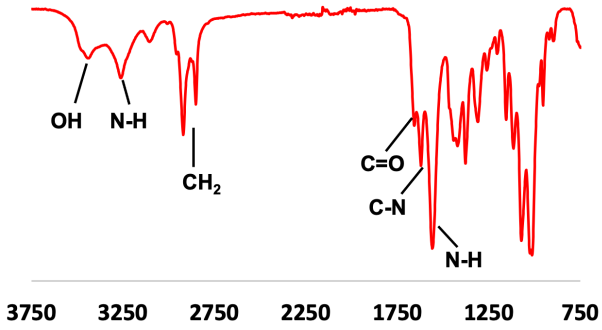

Figure SI 10. FT-IR spectrum for chitin extracted from *E. cuvieri*.

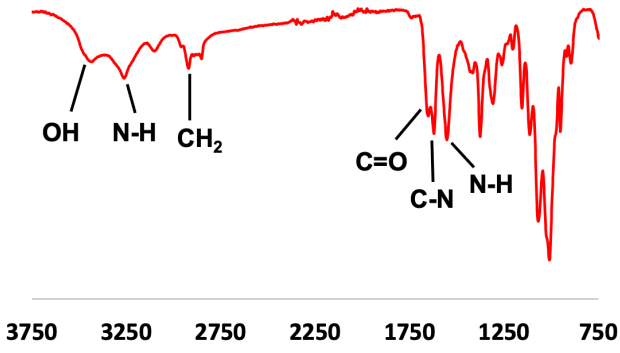

Figure SI 11. FT-IR spectrum for chitin extracted from *E. magnificus*.

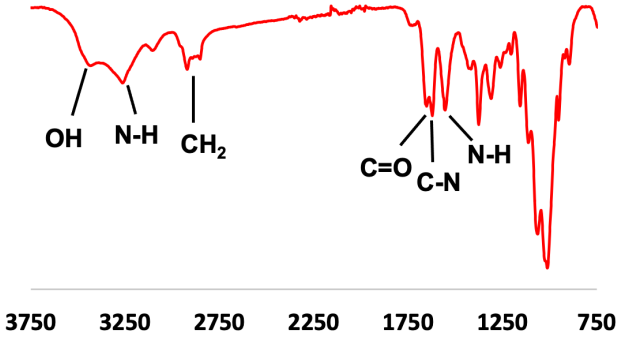

Figure SI 12. FT-IR spectrum for chitin extracted from *L. albicornis*.

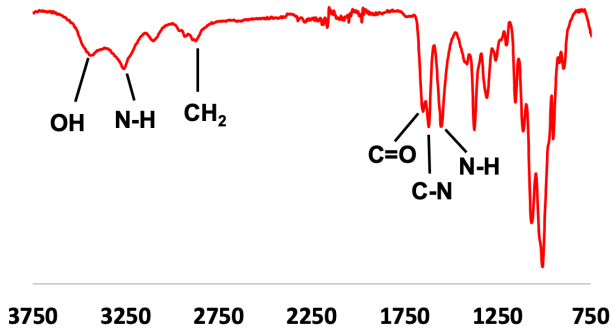

Figure SI 13. FT-IR spectrum for chitin extracted from *L. gigas*.

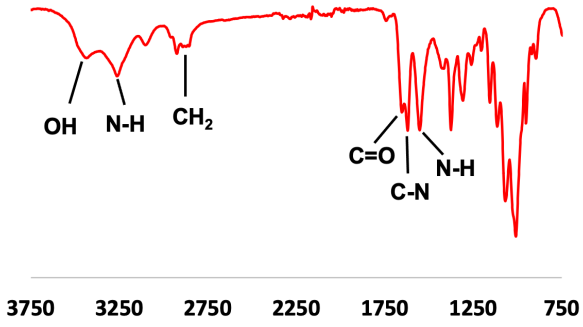

Figure SI 14. FT-IR spectrum for chitin extracted from *L. sturmii*.

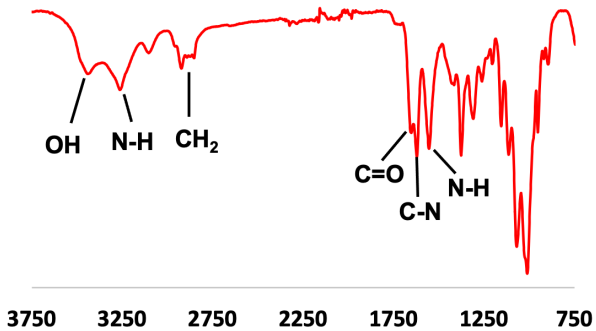

Figure SI 15. FT-IR spectrum for chitin extracted from *H. saxosus*.

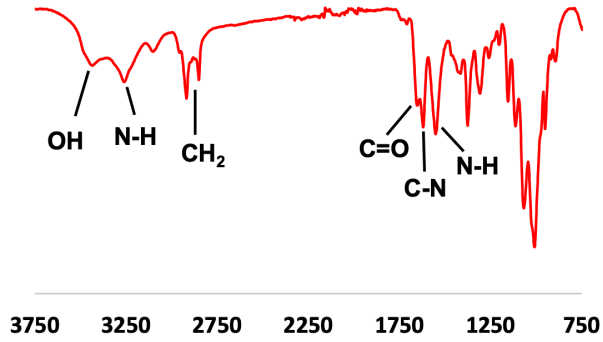

Figure SI 16. FT-IR spectrum for chitin extracted from *P. reticulatus*.

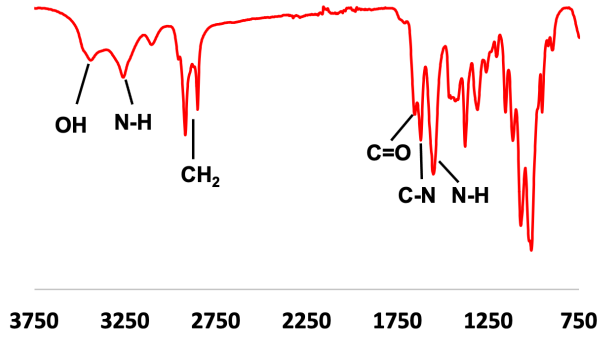

Figure SI 17. FT-IR spectrum for chitin extracted from *P. purpureus*.

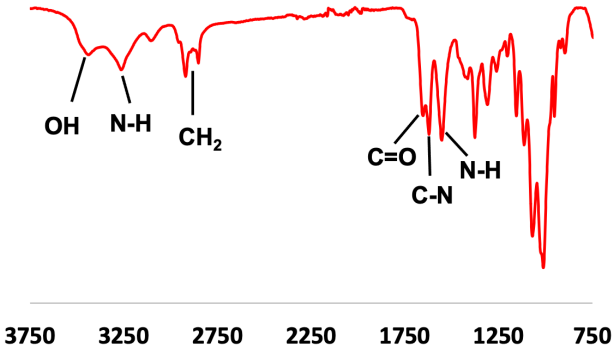

Figure SI 18. FT-IR spectrum for chitin extracted from *S. gigas*.

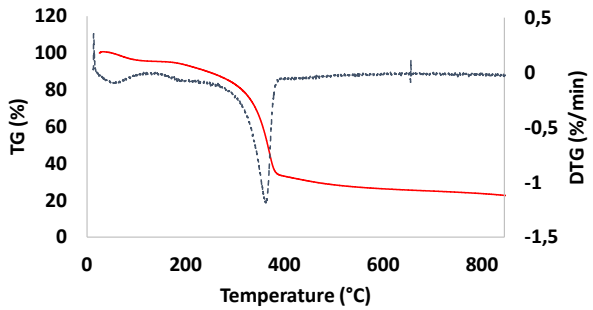

Figure SI 19. Thermal analysis (TGA in red and DTG in blue) of chitin extracted from *E. cuvieri*.

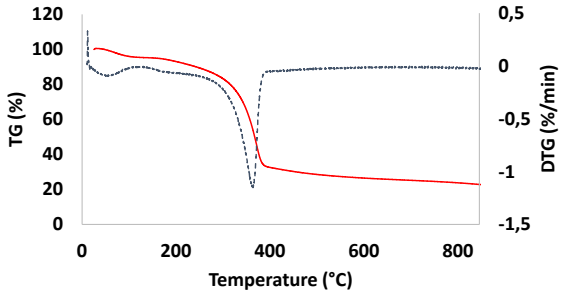

Figure SI 20. Thermal analysis (TGA in red and DTG in blue) of chitin extracted from *E. magnificus*.

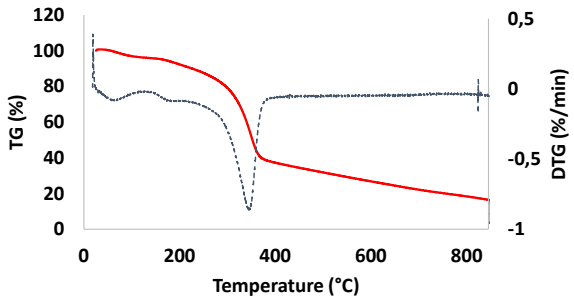

Figure SI 21. Thermal analysis (TGA in red and DTG in blue) of chitin extracted from *L. albicornis*.

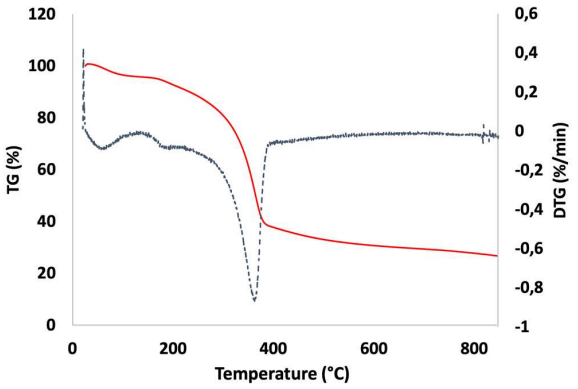

Figure SI 22. Thermal analysis (TGA in red and DTG in blue) of chitin extracted from *L. gigas*.

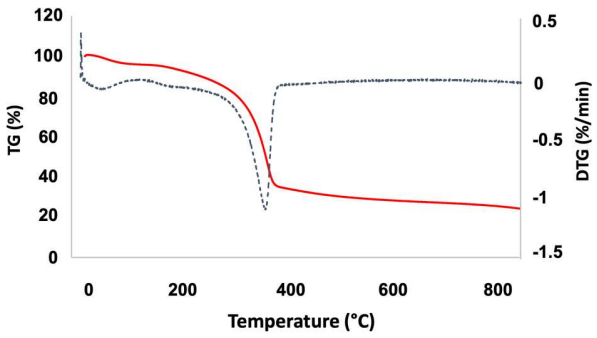

Figure SI 23. Thermal analysis (TGA in red and DTG in blue) of chitin extracted from *L. sturmii*.

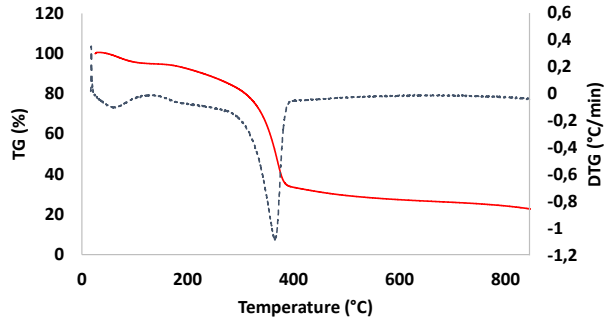

Figure SI 24. Thermal analysis (TGA in red and DTG in blue) of chitin extracted from *H. saxosus*.

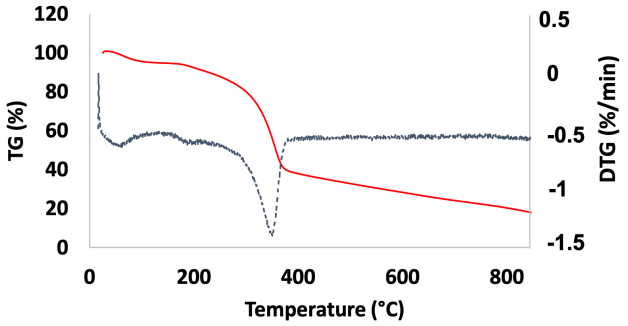

Figure SI 25. Thermal analysis (TGA in red and DTG in blue) of chitin extracted from *P. reticulatus*.

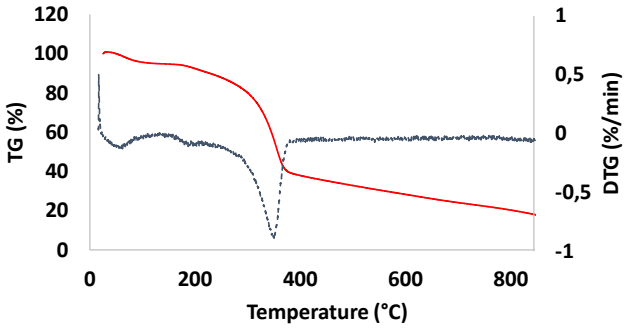

Figure SI 26. Thermal analysis (TGA in red and DTG in blue) of chitin extracted from *P. purpureus*.

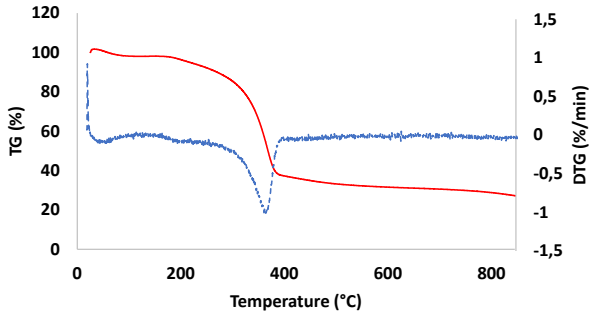

Figure SI 27. Thermal analysis (TGA in red and DTG in blue) of chitin extracted from *S. gigas*.

References

[1] M. Kaya; M. Mujtaba; H. Ehrlich; A. M. Salaberria; T. Baran; C. T. Amemiya; R. Galli; L. Akyuz; I. Sargin, J. Labidi, On chemistry of γ-chitin, *Carbohydrate Polymers*, 176 (2017), 177-186.

[2] J. D. Bumgardner; V. Murali; H. Su; O. Jenkins; D. Velasquez-Pulgarin; J. A. Jennings; A. Sivashanmugam, R. Jayakumar, Characterization of chitosan matters, *Chitosan Based Biomaterials*, 1 (2017), 81-114.

[3] A. A. Leke-Aladekoba, Comparison of extraction methods and characterisation of chitin and chitosan with antimicrobial and antioxidant properties from black soldier fly (Hermetia illucens) meal, Dalhousie University, (2018).

[4] Y. Chen; Y. Liu; Q. Dong; C. Xu; S. Deng; Y. Kang; M. Fan, L. Li, Application of functionalized chitosan in food: A review, *International Journal of Biological Macromolecules*, 235 (2023), 123716.

[5] L. Nicolle; C. M. Journot, S. Gerber-Lemaire, Chitosan functionalization: Covalent and non-covalent interactions and their characterization, *Polymers*, 13 (2021), 4118.

[6] I. O. Saheed; W. Da Oh, F. B. M. Suah, Chitosan modifications for adsorption of pollutants–A review, *Journal of hazardous materials*, 408 (2021), 124889.

[7] C. Ardean; C. M. Davidescu; N. S. Nemeş; A. Negrea; M. Ciopec; N. Duteanu; P. Negrea; D. Duda-Seiman, V. Musta, Factors influencing the antibacterial activity of chitosan and chitosan modified by functionalization, *International Journal of Molecular Sciences*, 22 (2021), 7449.

[8] S. Rashki; K. Asgarpour; H. Tarrahimofrad; M. Hashemipour; M. S. Ebrahimi; H. Fathizadeh; A. Khorshidi; H. Khan; Z. Marzhoseyni, M. Salavati-Niasari, Chitosan-based nanoparticles against bacterial infections, *Carbohydrate Polymers*, 251 (2021),

117108.

[9] S. Peter; N. Lyczko; D. Gopakumar; H. J. Maria; A. Nzihou, S. Thomas, Chitin and chitosan based composites for energy and environmental applications: a review, *Waste and Biomass Valorization*, 12 (2021), 4777-4804.

[10] S. Khattak; F. Wahid; L.-P. Liu; S.-R. Jia; L.-Q. Chu; Y.-Y. Xie; Z.-X. Li, C. Zhong, Applications of cellulose and chitin/chitosan derivatives and composites as antibacterial materials: Current state and perspectives, *Applied microbiology and biotechnology*, 103 (2019), 1989-2006.

[11] T. Hahn; E. Tafi; A. Paul; R. Salvia; P. Falabella, S. Zibek, Current state of chitin purification and chitosan production from insects, *Journal of Chemical Technology & Biotechnology*, 95 (2020), 2775-2795.

[12] M.N. Marzieh; F. Zahra; E. Tahereh, K. N. Sara, Comparison of the physicochemical and structural characteristics of enzymatic produced chitin and commercial chitin, *International Journal of Biological Macromolecules*, 139 (2019), 270-276.

[13] L. D. Fernando; M. C. Dickwella Widanage; J. Penfield; A. S. Lipton; N. Washton; J. P. Latgé; P. Wang; L. Zhang, T. Wang, Structural Polymorphism of Chitin and Chitosan in Fungal Cell Walls From Solid-State NMR and Principal Component Analysis, *Frontiers in Molecular Biosciences*, 8 (2021).

[14] M. Salavati, Mechanical Properties of α-Chitin and Chitosan Biocomposite: A Molecular Dynamic Study, *Journal of Composites Science*, 7 (2023), 464.

[15] R. A. Muzzarelli, Chitin nanostructures in living organisms, *Chitin: Formation and diagenesis*, (2011), 1-34.

[16] M. Feng; X. Lu; D. Hou, S. Zhang, Solubility, chain characterization, and derivatives of chitin, *Handbook of Chitin and Chitosan*, (2020), 101-129.

[17] S. Kumari, R. Kishor, Chitin and chitosan: origin, properties, and applications,

Handbook of chitin and chitosan, (2020), 1-33.

[18] M. T. Yen, J. L. Mau, Selected physical properties of chitin prepared from shiitake stipes, *LWT - Food Science and Technology*, 40 (2007), 558-563.

[19] F. A. A. Sagheer; M. A. Al-Sughayer; S. Muslim, M. Z. Elsabee, Extraction and characterization of chitin and chitosan from marine sources in Arabian Gulf, *Carbohydrate Polymers*, 77 (2009), 410-419.

[20] N. Morin-Crini; E. Lichtfouse; G. Torri, G. Crini, Fundamentals and applications of chitosan, *Sustainable agriculture reviews 35: chitin and chitosan: history, fundamentals and innovations*, (2019), 49-123.

[21] A. Pellis; G. M. Guebitz, G. S. Nyanhongo, Chitosan: Sources, processing and modification techniques, *Gels*, 8 (2022), 393.

[22] J. D. Bumgardner; V. P. Murali; H. Su; O. D. Jenkins; D. Velasquez-Pulgarin; J. A. Jennings; A. Sivashanmugam, R. Jayakumar, Characterization of chitosan matters, *Chitosan Based Biomaterials,* 1 (2017), 81-114.

[23] C. P. Jiménez-Gómez, J. A. Cecilia, Chitosan: a natural biopolymer with a wide and varied range of applications, *Molecules*, 25 (2020), 3981.

[24] N. A. Zainol Abidin; F. Kormin; N. A. Zainol Abidin; N. A. F. Mohamed Anuar, M. F. Abu Bakar, The Potential of Insects as Alternative Sources of Chitin: An Overview on the Chemical Method of Extraction from Various Sources, *International Journal of Molecular Sciences*, 21 (2020), 4978.

[25] Q. Luo; Y. Wang; Q. Han; L. Ji; H. Zhang; Z. Fei, Y. Wang, Comparison of the physicochemical, rheological, and morphologic properties of chitosan from four insects, *Carbohydrate Polymers*, 209 (2019), 266-275.

[26] M. Mehranian; R. F. Pourabad; N. S. Bashir, S. Taieban, Physicochemical characterization of chitin from the Mediterranean flour moth, Ephestia kuehniella Zeller

(Lepidoptera: Pyralidae), *Journal of Macromolecular Science, Part A*, 54 (2017), 720-726.

[27] M. Kaya; B. Bitim; M. Mujtaba, T. Koyuncu, Surface morphology of chitin highly related with the isolated body part of butterfly (Argynnis pandora), *International journal of biological macromolecules*, 81 (2015), 443-449.

[28] S. J. Wu; S. K. Pan; H. B. Wang, J. H. Wu, Preparation of chitooligosaccharides from cicada slough and their antibacterial activity, *International journal of biological macromolecules*, 62 (2013), 348-351.

[29] Z. Xia; J. Chen, S. Wu, Hypolipidemic activity of the chitooligosaccharides from Clanis bilineata (Lepidoptera), an edible insect, *International journal of biological macromolecules*, 59 (2013), 96-98.

[30] S. Wu; M. Lu, S. Wang, Antiageing activities of water-soluble chitosan from Clanis bilineata larvae, *International journal of biological macromolecules*, 102 (2017), 376-379.

[31] M. Kaya; I. Sargin; V. Aylanc; M. N. Tomruk; S. Gevrek; I. Karatoprak; N. Colak; Y. G. Sak, E. Bulut, Comparison of bovine serum albumin adsorption capacities of α-chitin isolated from an insect and β-chitin from cuttlebone, *Journal of Industrial and Engineering Chemistry*, 38 (2016), 146-156.

[32] M. Kaya; V. Baublys; E. Can; I. Šatkauskienė; B. Bitim; V. Tubelytė, T. Baran, Comparison of physicochemical properties of chitins isolated from an insect (Melolontha melolontha) and a crustacean species (Oniscus asellus), *Zoomorphology*, 133 (2014), 285-293.

[33] M. Kaya; E. Bulut; M. Mujtaba; K. Sivickis; I. Sargin; B. Akyuz, S. Erdogan, Gender Influences Differentiation of Chitin among Body Parts, *Archives of insect biochemistry and physiology*, 93 (2016), 96-109.

[34] M. Kaya; T. Baran; S. Erdogan; A. Mentes; M. A. Ozusaglam, Y. S. Cakmak, Physicochemical comparison of chitin and chitosan obtained from larvae and adult Colorado potato beetle (Leptinotarsa decemlineata), *Materials Science and Engineering: C*, 45 (2014), 72-81.

[35] J. Ma; C. Xin, C. Tan, Preparation, physicochemical and pharmaceutical characterization of chitosan from Catharsius molossus residue, *International journal of biological macromolecules*, 80 (2015), 547-556.

[36] N. H. Marei; E. A. El-Samie; T. Salah; G. R. Saad, A. H. Elwahy, Isolation and characterization of chitosan from different local insects in Egypt, *International journal of biological macromolecules*, 82 (2016), 871-877.

[37] N. Marei; A. H. M. Elwahy; T. A. Salah; Y. El Sherif, E. A. El-Samie, Enhanced antibacterial activity of Egyptian local insects' chitosan-based nanoparticles loaded with ciprofloxacin-HCl, *International journal of biological macromolecules*, 126 (2019), 262-272.

[38] Y. Song; M. Kim; C. Moon; D. Seo; Y. Han; Y. Jo; M. Noh; Y. Park; S. Kim; Y. Kim, W. Jung, Extraction of chitin and chitosan from larval exuvium and whole body of edible mealworm, Tenebrio molitor, *Entomological Research*, 48 (2018), 227-233.

[39] A. I. Saenz-Mendoza; P. B. Zamudio-Flores; M. C. Garcia-Anaya; C. R. Velasco; C. H. Acosta-Muniz; J. de Jesus Ornelas-Paz; M. Hernandez-Gonzalez; A. Vargas-Torres; M. A. Aguilar-Gonzalez, R. Salgado-Delgado, Characterization of insect chitosan films from Tenebrio molitor and Brachystola magna and its comparison with commercial chitosan of different molecular weights, *International journal of biological macromolecules*, 160 (2020), 953-963.

[40] Y. J. Son; I. K. Hwang; C. W. Nho; S. M. Kim, S. H. Kim, Determination of carbohydrate composition in mealworm (Tenebrio molitor L.) larvae and

characterization of mealworm chitin and chitosan, *Foods*, 10 (2021), 640.

[41] A. Nafary; S. A. Mousavi Nezhad, S. Jalili, Extraction and Characterization of Chitin and Chitosan from Tenebrio Molitor Beetles and Investigation of its Antibacterial Effect Against Pseudomonas aeruginosa, *Advanced Biomedical Research*, 12 (2023), 96.

[42] C.-S. Shin; D.-Y. Kim, W.-S. Shin, Characterization of chitosan extracted from Mealworm Beetle (Tenebrio molitor, Zophobas morio) and Rhinoceros Beetle (Allomyrina dichotoma) and their antibacterial activities, *International Journal of Biological Macromolecules*, 125 (2019), 72-77.

[43] C. Y. Soon; Y. B. Tee; C. H. Tan; A. T. Rosnita, A. Khalina, Extraction and physicochemical characterization of chitin and chitosan from Zophobas morio larvae in varying sodium hydroxide concentration, *International Journal of Biological Macromolecules*, 108 (2018), 135-142.

[44] Y. Zhatkanbayev; Z. Zhatkanbayeva; Z. Iskakova; A. Kolpek; A. Serikov; N. Moldagulova; G. Danlybayeva; A. Sarsenova, S. Anuarbekova, Application of Chitosan-Based Hydrogel Obtained from Insects in Pine Planting, *International Journal of Biomaterials*, 2023 (2023), 8175405.

[45] M. Kabalak; D. Aracagok, M. Torun, Extraction, characterization and comparison of chitins from large bodied four Coleoptera and Orthoptera species, *International Journal of Biological Macromolecules*, 145 (2020), 402-409.

[46] R. Badawy, H. Mohamed, Chitin extration, Composition of Different Six Insect Species and Their Comparable Characteristics with That of the Shrimp, *Journal of American science*, 11 (2015), 127.

[47] P. Jagdale, Extraction and characterization of chitin from granary weevil, Sitophilus granaries L. (Coleoptera- Curculionidae), *Arthropods*, 4 (2022), 176.

[48] M. Kaya; V. Baublys; I. Sargin; I. Šatkauskienė; A. Paulauskas; B. Akyuz; E. Bulut;

V. Tubelytė; T. Baran; O. Seyyar; M. Kabalak, H. Yurtmen, How Taxonomic Relations Affect the Physicochemical Properties of Chitin, *Food Biophysics*, 11 (2015), 10-19.

[49] I. B. Amor; H. Hemmami; S. E. Laouini; A. G. Abdelaziz, A. Barhoum, Influence of chitosan source and degree of deacetylation on antibacterial activity and adsorption of AZO dye from water, *Biomass Conversion and Biorefinery*, (2023).

[50] K. Ssekatawa; D. K. Byarugaba; E. M. Wampande; T. N. Moja; E. Nxumalo; M. Maaza; J. Sackey; F. Ejobi, J. B. Kirabira, Isolation and characterization of chitosan from Ugandan edible mushrooms, Nile perch scales and banana weevils for biomedical applications, *Scientific Reports*, 11 (2021), 4116.

[51] J. A. Torres-Castillo; S. R. Sinagawa-García; M. Lara-Villalón; G. C. G. Martínez-Ávila; A. Mora-Olivo, F. A. Reyes-Soria, Evaluation of Biochemical Components from （Pterophylla beltrani）(Bolivar & Bolivar) (Orthoptera: Tettigoniidae): A Forest Pest from Northeastern Mexico, *Southwestern Entomologist*, 40 (2015), 741-751, 711.

[52] S. Erdogan, M. Kaya, High similarity in physicochemical properties of chitin and chitosan from nymphs and adults of a grasshopper, *International Journal of Biological Macromolecules*, 89 (2016), 118-126.

[53] E. B. Ibitoye; I. H. Lokman; M. N. M. Hezmee; Y. M. Goh; A. B. Z. Zuki, A. A. Jimoh, Extraction and physicochemical characterization of chitin and chitosan isolated from house cricket, *Biomedical Materials*, 13 (2018), 025009.

[54] M. Kaya; E. Lelesius; R. Nagrockaite; I. Sargin; G. Arslan; A. Mol; T. Baran; E. Can, B. Bitim, Differentiations of chitin content and surface morphologies of chitins extracted from male and female grasshopper species, *PLoS One*, 10 (2015), e0115531.

[55] M. Kaya; T. Baran; M. Asan-Ozusaglam; Y. S. Cakmak; K. O. Tozak; A. Mol; A. Mentes, G. Sezen, Extraction and characterization of chitin and chitosan with antimicrobial and antioxidant activities from cosmopolitan Orthoptera species (Insecta),

Biotechnology and Bioprocess Engineering, 20 (2015), 168-179.

[56] M. Kaya; S. Erdogan; A. Mol, T. Baran, Comparison of chitin structures isolated from seven Orthoptera species, *International journal of biological macromolecules*, 72 (2015), 797-805.

[57] M. Kim; Y. Song; D. Seo; Y. Han; Y. Jo; M. Noh; Y. Yang; Y. Park; S. Kim, C. Choi, Extraction of chitin and chitosan from the exoskeleton of the cockroach (Periplaneta americana L.), *Journal of Chitin and Chitosan*, 22 (2017), 76-81.

[58] K. S. Chae; C. S. Shin, W. S. Shin, Characteristics of cricket (Gryllus bimaculatus) chitosan and chitosan-based nanoparticles, *Food science and biotechnology*, 27 (2018), 631-639.

[59] M.-W. Kim; Y.-S. Song; Y. S. Han; Y. H. Jo; M. H. Choi; Y.-K. Park; S. H. Kang; S.-A. Kim; C. Choi, W.-J. Jung, Production of chitin and chitosan from the exoskeleton of adult two-spotted field crickets (Gryllus bimaculatus), *Entomological Research*, 47 (2017), 279-285.

[60] M. Psarianos; S. Ojha; R. Schneider, O. K. Schluter, Chitin Isolation and Chitosan Production from House Crickets (Acheta domesticus) by Environmentally Friendly Methods, *Molecules*, 27 (2022).

[61] M. Malm; A. M. Liceaga; F. San Martin-Gonzalez; O. G. Jones; J. M. Garcia-Bravo, I. Kaplan, Development of chitosan films from edible crickets and their performance as a bio-based food packaging material, *Polysaccharides*, 2 (2021), 744-758.

[62] M. Psarianos; G. Dimopoulos; S. Ojha; A. C. M. Cavini; S. Bußler; P. Taoukis, O. K. Schlüter, Effect of pulsed electric fields on cricket (Acheta domesticus) flour: Extraction yield (protein, fat and chitin) and techno-functional properties, *Innovative Food Science & Emerging Technologies*, 76 (2022).

[63] M. Malm, A. M. Liceaga, Physicochemical Properties of Chitosan from Two

Commonly Reared Edible Cricket Species, and Its Application as a Hypolipidemic and Antimicrobial Agent, *Polysaccharides*, 2 (2021), 339-353.

[64] M. Kaya; M. Mujtaba; E. Bulut; B. Akyuz; L. Zelencova, K. Sofi, Fluctuation in physicochemical properties of chitins extracted from different body parts of honeybee, *Carbohydrate Polymers*, 132 (2015), 9-16.

[65] D. Tsaneva; Z. Petkova; N. Petkova; M. Stoyanova; A. Stoyanova, P. Denev, Isolation and characterization of chitin and biologically active substances from honeybee (Apis mellifera), *Journal of Pharmaceutical Sciences and Research*, 10 (2018), 884-888.

[66] E. Kovaleva; A. Pestov; D. Stepanova, L. Molochnikov, Characterization of chitin and its complexes extracted from natural raw sources, 1772 (2016).

[67] M. Kaya; N. Bagriacik; O. Seyyar, T. Baran, Comparison of chitin structures derived from three common wasp species (Vespa crabro Linnaeus, 1758, Vespa orientalis Linnaeus, 1771 and Vespula germanica (Fabricius, 1793)), *Archives of insect biochemistry and physiology*, 89 (2015), 204-217.

[68] X. Feás; M. P. Vázquez-Tato; J. A. Seijas; A. Pratima G. Nikalje, F. Fraga-López, Extraction and Physicochemical Characterization of Chitin Derived from the Asian Hornet, Vespa velutina Lepeletier 1836 (Hym.: Vespidae), *Molecules*, 25 (2020), 384.

[69] E. E. Essa; D. Hamza; M. M. Khalil; H. Zaher; D. Salah; A. M. Alnemari; M. H. Rady, S. A. Momen, The antibacterial activity of Egyptian wasp chitosan-based nanoparticles against important antibiotic-resistant pathogens, *Molecules*, 27 (2022), 7189.

[70] M. Kaya; K. Sofi; I. Sargin, M. Mujtaba, Changes in physicochemical properties of chitin at developmental stages (larvae, pupa and adult) of Vespa crabro (wasp), *Carbohydrate Polymers*, 145 (2016), 64-70.

[71] L. Soetemans; M. Uyttebroek, L. Bastiaens, Characteristics of chitin extracted from

black soldier fly in different life stages, *International Journal of Biological Macromolecules*, 165 (2020), 3206-3214.

[72] A. Wasko; P. Bulak; M. Polak-Berecka; K. Nowak; C. Polakowski, A. Bieganowski, The first report of the physicochemical structure of chitin isolated from Hermetia illucens, *International Journal of Biological Macromolecules*, 92 (2016), 316-320.

[73] D. Purkayastha, S. Sarkar, Physicochemical structure analysis of chitin extracted from pupa exuviae and dead imago of wild black soldier fly (Hermetia illucens), *Journal of Polymers and the Environment*, 28 (2019), 445-457.

[74] E. D'Hondt; L. Soetemans; L. Bastiaens; M. Maesen; V. Jespers; B. Van den Bosch; S. Voorspoels, K. Elst, Simplified determination of the content and average degree of acetylation of chitin in crude black soldier fly larvae samples, *Carbohydrate Research*, 488 (2020), 107899.

[75] H. Wang; K. U. Rehman; W. Feng; D. Yang; R. U. Rehman; M. Cai; J. Zhang; Z. Yu, L. Zheng, Physicochemical structure of chitin in the developing stages of black soldier fly, *International Journal of Biological Macromolecules*, 149 (2020), 901-907.

[76] A. Antonov; G. Ivanov; N. Pastukhova, G. Bovykina, Production of chitin from dead Hermetia Illucens, *IOP Conference Series: Earth and Environmental Science*, 315 (2019), 042003.

[77] A. Khayrova; S. Lopatin, V. Varlamov, Black soldier fly Hermetia illucens as a novel source of chitin and chitosan, *International Journal of Sciences*, 8 (2019), 81-86.

[78] A. Caligiani; A. Marseglia; G. Leni; S. Baldassarre; L. Maistrello; A. Dossena, S. Sforza, Composition of black soldier fly prepupae and systematic approaches for extraction and fractionation of proteins, lipids and chitin, *Food research international*, 105 (2018), 812-820.

[79] H. P. Teo; K. W. Law; W. C. Eric Chan, O. Y. Michelle Soo, Antibacterial Properties

of Chitosan Isolated from the Black Soldier Fly, Hermetia illucens, *Sains Malaysiana*, 51 (2022), 3923-3935.

[80] M. K. Lagat; S. Were; F. Ndwigah; V. J. Kemboi; C. Kipkoech, C. M. Tanga, Antimicrobial Activity of Chemically and Biologically Treated Chitosan Prepared from Black Soldier Fly (Hermetia illucens) Pupal Shell Waste, *Microorganisms*, 9 (2021), 2417.

[81] A. Guarnieri; M. Triunfo; C. Scieuzo; D. Ianniciello; E. Tafi; T. Hahn; S. Zibek; R. Salvia; A. De Bonis, P. Falabella, Antimicrobial properties of chitosan from different developmental stages of the bioconverter insect Hermetia illucens, *Scientific Reports*, 12 (2022), 8084.

[82] V. J. Kemboi; C. Kipkoech; M. Njire; S. Were; M. K. Lagat; F. Ndwiga; J. M. Wesonga, C. M. Tanga, Biocontrol potential of chitin and chitosan extracted from black soldier fly pupal exuviae against bacterial wilt of tomato, *Microorganisms*, 10 (2022), 165.

[83] M. K. Lagat, Biological and chemical extraction of chitin and chitosan from the black soldier fly (Hermetia illucens) exoskeleton and antimicrobial activity against selected human pathogenic microbes, JKUAT-COPAS, 2022.

[84] M. Triunfo; E. Tafi; A. Guarnieri; R. Salvia; C. Scieuzo; T. Hahn; S. Zibek; A. Gagliardini; L. Panariello; M. B. Coltelli; A. De Bonis, P. Falabella, Characterization of chitin and chitosan derived from Hermetia illucens, a further step in a circular economy process, *Scientific Report*, 12 (2022), 6613.

[85] M.-B. Coltelli; L. Panariello; A. Vannozzi; V. Gigante; A. Gagliardini; P. Morganti; P. Cinelli; A. Lazzeri; A. De Bonise, P. Falabella, Chitin and its derivatives: nanostructured materials from different marine and terrestrial sources, *Chemical Engineering Transactions*, 93 (2022), 295-300.

[86] Y. H. Lee; S. C. Kim; K. D. Nam; T. H. Kim; B. O. Jung; Y.-I. Park; A. Synytsya, J. K. Park, Chitosan isolated from black soldier flies Hermetia illucens: Structure and enzymatic hydrolysis, *Process Biochemistry*, 118 (2022), 171-181.

[87] A. Khayrova; S. Lopatin; B. Shagdarova; O. Sinitsyna; A. Sinitsyn, V. Varlamov, Evaluation of antibacterial and antifungal properties of low molecular weight chitosan extracted from Hermetia illucens relative to crab chitosan, *Molecules*, 27 (2022), 577.

[88] K. Zlotko; A. Wasko; D. M. Kaminski; I. Budziak-Wieczorek; P. Bulak, A. Bieganowski, Isolation of chitin from black soldier fly (Hermetia illucens) and its usage to metal sorption, *Polymers* 13 (2021), 818.

[89] M. Kaya; B. Akyuz; E. Bulut; I. Sargin; F. Eroglu, G. Tan, Chitosan nanofiber production from Drosophila by electrospinning, *International Journal of Biological Macromolecules*, 92 (2016), 49-55.

[90] M.-W. Kim; Y. S. Han; Y. H. Jo; M. H. Choi; S. H. Kang; S.-A. Kim, W.-J. Jung, Extraction of chitin and chitosan from housefly, Musca domestica, pupa shells, *Entomological Research*, 46 (2016), 324-328.

[91] S. Ilk; A. Ramanauskaite; B. Koc Bilican; P. Mulercikas; D. Cam; M. S. Onses; I. Torun; S. Kazlauskaite; V. Baublys; O. Aydin; L. S. Zang, M. Kaya, Usage of natural chitosan membrane obtained from insect corneal lenses as a drug carrier and its potential for point of care tests, *Materials Science and Engineering: C*, 112 (2020), 110897.

[92] M. Kaya; T. Baran; A. Mentes; M. Asaroglu; G. Sezen, K. O. Tozak, Extraction and Characterization of α-Chitin and Chitosan from Six Different Aquatic Invertebrates, *Food Biophysics*, 9 (2014), 145-157.

[93] A. Mol; M. Kaya; M. Mujtaba, B. Akyuz, Extraction of high thermally stable and nanofibrous chitin from Cicada (Cicadoidea), *Entomological Research*, 48 (2018), 480-489.

[94] A. Sharbidre; S. Sargar; H. Gogoi, R. Patil, Characterization of chitin content extracted from edible insect, Coridius nepalensis (Westwood, 1837) (Hemiptera: Dinidoridae), *International Journal of Tropical Insect Science*, 41 (2021), 1893-1900.

[95] F. Jiang; X. Li; Y. Duan; Q. Li; Y. Qu; G. Zhong; M. Qiu; J. Zhang; C. Zhang, X. Pan, Extraction and characterization of chitosan from Eupolyphaga sinensis Walker and its application in the preparation of electrospinning nanofiber membranes, *Colloids and Surfaces B: Biointerfaces*, 222 (2023), 113030.

[96] M. Kaya; I. Sargin; I. Sabeckis; D. Noreikaite; D. Erdonmez; A. M. Salaberria; J. Labidi; V. Baublys, V. Tubelyte, Biological, mechanical, optical and physicochemical properties of natural chitin films obtained from the dorsal pronotum and the wing of cockroach, *Carbohydrate Polymers*, 163 (2017), 162-169.

[97] H. Basseri; R. Bakhtiyari; S. J. Hashemi; M. Baniardelani; H. Shahraki, L. Hosainpour, Antibacterial/Antifungal Activity of Extracted Chitosan From American Cockroach (Dictyoptera: Blattidae) and German Cockroach (Blattodea: Blattellidae), *Journal of medical entomology*, 56 (2019), 1208-1214.

[98] D. Wanule; J. Balkhande; P. Ratnakar; A. Kulkarni, C. Bhowate, Extraction and FTIR analysis of chitosan from American cockroach, Periplaneta americana, *Extraction*, 3 (2014), 299-304.

[99] M. Kaya, T. Baran, Description of a new surface morphology for chitin extracted from wings of cockroach (Periplaneta americana), *Int J Biol Macromol*, 75 (2015), 7-12.

[100] S. Chen; X. Wei; Z. Sui; M. Guo; J. Geng; J. Xiao, D. Huang, Preparation of Antioxidant and Antibacterial Chitosan Film from Periplaneta americana, *Insects*, 12 (2021), 53.

[101] M. Mahmoud T; H. Mostafa I; B. Ahmed S; M. Aly F, A.-S. Mohammad R. K, Antibacterial and antiviral activities of chitosan nanoparticles from the American

cockroach, Periplaneta americana, *Journal of Applied Pharmaceutical Science*, (2022).

[102] M. Kamal; E. Adly; S. A. Alharbi; A. S. Khaled; M. H. Rady, N. A. Ibrahim, Exploring Simplified Methods for Insect Chitin Extraction and Application as a Potential Alternative Bioethanol Resource, *Insects*, 11 (2020), 788.

[103] M. Kaya; I. Sargin; I. Al-Jaf; S. Erdogan, G. Arslan, Characteristics of corneal lens chitin in dragonfly compound eyes, *International journal of biological macromolecules*, 89 (2016), 54-61.

[104] G. Tan; M. Kaya; A. Tevlek; I. Sargin, T. Baran, Antitumor activity of chitosan from mayfly with comparison to commercially available low, medium and high molecular weight chitosans, *In Vitro Cellular & Developmental Biology-Animal*, 54 (2018), 366-374.

[105] H. Greven; M. Kaya; K. Junker; L. Akyuz, C. T. Amemiya, Characterization of tongue worm (Pentastomida) chitin supports α- rather than β-chitin, *Zoologischer Anzeiger*, 279 (2019), 111-115.

[106] A. Nafisah; Nahrowi; R. Mutia, A. Jayanegara, Chemical composition, chitin and cell wall nitrogen content of Black Soldier Fly (Hermetia illucens) larvae after physical and biological treatment, *IOP Conference Series: Materials Science and Engineering*, 546 (2019), 042028.

[107] H. Srinivasan; V. Kanayairam, R. Ravichandran, Chitin and chitosan preparation from shrimp shells Penaeus monodon and its human ovarian cancer cell line, PA-1, *International Journal of Biological Macromolecules*, 107 (2018), 662-667.

[108] F. Al Sagheer; M. Al-Sughayer; S. Muslim, M. Elsabee, Extraction and characterization of chitin and chitosan from marine sources in Arabian Gulf, *Carbohydrate Polymers*, 77 (2009), 410-419.

[109] J. Synowiecki, N. A. Al-Khateeb, Production, Properties, and Some New

Applications of Chitin and Its Derivatives, *Critical Reviews in Food Science and Nutrition*, 43 (2003), 145-171.

[110] X. Feas; M. P. Vazquez-Tato; J. A. Seijas; G. N. A. Pratima, F. Fraga-Lopez, Extraction and Physicochemical Characterization of Chitin Derived from the Asian Hornet, Vespa velutina Lepeletier 1836 (Hym.: Vespidae), *Molecules*, 25 (2020), 384.

[111] E. E. Essa; D. Hamza; M. M. H. Khalil; H. Zaher; D. Salah; A. M. Alnemari; M. H. Rady, S. A. A. Mo Men, The antibacterial activity of Egyptian wasp chitosan-based nanoparticles against important antibiotic-resistant pathogens, *Molecules*, 27 (2022), 7189.

[112] Z. G. Umar; M. E. Abalaka; S. Y. Daniyan; H. Babayi, K. A. Adeniyi, Physicochemical and bio-metabolite characterizations of chitosan isolated from American cockroach (Periplaneta americana) and cricket (Acheta domesticus), *Federal University of Technology*, 02 (2022), 25-36.

[113] E. Cheraghi; M. Kababian; E. Moradi-Asl; S. M. M. Bafrouyi, A. Saghafipour, Structure and antibacterial activity of chitosan from the American cockroach, the German cockroach and the mealworm beetle, *Journal of Arthropod-Borne Diseases*, 16 (2022), 325.

[114] A. Jantzen da Silva Lucas; E. Quadro Oreste; H. Leao Gouveia Costa; H. Martin Lopez; C. Dias Medeiros Saad, C. Prentice, Extraction, physicochemical characterization, and morphological properties of chitin and chitosan from cuticles of edible insects, *Food Chemistry*, 343 (2021), 128550.

[115] A. Khayrova; S. Lopatin, V. Varlamov, Black Soldier Fly Hermetia illucens as a Novel Source of Chitin and Chitosan, *International Journal of Sciences*, 8 (2019), 81-86.

[116] C. Song; H. Yu; M. Zhang; Y. Yang, G. Zhang, Physicochemical properties and

antioxidant activity of chitosan from the blowfly Chrysomya megacephala larvae, *International Journal of Biological Macromolecules*, 60 (2013), 347-354.

[117] F. Jiang; X. Li; Y. Duan; Q. Li; Y. Qu; G. Zhong; M. Qiu; J. Zhang; C. Zhang, X. Pan, Extraction and characterization of chitosan from Eupolyphaga sinensis Walker and its application in the preparation of electrospinning nanofiber membranes, *Colloids Surf B Biointerfaces*, 222 (2023), 113030.

[118] G. Tan; M. Kaya; A. Tevlek; I. Sargin, T. Baran, Antitumor activity of chitosan from mayfly with comparison to commercially available low, medium and high molecular weight chitosans, *In Vitro Cell Dev Biol Anim*, 54 (2018), 366-374.

[119] Y. N. Tan; Y. L. Chin, W. N. Chen, Comparison of sustainable lipid and protein removal methods for the isolation of insect chitin from black soldier fly exoskeleton, *ACS Food Science & Technology*, 1 (2021), 698-706.

[120] Y.-S. Lin; S.-H. Liang; W.-L. Lai; J.-X. Lee; Y.-P. Wang; Y.-T. Liu; S.-H. Wang, M.-H. Lee, Sustainable extraction of chitin from spent pupal shell of black soldier fly, *Processes*, 9 (2021).

[121] K. S. Egorova; E. G. Gordeev, V. P. Ananikov, Biological activity of ionic liquids and their application in pharmaceutics and medicine, *Chemical Reviews*, 117 (2017), 7132-7189.

[122] J. L. Shamshina, N. Abidi, Isolation of chitin nano-whiskers directly from crustacean biomass waste in a single step with acidic ionic liquids, *ACS Sustainable Chemistry & Engineering*, 10 (2022), 11846-11855.

[123] E. S. Morais; A. M. d. C. Lopes; M. G. Freire; C. S. Freire; J. A. Coutinho, A. J. Silvestre, Use of ionic liquids and deep eutectic solvents in polysaccharides dissolution and extraction processes towards sustainable biomass valorization, *Molecules*, 25 (2020), 3652.

[124] Z. Li; C. Liu; S. Hong; H. Lian; C. Mei; J. Lee; Q. Wu; M. A. Hubbe, M.-C. Li, Recent advances in extraction and processing of chitin using deep eutectic solvents, *Chemical Engineering Journal*, 446 (2022), 136953.

[125] M. Khajavian; V. Vatanpour; R. Castro-Muñoz, G. Boczkaj, Chitin and derivative chitosan-based structures—Preparation strategies aided by deep eutectic solvents: A review, *Carbohydrate Polymers*, 275 (2022), 118702.

[126] G. Huet; C. Hadad; J. M. Gonzalez-Dominguez; M. Courty; A. Jamali; D. Cailleu, A. N. van Nhien, IL versus DES: Impact on chitin pretreatment to afford high quality and highly functionalizable chitosan, *Carbohydrate Polymers*, 269 (2021), 118332.

[127] Z. Li; M.-C. Li; C. Liu; X. Liu; Y. Lu; G. Zhou; C. Liu, C. Mei, Microwave-assisted deep eutectic solvent extraction of chitin from crayfish shell wastes for 3D printable inks, *Industrial Crops and Products*, 194 (2023), 116325.

[128] A. M. de Oliveira; T. T. Franco, E. N. d. Oliveira Junior, Physicochemical characterization of thermally treated chitosans and chitosans obtained by alkaline deacetylation, *International Journal of Polymer Science*, 2014 (2014).

[129] K. Gzyra‐Jagieła; B. Pęczek; M. Wiśniewska‐Wrona, N. Gutowska, Physicochemical properties of chitosan and its degradation products, *Chitin and Chitosan: Properties and Applications*, (2019), 61-80.

[130] R. M. Abdel-Rahman; R. Hrdina; A. M. Abdel-Mohsen; M. M. G. Fouda; A. Y. Soliman; F. K. Mohamed; K. Mohsin, T. D. Pinto, Chitin and chitosan from Brazilian Atlantic Coast: Isolation, characterization and antibacterial activity, *International Journal of Biological Macromolecules*, 80 (2015), 107-120.

[131] F. Sedaghat; M. Yousefzadi; H. Toiserkani, S. Najafipour, Chitin from Penaeus merguiensis via microbial fermentation processing and antioxidant activity, *International Journal of Biological Macromolecules*, 82 (2016), 279-283.

[132] D. Purkayastha, S. Sarkar, Physicochemical Structure Analysis of Chitin Extracted from Pupa Exuviae and Dead Imago of Wild Black Soldier Fly (Hermetia illucens), *Journal of Polymers and the Environment*, 28 (2020), 445-457.

[133] T. Marmier; C. R. Szczepanski; C. Candet; A. Zenerino; R. P. Godeau, G. Godeau, Investigation on Mecynorhina torquata Drury, 1782 (Coleoptera, Cetoniidae, Goliathini) cuticle: Surface properties, chitin and chitosan extraction, *International Journal of Biological Macromolecules*, 164 (2020), 1164-1173.

[134] X. Y. Godeau; F. J. Andrianandrasana; O. Volkova; C. R. Szczepanski; A. Zenerino; O. Montreuil; R. P. Godeau; P. Kuzhir, G. Godeau, Investigation on dung beetle's (Heliocopris Hope, 1838) chitosan valorisation for hydrogel 3D printing, *International Journal of Biological Macromolecules*, 199 (2022), 172-180.

[135] P. Fournier; C. R. Szczepanski; R. P. Godeau, G. Godeau, Chitosan extraction from Goliathus orientalis Moser, 1909: Characterization and comparison with commercially available chitosan, *Biomimetics*, 5 (2020), 15.

[136] M. R. Kasaai, A review of several reported procedures to determine the degree of N-acetylation for chitin and chitosan using infrared spectroscopy, *Carbohydrate Polymers*, 71 (2008), 497-508.

[137] Y. S. Song; Y. H. Jo; Y. S. Han, W. J. Jung, Production of chitin‐ and chitosan‐oligosaccharide using the edible insect, Tenebrio molitor, *Entomological Research*, 52 (2022), 207-213.

[138] N. F. Goularte; T. Kallem, L. Cegelski, Chemical and Molecular Composition of the Chrysalis Reveals Common Chitin-Rich Structural Framework for Monarchs and Swallowtails, *Journal of Molecular Biology*, 434 (2022), 167456.

[139] M. Kaya; A. M. Salaberria; M. Mujtaba; J. Labidi; T. Baran; P. Mulercikas, F. Duman, An inclusive physicochemical comparison of natural and synthetic chitin films,

International Journal of Biological Macromolecules, 106 (2018), 1062-1070.

[140] T. Hahn; E. Tafi; N. von Seggern; P. Falabella; R. Salvia; J. Thomä; E. Febel; M. Fijalkowska; E. Schmitt; L. Stegbauer, S. Zibek, Purification of Chitin from Pupal Exuviae of the Black Soldier Fly, *Waste and Biomass Valorization*, 13 (2021), 1993-2008.

[141] M. Chalghaf; K. Charradi; R. Ksouri; Q. A. Alsulami; A. Jaouani; S. M. A. S. Keshk, E. A. Hayouni, Physicochemical characterization of chitin extracted by different treatment sequences from an edible insect, *International Journal of Biological Macromolecules*, 253 (2023), 127156.

[142] S. Sharma; N. Kaur; R. Kaur, R. Kaur, A review on valorization of chitinous waste, *Journal of Polymer Research*, 28 (2021), 1-20.

[143] C. Qiao; X. Ma; X. Wang, L. Liu, Structure and properties of chitosan films: Effect of the type of solvent acid, *Lwt*, 135 (2021), 109984.

[144] R. Chatterjee; M. Maity; M. S. Hasnain, A. K. Nayak, Chitosan: source, chemistry, and properties, *Chitosan in Drug Delivery*, (2022), 1-22.

[145] G. Kapadnis; A. Dey; P. Dandekar, R. Jain, Effect of degree of deacetylation on solubility of low‐molecular‐weight chitosan produced via enzymatic breakdown of chitosan, *Polymer International*, 68 (2019), 1054-1063.

[146] J. C. Roy; F. Salaün; S. Giraud; A. Ferri; G. Chen, J. Guan, Solubility of chitin: solvents, solution behaviors and their related mechanisms, *Solubility of polysaccharides*, 3 (2017), 20-60.

[147] E. S. de Alvarenga, Characterization and properties of chitosan, *Biotechnology of Biopolymers*, 91 (2011), 48-53.

[148] W. Wang; Q. Meng; Q. Li; J. Liu; M. Zhou; Z. Jin, K. Zhao, Chitosan derivatives and their application in biomedicine, *International Journal of Molecular Sciences*, 21 (2020), 487.

[149] A. Jain; A. Gulbake; S. Shilpi; A. Jain; P. Hurkat, S. K. Jain, A new horizon in modifications of chitosan: syntheses and applications, *Critical Reviews™ in Therapeutic Drug Carrier Systems*, 30 (2013).

[150] A. H. Chisty; R. A. Masud; M. M. Hasan; M. N. Khan; A. K. Mallik, M. M. Rahman, PEGylated chitin and chitosan derivatives, *Handbook of chitin and chitosan*, (2020), 59-100.

[151] T. Liu; Y. Wang; B. Li; H. Deng; Z. Huang; L. Qian, X. Wang, Urea free synthesis of chitin-based acrylate superabsorbent polymers under homogeneous conditions: Effects of the degree of deacetylation and the molecular weight, *Carbohydrate Polymers*, 174 (2017), 464-473.

[152] S.-K. Kim, Chitin and chitosan derivatives: advances in drug discovery and developments, *CRC press*, (2013).

[153] R. Jayakumar; M. Prabaharan; P. S. Kumar; S. Nair, H. Tamura, Biomaterials based on chitin and chitosan in wound dressing applications, *Biotechnology advances*, 29 (2011), 322-337.

[154] H. Jafari; M. Pirouzifard; M. A. Khaledabad, H. Almasi, Effect of chitin nanofiber on the morphological and physical properties of chitosan/silver nanoparticle bionanocomposite films, *International Journal of Biological Macromolecules*, 92 (2016), 461-466.

[155] T. Furuike; D. Komoto; H. Hashimoto, H. Tamura, Preparation of chitosan hydrogel and its solubility in organic acids, *International Journal of Biological Macromolecules*, 104 (2017), 1620-1625.

[156] R. Rashid; I. Shafiq; P. Akhter; M. J. Iqbal, M. Hussain, A state-of-the-art review on wastewater treatment techniques: the effectiveness of adsorption method, *Environ. Sci. Pollut. Res.*, 28 (2021), 9050-9066.

[157] P. Bhatt; S. Joshi; G. M. U. Bayram; P. Khati, H. Simsek, Developments and application of chitosan-based adsorbents for wastewater treatments, *Environmental Reseach*, 226 (2023), 115530.

[158] T. Jozwiak; U. Filipkowska; T. Bakula; B. Bralewska-Piotrowicz; K. Karczmarczyk; M. Gierszewska; E. Olewnik-Kruszkowska; N. Szyrynska, B. Lewczuk, The use of chitin from the Molts of Mealworm (Tenebrio molitor) for the removal of anionic and cationic dyes from aqueous solutions, *Materials*, 16 (2023), 545.

[159] X.-Q. Dou, C.-L. Feng, Amino Acids and Peptide-Based Supramolecular Hydrogels for Three-Dimensional Cell Culture, *Adv. Mater.*, 29 (2017), 1604062.

[160] G. A. Engwa, Free radicals and the role of plant phytochemicals as antioxidants against oxidative stress-related diseases, *Phytochemicals: source of antioxidants and role in disease prevention. BoD–Books on Demand*, 7 (2018), 49-74.

[161] A. K. Shetty; M. Kodali; R. Upadhya, L. N. Madhu, Emerging anti-aging strategies-scientific basis and efficacy, *Aging and disease*, 9 (2018), 1165.

[162] X. Cui; Q. Lin, Y. Liang, Plant-derived antioxidants protect the nervous system from aging by inhibiting oxidative stress, *Frontiers in aging neuroscience*, 12 (2020), 209.

[163] E. Tafi; M. Triunfo; A. Guarnieri; D. Ianniciello; R. Salvia; C. Scieuzo; A. Ranieri; A. Castagna; S. Lepuri, T. Hahn, Preliminary investigation on the effect of insect-based chitosan on preservation of coated fresh cherry tomatoes, *Scientific Reports*, 13 (2023), 7030.

[164] Y.-C. Chung; Y. P. Su; C.-C. Chen; G. Jia; H. L. Wang; J. G. Wu, J. G. Lin, Relationship between antibacterial activity of chitosan and surface characteristics of cell wall, *Acta pharmacologica sinica*, 25 (2004), 932-936.

[165] P. S. Bhavsar; G. Dalla Fontana, M. Zoccola, Sustainable superheated water

hydrolysis of black soldier fly exuviae for chitin extraction and use of the obtained chitosan in the textile field, *ACS Omega*, 6 (2021), 8884-8893.

[166] M. Kaya; I. Sargin; P. Mulerčikas; J. Labidi; A. M. Salaberria; Y. S. Cakmak; S. Kazlauskaitė; D. Erdonmez, V. Baublys, Conversion of waste parasitic insect (Hylobius abietis L.) into antioxidative, antimicrobial and biodegradable films, *Journal of Renewable Materials*, 7 (2019), 215-226.

[167] A. I. Hasaballah, Crude and chitosan nano-particles extracts of some maggots as antioxidant and anticancer agents, *Journal of Advances in Biology & Biotechnology*, 21 (2019), 1-8.

[168] M. Mahboub; M. Hassan; A. Bream; A. Mohamed, M. Abdel-Samad, Preparation, characterization and anticancer activity of chitosan prepared from the American cockroach, Periplaneta americana, *Egyptian Academic Journal of Biological Sciences. A, Entomology*, 14 (2021), 163-171.

[169] V. Patrulea; V. Ostafe; G. Borchard, O. Jordan, Chitosan as a starting material for wound healing applications, *European Journal of Pharmaceutics and Biopharmaceutics*, 97 (2015), 417-426.

[170] I. Bano; M. Arshad; T. Yasin; M. A. Ghauri, M. Younus, Chitosan: A potential biopolymer for wound management, *International Journal of Biological Macromolecules*, 102 (2017), 380-383.

[171] N. H. Marei; W. El-Mazny; A. El-Shaer; K. D. Zaki; Z. S. Hussein, E. M. Abd-El-Samie, Enhanced wound healing activity of desert locust (Schistocerca gregaria) vs. shrimp (Penaeus monodon) chitosan based scaffolds, *International Journal of Biological Macromolecules*, 97 (2017), 23-33.

[172] E. B. Denkbas, R. M. Ottenbrite, Perspectives on: Chitosan Drug Delivery Systems Based on their Geometries, *Journal of Bioactive and Compatible Polymers*, 21 (2006),

351-368.

[173] S. M. Ahsan; M. Thomas; K. K. Reddy; S. G. Sooraparaju; A. Asthana, I. Bhatnagar, Chitosan as biomaterial in drug delivery and tissue engineering, *International Journal of Biological Macromolecules*, 110 (2018), 97-109.

[174] S. Jana, S. Jana, Functional chitosan: Drug delivery and biomedical applications, *Springer*, (2020).

[175] M. Glab; S. Kudlacik-Kramarczyk; A. Drabczyk; M. D. Guigou; A. Sobczak-Kupiec; D. Mierzwinski; P. Gajda; J. Walter, B. Tyliszczak, Multistep chemical processing of crickets leading to the extraction of chitosan used for synthesis of polymer drug carriers, *Materials*, 14 (2021), 5070.

[176] M. Keshvardoostchokami; M. Majidi; A. Zamani, B. Liu, A review on the use of chitosan and chitosan derivatives as the bio-adsorbents for the water treatment: Removal of nitrogen-containing pollutants, *Carbohydrate polymers*, 273 (2021), 118625.

[177] M. N. Sakib; A. K. Mallik, M. M. Rahman, Update on chitosan-based electrospun nanofibers for wastewater treatment: A review, *Carbohydrate Polymer Technologies and Applications*, 2 (2021), 100064.

[178] S. A. Qamar; M. Ashiq; M. Jahangeer; A. Riasat, M. Bilal, Chitosan-based hybrid materials as adsorbents for textile dyes–A review, *Case Studies in Chemical and Environmental Engineering*, 2 (2020), 100021.

[179] A. C. Sadiq; A. Olasupo; W. S. W. Ngah; N. Y. Rahim, F. B. M. Suah, A decade development in the application of chitosan-based materials for dye adsorption: A short review, *International Journal of Biological Macromolecules*, 191 (2021), 1151-1163.

[180] H. El Knidri; R. Belaabed; A. Addaou; A. Laajeb, A. Lahsini, Extraction, chemical modification and characterization of chitin and chitosan, *International Journal of Biological Macromolecules*, 120 (2018), 1181-1189.

[181] M. Lavertu; Z. Xia; A. N. Serreqi; M. Berrada; A. Rodrigues; D. Wang; M. D. Buschmann, A. Gupta, A validated 1H NMR method for the determination of the degree of deacetylation of chitosan, *Journal of Pharmaceutical and Biomedical Analysis*, 32 (2003), 1149-1158.

[182] R. Czechowska-Biskup; D. Jarosińska; B. Rokita; P. Ulański, J. M. Rosiak, Determination of degree of deacetylation of chitosan-comparision of methods, *Progress on Chemistry and Application of Chitin and its Derivatives*, (2012), 5-20.

[183] J. Wang, X. Guo, Adsorption kinetic models: Physical meanings, applications, and solving methods, *Journal of Hazardous materials*, 390 (2020), 122156.

[184] S. Lagergren, About the Theory of So-Called Adsorption of Soluble Substances, 24 (1898), 1–39.

[185] Y. Ho, Wase, DAJ, C. CF Forster, Removal of lead ions from aqueous solution using sphagnum moss peat as adsorbent, *Water Sa*, 22 (1996), 219-224.

[186] I. Langmuir, The constitution and fundamental properties of solids and liquids. Part I. Solids, *Journal of the American chemical society*, 38 (1916), 2221-2295.

[187] H. Freundlich, Über die adsorption in lösungen, *Zeitschrift für physikalische Chemie*, 57 (1907), 385-470.

[188] J. W. Gibbs, On the equilibrium of heterogeneous substances, *American Journal of Science*, 3 (1878), 441-458.

[189] X. Zhou, X. Zhou, The unit problem in the thermodynamic calculation of adsorption using the Langmuir equation, *Chemical Engineering Communications*, 201 (2014), 1459-1467.

[190] T. Fischetti; N. Celikkin; N. Contessi Negrini; S. Farè, W. Swieszkowski, Tripolyphosphate-crosslinked chitosan/gelatin biocomposite ink for 3D printing of uniaxial scaffolds, *Frontiers in Bioengineering and Biotechnology*, 8 (2020).

[191] Z. He; Y. Sun; J. Cao, Y. Duan, Degradation behavior and biosafety studies of the mPEG–PLGA–PLL copolymer, *Physical Chemistry Chemical Physics*, 18 (2016), 11986-11999.

[192] S. Shin; D. J. Clarke; A. R. Lemmon; E. Moriarty Lemmon; A. L. Aitken; S. Haddad; B. D. Farrell; A. E. Marvaldi; R. G. Oberprieler, D. D. McKenna, Phylogenomic data yield new and robust insights into the phylogeny and evolution of weevils, *Mol. Biol. Evol.*, 35 (2018), 823-836.

[193] X. Y. Godeau; F. J. Andrianandrasana; O. Volkova; C. R. Szczepanski; A. Zenerino; O. Montreuil; R.-P. Godeau; P. Kuzhir, G. Godeau, Investigation on dung beetle's (Heliocopris Hope, 1838) chitosan valorisation for hydrogel 3D printing, *Int. J. Biol. Macromol.*, 199 (2022), 172-180.

[194] A. Percot; C. Viton, A. Domard, Optimization of chitin extraction from shrimp shells, *Biomacromolecules*, 4 (2003), 12-18.

[195] C. Pouya; D. Stavenga, P. Vukusic, Discovery of ordered and quasi-ordered photonic crystal structures in the scales of the beetle Eupholus magnificus, *Optics express*, 19 (2011), 11355-11364.

[196] Y. Liu; R. Xing; H. Yang; S. Liu; Y. Qin; K. Li; H. Yu, P. Li, Chitin extraction from shrimp (Litopenaeus vannamei) shells by successive two-step fermentation with Lactobacillus rhamnoides and Bacillus amyloliquefaciens, *Int. J. Biol. Macromol.*, 148 (2020), 424-433.

[197] W. Sajomsang, P. Gonil, Preparation and characterization of α-chitin from cicada sloughs, *Materials Science and Engineering: C*, 30 (2010), 357-363.

[198] T. S. Trung; L. H. Tram; N. Van Tan; N. Van Hoa; N. C. Minh; P. T. Loc, W. F. Stevens, Improved method for production of chitin and chitosan from shrimp shells, *Carbohydrate Research*, 489 (2020), 107913.

[199] L. Huang; S. Bi; J. Pang; M. Sun; C. Feng, X. Chen, Preparation and characterization of chitosan from crab shell (Portunus trituberculatus) by NaOH/urea solution freeze-thaw pretreatment procedure, *International Journal of Biological Macromolecules*, 147 (2020), 931-936.

[200] G. Hao; Y. Hu; L. Shi; J. Chen; A. Cui; W. Weng, K. Osako, Physicochemical characteristics of chitosan from swimming crab (Portunus trituberculatus) shells prepared by subcritical water pretreatment, *Scientific Reports*, 11 (2021), 1646.

[201] A. Hosney; S. Ullah, K. Barčauskaitė, A Review of the Chemical Extraction of Chitosan from Shrimp Wastes and Prediction of Factors Affecting Chitosan Yield by Using an Artificial Neural Network, *Marine Drugs*, 20 (2022), 675.

[202] Y. Villegas-Peralta; J. López-Cervantes; T. J. Madera Santana; R. G. Sánchez-Duarte; D. I. Sánchez-Machado; M. d. R. Martínez-Macías, M. A. Correa-Murrieta, Impact of the molecular weight on the size of chitosan nanoparticles: characterization and its solid-state application, *Polymer Bulletin*, 78 (2021), 813-832.

[203] Y. Tan; M. S. R. Rajoka; Z. Ke; H. M. Mehwish; W. Deng; J. Li; W. Qin; L. Zhao, Y. Wu, Effect of Squid Cartilage Chitosan Molecular Structure on the Properties of Its Monofilament as an Absorbable Surgical Suture, *Polymers*, 14 (2022), 1306.

[204] S. P. Chawla; S. R. Kanatt, A. K. Sharma, Chitosan, in: K.G. Ramawat, J.-M. Mérillon (Eds.), Polysaccharides: Bioactivity and Biotechnology, Springer International Publishing, Cham, 2015, pp. 219-246.

[205] W. H. Miller, A treatise on crystallography, *For J. & JJ Deighton*, (1839).

[206] G. L. Clark, A. F. Smith, X-ray diffraction studies of chitin, chitosan, and derivatives, *The Journal of Physical Chemistry*, 40 (2002), 863-879.

[207] H. Wu; J. Zhou; S. Zhang; P. Niu; H. Li; Z. Liu; N. Zhang; C. Li; L. Wang, Y. Wang, A Comparative Study of Removal of Acid Red 27 by Adsorption on Four Different

Chitosan Morphologies, *Polymers*, 16 (2024), 1019.

[208] D. Rigotti, Polymer composites for sustainable 3D printing materials, *Univerista Di Trento*, (2019).

[209] H. Yan; Y. Feng; W. Hu; C. Cheng; R. Liu; C. Wang; J. Li, Q. Lin, Preparation and evaluation of alginate-chitosan-bentonite based beads for the delivery of pesticides in controlled-release formulation, *Asian Journal of Chemistry*, 25 (2013), 9936.

[210] T. Vieira; V. Becegato, A. Paulino, Equilibrium Isotherms, Kinetics, and Thermodynamics of the Adsorption of 2,4-Dichlorophenoxyacetic Acid to Chitosan-Based Hydrogels, *Water, Air, & Soil Pollution*, 232 (2021).

[211] K. V. Harish Prashanth; F. S. Kittur, R. N. Tharanathan, Solid state structure of chitosan prepared under different N-deacetylating conditions, *Carbohydrate Polymers*, 50 (2002), 27-33.

[212] K. S. S. Yuvarani I, Venkatesan J, Kim, S. K.,Sudha, P. N., Preparation and characterization of curcumin coated chitosan-alginate blend for wound dressing application, *Journal of Biomaterials and Tissue Engineering*, 2 (2012), 54-60.

[213] J. Peng; X. Wang, T. Lou, Preparation of chitosan/gelatin composite foam with ternary solvents of dioxane/acetic acid/water and its water absorption capacity, *Polymer Bulletin*, 77 (2020), 5227-5244.

[214] W. Srihata; T. Jamnongkan; U. Rattanasak; S. Boonsang, S. Kaewpirom, Enhanced electrostatic dissipative properties of chitosan/gelatin composite films filled with reduced graphene oxide, *Journal of Materials Science: Materials in Electronics*, 28 (2017), 999-1010.

[215] S. Brunauer; P. H. Emmett, E. Teller, Adsorption of gases in multimolecular layers, *Journal of the American chemical society*, 60 (1938), 309-319.

[216] I. Ben Amor; H. Hemmami; S. E. Laouini ; S. Zeghoud; M. Benzina; S. Achour;

A. Naseef; A. Alsalme, A. Barhoum, Use of Insect-Derived Chitosan for the Removal of Methylene Blue Dye from Wastewater: Process Optimization Using a Central Composite Design, *Materials*, 16 (2023), 5049.

[217] A. Fernández-Pérez; T. Valdés-Solís, G. Marbán, Visible light spectroscopic analysis of Methylene Blue in water; the resonance virtual equilibrium hypothesis, *Dyes and Pigments*, 161 (2019), 448-456.

[218] A. Prasetyaningrum; S. Arrois; F. Lafifa; A. Z. Mubarok; F. Fani; N. A. Handayani; R. Ratnawati, B. Jos, Encapsulation of Lemongrass Extract (Cymbopogon citratus) Coated Alginate/Chitosan Using Gelation Method, *Reaktor*, 21 (2021), 9.

[219] Z. Feyissa; G. D. Edossa; N. K. Gupta, D. Negera, Development of double crosslinked sodium alginate/chitosan based hydrogels for controlled release of metronidazole and its antibacterial activity, *Heliyon*, 9 (2023), e20144.

[220] A. Niculescu, A. Grumezescu, Applications of Chitosan-Alginate-Based Nanoparticles—An Up-to-Date Review, *Nanomaterials*, 12 (2022), 186.

[221] E. Salehi, A. Farahani, Macroporous chitosan/polyvinyl alcohol composite adsorbents based on activated carbon substrate, *Journal of Porous Materials*, 24 (2017), 1197-1207.

[222] D. Allouss; Y. Essamlali; O. Amadine; A. Chakir, M. Zahouily, Response surface methodology for optimization of methylene blue adsorption onto carboxymethyl cellulose-based hydrogel beads: adsorption kinetics, isotherm, thermodynamics and reusability studies, *RSC Advances*, 9 (2019), 37858-37869.

[223] P. Sirajudheen; N. C. Poovathumkuzhi; S. Vigneshwaran; B. M. Chelaveettil, S. Meenakshi, Applications of chitin and chitosan based biomaterials for the adsorptive removal of textile dyes from water — A comprehensive review, *Carbohydrate Polymers*, 273 (2021), 118604.

[224] N. S. Abdul Mubarak; N. N. Bahrudin; A. H. Jawad; B. H. Hameed, S. Sabar, Microwave enhanced synthesis of sulfonated chitosan-montmorillonite for effective removal of methylene blue, *Journal of Polymers and the Environment*, 29 (2021), 4027-4039.

[225] S. Canossa; C. Graiff; D. Crocco, G. Predieri, Water Structures and Packing Efficiency in Methylene Blue Cyanometallate Salts, *Crystals*, 10 (2020), 558.

[226] D. A. Ahmad Ruzaidi; M. M. Mahat; Z. Mohamed Sofian; N. A. Nor Hashim; H. Osman; M. A. Nawawi; R. Ramli; K. A. Jantan; M. F. Aizamddin; H. H. Azman; Y. H. Robin Chang, H. H. Hamzah, Synthesis and Characterization of Porous, Electro-Conductive Chitosan–Gelatin–Agar-Based PEDOT: PSS Scaffolds for Potential Use in Tissue Engineering, *Polymers*, 13 (2021), 2901.

[227] S. Sethi; Medha, B. S. Kaith, A review on chitosan-gelatin nanocomposites: Synthesis, characterization and biomedical applications, *Reactive and Functional Polymers*, 179 (2022), 105362.

[228] M. Joudi; H. Nasserlah; H. Hafdi; J. Mouldar; B. Hatimi; M. A. E. Mhammedi, M. Bakasse, Synthesis of an efficient hydroxyapatite–chitosan ‑ montmorillonite thin film for the adsorption of anionic and cationic dyes: adsorption isotherm, kinetic and thermodynamic study, *SN Applied Sciences*, 2 (2020), 1078.

[229] K. Valizadeh; A. Bateni; N. Sojoodi; M. R. Ataabadi; A. H. Behroozi; A. Maleki, Z. You, Magnetized inulin by Fe3O4 as a bio-nano adsorbent for treating water contaminated with methyl orange and crystal violet dyes, *Scientific Reports*, 12 (2022), 22034.

[230] Z. Chen; Z.-B. Zhang; J. Zeng; Z.-J. Zhang; S. Ma; C.-M. Tang, J.-Q. Xu, Preparation of polyethyleneimine-modified chitosan/Ce-UIO-66 composite hydrogel for the adsorption of methyl orange, *Carbohydrate Polymers*, 299 (2023), 120079.

[231] N. S. Abdul Mubarak; T. W. Chuan; H. P. Khor; A. H. Jawad; L. D. Wilson, S. Sabar, Immobilized Fe-Loaded Chitosan Film for Methyl Orange Dye Removal: Competitive Ions, Reusability, and Mechanism, *Journal of Polymers and the Environment*, 29 (2021), 1050-1062.

[232] Y. Liu; S. Huang; X. Zhao, Y. Zhang, Fabrication of three-dimensional porous β-cyclodextrin/chitosan functionalized graphene oxide hydrogel for methylene blue removal from aqueous solution, *Colloids and Surfaces A: Physicochemical and Engineering Aspects*, 539 (2018), 1-10.

[233] X. Zhao; X. Wang, T. Lou, Preparation of fibrous chitosan/sodium alginate composite foams for the adsorption of cationic and anionic dyes, *Journal of Hazardous Materials*, 403 (2021), 124054.

[234] E. S. Dragan; M. M. Lazar; M. V. Dinu, F. Doroftei, Macroporous composite IPN hydrogels based on poly(acrylamide) and chitosan with tuned swelling and sorption of cationic dyes, *Chemical Engineering Journal*, 204-206 (2012), 198-209.

[235] C. Qi; L. Zhao; Y. Lin, D. Wu, Graphene oxide/chitosan sponge as a novel filtering material for the removal of dye from water, *Journal of Colloid and Interface Science*, 517 (2018), 18-27.

[236] T. S. Vo; T. T. B. C. Vo; J. W. Suk, K. Kim, Recycling performance of graphene oxide-chitosan hybrid hydrogels for removal of cationic and anionic dyes, *Nano Convergence*, 7 (2020), 4.

[237] Y. Jiang; J.-L. Gong; G.-M. Zeng; X.-M. Ou; Y.-N. Chang; C.-H. Deng; J. Zhang; H.-Y. Liu, S.-Y. Huang, Magnetic chitosan–graphene oxide composite for anti-microbial and dye removal applications, *International Journal of Biological Macromolecules*, 82 (2016), 702-710.

[238] M. T. Nakhjiri; G. B. Marandi, M. Kurdtabar, Poly(AA-co-VPA) hydrogel cross-

linked with N-maleyl chitosan as dye adsorbent: Isotherms, kinetics and thermodynamic investigation, *International Journal of Biological Macromolecules*, 117 (2018), 152-166.

[239] D. Li; Q. Li; D. Mao; N. Bai, H. Dong, A versatile bio-based material for efficiently removing toxic dyes, heavy metal ions and emulsified oil droplets from water simultaneously, *Bioresource Technology*, 245 (2017), 649-655.

[240] Q. Peng; M. Liu; J. Zheng, C. Zhou, Adsorption of dyes in aqueous solutions by chitosan–halloysite nanotubes composite hydrogel beads, *Microporous and Mesoporous Materials*, 201 (2015), 190-201.

[241] A. Sabzevari, A. Kakanejadifard, Synthesis and characterization of grapheme–chitosan hydrogel as adsorbent for methyl orange, *Polymer Bulletin*, 81 (2024), 8607-8625.

[242] S. Zhao; F. Zhou; L. Li; M. Cao; D. Zuo, H. Liu, Removal of anionic dyes from aqueous solutions by adsorption of chitosan-based semi-IPN hydrogel composites, *Composites Part B: Engineering*, 43 (2012), 1570-1578.

[243] W. Wang; H. Zhang; J. Shen, M. Ye, Facile preparation of magnetic chitosan/poly (vinyl alcohol) hydrogel beads with excellent adsorption ability via freezing-thawing method, *Colloids and Surfaces A: Physicochemical and Engineering Aspects*, 553 (2018), 672-680.

[244] A. S. Kulkarni; A. M. Sajjan; T. M. Y. Khan; I. A. Badruddin; S. Kamangar; N. R. Banapurmath; N. H. Ayachit; M. Ashwini, A. Sharanappa, Development and Characterization of Biocompatible Membranes from Natural Chitosan and Gelatin for Pervaporative Separation of Water–Isopropanol Mixture, *Polymers*, 13 (2021), 2868.

[245] S. Ansari; M. A. I. Rashid; P. R. Waghmare, D. S. Nobes, Measurement of the flow behavior index of Newtonian and shear-thinning fluids via analysis of the flow velocity characteristics in a mini-channel, *SN Applied Sciences*, 2 (2020), 1787.

[246] C. W. Macosko, Rheology principles, *Measurements and Applications*, (1994).

[247] M. Nieto-Suárez; M. A. López-Quintela, M. Lazzari, Preparation and characterization of crosslinked chitosan/gelatin scaffolds by ice segregation induced self-assembly, *Carbohydr. Polym.*, 141 (2016), 175-183.

[248] C.-M. Moysidou; C. Barberio, R. M. Owens, Advances in Engineering Human Tissue Models, *Front. Bioeng. Biotechnol.*, 8 (2021).

[249] M. Samiei; E. Dalir Abdollahinia; N. Amiryaghoubi; M. Fathi; J. Barar, Y. Omidi, Injectable thermosensitive chitosan/gelatin hydrogel for dental pulp stem cells proliferation and differentiation, *Bioimpacts*, 13 (2023), 63-72.